Western Graduate&PostdoctoralStudies

Western University
Scholarship@Western

Electronic Thesis and Dissertation Repository

7-18-2018 10:00 AM

Coinage Metal Chalcogenide Clusters with N-Heterocyclic Carbene Ancillary Ligands

Alex Polgar, *The University of Western Ontario*

Supervisor: Corrigan, John F., *The University of Western Ontario*

A thesis submitted in partial fulfillment of the requirements for the Master of Science degree in Chemistry

© Alex Polgar 2018

Follow this and additional works at: https://ir.lib.uwo.ca/etd

Part of the Inorganic Chemistry Commons

Recommended Citation

Polgar, Alex, "Coinage Metal Chalcogenide Clusters with N-Heterocyclic Carbene Ancillary Ligands" (2018). *Electronic Thesis and Dissertation Repository*. 5468.
https://ir.lib.uwo.ca/etd/5468

This Dissertation/Thesis is brought to you for free and open access by Scholarship@Western. It has been accepted for inclusion in Electronic Thesis and Dissertation Repository by an authorized administrator of Scholarship@Western. For more information, please contact wlswadmin@uwo.ca.

Abstract

This thesis describes the synthesis and characterization of homo- and heterometallic group 11 – group 16 clusters with *N*-heterocyclic carbene (NHC) ligands. The clusters were prepared from reactive group 11 trimethylsilylchalcogenolate reagents (NHC-M-ESiMe$_3$; M = Cu, Au; E = S, Se, Te) by silane deprotection reactions with phosphine- or phosphite-solubilized group 11 acetates (R_3P-M-OAc; M = Cu, Ag, Au). Clusters were characterized by combustion analysis and spectroscopic methods in solution and the solid state. The clusters were phosphorescent at low temperatures with emission energies that depend on the metal/chalcogen composition, ancillary NHC ligand, cluster geometry and nuclearity, and local environment. Lower energy photoluminescence is associated with higher atomic number chalcogenide ligands and correlates with the M→S metal-to-ligand charge transfer energy, for which M = Ag > Cu > Au. Quantum yield of emission is increased in a cluster of high nuclearity and connectivity because of increased molecular rigidity and thermally activated delayed fluorescence. Quantum chemical calculations point to a common mode of emission from all clusters, originating from a charge transfer process from metal-chalcogenide core to the NHC ancillary ligands.

Co-Authorship Statement

The work described in this thesis contains contributions from the author as well as co-workers Angel Zhang, Dr. Martin J. Stillman, Dr. Florian Weigend, Dr. Sergei Lebedkin, and Dr. John F. Corrigan. The contributions of each are described below.

Chapter 1 was written by the author and edited by Dr. Corrigan.

Chapter 2 describes a series of compounds synthesized by the author. Dr. Corrigan performed all crystallographic experiments, structural solution and refinement. Angel Zhang and Dr. Stillman assisted the author with measurements of steady-state and time-resolved photoluminescence in frozen glass matrices at 77K. Dr. Lebedkin assisted the author with temperature-dependent measurements of steady-state and time-resolved photoluminescence in the crystalline state. Dr. Weigend performed the quantum chemical calculations. The chapter was written by the author and edited by Dr. Corrigan.

Chapter 3 describes a series of compounds synthesized by the author. Dr. Corrigan performed all crystallographic experiments and structural solution. Structural refinement was performed by the author and Dr. Corrigan. Angel Zhang and Dr. Stillman assisted the author with measurements of steady-state and time-resolved photoluminescence at in frozen glass matrices 77K. Quantum chemical calculations were performed by the author. The chapter was written by the author and edited by Dr. Corrigan.

Chapter 4 describes compounds synthesized by the author. Dr. Corrigan performed all crystallographic experiments and structural solution. Structural refinement was performed by the author and Dr. Corrigan. Dr. Lebedkin assisted the author with temperature-dependent measurements of steady-state and time-resolved photoluminescence in the crystalline state. Quantum chemical calculations were performed by the author. The chapter was written by the author and edited by Dr. Corrigan.

Chapter 5 was written by the author and edited by Dr. Corrigan.

Acknowledgements

I am grateful to my supervisor Dr. John F. Corrigan for all that he has done for me over the past three years that I have been privileged to work with him. He is a model of what it means to be a good scientist and a good person. I am especially grateful for all the opportunities he has given me to present at conferences, to conduct research abroad, and to freely explore the scope of my research.

Thanks to the members of the Corrigan group past and present. Thanks to Vaishnavi and Kyle for showing me the ropes when I started here in my undergraduate. Thanks to Stefan for showing me how to do chemistry the German (*i.e*. correct) way. Thanks to my surrogate group members in the first year of my MSc: Wilson, Praveen, Alex, Tommy, and Raj. And thanks to the new Corrigan group members Jay, Richard, and Khayrat for making my last year so enjoyable.

I have been in the Department of Chemistry at Western for six years and am grateful for all the wonderful people to have taught and collaborated with me. A special thanks to Dr. Viktor Staroverov, who took me on as a USRA student after second year and introduced me to what it means to do scientific research. Thanks to Dr. Martin Stillman and Angel Zhang for the fruitful collaboration over the past two years. Thanks to the support staff – Mat in NMR, Paul in X-Ray, Doug in Mass Spec, Jon and John in the electronics shop, Yves and Mike at the glassblowing shop, and the folks down in ChemStores – for being so good at what they do.

A big thank you to my committee members Dr. Ragogna, Dr. Puddephatt, and Dr. Goncharova for taking the time to read this thesis.

Finally, I could not have done this without the support of my family. Thank you for everything!

Table of Contents

Abstract i
Co-Authorship Statement ii
Acknowledgements iii
List of Figures vii
List of Tables viii
List of Charts and Schemes viii
List of Appendices ix
List of Abbreviations x
Chapter 1 1
1 Introduction 1
1.1 Group 11 Chalcogen Compounds 1
1.1.1 Group 11 Chalcogenolate Compounds 1
1.1.2 Group 11 Chalcogenide Clusters 5
1.1.3 Group 11 Chalcogenolate-Chalcogenide Clusters 7
1.1.4 Group 11 Silylchalcogenolate Reagents 8
1.2 Luminescent Metal Complexes 10
1.2.1 Principles of Luminescence Spectroscopy 10
1.2.2 d^6 and d^8 Platinum Group Complexes 12
1.2.3 d^{10} Group 11 Complexes 14
1.2.4 d^{10} Group 11 Complexes with Chalcogen-Containing Ligands 17
1.3 Scope of the Thesis 19
1.4 References 20
Chapter 2 24
2 A *N*-Heterocyclic Carbene Stabilized Coinage Metal Chalcogenide Framework with Highly Tunable Optical Properties 24
2.1 Introduction 24

2.2 Results and Discussion 25
2.3 Experimental Section 33
2.3.1 General Considerations 33
2.3.2 Synthesis 34
2.3.3 X-Ray Crystallography Details 38
2.4 Conclusions and Outlook 39
2.5 References 40
Chapter 3 42
3 Plug and Play: Tunable Metal/Chalcogen Composition in Copper(I)-Chalcogenide Self-Assemblies Enabled by Cyclic (Alkyl)(amino)carbenes 42
3.1 Introduction 42
3.2 Results and Discussion 43
3.3 Experimental Section 51
3.3.1 General Considerations 51
3.3.2 Synthesis 52
3.3.3 X-Ray Crystallography Details 55
3.4 Conclusions and Outlook 57
3.5 References 58
Chapter 4 60
4 Gold(I)-Copper(I)-Sulfido Clusters: Structure-Dependent Luminescence and Thermally Activated Delayed Fluorescence 60
4.1 Introduction 60
4.2 Results and Discussion 61
4.3 Experimental Section 66
4.3.1 General Considerations 66
4.3.2 Synthesis 68

4.3.3 X-Ray Crystallography Details 69
4.4 Conclusions and Outlook 70
4.5 References 71
Chapter 5 73
5 Conclusions and Outlook 73
5.1 Summary and Conclusions 73
5.2 Outlook – NHCs in Nanocluster Chemistry 77
5.3 Outlook – Metal Chalcogenide-Metallachalcogenolate clusters 78
5.4 Outlook – Modulation of the Ancillary NHC Ligands 78
5.5 References 79
Appendices 80
Appendix 1. Permission to Reuse Copyright Material 80
Appendix 2. Supporting Information for Chapter 2 82
Appendix 3. Supporting Information for Chapter 3 97
Appendix 4. Supporting Information for Chapter 4 110
Curriculum Vitae 114

List of Figures

Figure 1.1 Molecular structures of 1D and 2D group 11 chalcogenolate coordination polymers in the crystal 2

Figure 1.2 Molecular structures of group 11 chalcogenolate oligomers in the crystal 3

Figure 1.3 Molecular structures of trialkylphosphine-stabilized group 11 chalcogenolate clusters in the crystal 4

Figure 1.4 Molecular structures of phosphine-stabilized group 11 chalcogenide clusters in the crystal 6

Figure 1.5 Molecular structures of phosphine-stabilized ternary group 11 chalcogenide clusters in the crystal 7

Figure 1.6 Molecular structures of group 11 chalcogenolate-chalcogenide clusters in the crystal with (A) and without (B) ancillary phosphine ligands 8

Figure 1.7 Jablonski diagram for the electronic transitions involved in light absorption, fluorescence, and phosphorescence 11

Figure 1.8 Molecular structures of luminescent group 11 chalcogenide clusters in the crystal . 18

Figure 2.1 Stacked ^{1}H NMR Spectra of **2.1a** (black), **2.1b** (red), and **2.1c** (blue) in $CDCl_3$ at 298K 26

Figure 2.2 Molecular structures of **2.2a,b** and **2.3a-c** in the crystal 28

Figure 2.3 ^{1}H NMR spectra for **2.2b** in $CDCl_3$ at 298K. Inset is the ^{77}Se{^{1}H} NMR spectrum in $CDCl_3$ at 273K 30

Figure 2.4 Photoluminescence emission (PL) and excitation (PLE) spectra for **2.2-3** in glassy 2-MeTHF at 77K (top) and as a crystalline powder (bottom) 31

Figure 2.5 A) Orbital energy diagram for **2.2-3**. B) Difference density plot for the first singlet excited state of **2.2a** 32

Figure 3.1 ^{1}H NMR spectra for **3.1-2** in $CDCl_3$ at 298K 44

Figure 3.2 Molecular structures of **3.3**–**5** in the crystal 46

Figure 3.3 Absorption spectra of **A**) mononuclear complexes **3.1-2** and **CAAC^{Cy}** **C**) cluster compounds **3.3-5** in 2-MeTHF at 298K. Photoluminescence excitation (PLE) and emission (PL) spectra of **B**) mononuclear complexes **3.1-2** and **CAAC^{Cy}** and **D**) cluster compounds **3.3-5** in glassy 2-MeTHF at 77K 48

Figure 3.4 Orbital energy diagram for the singlet states of **3.3-5**. Below, the HOMO and LUMO for **3.3a** are plotted 50
Figure 4.1 Molecular structures of **4.1** (left) and **4.2** (right) in the crystal 62
Figure 4.2 A) Simulated (lower, red) and experimental (upper, black) ^{1}H NMR spectra for the aromatic region of **4.1.** B) Experimental ^{1}H NMR spectrum for the aliphatic region of **4.1** 64
Figure 4.3 Temperature-dependent emission spectra of A) **4.1** and B) **4.2** in the solid state from 77K to 298K (solid lines). C) Temperature-dependence of the phosphorescence lifetime (black circles) and radiative rate constant $k_r = \Phi_{PL}/\tau$ (blue squares) of **4.1** 65
Figure 4.4 Highest occupied molecular orbital (HOMO) and lowest unoccupied molecular orbital (LUMO) isosurfaces (isoval = 0.03) for **4.1** 66

List of Tables

Table 2.1 Selected bonds lengths (Å) and angles (°) for **2.2-3** 29
Table 2.2 Summary of spectroscopic data for **2.2-3** in frozen 2-MeTHF and the solid state at 77K 31
Table 3.1 Selected bonds lengths (Å) and angles (°) for **3.3-5** 47
Table 3.2 Spectroscopic data for **3.1-5** and **CAAC^{Cy}** in frozen (77K) 2-MeTHF 49
Table A2.1 Crystallographic data for **2.2-3**..... 96
Table A3.1 Crystallographic data for **3.3-5**..... 109
Table A4.1 Crystallographic data for **4.1** and **4.2** 113

List of Charts and Schemes

Scheme 1.1 Ternary metal chalcogenide clusters synthesized from group 11 silylchalcogenolate compounds stabilized by tertiary phosphines 9
Scheme 1.2 Ternary metal chalcogenide clusters synthesized from group 11 silylchalcogenolate compounds stabilized by NHCs 10
Chart 1.1 Examples of intensely luminescent organometallic complexes and their spectroscopic parameters 13
Chart 1.2 Examples of intensely luminescent complexes of d^{10} coinage metals and their spectroscopic parameters 15

Chart 1.3 Examples of intensely luminescent complexes which operate by the TADF mechanism and their spectroscopic parameters 16
Scheme 2.1 Synthesis of **2.1a-c** 25
Scheme 2.2 Synthesis of **2.2a,b** and **2.3a-c** 27
Scheme 3.1 Synthesis of **CAAC^{Cy}** and **3.1 – 3.5** 45
Scheme 4.1 Syntheses of A) **4.1** and B) **4.2**. 62
Chart 5.1 New compounds reported in Section 2 and their associated spectroscopic parameters at 77K 74
Chart 5.2 New compounds reported in Section 3 and their associated spectroscopic parameters at 77K 75
Chart 5.3 New compounds reported in Section 3 and their associated spectroscopic parameters 77

List of Appendices

Appendix 1 Permission to Reuse Copyright Material 80
Appendix 2 Supporting Information for Chapter 2..... 82
Appendix 3 Supporting Information for Chapter 3..... 97
Appendix 4 Supporting Information for Chapter 4..... 110

List of Abbreviations

°C	Degrees Celsius
δ	Chemical Shift
ε	Molar Absorptivity
γ	Magnetogyric Ratio
λ_{em}	Emission wavelength
λ_{ex}	Excitation wavelength
μs	Microsecond
$\tilde{\nu}_{ST}$	Stokes shift
Φ_{PL}	Photoluminescence Quantum Yield
ζ	Spin-Orbit Coupling Constant
γ	Magnetogyric Ratio
τ	Excited state lifetime (decay time)
1D	One-dimensional
2D	Two-dimensional
3D	Three-dimensional
Å	Angstrom
a. u.	Arbitrary Units
Ad	Adamantyl
Ar	Aromatic Group
C^N	Bidentate ligand with C and N donors
CAAC	Cyclic (Alkyl)(amino)carbene
$CAAC^{Cy}$	2-(2,6-diisopropylphenyl)-3,3-dimethyl-2-azaspiro[4.5]dec-1-ylidene
CC	Cluster-Centered
CLCT	Cluster-to-Ligand Charge Transfer
cm	Centimeter
CT	Charge Transfer
Dipp	2,6-diisopropylphenyl
DFT	Density Functional Theory
dpepp	$\{Ph_2P(CH_2)_2\}_2PPh$
dppe	Bis(diphenylphosphino)ethane – $Ph_2P(CH_2)_2PPh_2$
dpph	Bis(diphenylphosphino)heptane – $Ph_2P(CH_2)_7PPh_2$
dppm	Bis(diphenylphosphino)methane – $Ph_2PCH_2PPh_2$
dppp	Bis(diphenylphosphino)propane – $Ph_2P(CH_2)_3PPh_2$
dpppt	Bis(diphenylphosphino)pentane – $Ph_2P(CH_2)_5PPh_2$
E	Chalcogen: S, Se, or Te
ER	Chalcogenolate
Et	Ethyl – C_2H_5
eV	Electron Volt – 1.6022×10^{-19} J

F	Structure Factor
FWHM	Full-Width at Half Maximum
FMO	Frontier Molecular Orbital
HMBC	Heteronuclear Multiple Bond Correlation
HOMO	Highest Occupied Molecular Orbital
Hz	Hertz (s^{-1})
I	Nuclear Spin Quantum Number
IL	Intraligand
*i*Pr	Isopropyl – $CH(CH_3)_2$
*i*Pr$_2$-bimy	1,3-diisopropylbenzimidazolin-2-ylidene
IPr	1,3-bis(2,6-diisopropylphenyl)imidazole-2-ylidene
IPr*	1,3-bis(2,6-(diphenylmethyl)-4-methylphenyl)imidazol-2-ylidene
ISC	Intersystem Crossing – $T_1 \rightarrow S_1$
J	NMR Coupling constant
K	Degrees Kelvin
k	Decay rate constant
kJ	Kilojoule
k_r	Radiative decay rate constant
k_{nr}	Non-radiative decay rate constant
L	Neutral, 2 electron donor ligand
LF	Ligand Field
LLCT	Ligand-to-Ligand Charge Transfer
LMCT	Ligand-to-Metal Charge Transfer
LMMCT	Ligand-to-Metal-Metal Charge Transfer
M	Transition or Post-Transition Metal
MLCT	Metal-to-Ligand Charge Transfer
MMLCT	Metal-Metal-to-Ligand Charge Transfer
Me	Methyl – CH_3
2-MeTHF	2-methyltetrahydrofuran
NHC	*N*-Heterocyclic Carbene
NIR	Near infrared
nm	nanometer
NMR	Nuclear Magnetic Resonance
*n*Pr	*n*-Propyl – C_3H_5
OAC	Acetate – $CH_3C(O)O$
OLED	Organic Light Emitting Diode
P^N	Bidentate ligand with P and N donors
Ph	Phenyl – C_6H_5
PL	Photoluminescence
PLE	Photoluminescence Excitation

PNP^{nPr}	$Ph_2PN(nPr)PPh_2$
PNP^{Tol}	$Ph_2PN(p\text{-}CH_3C_6H_4)PPh_2$
ppm	Parts-per-million
PXRD	Powder X-ray Diffraction
py	pyridyl
R	Organic group
R_3P	Tertiary phosphine
s	Second
S_0	Ground singlet state
S_n	Singlet electronic state
SCXRD	Single-Crystal X-ray Diffraction
SOC	Spin-Orbit Coupling
T_n	Triplet electronic state
TADF	Thermally Activated Delayed Fluorescence
*t*Bu	Tertiary-butyl – $C(CH_3)_3$
TDDFT	Time-Dependent Density Functional Theory
THF	Tetrahydrofuran
THT	Tetrahydrofthiophene
UV-Vis	Ultraviolet-Visible
$\%V_{bur}$	Percent Buried Volume
X	Anionic, 2 electron donor ligand
XLCT	Anion-to-Ligand Charge Transfer

Chapter 1

1 Introduction

(Adapted from: A. M. Polgar, J. F. Corrigan in *Selenium and Tellurium Reagents - In Chemistry and Materials Science*; R. Laitinen Ed., De Gruyter, 2018)

1.1 Group 11 Chalcogen Compounds

Chalcogen-containing ligands are employed in many areas of inorganic and materials chemistry. Considering only their complexes with the group 11 metals Cu, Ag, and Au, these still comprise some of the most structurally diverse assemblies in modern synthetic chemistry – ranging in size from small clusters of metal atoms up to nanoscale "cut-outs" of bulk metal chalcogenides and infinite three-dimensional network solids. An impressive set of physical properties may be accessed in these systems as a function of their composition and structure. Metal chalcogen compounds therefore occupy a special position in materials science.

1.1.1 Group 11 Chalcogenolate Compounds

The combination of group 11 salts with organic chalcogenolate ligands RE^- (E = S, Se, Te; R = organic group) gives rise to metal chalcogenolate oligomers $[M(ER)]_n$.[1-3] The value of *n* and the molecular structure is predominantly a function of the steric and electronic nature of R. Small groups favour the formation of one- and two-dimensional (1D and 2D) coordination polymers. These tend to be highly insoluble and crystallographic structural data is relatively sparse (see Figure 1.1 for examples). The 1D coordination polymer $[Cu(SMe)]_n$ was prepared by thermal decomposition of $[Cu_4(SMe)_6]^{2-}$ and its structure was solved by powder X-ray diffraction (PXRD).[4] It consists of stacked Cu_3S_3 hexagons fused in one dimension. All Cu(I) atoms have trigonal planar geometry and all SMe are pyramidal and μ_3-bridging. $[Cu(SePh)]_n$ was prepared by refluxing Cu_2O and PhSeH in methanol and its 1D chain structure was determined by PXRD.[5] All Cu(I) atoms are trigonal planar coordinated with μ_3-SePh bridging ligands. The addition of $AgNO_3$ to an acetonitrile solution of [(2,4,6-(*i*Pr)$_3$-C_6H_2-SH] and NEt_3 produces the 1D polymer [Ag(S-C_6H_2-2,4,6-(*i*Pr)$_3$)]$_n$ which has a structure like two linear $[Ag(\mu\text{-SR})]_n$ chains aggregated primarily through argentophilic interactions.[6] 2D coordination polymers such as $[Cu(p\text{SPhOH})]_n$ and

$[Ag(SePh)]_n$ have been reported,[7,8] with structural determination by single crystal X-ray diffraction analysis for the latter. $[Ag(SePh)]_n$ was prepared from $AgCl{\cdot}PPh_3$ in THF with the addition of PhSeLi. It contains all μ_4-bridging SePh ligands above and below a layer of fused Ag_6 hexagons.

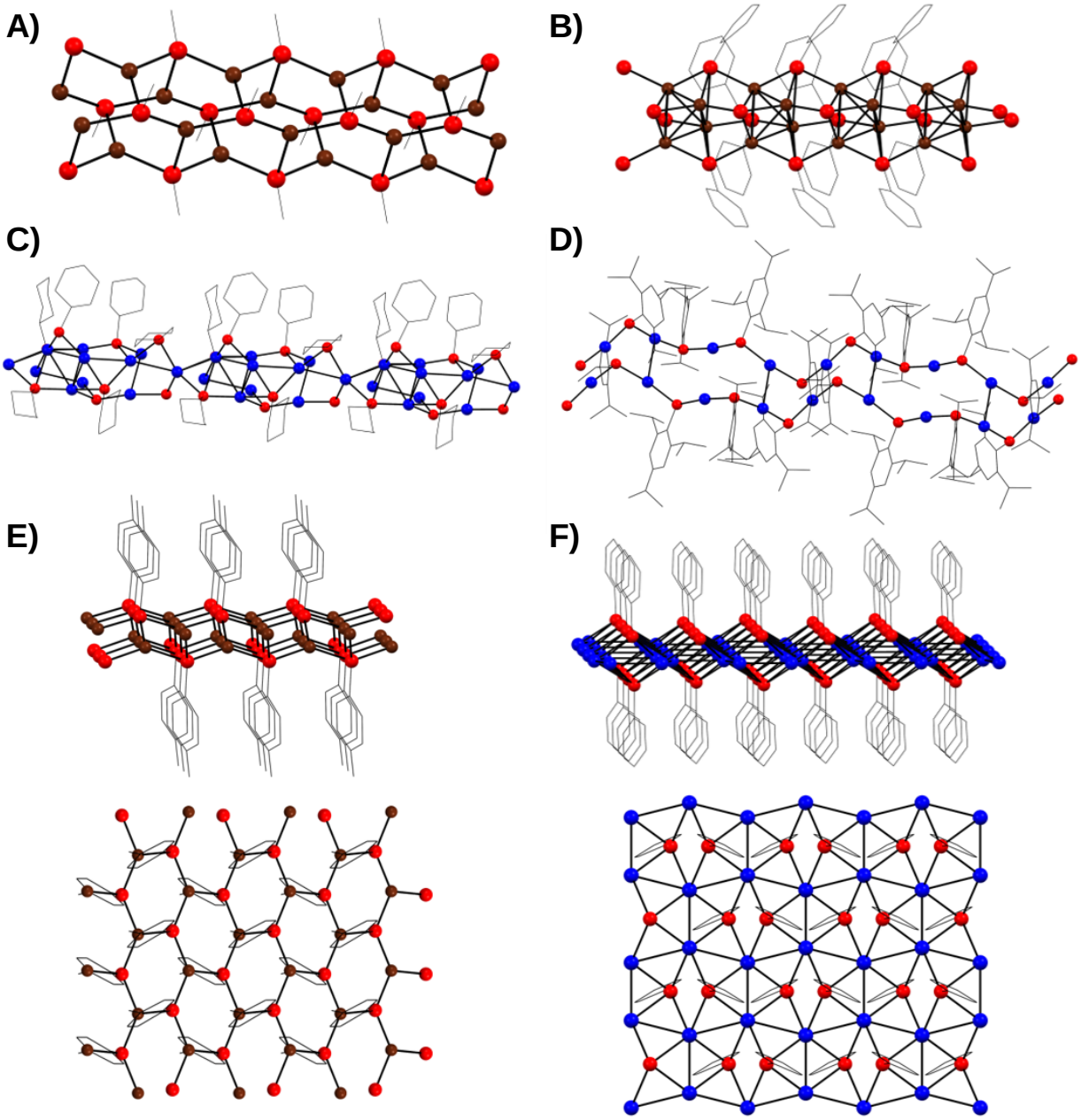

Figure 1.1 Molecular structures of 1D and 2D group 11 chalcogenolate coordination polymers in the crystal. A) $[Cu(SMe)]_n$, B) $[Cu(SePh)]_n$, C) $[Ag(SCy)]_n$, D) $[Ag(S\text{-}C_6H_2\text{-}2,4,6\text{-}(i\text{Pr})_3)]_n$, side and top view of E) $[Cu(p\text{SPhOH})]_n$ and F) $[Ag(SePh)]_n$. Cu = brown sphere, Ag = blue sphere, E = red sphere, R = wireframe.

When larger R groups are present, association into polymers is suppressed and smaller, cyclic oligomers form, many of which have been structurally characterized by single-crystal X-ray diffraction (SCXRD) methods. Because of the pyramidal coordination of chalcogenolate ligands, the R group is directed towards the surface of the oligomer. Smaller cyclic or polycyclic structures maximize the surface area available to orient the R groups about the surface. With the bulky adamantly (Ad) group, mononuclear complexes $[M(SAd)_2]^-$ (M = Cu, Ag, Au) have been prepared by the addition NaSAd and $[HNEt_3]Cl$ to a methanolic solution of the metal salt.[9] A common oligomeric motif is the cyclic tetramer $[M(ER)]_4$ (Figure 1.2). Arnold and co-workers prepared $[Au(EC(SiMe_3)_3)]_4$ and $[Ag(EC(SiMe_3)_3)]_4$ with the sterically hindered $-C(SiMe_3)_3$ group by the reaction of $Li[EC(SiMe_3)_3]$ with AuCl(THT) (THT = tetrahydrothiophene) or $AgNO_3$ in organic solvents.[10,11] Slightly smaller R groups, for example monosubstituted phenylthiols give rise to polycyclic systems like $[Cu(o\text{-}S(C_6H_4)SiMe_3)]_{12}$ and $\{Br@[Ag(p\text{-}S(C_6H_4)tBu)]_{36}\}^-$. $[Cu(o\text{-}SPhSiMe_3)]_{12}$ is prepared by the combination of $[Cu(NCMe)_4]PF_6$ and $o\text{-}Me_3SiPhSH$ in methanol.[12] The core structure consists of two parallel Cu_3S_3 rings connected through six linear CuS_2 sites. The preparation of $\{Br@[Ag(p\text{-}S(C_6H_4)tBu)]_{36}\}^-$ takes advantage of the ability of bromide ions to sever the silver-thiolate bonds in the coordination polymer $\{[Ag_{10}(p\text{-}S(C_6H_4)tBu)_{12}]^{2-}\}_n$.[13] Addition of an acetonitrile solution of $[(C_4H_9)_4N]Br$ to this polymer causes the aggregation of the symmetrical silver-thiolate cluster shown in Figure 1.2.

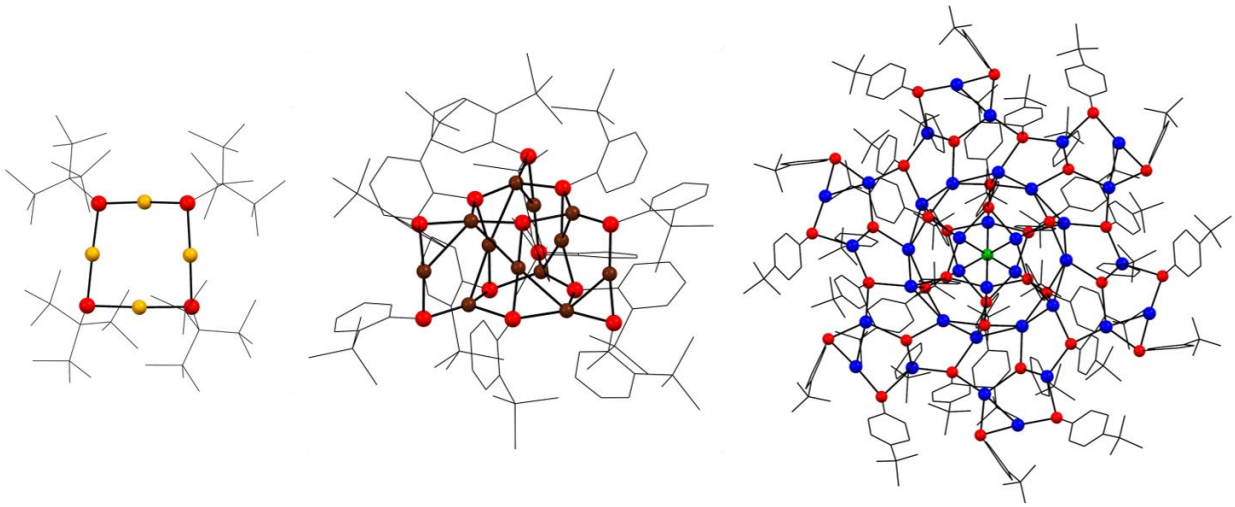

Figure 1.2 Molecular structures of group 11 chalcogenolate oligomers in the crystal. From left to right: $[Au(EC(SiMe_3)_3)]_4$, $[Cu(o\text{-}S(C_6H_4)SiMe_3)]_{12}$, and $\{Br@[Ag(p\text{-}S(C_6H_4)tBu)]_{36}\}^-$. Cu = brown sphere, Ag = blue sphere, E = red sphere, Br = green sphere, R = wireframe.

When reactions between metal salts and chalcogenolates are carried out in the presence of ancillary ligands, ligand-stabilized metal chalcogenolate clusters $[(L)_n(MER)_m]$ result. The size and structure of the resultant cluster is dependent on the reaction stoichiometry, the chalcogenolate ligand, the ancillary ligand, and the metal center. Another method uses ancillary ligands to coordinate to pre-formed metal chalcogenolate polymer, in which case the product spectrum is mostly sensitive to the nature and amount of the solubilizing ligand. Larger ligands or ligands used in excess favour condensation of smaller clusters. Krautscheid provided a systematic demonstration of these effects for the copper(I) chalcogenolate system in the presence of trialkyl phosphines of various sizes.[14] The reaction of *n* equivalents of CuOAc and Me_3SiEPh (E = S, Se, Te) in the presence of *m* equivalents of R_3P leads to elimination of $AcOSiMe_3$ and concomitant formation of phosphine-stabilized copper(I)-chalcogenolate complexes $[(R_3P)_m(CuEPh)_n]$ of various structures and nuclearity (number of metal atoms; Figure 1.3).

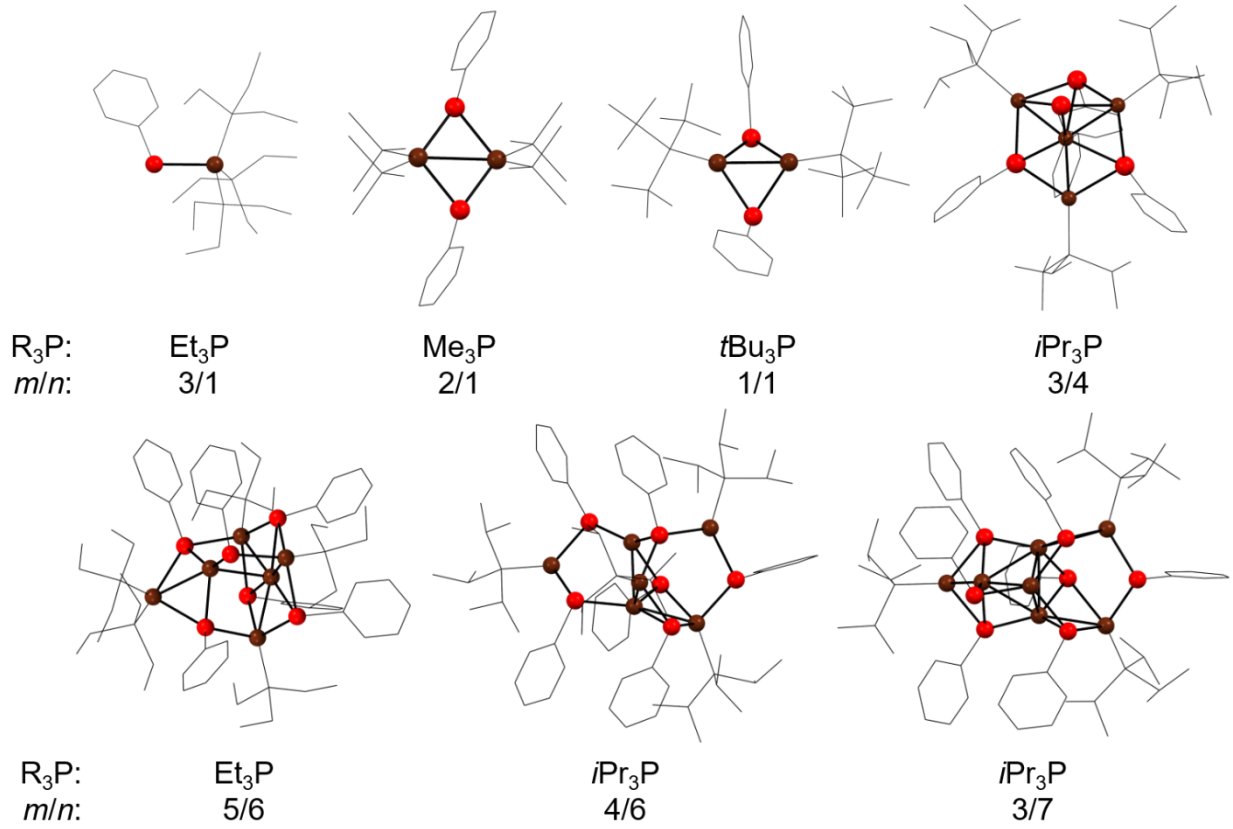

Figure 1.3 Molecular structures of trialkylphosphine-stabilized group 11 chalcogenolate clusters in the crystal. The molecular formula of each structure is $[(R_3P)_m(CuEPh)_n]$, with the phosphine and values of *m* and *n* specified below each structure. Cu = brown sphere, E = red sphere, R, PR_3 = wireframe.

1.1.2 Group 11 Chalcogenide Clusters

Group 11 chalcogenolates aggregate into 1D and 2D polymers and oligomers because of the structure directing influence of the organic group. Growth in three dimensions is prohibited by the pyramidal coordination of the chalcogenolate and the apical position of the organic group. Chalcogenides (E^{2-}) do not have this restriction and form high-connectivity, three-dimensional (3D) binary solids with the d^{10} group 11 metals, M_2E, in which E adopts various metal-bridging modes. As with the chalcogenolates, aggregation into extended solids is suppressed by ancillary ligands, leading to ligand-stabilized metal chalcogenide clusters $[(L)_n(M_2E)_m]$.[15-19] The structural trends for Cu(I), Ag(I), and Au(I) differ markedly because of their preference for different coordination modes and ability to aggregate through metallophilic interactions.

Au(I) chalcogenides have a greater propensity than Ag(I) or Cu(I) to form low-nuclearity clusters.[20] Considering clusters with only a single chalcogenide ligand, Au(I) forms clusters of nuclearity 2 – 6 (*i.e.* $[(\mu\text{-E})(AuPR_3)_2]$ to $[(\mu_6\text{-E})(AuPR_3)_6]^{4+}$), with structural characterization for the dinuclear to tetranuclear clusters (Figure 1.4).[21-24] Ag(I) and Cu(I) only form the tetranuclear cluster $[(\mu_4\text{-E})M_4(P\text{^}P)_4]^{4+}$ (P^P = bidentate phosphine; see Figure 1.8) with a single chalcogenide and phosphine ancillary ligands.[25-29] $[(\mu\text{-E})(AuPR_3)_2]$ is synthesized in alcoholic solutions by the combination of $AuCl(PR_3)$ with E^{2-} sources like Li_2S or selenourea. Starting from $[(\mu\text{-E})(AuPR_3)_2]$, cluster growth is attained by sequential addition of one to four equivalents of $[R_3PAu]OTf$. The stability of low-connectivity, electron deficient clusters like $[(\mu_6\text{-E})(AuPR_3)_6]^{4+}$ is enhanced by the strong metallophilic interactions for Au(I) (See 1.2.3).

Whereas the largest gold-chalcogenide clusters have nuclearities below 50, Cu(I) and Ag(I) clusters commonly have more than 100, for example $[Cu_{146}Se_{73}(PPh_3)_{30}]$ and $[Ag_{188}S_{94}(PnPr_3)_{20}]$ (Figure 1.4).[30,31] These are prepared by the addition of $E(SiMe_3)_2$, an organic-soluble E^{2-} source, to a mixture of CuOAc or AgOAc and a tertiary phosphine. All high nuclearity Au(I) chalcogenide clusters require bidentate or tridentate phosphines, whereas high nuclearity Ag(I) and Cu(I) clusters usually incorporate monodentate phosphines. This points to different driving forces for aggregation of high-nuclearity clusters. In the case of low-connectivity Au(I) chalcogenide clusters, aggregation occurs by bridging $[Au_3S]$ units through the ancillary ligand framework.[32] Cu(I) and Ag(I) clusters have higher connectivity and aggregate instead through bridging chalcogenide ligands.

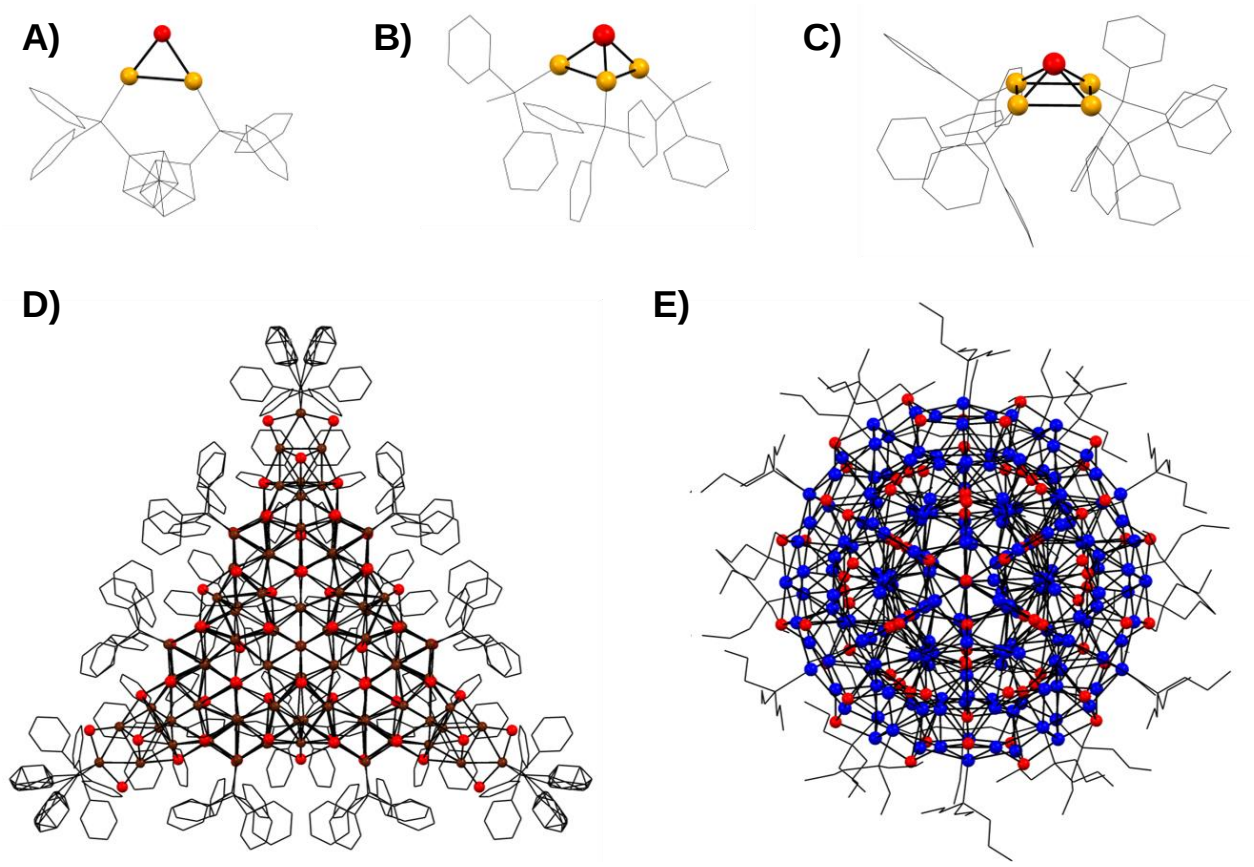

Figure 1.4 Molecular structures of phosphine-stabilized group 11 chalcogenide clusters in the crystal. A) [(μ-E)Au_2(μ-dppf)], B) [(μ_3-S)$(AuPPh_2Me)_3]^+$, C) [(μ_4-S)$(AuPPh_3)_4]^{2+}$, D) $[Cu_{146}Se_{73}(PPh_3)_{30}]$ and E) $[Ag_{188}S_{94}(PnPr_3)_{20}]$. Cu = brown sphere, Ag = blue sphere, Au = orange sphere, E = red sphere, PR_3 = wireframe.

Ternary, or heterometallic, chalcogenide clusters (M-M′-E) have received increasing interest over the past few years because of their distinct structural chemistry and unique properties. One method of preparing these systems, pioneered by Fenske, involves mixing two metal halide or acetate salts in the presence of $E(SiMe_3)_2$.[33,34] Eichhöfer has used this method to prepare ternary Cu(I)-Sn(IV)-E clusters $[Cu_6E_6(SnPh)_2(PPh_2Et)_6]$ from mixture of CuOAc, $PhSnCl_3$, PPh_2Et and $E(SiMe_3)_2$ in organic solvents.[35] These clusters have a narrow optical bandgap, leading to near-infrared photoluminescence which is bathochromically shifted as a function of the chalcogenide (λ_{em} = 800, 920, and 1280 nm for E = S, Se, and Te, respectively). Another successful method for producing ternary chalcogenide clusters uses multifunctional ancillary ligands. Wang *et al.* and later Laguna and co-workers prepared ternary group 11 chalcogenide clusters [(μ_3-E)$(Au(P\^N))_3M]^{2+}$ (P^N = pyridylphosphine, M = Ag, Cu) from [(μ_3-E)$(Au(P\^N))_3]^+$ and $AgBF_4$

or $[Cu(MeCN)_4]PF_6$ by exploiting the coordinating ability of the unbound pyridyl groups.[36-38] These clusters were brightly photoluminescent with emission maxima that could be tuned based on the identity of the chalcogen and the heterometal M.

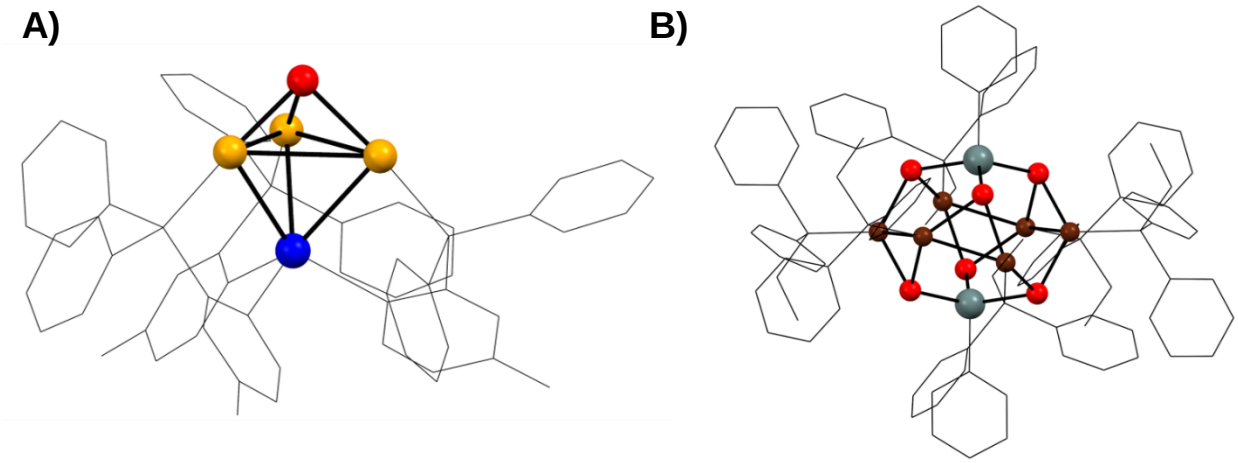

Figure 1.5 Molecular structures of phosphine-stabilized ternary group 11 chalcogenide clusters in the crystal. A) $[(\mu_3\text{-S})(Au(PPh_2py))_3Ag]^{2+}$ and B) $[Cu_6S_6(SnPh)_2(PPh_2Et)_6]$ Cu = brown sphere, Ag = blue sphere, Au = orange sphere, Sn = grey sphere, E = red sphere, PR_3 = wireframe.

1.1.3 Group 11 Chalcogenolate-Chalcogenide Clusters

Combining the surface-passivating effects of chalcogenolates with the ability of chalcogenides to direct growth in three dimensions gives rise to massive group 11 chalcogenolate-chalcogenide clusters, such as $[Ag_{490}S_{188}(StC_5H_{11})_{14}]$.[39] Not including the ligands, this cluster has a diameter of more than 3 nm. The impressive size of this clusters arises from a silver sulfide core, passivated by a silver thiolate shell. Additional surface stabilization by phosphine ligands has been realized, for example in the clusters $[Ag_{320}S_{130}(StBu)_{60}(dppp)_{12}]$ (dppp = 1,4-bis-(diphenylphosphino)propane) and $[Cu_{136}S_{56}(SCH_2C_4H_3O)_{24}(dpppt)_{10}]$ (dpppt = 1,5-bis(diphenyl-phosphino)pentane). $[Ag_{320}S_{130}(StBu)_{60}(dppp)_{12}]$ is prepared from the coordination polymer $[Ag(StBu)]_n$ upon solubilizing with a bidentate phosphine, dppp, with the addition of $S(SiMe_3)_2$ in toluene/chloroform to precipitate cluster growth.[39] Likewise, $[Cu_{136}S_{56}(SCH_2C_4H_3O)_{24}(dpppt)_{10}]$ is prepared from $[Cu(SCH_2C_4H_3O)]_n$, dpppt, and $S(SiMe_3)_2$ in toluene.[40] Analogous chemistry for Au(I) is non-existent, probably due to the lower coordination number of Au(I) blocking core growth. While the structural chemistry of these clusters is certainly impressive, a commonly

encountered problem is the insolubility or instability of these clusters in solution, which hampers their characterization and range of application. Fenske has shown that the use of thiolates with solubilizing 4-*t*Bu(C_6H_4) groups allows for the synthesis of the first organic soluble nanoscopic silver-sulfide-thiolate $[Ag_{115}S_{34}(SCH_2C_6H_4tBu)_{47}(dpph)_6]$ (dpph = 1,6-(diphenylphosphino)-hexane).[41]

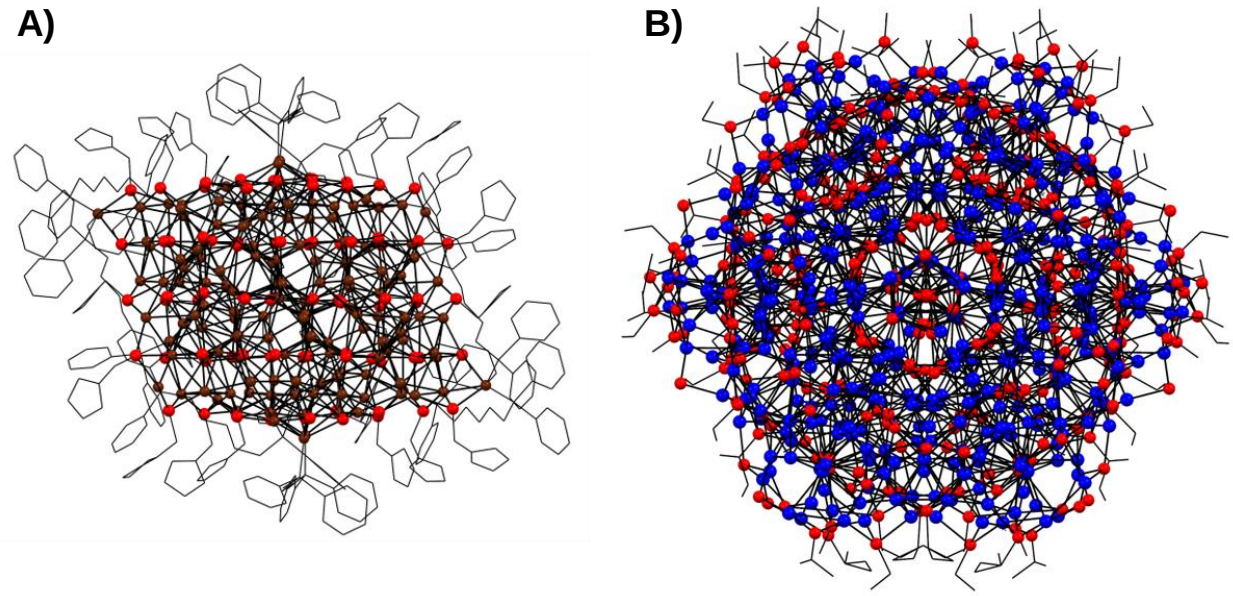

Figure 1.6 Molecular structures of group 11 chalcogenolate-chalcogenide clusters in the crystal with (A) and without (B) ancillary phosphine ligands. A) $[Cu_{136}S_{56}(SCH_2C_4H_3O)_{24}(dpppt)_{10}]$, B) $[Ag_{490}S_{188}(StC_5H_{11})_{14}]$. Cu = brown sphere, Ag = blue sphere, E = red sphere, R, PR_3 = wireframe.

1.1.4 Group 11 Silylchalcogenolate Reagents

Group 11 acetates and halides react with silylated chalcogen sources such as Me_3SiER and $E(SiMe_3)_2$ in organic solvents to yield polynuclear metal chalcogen clusters. Formation of a strong Si-X (X = halide, OAc) bond via the elimination of a silane drives the generation of new bonds between the metal and bridging chalcogen ligands. When ancillary ligands are applied in excess or are sterically bulky, terminal coordination of -$ESiMe_3$ ligands can be enforced to yield group 11 trimethylsilylchalcogenolate complexes $[L_nMESiMe_3]$.[42] The utility of these reagents is in their ability to controllably react with a second metal salt after initial complex formation to form ternary M-M′-E cluster systems (Scheme 1.1). The reactivity of these complexes with metal salts draws the analogy to organic chalcogenolates RE^- where the R group contains a metal center, or

"metallachalcogenolates". Examples of ternary chalcogenide systems prepared from group 11 trimethylsilylchalcogenolates are given in Scheme 1.1.[43-48] Krautscheid has shown that when the electron rich metal complex Me_3In is combined with the copper(I) trimethylsilylchalcogenolate reagent $[(i Pr_3P)_2CuESiMe_3]$, silane elimination is suppressed and the Lewis acid-base adduct $[(i Pr_3P)_2Cu(\mu\text{-}ESiMe_3)(InMe_3)]$ (E = S, Se) forms instead.[47]

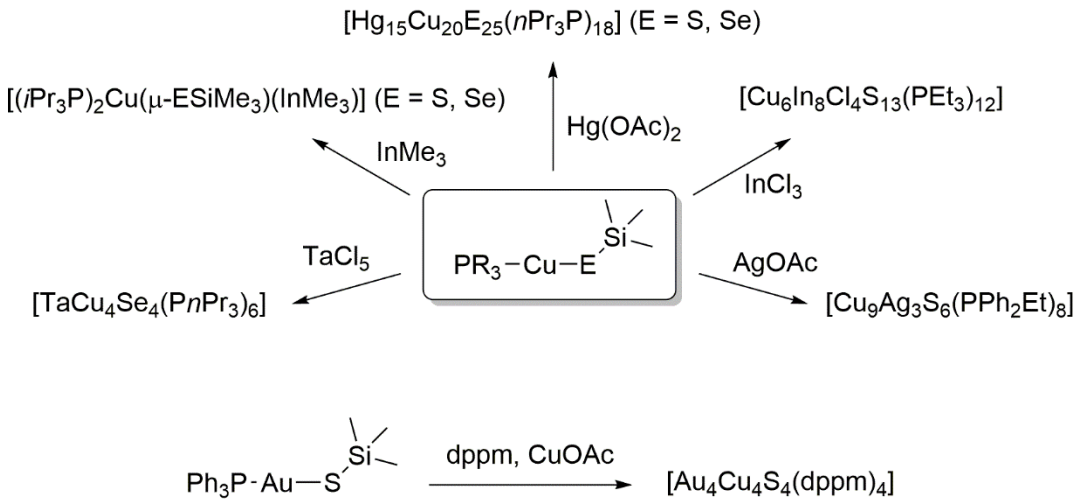

Scheme 1.1 Ternary metal chalcogenide clusters synthesized from group 11 silylchalcogenolate compounds stabilized by tertiary phosphines.

Phosphine-stabilized group 11 trimethylsilylchalcogenolates, despite their beneficial reactivity patterns, are limited in their application by their thermal instability in solution and/or the solid state.[43,44,46,49] Computational studies by Jacobsen have suggested that the origin of this instability comes from dissociation of the phosphine ligands in solution.[50] In 2015, Corrigan and Hillhouse showed that decomposition by this mechanism could be avoided by using *N*-heterocyclic carbene (NHC) ancillary ligands.[51,52] For example, the NHC-ligated silver(I) trimethylsilyl-selenolate $[(IPr)AgSeSiMe_3]$ (IPr = 1,3-bis(2,6-diisopropylphenyl)imidazole-2-ylidene) is thermally stable up to the melting point 170 °C,[53] whereas $[(EtPh_2P)AgSeSiMe_3]$ decomposes at its melting point of -35°C.[46] The drastic improvement in thermal stability is surely linked to the improved σ-donor properties of NHCs relative to phosphines.

The reactions of $[(NHC)CuESiMe_3]$ compounds has been investigated by the Corrigan and Hillhouse groups.[51-54] Hillhouse showed that bulky NHCs could be used to prepare low nuclearity copper sulfido clusters $[\{(IPr)Cu\}_3(\mu_3\text{-}S)]$ and $[\{(IPr^*)Cu\}_2(\mu\text{-}S)]$ (IPr* = 1,3-bis(2,6-

(diphenylmethyl)-4-methylphenyl)imidazol-2-ylidene), the latter of which has small-molecule activation ability similar to the N_2O reductase enzyme, as shown recently by Mankad.[55] Corrigan has utilized copper(I) and silver(I) silylchalcogenolates for the preparation of ternary Cu(I)-Hg(II)-S and Ag(I)-Hg(II)-S clusters. When a bulky carbene is used, small trinuclear clusters [{(IPr)MS}$_2$Hg] are obtained. The smaller carbene 1,3-diisopropylbenzimidazolin-2-ylidene (*i*Pr$_2$-bimy) results in a dimeric Cu-ESiMe$_3$ complex [(*i*Pr$_2$-bimy)Cu(μ-ESiMe$_3$)]$_2$ which, upon reaction which Hg(OAc)$_2$ at low temperature, forms the higher nuclearity cluster [(*i*Pr$_2$-bimy)$_6$Cu$_{10}$S$_8$Hg$_3$]. This cluster emits in the NIR region in the solid state, with a broad band centered around 800 nm.

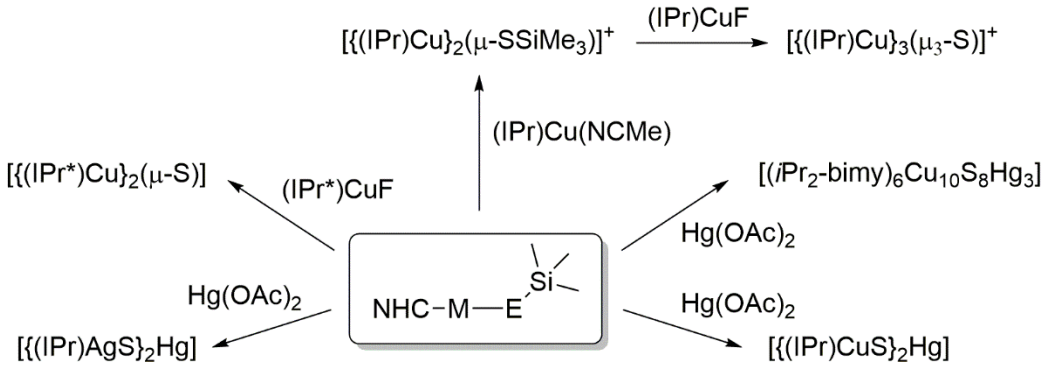

Scheme 1.2 Ternary metal chalcogenide clusters synthesized from group 11 silylchalcogenolate compounds stabilized by NHCs.

1.2 Luminescent Metal Complexes

1.2.1 Principles of Luminescence Spectroscopy

Luminescence is the release of energy in the form of light from an excited electronic state of a molecule or material. When the excited state is generated by absorption of a photon, photoluminescence is said to occur. Photoluminescence can be broadly divided into two categories: fluorescence and phosphorescence. Fluorescence involves the emission of a photon from an excited state where all electron spins are paired (a singlet state, S_n). Phosphorescence involves an excited state with two unpaired electron spins (triplet, T_n). Absorption from S_0 to excited singlet states S_n is followed by rapid relaxation down to the lowest vibrationally excited level (internal conversion). From here either prompt fluorescence ($S_1 \rightarrow S_0$), intersystem crossing to the triplet state (ISC; $S_1 \rightarrow T_1$) or other non-radiative deactivation processes can occur. These excited state dynamics are represented in a Jablonski diagram (Figure 1.6).[56]

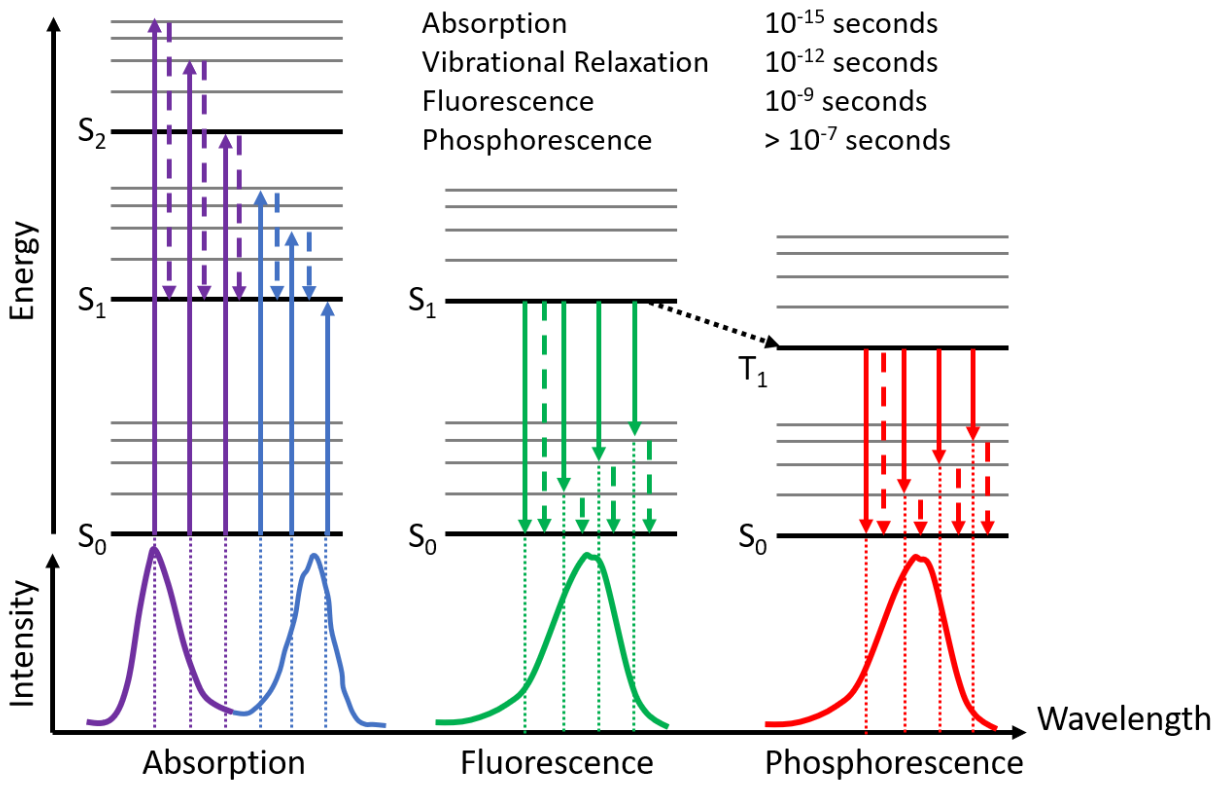

Figure 1.7 Top: Jablonski diagram for the electronic transitions involved in light absorption, fluorescence, and phosphorescence. Electronic excited states are indicated by solid black lines. Vibrationally excited states are grey lines. Solid arrows indicate the absorption or emission of a photon. Dashed lines indicate vibrational relaxation. A dotted black line indicates intersystem crossing from a singlet to triplet excited state. Bottom: steady-state spectra for the stated type of electronic transition from top figure. Adapted from reference 56.

Photoluminescence is principally characterized by three parameters: the wavelength of maximum emission intensity (λ_{em}), the efficiency of photoluminescence (photoluminescence quantum yield, Φ_{PL}), and the excited state decay time (τ). λ_{em} is determined by the energetic spacing between excited and ground states and, for metal complexes, usually falls in the ultraviolet-visible-near-infrared (UV-Vis-NIR; ca. 300 – 1200 nm) region of the electromagnetic spectrum. Φ_{PL} is the ratio of the number of photons absorbed by a molecule relative to the number emitted. It is related to the rate constants for radiative (k_r) and non-radiative (k_{nr}) excited state processes. As captured in Equation 1.1, faster radiative decay and slower non-radiative decay leads to improved quantum yield.[57]

$$\Phi_{PL} = \frac{k_r}{k_r + k_{nr}} \quad \textbf{(1.1)}$$

Excited state lifetime is related to k_r and k_{nr} by Equation 1.2

$$\tau = \frac{1}{k_r + k_{nr}} \quad \textbf{(1.2)}$$

From which it follows $k_r = \Phi_{PL}/\tau$, allowing k_r and k_{nr} to be calculated from experimental measurements of Φ_{PL} and τ. k_r is determined by the probability of an electronic transition. Certain transitions (e.g. those involving a spin-flip or retention of orbital parity) are said to be forbidden and are associated with lower values of k_r. Since phosphorescence involves a change in electron spin, it is formally forbidden and therefore occurs at a slower rate than fluorescence. Consequently, typical values of τ for fluorescence are on the order of nanoseconds, whereas phosphorescence decay times are on the order of several microseconds or longer. k_{nr} is sensitive to internal factors like flexible molecular structures leading to vibrational relaxation and external factors such as collisional quenching, electron, or energy transfer with other molecular species.

1.2.2 d^6 and d^8 Platinum Group Complexes

Complexes of d^8 and d^6 platinum group (Ru, Rh, Pd, Os, Ir, and Pd) metals have long been at the forefront of research into luminescent d-block complexes.[58] The octahedral d^6 compound $[Ru(bpy)_3]^{2+}$ (bpy = 2,2′-bipyridine) is perhaps the prototypical example of a luminescent metal complex.[59] In room-temperature solution, it emits bright red phosphorescence (λ_{em} = 606 nm, Φ_{PL} = 0.075, τ = 0.87 μs).[60] The understanding of the relationship between the structure of a complex and its emissive properties has led to thousands of metal complexes, with λ_{em} tunable across much of the UV-Vis-NIR spectrum, quantum yields approaching or even converging to 1, and τ generally ranging from nanoseconds to microseconds. Examples of luminescent complexes of the platinum group metals, Re(I), and Au(III) are displayed in Chart 1.1.[61-66] Luminescent metal complexes have been applied in the development of organic electronics,[67,68] and sensing materials,[69] with C^N cyclometalated Pt(II) and Ir(III) complexes present in commercial technologies.[70,71]

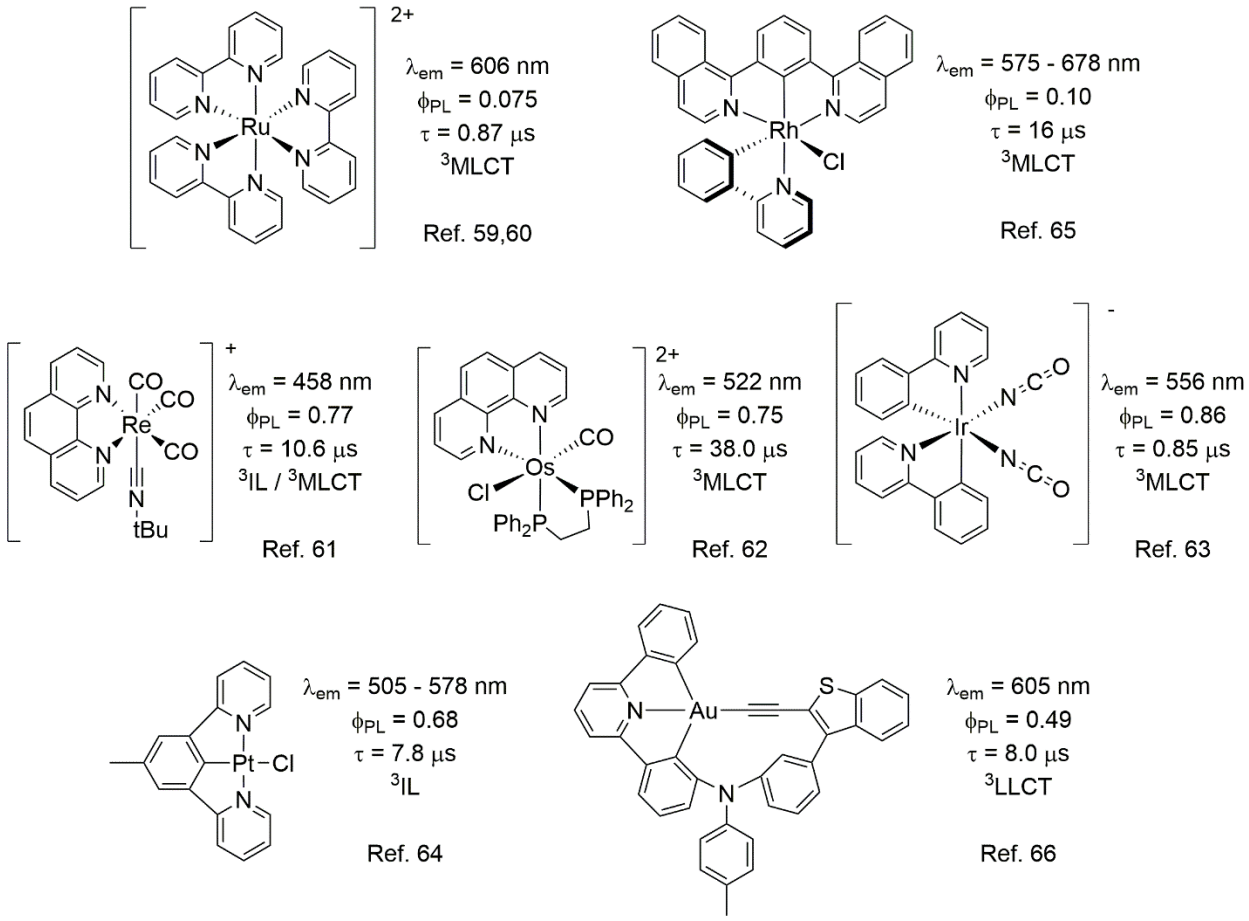

Chart 1.1. Examples of intensely luminescent organometallic complexes and their spectroscopic parameters. All quantities refer to luminescence in solution at 298K.

The excited states for classical transition metal complexes are broadly categorized into three types. (i) Ligand-field (LF) or d-d states involve the promotion of an electron from an occupied d-orbital into an unoccupied d-orbital. (ii) Intraligand (IL) transitions are localized in the ligand sphere and often involve promotion of electron from a π orbital into an antibonding π^* in an aromatic system (also termed π-π^*). (iii) Charge transfer (CT) states involve movement of charge from one part of the molecule to another. CT states typically involve the transfer an electron from a d-orbital to a π^* orbital of the ligand (MLCT; d-π^*), or transfer of an electron in a π orbital into an unfilled d orbital (LMCT; π-d). Polynuclear complexes may involve d orbitals on several metal atoms, and the d-π^* state that can arise is termed metal-metal-to-ligand charge transfer (MMLCT). In heteroleptic complexes, CT between different ligands becomes possible. This is termed ligand-ligand charge transfer (LLCT or XLCT if one ligand is anionic).

LF states are Laporte forbidden, so they produce weak absorptions ($\varepsilon < 10^3$ M^{-1} cm^{-1}), are usually weakly emissive, and moreover may lead to photodecomposition by ligand loss.[72] These undesirable characteristics are avoided by designing ligands which raise the energy of LF states. Strong-field, cyclometalating C^N ligands have become popular because they raise the ligand-field splitting parameter and hence the d-d energy gap. ^{1}IL transitions are fully allowed and can lead to efficient fluorescence in metal compounds. Because ^{1}IL states are typically at higher energies than LF or CT, internal conversion usually renders these states non-emissive.[73] Conversely, ^{3}IL emission occurs at lower energies and is induced by the heavy atom effect of the metal center. Spin-orbit coupling (SOC) is the process by which singlet and triplet states are mixed, allowing for changes in electronic angular momentum to couple to the flip of an electron spin. This is crucial for fast rates of intersystem crossing (ISC) from S_n to T_n. The efficiency of SOC increases with the atomic number so complexes of heavy atoms like Pt and Ir can have efficient ISC to low-lying, ^{3}IL states. CT states are commonly observed emissive states for d-block complexes, due to the difference in the oxidizing/reducing abilities of metal ions and ligands. $[Ru(bpy)_3]^{2+}$, for example, emits from a ^{3}MLCT state formally involving partial oxidation of the metal and partial reduction of the ligand. Clearly, more efficient use of MLCT states can be obtained for metal ions with low oxidation potentials and ligands that are readily reduced. This principle is useful for tuning emission energy by variation of the ligand. Structural modifications such as extended conjugation or the implementation of electron withdrawing groups make the ligand easier to reduce, resulting in lower-lying MLCT states.

1.2.3 d^{10} Group 11 Complexes

The photochemistry and photophysical properties of d^{10} complexes has generated interest over the past few decades to rival conventional d^6 and d^8 emitters.[74,75] Because d^{10} metals have a filled d-shell, d-d states are not present in their complexes. This is beneficial because these states could otherwise quench emission by thermal equilibration or energy transfer.[76] Phosphorescence usually arises from ^{3}MLCT states for Cu(I) since it has a low oxidation potential and either ^{3}MLCT, ^{3}LLCT, or ^{3}IL states for Ag(I) or Au(I) due to their high spin-orbit coupling constants (ζ_{Ag} = 1779 cm^{-1} and ζ_{Au} = 5104 cm^{-1}).[77] The ability of group 11 metals to form polynuclear complexes further diversifies their excited states by allowing for MMLCT or LF states modified

by metallophilic interactions (*vide infra*), often with low energy photoluminescence. Examples of luminescent group 11 complexes are provided in Chart 1.2.[78-81]

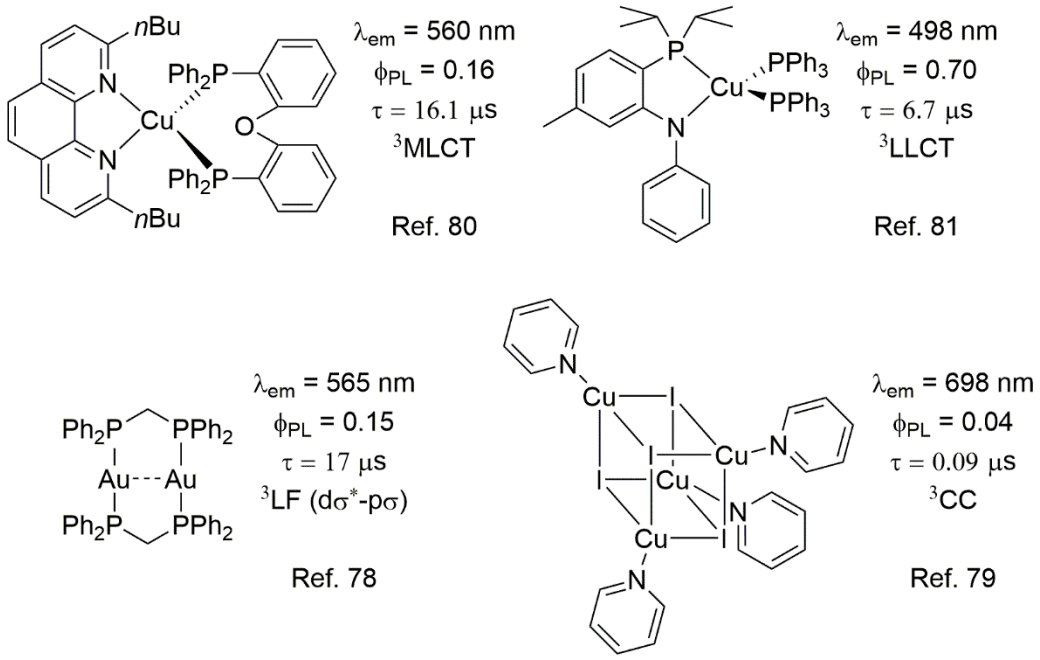

Chart 1.2 Examples of intensely luminescent complexes of d^{10} coinage metals and their spectroscopic parameters. All quantities refer to luminescence in solution at 298K.

Cluster complexes of d^{10} metals have been shown to emit from a diverse range of excited states, enhanced by metal-metal interactions.[78,79] Throughout the 1970's and 1980's a large body of evidence had amassed for the existence of attractive non-covalent interactions between d^{10} metal centers, termed "metallophilicity".[82] Evidence for their existence came in the form of inter- and intramolecular aggregation of M(I) centers into chains, sheets, and clusters, often without bridging ligands. In gold, this tendency was observed with such regularity that it was given the separate name "aurophilicity" by Schmidbaur.[83,84] Ford and others showed that for tetranuclear $[Cu_4I_4(L)_4]$ clusters, the presence of short Cu(I)-Cu(I) contacts (< 2.80 Å) predicted a low energy ^{3}CC (cluster-centred) emission.[79] Several studies also confirmed that low energy emission in polynuclear Au(I) complexes was correlated to short Au(I)-Au(I) contacts (< 3.32 Å).[78,85,86] A theoretical explanation for the connection between metallophilicity and low energy excited states was proposed by Hoffman in polynuclear d^{10}-d^{10} systems,[87,88] and for dinuclear Au(I) complexes by Fackler.[89] A hybridization between a high-lying occupied 5d orbital of σ* symmetry with respect to M-M bond

formation and unoccupied 6s and 6p orbitals of σ symmetry both increases the formal M-M bond order and decreases the σ*(d)→σ(s/p) state energy. More advanced treatments of aurophilicity by Pyykkö have pointed to the importance of relativistic effects in stabilizing the s and p orbitals while destabilizing and expanding the d orbitals.[90] The main attractive force is thought to be based on electron correlation, enhanced by relativistic effects in gold, with estimates for the interaction energy estimated between 20 and 40 kJ mol^{-1} (similar to that of a strong hydrogen bond).[82]

In the past decade or so, interest in luminescent d^{10} coinage metal complexes has intensified because of their ability to exhibit thermally activated delayed fluorescence (TADF).[91] Upon entering the triplet excited state, molecules that exhibit TADF can thermally populate S_1 by reverse intersystem crossing. The benefit of this mechanism is efficient fully-allowed $S_1 \rightarrow S_0$ emission from metal complexes. High quantum yields ($\Phi_{PL} > 0.9$) are common in the solid state, as shown in Chart 1.3.[92-95] The interest in TADF materials is due to their ability to harvest both singlet and triplet excitons in electroluminescent devices (e.g. organic light emitting diodes, OLEDs).[96,97] This provides a theoretical four-fold increase in device efficiency compared to fluorescent OLEDS which only harvest ¼ of the generated excitons (only singlet excitons). Furthermore, compared to phosphorescent OLEDs based on platinum group metals, which also harvest both singlet and triplet excitons, TADF complexes allow the use of more abundant and less toxic metals like Cu and Ag.

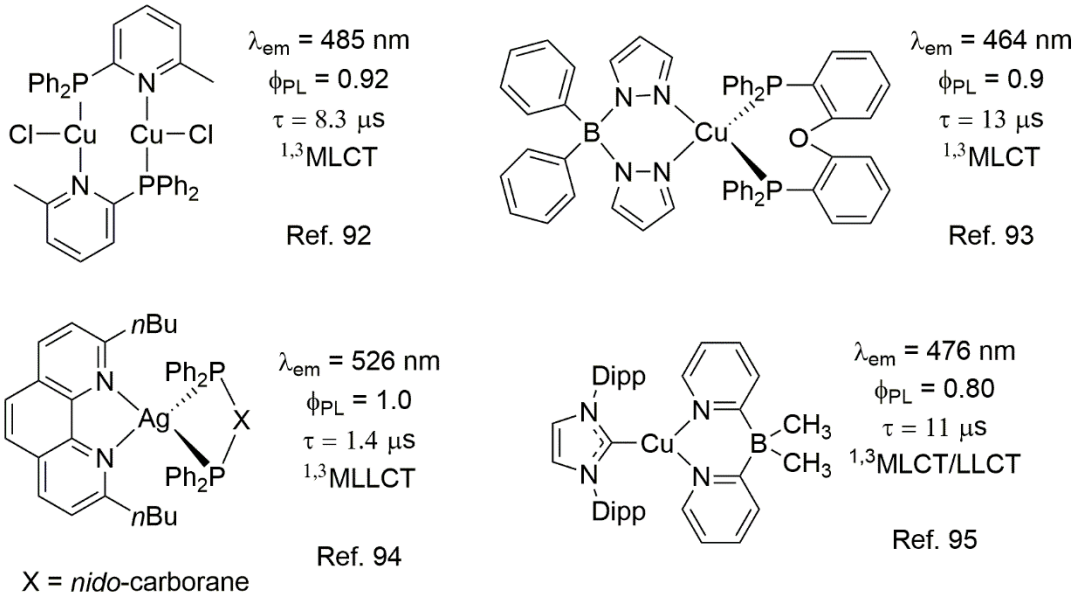

Chart 1.3 Examples of intensely luminescent complexes which operate by the TADF mechanism and their spectroscopic parameters. Parameters are given for complexes in the solid state at 298K.

1.2.4 d^{10} Group 11 Complexes with Chalcogen-Containing Ligands

There is a growing literature regarding photoluminescence from group 11 chalcogenolate and chalcogenide complexes and clusters.[20,98] Although early reports focused on luminescent copper(I) and silver(I) clusters like $[M_6(mtc)_6]$ (M = Cu, Ag, λ_{em} = 596 – 767 nm; mtc = di-*n*-propylmonothiocarbamate)[99] and $[(\mu_4\text{-E})M_4(dppm)_4]$ (M = Cu, Ag, E = S, Se, Te, λ_{em} = 516 – 628 nm),[25-27] gold(I) chalcogenides are the most developed with a strong understanding of structure-property relationships. Yam and co-workers reported emissions from a series of gold-sulfido clusters with bidentate phosphine ligands $[Au_6(\mu\text{-}PNP^{Tol})_3(\mu_3\text{-}S)_2]^{2+}$ (**$Au_6S_2^{2+}$**; PNP^{Tol} = $Ph_2PN(p\text{-}CH_3C_6H_4)PPh_2$),[100] $[Au_{10}(\mu\text{-}PNP^{nPr})_4(\mu_3\text{-}S)_4]^{2+}$ (**$Au_{10}S_4^{2+}$**; PNP^{nPr} = $Ph_2PN(^nPr)PPh_2$),[101] and $[Au_{12}(\mu\text{-dppm})_6(\mu_3\text{-}S)_4]^{4+}$ (**$Au_{12}S_4^{4+}$**; dppm = $Ph_2PCH_2PPh_2$).[102] At ambient temperatures in solution, **$Au_{10}S_4^{2+}$** and **$Au_{12}S_4^{4+}$** emit in the yellow-green region with λ_{em} of 510 and 546 nm and lifetimes of 100 and 250 ns, respectively. **$Au_6S_2^{2+}$** has a weak near-infrared (NIR) emission centered at 810 nm which is replaced by yellow emission (λ_{em} = 562 nm) upon cooling solutions to 77K. The clusters are also emissive in the solid state with emission maxima shifted towards the red compared to the solution state (λ_{em} = 603 nm **$Au_6S_2^{2+}$**, 635 nm **$Au_{10}S_4^{2+}$**, 648 nm **$Au_{12}S_4^{4+}$**). This shift in emission wavelength is also accompanied by increased intensity, and a tenfold or greater increase of excited state lifetime in the solid state. Phosphorescence from these clusters was assigned to ^{3}LMMCT; $S^{2-} \rightarrow Au\cdots Au$ with admixture from metal-perturbed ^{3}IL states. The emissions of other gold(I)-sulfido clusters occur at similar energies, for example in the octadecanuclear cluster $[Au_{18}(\mu\text{-dpepp})_6(\mu_3\text{-}S)_6]^{6+}$ (**$Au_{18}S_6^{6+}$**; dpepp = $\{Ph_2P(CH_2)_2\}_2PPh$; λ_{em} = 500 nm in CH_3CN at 298K).[103]

Gold(I) selenide clusters tend to have bathochromically shifted emissions compared to their sulfur counterparts. **$Au_{10}Se_4^{2+}$** is structurally analogous to **$Au_{10}S_4^{2+}$** and has λ_{em} = 554 nm in solution and 584 nm as a solid at 298K.[104] **$Au_6Se_2^{2+}$** has an unusual NIR emission at ca. 810 nm. Variation of the PNP ligand in **$Au_{10}S_4^{2+}$**, **$Au_{10}Se_4^{2+}$**, **$Au_6Se_2^{2+}$**, and **$Au_6Se_2^{2+}$** resulted in emission maxima shifting over a range of ca. 50 nm, depending on whether electron donating or withdrawing groups are on the ligands. Fenske and co-workers prepared the gold(I) selenide clusters $[Au_{10}(\mu\text{-dpppt})_4(\mu_3\text{-}Se)_4]^{2+}$ (**$Au_{10}Se_4^{2+}$**; dpppt = $Ph_2P(CH_2)_5PPh_2$) and $[Au_{18}(\mu\text{-dppe})_6(\mu_3\text{-}Se)_8]^{2+}$ (**$Au_{18}Se_8^{2+}$**; dppe = $Ph_2P(CH_2)_2PPh_2$).[105] **$Au_{18}Se_8^{2+}$** emits red light with λ_{em} = 628 nm in CH_2Cl_2 at 293K. The quantum yield of its emission is low in solution (<1%) but increases to ca. 80% as a powder at 77K. On the other hand, **$Au_{10}Se_4^{2+}$** is a weak NIR emitter at all temperatures

with emission maxima between 880 nm (solution, 293K) and 1020 nm (powder, 77K). There are currently no published reports of luminescence from gold(I) telluride complexes.

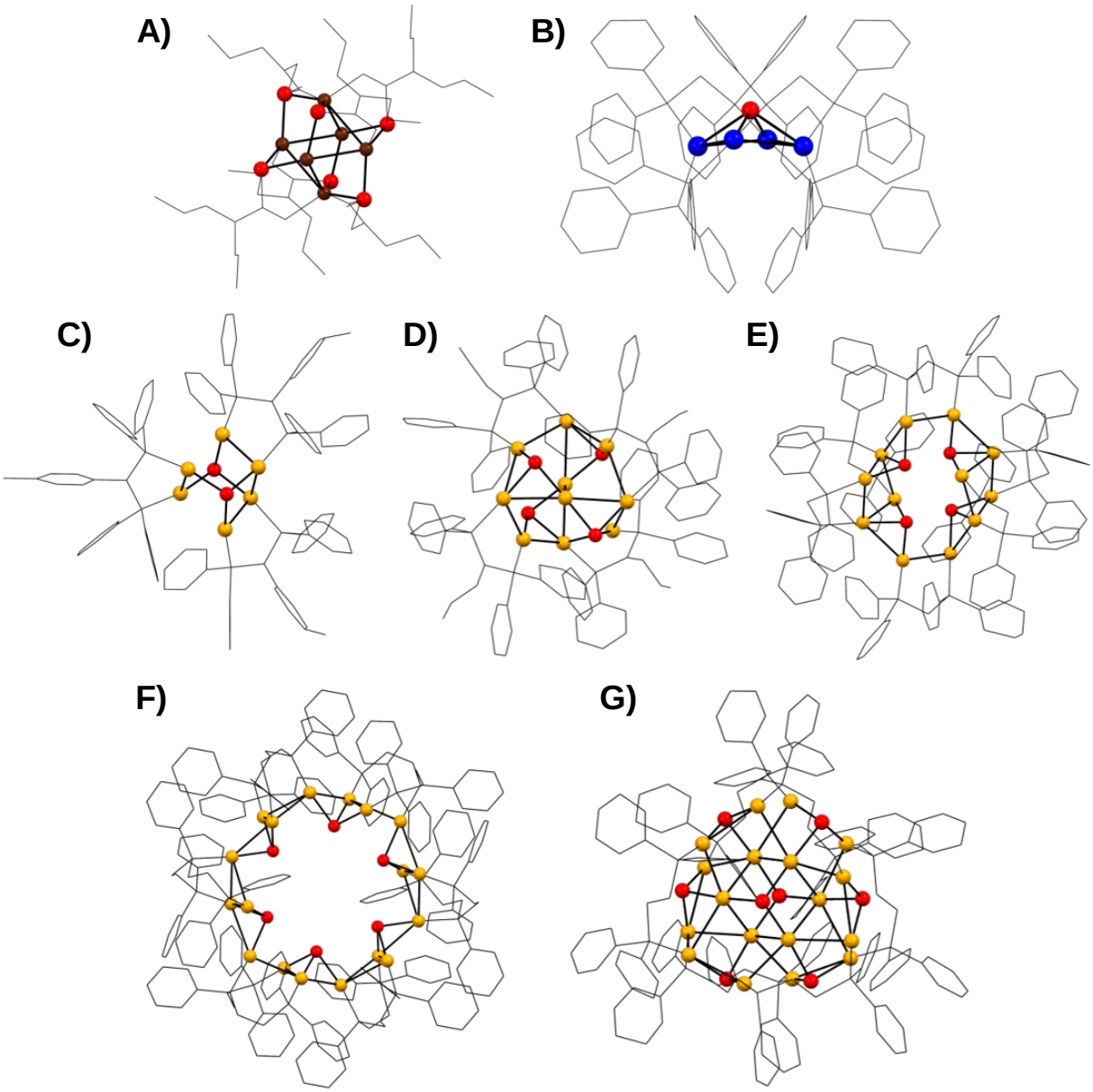

Figure 1.8 Molecular structures of luminescent group 11 chalcogenide clusters in the crystal. A) $[Cu(mtc)]_6$, B) $[(\mu_4\text{-}S)Ag_4(dppm)_4]^+$, C) $\mathbf{Au_6S_2}^{2+}$, D) $\mathbf{Au_{10}S_4}^{2+}$, E) $\mathbf{Au_{12}S_4}^{4+}$, F) $\mathbf{Au_{18}S_6}^{6+}$, G) $\mathbf{Au_{18}Se_8}^{2+}$. Cu = brown sphere, Ag = blue sphere, Au = orange sphere, E = red sphere, R, PR_3 = wireframe.

Ternary coinage metal chalcogenide clusters also can exhibit bright emissions in solution and the solid state. Wang and co-workers prepared ternary Au(I)-Ag(I)-E clusters [(μ_3-

S){Au(PPh$_2$py)}$_3$Ag]$^{2+}$ (**Au$_3$AgS**$^{2+}$; py = pyridyl; see Section 1.1.2, Figure 1.5), and [(μ_3-Se){Au(PPh$_2$py)}$_3$Ag]$^{2+}$ (**Au$_3$AgSe**$^{2+}$) by exploiting the Ag$^+$ complexation ability of the free pyridyl moieties in [(μ_3-E){Au(PPh$_2$py)}$_3$]$^+$ (**Au$_3$E^{py+}**).[36] Whereas **Au$_3$E^{py+}** is non-luminescent, **Au$_3$AgS**$^{2+}$ and **Au$_3$AgSe**$^{2+}$ are brightly green (554 nm) and red (670 nm) emissive, respectively, with microsecond decay times in the solid state at 298K. Similar to the binary systems described previously, the emission is attributed to ^{3}LMMCT ($E^{2-} \rightarrow Au_3Ag$) with metal-centered (MC) contributions. Complexing **Au$_3$E^{py+}** with Cu$^+$ instead of Ag$^+$ results in the clusters [(μ_3-S){Au(PPh$_2$py)}$_3$Cu]$^{2+}$ (**Au$_3$CuS**$^{2+}$) and [(μ_3-Se){Au(PPh$_2$py)}$_3$Cu]$^{2+}$ (**Au$_3$CuSe**$^{2+}$), which have similar emission energies compared to the Ag$^+$ congeners (λ_{em}^{max} = 590 nm **Au$_3$CuS**$^{2+}$, 650 nm **Au$_3$CuSe**$^{2+}$). The ternary octanuclear Au(I)-Cu(I)-S cluster [Au$_4$Cu$_4$(μ_3-S)$_4$(μ-dppm)$_2$] (**Au$_4$Cu$_4$S$_4$**) was prepared by Corrigan and co-workers.[48] It exhibited long-lived (68 μs) phosphorescence in the solid state at 653 nm.

1.3 Scope of the Thesis

This thesis is concerned with the reaction chemistry of NHC-stabilized group 11 trimethylsilylchalcogenolate reagents for the preparation of luminescent homo- and heterometallic group 11 chalcogenide clusters. Chapter 2 focuses on new gold(I) trimethylsilylchalcogenolate complexes and their application in the preparation of a series of NHC-stabilized homometallic Au(I) and heterometallic Au(I)-Ag(I) chalcogenide clusters with tunable luminescence properties. Chapter 3 is concerned with variation of the ancillary carbene ligand from an NHC to a cyclic (alkyl)(amino)carbene (CAAC). The enhanced ligation properties of CAACs enables the preparation of a series of phosphorescent homometallic Cu(I) chalcogenide and heterometallic Cu(I)-Ag(I) and Cu(I)-Au(I) chalcogenide clusters which are inaccessible from conventional NHCs. Chapter 4 concerns two Au(I)-Cu(I)-S clusters with distinct structural features and the effect of this structural variation on the luminescence properties. Chapter 5 summarizes the results and conclusions of the previous chapters and suggests future directions for the project.

1.4 References

[1] I. G. Dance. *Polyhedron* **1986**, *5*, 1037.
[2] J. Arnold. *The Chemistry of Metal Complexes with Selenolate and Tellurolate Ligands*. Progress in Inorganic Chemistry, Vol 43. **1995**, John Wiley & Sons, Inc.
[3] O. Veselska, A. Demessence. *Coord. Chem. Rev.* **2018**, *355*, 240.
[4] M. Baumgartner, H. Schmalle, C. Baerlocher. *J. Solid State Chem.* **1993**, *107*, 63.
[5] C.-M. Che, C.-H. Li, S. S.-Y. Chui, V. A. L. Roy, K.-H. Low. *Chem. Eur. J.* **2008**, *14*, 2965.
[6] K. Tang, J. Yang, Q. Yang, Y. Tang. *J. Chem. Soc. Dalton Trans.* **1989**, *0*, 2297.
[7] K.-H. Low, V. A. L. Roy, S. S.-Y. Chui, S. L.-F. Chan, C.-M. Che. *Chem. Commun.* **2010**, *46*, 7328.
[8] H. L. Cuthbert, A. I. Wallbank, N. J. Taylor, J. F. Corrigan. *Z. Anorg. Allg. Chem.* **2002**, *628*, 2483.
[9] K. Fujisawa, S. Imai, Y. Moro-oka. *Chem. Lett.* **1998**, *27*, 167.
[10] P. J. Bonasia, D. E. Gindelberger, J. Arnold. *Inorg. Chem.* **1993**, *32*, 5216.
[11] P. J. Bonasia, G. P. Mitchell, F. J. Hollander, J. Arnold. *Inorg. Chem.* **1994**, *33*, 1979.
[12] E. Block, M. Gernon, H. Kang, G. Ofori-Okai, J. Zubieta. *Inorg. Chem.* **1989**, *28*, 1263.
[13] X. Liu, H. Yang, N. Zheng, L. Zheng. *Eur. J. Inorg. Chem.* **2010**, 2084.
[14] O. Kluge, K. Grummt, R. Biedermann, H. Krautscheid. *Inorg. Chem.* **2011**, *50*, 4742.
[15] S. Dehnen, A. Eichhöfer, D. Fenske. *Eur. J. Inorg. Chem.* **2002**, 279.
[16] M. W. DeGroot, J. F. Corrigan. *High Nuclearity Clusters: Metal Chalcogenide Polynuclear Complexes.* Comprehensive Coordination Chemistry, II. ed. M. Fujita,A.Powelland C. Creutz, **2004**, vol. 7, pp. 57–113
[17] J. F. Corrigan, O. Fuhr, D. Fenske. *Adv. Mater.* **2009**, *21*, 1867.
[18] O. Fuhr, S. Dehnen, D. Fenske. *Chem. Soc. Rev.* **2013**, *42*, 1871.
[19] Y.-P. Xie, J.-L. Jin, G.-X. Duan, X. Lu, T. C. W. Mak, *Coord. Chem. Rev.* **2017**, *331*, 54.
[20] M. C. Gimeno, A. Laguna, *Chem. Soc. Rev.* **2008**, *37*, 1952.
[21] F. Canales, M. C. Gimeno, A. Laguna, P. G. Jones, *J. Am. Chem. Soc.* **1996**, *118*, 4839.
[22] F. Canales, M. C. Gimeno, A. Laguna, M. D. Villacampa. *Inorg. Chim. Acta* **1996**, *244*, 95.
[23] S. Canales, O. Crespo, M. C. Gimeno, P. G. Jones, A. Laguna. *Chem. Commun.* **1999**, *0*, 679.
[24] S. Canales, O. Crespo, M. C. Gimeno, P. G. Jones, A. Laguna, F. Mendizabal. *Organometallics* **2000**, *19*, 4985.
[25] V. W.-W. Yam, W.-K. Lee, T.-F. Lai. *J. Chem. Soc. Chem. Commun.* **1993**, *4*, 1571.
[26] V. W.-W. Yam, K. K.-W. Lo, K.-K. Cheung. *Inorg. Chem.* **1996**, *35*, 3459.
[27] V. W.-W. Yam, K. K.-W. Lo, C.-R. Wang, K.-K. Cheung. *Inorg. Chem.* **1996**, *35*, 5116.
[28] B. J. Johnson, S. V. Lindeman, N. P. Mankad. *Inorg. Chem.* **2014**, *53*, 10611.
[29] B. J. Johnson, W. E. Antholine, S. V. Lindeman, M. J. Graham, N. P. Mankad. *J. Am. Chem. Soc.* **2016**, *138*, 13107.
[30] H. Krautscheid, D. Fenske, G. Baum, M. Semmelmann. *Angew. Chem. Int. Ed.* **1993**, *32*, 1303.
[31] X.-J. Wang, T. Langetepe, C. Persau, B.-S. Kang, G. M. Sheldrick, D. Fenske. *Angew. Chem. Int. Ed.* **2002**, *41*, 3818.
[32] W. W. Xu, X. C. Zeng, Y. Gao. *Nanoscale*, **2017**, *9*, 8990.
[33] E. Eichhöfer, D. Fenske. *J. Chem. Soc. Dalton Trans.* **2000**, *0*, 941.
[34] J. Olkowska-Oetzel, P. Sevillano, A. Eichhöfer, D. Fenske. *Eur. J. Inorg. Chem.* **2004**, 1100.

[35] E. Eichhöfer, M. Kühn, S. Lebedkin, M. Kehry, M. M. Kappes, F. Weigend. *Inorg. Chem.* **2017**, *56*, 9330.
[36] Q.-M. Wang, Y.-A. Lee, O. Crespo, J. Deaton, C. Tang, H. J. Gysling, M. C. Gimeno, C. Larraz, M. D. Villacampa, A. Laguna, R. Eisenberg, *J. Am. Chem. Soc.* **2004**, *126*, 9488.
[37] O. Crespo, M. C. Gimeno, A. Laguna, C. Larraz, M. D. Villacampa. *Chem. Eur. J.* **2007**, *13*, 235.
[38] L.-Q. Mo, J.-H. Jia, L.-j. Sun, Q.-M. Wang, *Chem. Commun.* **2012**, *48*, 8691.
[39] C. E. Anson, A. Eichhöfer, I. Issac, D. Fenske, O. Fuhr, P. Sevillano, C. Persau, D. Stalke, J. Zhang. *Angew. Chem. Int. Ed.* **2008**, *47*, 1326.
[40] M. L. Fu, I. Issac, D. Fenske, O. Fuhr, *Angew. Chem. Int. Ed.* **2010**, *49*, 6899.
[41] S. Bestgen, O. Fuhr, B. Breitung, Z. S. K. Chakravadhanula, G. Guthausen, F. Hennrich, W. Yu, M. M. Kappes, P. W. Roesky, D. Fenske, *Chem. Sci.* **2017**, *42*, 1871.
[42] M. W. DeGroot, J. F. Corrigan. *Z. Anorg. Allg. Chem.* **2006**, *632*, 19.
[43] D. T. T. Tran, N. J. Taylor, J. F. Corrigan, *Angew. Chem. Int. Ed.* **2000**, *39*, 935.
[44] D. T. T. Tran, L. M. C. Beltran, C. M. Kowalchuk, N. R. Trefiak, N. J. Taylor, J. F. Corrigan. *Inorg. Chem.* **2002**, *41*, 5693.
[45] R. Pätow, D. Fenske, *Z. Anorg. Allg. Chem.* **2003**, *629*, 1437.
[46] A. Borecki, J. F. Corrigan. *Inorg. Chem.* **2007**, *46*, 2478.
[47] R. Biedermann, O. Kluge, D. Fuhrmann, H. Krautscheid. *Eur. J. Inorg. Chem.* **2013**, *27*, 4727.
[48] A. M. Polgar, C. B. Khadka, M. Azizpoor Fard, B. Nikkel, T. O'Donnell, T. Neumann, K. Lahring, K. Thompson, C. Cadogan, F. Weigend, J. F. Corrigan. *Chem. Eur. J.* **2016**. *22*, 18378.
[49] I. Medina, H. Jacobsen, J. T. Mague, M. J. Fink. *Inorg. Chem.* **2006**, *45*, 8844.
[50] H. Jacobsen, M. J. Fink. *Eur. J. Inorg. Chem.* **2007**, *360*, 5294.
[51] M. Azizpoor Fard, F. Weigend, J. F. Corrigan. *Chem. Commun.* **2015**, *51*, 8361.
[52] J. Zhai, M. D. Hopkins, G. L. Hillhouse, *Organometallics*, **2015**, *34*, 4637.
[53] M. Azizpoor Fard, T. I. Levchenko, C. Cadogan, W. J. Humenny, J. F. Corrigan. *Chem. – Eur. J.* **2016**, *22*, 4543.
[54] J. Zhai, A. S. Filatov, G. L. Hillhouse, M. D. Hopkins. *Chem. Sci.* **2016**, *7*, 589.
[55] S. Bagherzadeh, N. P. Mankad. *Chem. Commun.* **2018**, *54*, 1097.
[56] P. Atkins, J. de Paula. *Physical Chemistry: Thermodynamics, Structure, and Change, 10th edition*. **2014**, W. H. Freeman and Company, New York, NY.
[57] J. R. Lakowicz. *Principles of Fluorescence Spectroscopy, 3rd edition.* **2006**, Springer Science, New York, NY.
[58] A. J. Lees. *Chem. Rev.* **1987**, *87*, 711.
[59] J. N. Demas, A. W. Adamson. *J. Am. Chem. Soc.* **1971**, *93*, 1800.
[60] A. Bouskila, B. Drahi, E. Amouyal, I. Sasaki, A. Gaudemer. *J. Photochem. Photobiol. A* **2004**, *163*, 381.
[61] L. Sacksteder, M. Lee, J. N. Demas, B. A. DeGraff. *J. Am. Chem. Soc.* **1993**, *115*, 8230.
[62] B. Carlson, G. D. Phelan, W. Kaminsky, L. Dalton, X. Jiang, S. Liu, A. K.-Y. Jen. *J. Am. Chem. Soc.* **2002**, *124*, 14162.
[63] Md. K. Nazeeruddin, R. Humphry-Baker, D. Berner, S. Rivier, L. Zuppiroli, M. Graetzel. *J. Am. Chem. Soc.* **2003**, *125*, 8790.
[64] J. A. G. Williams, A. Beeby, E. S. Davies, J. A. Weinstein, C. Wilson. *Inorg. Chem.* **2003**, *42*, 8609.
[65] L. F. Gildea, A. S. Batsanov, J. A. G. Williams. *Dalton Trans.* **2013**, *42*, 10388.

[66] B. Y.-W. Wong, H.-L. Wong, Y.-C. Wong, M.-Y. Chan, V. W.-W. Yam. *Angew. Chem. Int. Ed.* **2017**, *56*, 302.
[67] R. C. Evans, P. Douglas, C. J. Winscom. *Coord. Chem. Rev.* **2006**, *250*, 2093.
[68] P.-T. Chou, Y. Chi, M.-W. Chung, C.-C. Lin. *Coord. Chem. Rev.* **2011**, *255*, 2653.
[69] J. N. Demas, B. A. DeGraff. *Coord. Chem. Rev.* **2001**, *211*, 317.
[70] Y. You, S. Y. Park. *Dalton Trans.* **2009**, *9226*, 1267.
[71] J. Kalinowski, V. Fattori, M. Cocchi, J. A. G. Williams. *Coord. Chem. Rev.* **2011**, *255*, 2401.
[72] A. W. Adamson, W. L. Waltz, E. Zinato, D. W. Watts, P. D. Fleischauer, R. D. Lindhom. *Chem. Rev.* **1968**, *68*, 541.
[73] Y. Y. Chia, M. G. Tay. *Dalton Trans.* **2014**, *43*, 13159.
[74] A. Barbieri, G. Accorsi, N. Armaroli. *Chem. Commun.* **2008**, 2185
[75] V. W.-W. Yam, K. M.-C. Wong. *Chem. Commun.* **2011**, *47*, 11579.
[76] A. Vogler, H. Kunkley. *Coord. Chem. Rev.* **2001**, *219*, 489.
[77] M. Montalti, A. Credi, L. Prodi, M. T. Gandolfina, *Handbook of Photochemistry*, Taylor and Francis, Boca Raton, 2006.
[78] C.-M. Che, H.-L. Kwong, V. W.-W. Yam, K.-C. Cho. *J. Chem. Soc. Chem. Commun.* **1989**, *2*, 885.
[79] K. R. Kyle, J. DiBenedetto, P. C. Ford. *J. Chem. Soc. Chem. Commun.* **1989**, *2*, 714.
[80] D. G. Cuttell, S.-M. Kuang, P. E. Fanwick, D. R. McMillin, R. A. Walton. *J. Am. Chem. Soc.* **2002**, *124*, 6.
[81] A. J. M. Miller, J. L. Dempsey, J. C. Peters, *Inorg. Chem.* **2007**, *46*, 7244.
[82] P. Pyykkö. *Chem. Rev.* **1997**, *97*, 597.
[83] F. Scherbaum, A. Grohmann, B. Huber, C. Krüger, H. Schmidbaur, *Angew. Chem. Int. Ed.* **1988**, *27*, 1544.
[84] H. Schmidbaur, A. Schier. *Chem. Soc. Rev.* **2012**, *41*, 370.
[85] A. Vogler, H. Kunkley. *Chem. Phys. Lett.* **1988**, *150*, 135.
[86] M. A. Mansour, W. B. Connick, R. J. Lachicotte, H. J. Gysling, R. Eisenberg. *J. Am. Chem. Soc.* **1998**, *120*, 1329.
[87] A. Dedieu, R. Hoffmann. *J. Am. Chem. Soc.* **1978**, *100*, 2074.
[88] K. M. Merz, Jr. R. Hoffmann. *Inorg. Chem.* **1988**, *27*, 2120.
[89] C. King, J.-C. Wang, Md. N. I. Khan, J. P. Fackler, Jr. *Inorg. Chem.* **1989**, *28*, 2145.
[90] P. Pyykkö. *Angew. Chem. Int. Ed.* **2004**, *43*, 4412.
[91] R. Czerwieniec, M. J. Leitl, H. H. H. Homeier, H. Yersin. *Coord. Chem. Rev.* **2016**, *325*, 2.
[92] T. Hofbeck, U. Monkowius, H. Yersin. *J. Am. Chem. Soc.* **2015**, *137*, 399.
[93] R. Czerwieniec, J. Yu, H. Yersin. *Inorg. Chem.* **2011**, *50*, 8293.
[94] M. J. Leitl, V. A. Krylova, P. I. Djurovich, M. E. Thompson, H. Yersin. *J. Am. Chem. Soc.* **2014**, *136*, 16032.
[95] M. Z. Shafikov, A. F. Suleymanova, R. Czerwieniec, H. Yersin. *Chem. Mater.* **2017**, *29*, 1708.
[96] F. Dumur. *Org. Electron.* **2015**, *21*, 27.
[97] M. J. Leitl, D. M. Zink, A. Schinabeck, T. Baumann, D. Volz, H. Yersin. *Top. Curr. Chem. (Z)* **2016**, *374*, 1.
[98] V. W.-W. Yam, C.-L. Chan, C.-K. Li, K. M.-C. Wong. *Coord. Chem. Rev.* **2001**, *216-217*, 173.
[99] F. Sabin, C. K. Ryu, P. C. Ford, A. Vogler. *Inorg. Chem.* **1992**, *31*, 1941.
[100] V. W.-W. Yam, E. C.-C. Cheng, N. Zhu. *Angew. Chem. Int. Ed.* **2001**, *39*, 1763.
[101] V. W.-W. Yam, E. C.-C. Cheng, Z.-Y. Zhou. *Angew. Chem. Int. Ed.* **2000**, *39*, 1683.

[102] V. W.-W. Yam, E. C.-C. Cheng, K.-K. Cheung. *Angew. Chem. Int. Ed.* **1999**, *38*, 197.
[103] T. K.-M. Lee, N. Zhu, V. W.-W. Yam. *J. Am. Chem. Soc.* **2010**, *132*, 17646.
[104] E. C.-C. Cheng, W.-Y. Lo, T. K.-M. Lee, N. Zhu, V. W.-W. Yam. *Inorg. Chem.* **2014**, *53*, 3854.
[105] S. Lebedkin, T. Langetepe, P. Sevillano, D. Fenske, M. M. Kappes, *J. Phys. Chem. B* **2002**, *106*, 9019.

Chapter 2

2 A *N*-Heterocyclic Carbene Stabilized Coinage Metal Chalcogenide Framework with Highly Tunable Optical Properties

(A version of this work is presented in the Journal of the American Chemical Society. A. M. Polgar, F. Weigend, A. Zhang, M. J. Stillman, J. F. Corrigan. *J. Am. Chem. Soc.* **2017**, *139*, 14045 – 14048)

2.1 Introduction

Over the past 50 years, complexes of gold in the +1 oxidation state have been studied for their rich photophysical properties.[1-4] Early crystallographic studies of linear, rod-like [LAuX], $[L_2Au]^+$, and $[AuX_2]^-$ complexes revealed intermolecular aggregation of Au^+ centers into supramolecular oligomers, chains and sheets through a dispersive d^{10}-d^{10} attraction strengthened by relativistic effects, which has been termed "aurophilicity".[5,6] It was soon recognized that this interaction is correlated to photoluminescence in Au(I) complexes.[7] It was also shown that this effect could also exist intramolecularly, resulting in clustering of Au^+ centers about main group donor atoms.[8] Of these cluster compounds, gold(I) chalcogenides have shown particular promise for their stability, synthetic accessibility, and intense photoluminescence.[9]

When combined with phosphine ancillary ligands, gold(I) chalcogenides form clusters typically based on $[(\mu_3\text{-E})Au_3]^+$ units aggregated through aurophilic interactions and bridging diphosphines.[10] By varying parameters of the stabilizing phosphine such as Tolman cone angle, denticity, and the presence of other functional groups, many different cluster sizes and geometries have been prepared.[11-25] Curiously, there have been very few reports on gold(I) chalcogenide clusters with ancillary ligands other than phosphines.[26-28] This is in stark contrast to the rest of gold chemistry, where *N*-Heterocyclic carbene (NHC) ligands have overtaken phosphines as the ligand of choice for applications in catalysis,[29,30] medicine,[31,32] supramolecular assembly,[33,34] surface chemistry,[35] and nanocluster chemistry,[36,37] among others. NHC-Au(I) complexes have been shown to exhibit fascinating and tunable optical effects such as mechano-, iono-, and

vapochromism.[38-40] Furthermore, reports have emerged recently where NHCs stabilize chalcogenide clusters of other d-block metals.[41-44]

Herein, a fusion of the worlds of luminescent gold(I) chalcogenide clusters and NHC-Au(I) complexes is envisioned. Gold(I) trimethylsilylchalcogenolate reagents [(IPr)AuESiMe$_3$] (E = S (**2.1a**), Se (**2.1b**), Te (**2.1c**); IPr = 1,3-bis(2,6-diisopropylphenyl)imidazole-2-ylidene) are applied as precursors to homo- and heterometallic clusters with NHC ancillary ligands. Treatment of these synthons with [(L)M(OAc)] (L = Ph_3P, $(ArO)_3P$; M = Ag, Au) led to the concomitant formation of $AcOSiMe_3$ and Au-E-M motifs in the octanuclear clusters [$Au_4Ag_4(\mu_3\text{-}E)_4(IPr)_4$] (E = S (**2.2a**), Se (**2.2b**)) and [$Au_8(\mu_3\text{-}E)_4(IPr)_4$] (E = S (**2.3a**), Se (**2.3b**), Te (**2.3c**)). The present work demonstrates that NHCs have a special role to play in the continued development of gold(I) chalcogenide chemistry and its application towards new light emitting metal complexes.

2.2 Results and Discussion

The NHC-stabilized gold trimethylsilylchalcogenolates **2.1a-c** were prepared by salt metathesis of [(IPr)AuCl] with Li[ESiMe$_3$] in tetrahydrofuran (THF; Scheme 1). Repeated attempts to grow crystals for X-ray crystallography produced fragile and rapidly desolvating crystals unsuitable for diffraction analysis. The molecular structures are thus supported by 1D and 2D multinuclear NMR spectroscopy and elemental analysis. Given the propensity for gold(I) to adopt linear, terminally coordinated species, we propose mononuclear complexes with gold(I) ligated to one IPr ligand and one E(SiMe$_3$) in a linear fashion.

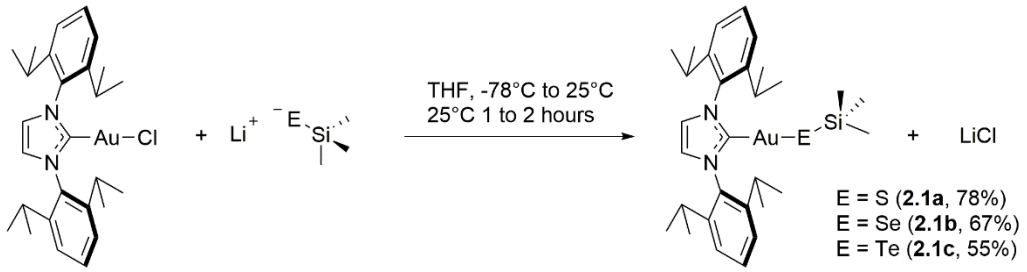

Scheme 2.1 Synthesis of **2.1a-c**.

The ^{1}H NMR spectra of **2.1a-c** in $CDCl_3$ at 298K exhibit a set of signals assigned to IPr and one high field singlet for the trimethylsilyl group (Figure 2.1). In the former, a triplet (7.48

ppm) and a doublet (7.28 – 7.29 ppm) in the aromatic region are assigned to the *para*- and *meta*-protons of the 2,6-diisopropylphenyl moiety, respectively. At slightly higher field (7.14 ppm), a singlet is present for the two vinylic protons of the imidazolylidene backbone. The presence of only one signal indicates the chemical equivalence of these protons. Consequently, the two diisopropylphenyl groups are also chemically equivalent. The signals for this group are a septet (2.61 – 2.63 ppm), corresponding to the methine proton of the isopropyl groups, and two doublets (1.37 – 1.38 ppm and 1.22 ppm) for the two diastereotopic methyl groups of the isopropyl moiety. The high field singlets for the -ESiMe$_3$ group are shifted as a function of the chalcogen atom, with the trend E = S (-0.11 ppm) < Se (0.01 ppm) < Te (0.18 ppm) mimicking what has been reported previously for $(R_3P)_nCuESiMe_3$.[45] In the $^{13}C\{^1H\}$ NMR spectra for **2.1a-c** in $CDCl_3$ at 298K, the high field trimethylsilyl signals shift downfield from S (6.4 ppm) to Se (7.0 ppm) to Te (8.2 ppm). Such trends violate the inductive effect (more electronegative chalcogen causes downfield chemical shifts). This points to the importance of anisotropic effects for the chemical shifts of the β-protons, as originally argued by Drake for the series $E(SiMe_3)_2$ (E = O, S, Se, Te).[46]

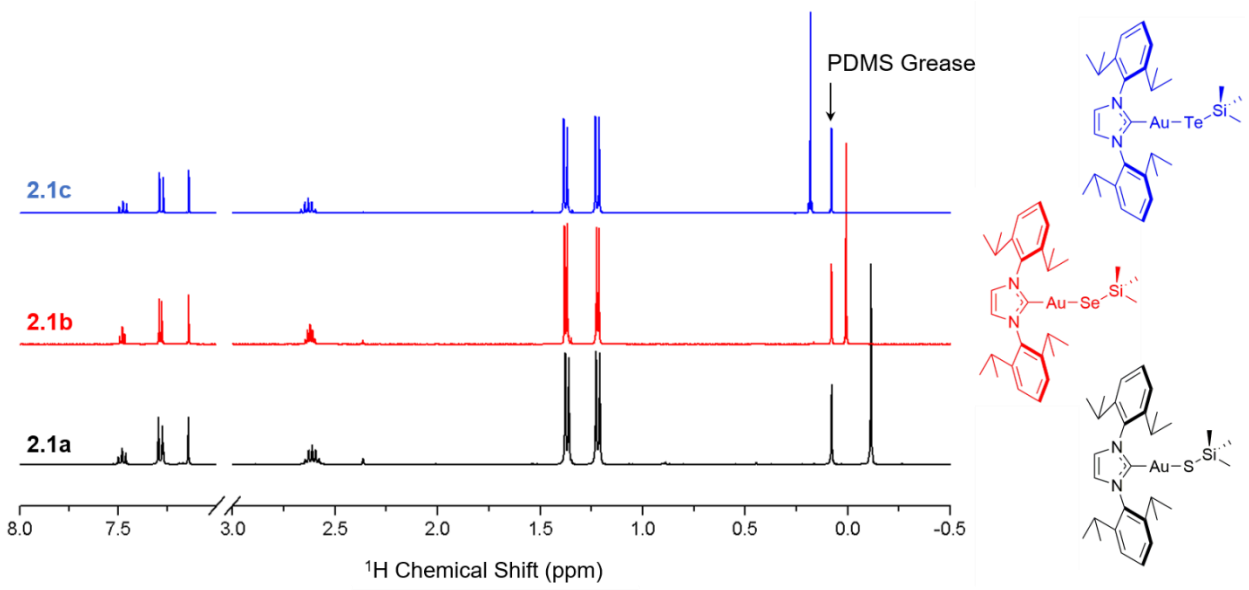

Figure 2.1 Stacked ^1H NMR Spectra of **2.1a** (black), **2.1b** (red), and **2.1c** (blue) in $CDCl_3$ at 298K.

For **2.1a-c**, the ^{29}Si NMR signals were determined by ^1H-^{29}Si Heteronuclear Multiple Bond Correlation (HMBC) experiments. In all cases, correlations between the high field singlets in the ^1H NMR and high field ^{29}Si signals (**2.1a**, 12 ppm; **2.1b**, 8 ppm; **2.1c**, -12 ppm) were detected,

which do correlate with the inductive effect of the adjacent chalcogen. For **2.1b** and **2.1c** ^{1}H-^{77}Se and ^{1}H-^{125}Te HMBC experiments were performed. A high field ^{77}Se signal at 32 ppm was correlated to the -SeSiMe$_3$ proton signals in **2.1b**. The ^{125}Te signal for **2.1c** occurred also at high field (-1071 ppm), comparing favourably to [Au(TeSi(SiMe$_3$)$_3$)]$_4$ (-1112 ppm).[47] The ^{125}Te{^{1}H} NMR spectrum shows, in addition to this signal, two satellites of relative intensity 2.6% to the main signal due to coupling of ^{125}Te to ^{29}Si (I = ½, 4.685% abundance) with $^{1}J_{\text{Si-Te}}$ = 296 Hz.[48]

Stoichiometric reactions of **2.1a** with a suspension of AgOAc at -78°C resulted in the production of intractable mixtures. The reaction was subsequently performed via ligation of AgOAc with a tertiary phosphine to retard uncontrolled cluster growth. Thus, reaction of **2.1a** and **2.1b** with [(Ph$_3$P)AgOAc] yielded the ternary Au-E-Ag clusters [Au$_4$Ag$_4$(μ_3-S)$_4$(IPr)$_4$] (**2.2a**) and [Au$_4$Ag$_4$(μ_3-Se)$_4$(IPr)$_4$] (**2.2b**), respectively (Scheme 2.2). The same structural framework could be obtained via a similar reaction in which Ag is replaced with Au. Reaction of **2.1a** with [(Ph$_3$P)AuOAc] resulted in the crystallization of the octanuclear gold(I)-sulfido cluster [Au$_8$(μ_3-S)$_4$(IPr)$_4$] (**2.3a**). However, NMR and mass spectral analysis indicated that the reaction also produced [(IPr)Au(PPh$_3$)]OAc (~33%). A weaker Lewis base (ArO)$_3$P (Ar = 2,4-^{t}Bu(C$_6$H$_3$)) was employed instead to promote P – Au bond scission. This modified procedure selectively yielded [Au$_8$(μ_3-S)$_4$(IPr)$_4$] and [Au$_8$(μ_3-Se)$_4$(IPr)$_4$] (**2.3b**). Reaction of **2.1c** with [(Ph$_3$P)AuOAc] allowed for the clean isolation of [Au$_8$(μ_3-Te)$_4$(IPr)$_4$] (**2.3c**) without observation of any cationic gold(I) species (Scheme 2.2).

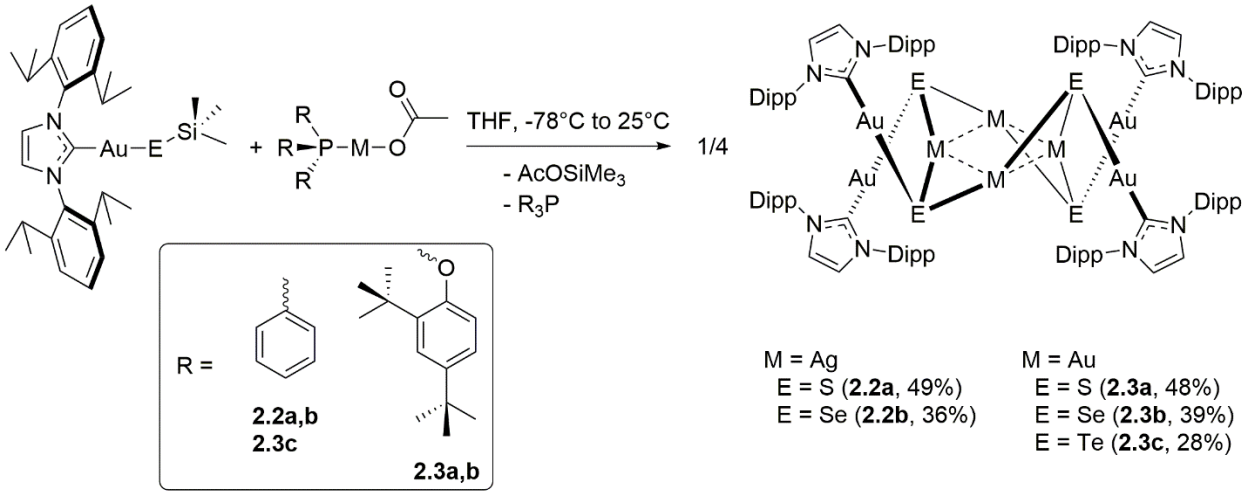

Scheme 2.2 Synthesis of **2.2a**,**b** and **2.3a-c**. Dipp = 2,6-diisopropylphenyl, AcO = acetate. Dashed lines drawn between the four central centers indicate metallophilic interactions. Any interactions between Au and M are omitted for clarity.

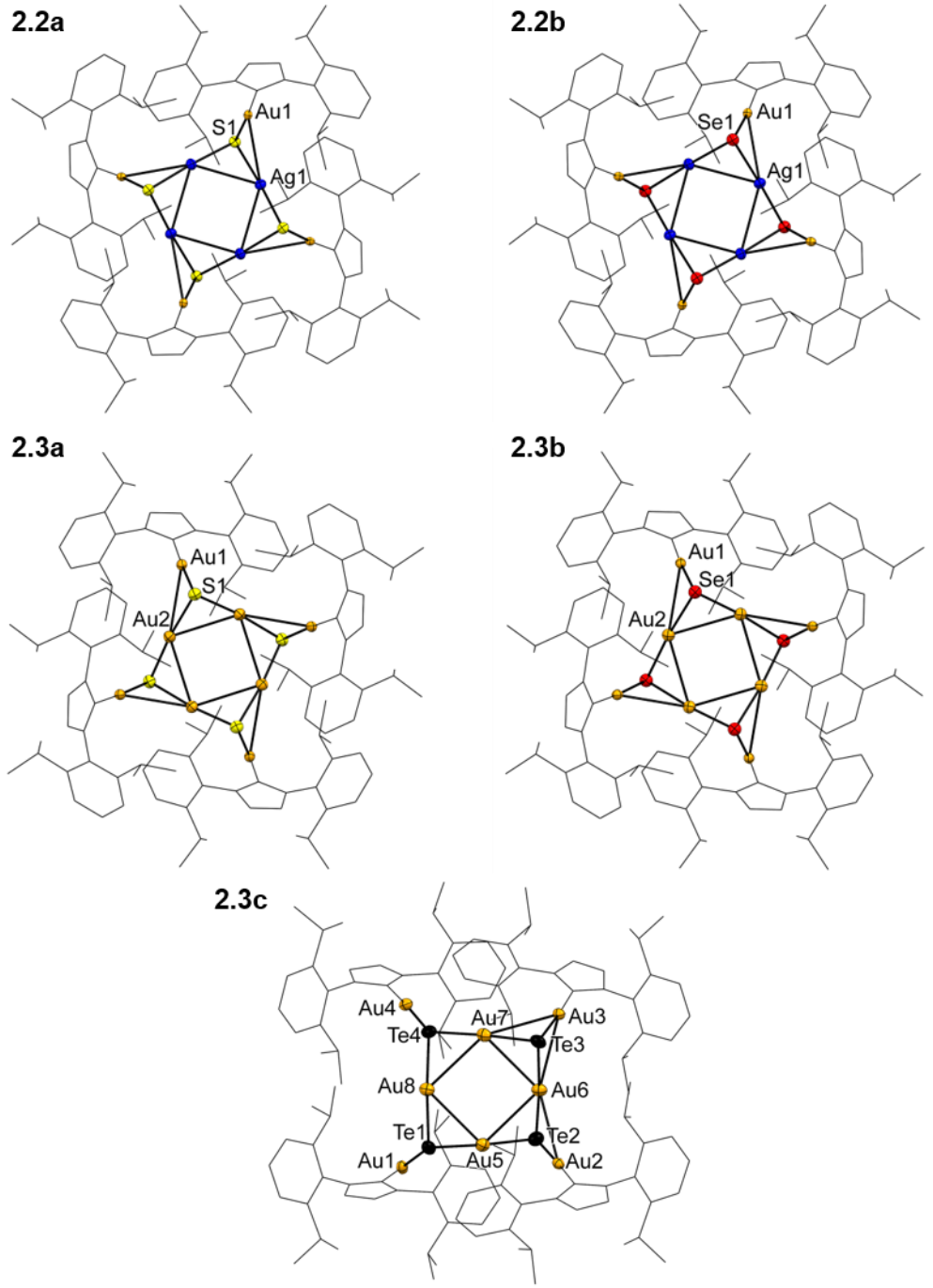

Figure 2.2 Molecular structures of **2.2a**,**b** and **2.3a-c** in the crystal. The core metal and chalcogen atoms are represented by thermal ellipsoids plotted at the 50% probability level. NHC ligands are represented as wireframe drawings. Bonds are drawn between two metal atoms when their separation is less than the sum of their van der Waals radii, but should not be interpreted as covalent. All hydrogen atoms and one co-crystallizing THF molecule for **2.3c** have been omitted for clarity. **2.2a**,**b** and **2.3a**,**b** crystallize about a $\bar{4}$ center, so only one quarter of the molecule is labelled. Colour scheme: S, yellow; Se, red; Te, black; Au, orange; Ag, blue.

Compounds **2.2a**, **2.2b**, **2.3a**, and **2.3b** are isostructural and isomorphous, crystalizing in the tetragonal space group $I\bar{4}$ and residing about a crystallographic $\bar{4}$ center (Figure 2.2). The molecules consist of a central $\{M_4E_4\}$ cycle (M = Ag (**2.2a**,**b**); Au (**2.3a**,**b**)) with the four "M" atoms close to planarity and the chalcogen atoms lying alternately above and below this plane. Each chalcogen atom is ligated to two M and one Au, forming a (μ_3-E)AuM_2 tetrahedron. Aurophilic and/or metallophilic interactions are present in all clusters, with the interaction becoming weaker (as judged by longer metal-metal contacts) when the size of the bridging chalcogen increases. Compound **2.3c** crystallizes as a THF solvate in the orthorhombic space group $P2_12_12_1$ and its geometry is distorted compared to the lighter congeners of this series, owing to both the longer Au−Te bonds and aurophilic contacts present. Selected structural parameters are presented in Table 2.1.

Table 2.1 Selected bonds lengths (Å) and angles (°) for **2.2-3**. See Figure 2.2 for the atomic numbering scheme.

	2.2a **M = Ag** **E = S**	**2.2b** **M = Ag** **E = Se**	**2.3a** **M = Au2** **E = S**	**2.3b** **M = Au2** **E = Se**	**2.3c** **M = Au**[a] **E = Te**
Au – E	2.2808(01)	2.3913(7)	2.2963(1)[b]	2.4001(8)[b]	2.5533(8) – 2.5649(8)[c]
M – E	2.391(1) – 2.407(1)	2.4864(7) – 2.5059(7)	2.322(2) – 2.336(2)	2.4315(8) – 2.4453(8)	2.585(1) – 2.6058(8)
M – M	3.0833(5)	3.1160(7)	3.0899(8)	3.1371(4)	3.1667(8) – 3.2068(8)
Au – M	3.1156(4)	3.1211(8)	3.1653(9)	3.1544(3)	3.2068(8) – 3.2311(7)
Au – E – M	83.26(3) – 89.86(4)	79.15(2) – 87.89(2)	86.20(5) – 91.30(5)	81.23(2) – 88.94(3)	74.55(2) – 91.72(3)
M – E – M	79.98(3)	77.24(2)	83.12(5)	80.07(2)	75.11(2) – 76.44(2)
C – Au – E	176.6(1)	176.04(9)	176.74(2)	176.25(15)	176.9(3) – 178.3(3)
E – M – E	176.65(4)	177.63(2)	174.25(2)	175.20(2)	175.99(3) – 176.98(3)

[a] M = Au5, Au6, Au7, Au8
[b] Au = Au1
[c] Au = Au1, Au2, Au3, Au4

^{1}H NMR spectra for **2.2-3** exhibit one set of signals for IPr, as expected from the S_4 molecular symmetry element in **2.2a**,**b** and **2.3a**,**b** (Figure 2.3). For **2.3c**, one set of IPr signals is observed also, despite its lower molecular symmetry. This suggests that the asymmetric Au_8Te_4 core relaxes in solution so that the overall environment for all four ligands is the same. Overall,

the ^{1}H NMR spectra for all clusters are very similar. The ^{13}C{^{1}H} NMR spectra are differentiated mainly in the position of the carbenic carbon (C_{NHC}) signals at downfield chemical shifts (186.2 – 192.5 ppm). The ^{77}Se{^{1}H} NMR spectra for **2.2b** and **2.3b** at 273K show one high field signal at -655 ppm and -517 ppm, respectively. While the signal for **2.3b** is a singlet, since Au is not NMR active, **2.2b** is a triplet due to coupling to ^{107}Ag (I = ½, 51.839% abundance) and ^{109}Ag (I = ½, 48.161% abundance), with a coupling constant $^{1}J_{Se\text{-}Ag}$ = 17 Hz (Figure 2.3). No resolution between individual ^{77}Se-^{107}Ag and ^{77}Se-^{109}Ag couplings could be obtained. Given the ratio of magnetogyric ratios $\gamma(^{109}Ag)/\gamma(^{107}Ag)$ = 1.1507 = $^{1}J(^{77}Se\text{-}^{107}Ag)/^{1}J(^{77}Se\text{-}^{109}Ag)$, and the measured coupling constant, the difference in the ^{77}Se-^{107}Ag and ^{77}Se-^{109}Ag coupling constants is not more than 3 Hz. Since the breadth of the signal (FWHM = 5 Hz) is greater than this, both isotopes can be treated as one with I = ½ to explain the apparent triplet pattern. ^{125}Te{^{1}H} NMR for **2.3c** shows one signal at -1050 ppm, shifted +21 ppm relative to **2.2c**.

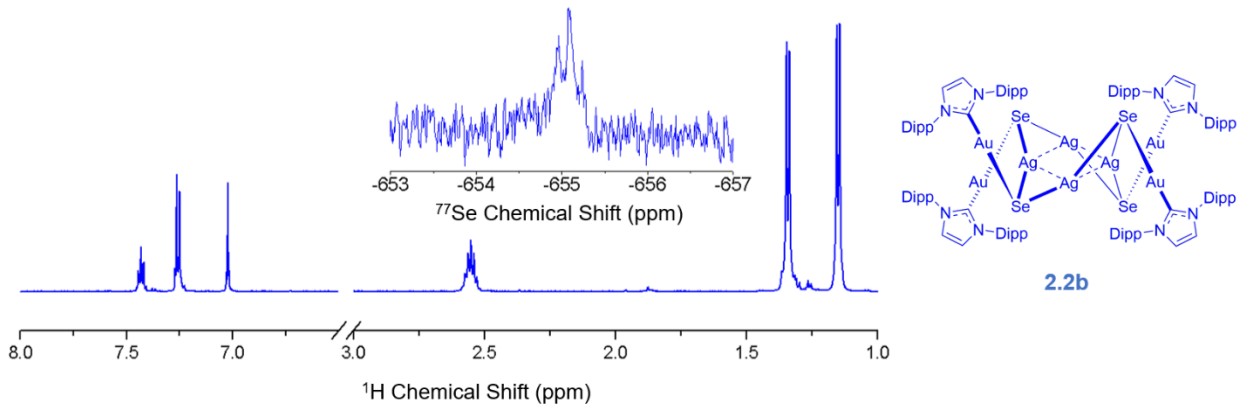

Figure 2.3 ^{1}H NMR spectra for **2.2b** in $CDCl_3$ at 298K. Inset is the ^{77}Se{^{1}H} NMR spectrum in $CDCl_3$ at 273K.

The luminescence of clusters **2.2a**,**b** and **2.3a**,**b** in glassy 2-methyl tetrahydrofuran (2-MeTHF) and the solid state have been measured at 77K (Figure 2.4). The spectroscopic results are summarized in Table 2.2. Except for **2.3c**, all clusters exhibit a single excitation band with λ_{ex} between 310 and 327 nm, increasing in wavelength in the order **2.2a** < **2.2b** < **2.3a** < **2.3b**. The same ordering applies to the λ_{em} of the solution-state emission spectra. This gives rise to emission colours ranging from yellow-green (**2.2a**) to red (**2.3b**). Each of the clusters exhibited large Stokes' shifts (> 14 000 cm^{-1}) and microsecond lifetimes of ca. 10 to 40μs, indicating a triplet parentage

for the emissions. The excitation spectra of **2.2a** and **2.2b** do not significantly change from solution to the solid state, but significant bathochromic shifting of the emission maxima is observed. Both the excitation and emission maxima of **2.3c** in the solid state occur at comparatively low energies, which are similar to those reported for the octanuclear gold(I) tellurolates $[Au_8(\mu\text{-TeR})_8(PR'_3)_4]$.[49]

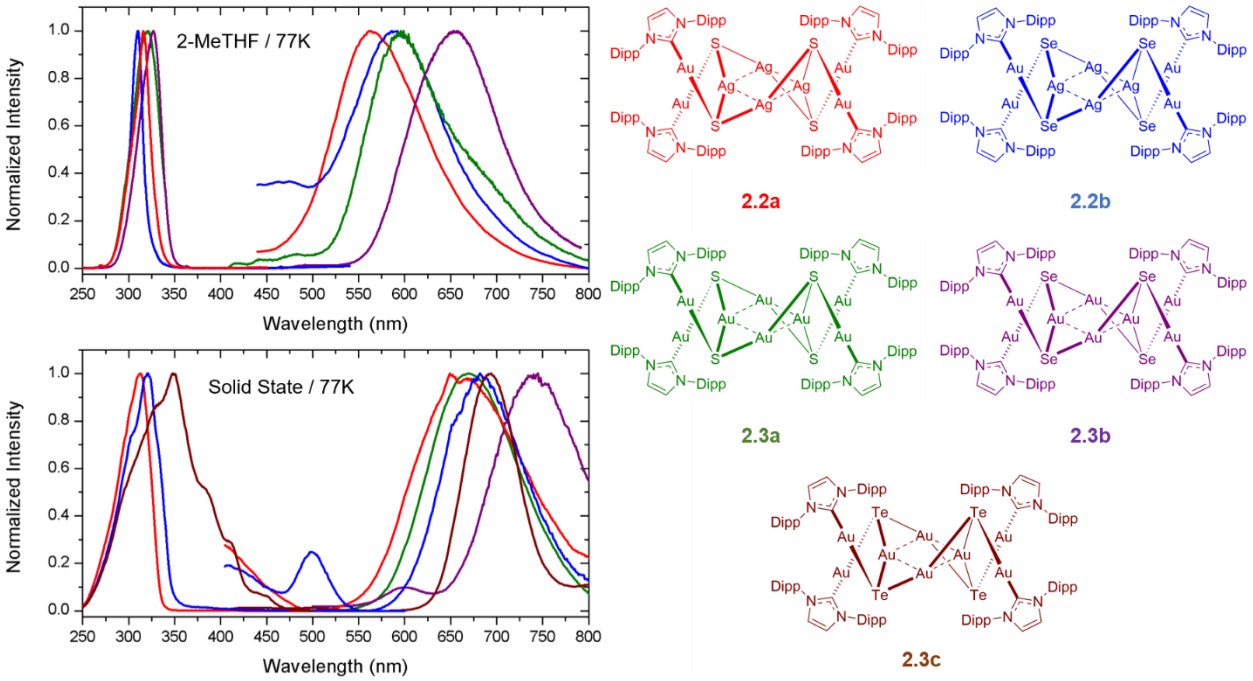

Figure 2.4 Photoluminescence emission (PL) and excitation (PLE) spectra for **2.2-3** in glassy 2-MeTHF at 77K (top) and as a crystalline powder (bottom).

Table 2.2 Summary of spectroscopic data for **2.2-3** in frozen 2-MeTHF and the solid state at 77K.

	2-Me-THF (77K)				Solid (77K)			
	λ_{ex} [nm]	λ_{em} [nm]	τ [µs]	$\tilde{\nu}_{ST}$ [cm^{-1}]	λ_{ex} [nm]	λ_{em} [nm]	τ [µs]	$\tilde{\nu}_{ST}$ [cm^{-1}]
2.2a	310	562	17.7	14500	313	669	19.2	17000
2.2b	316	592	20.5	14800	320	682	20.4	16600
2.3a	322	596	42.4	14300	-	670	31.0	-
2.3b	327	657	37.8	15400	-	745	30.3	-
2.3c	-	-	-	-	348	694	9.78	14300

For cluster **2.2a**, the character of the excitations causing the excitation band starting at a wavelength of ca. 350 nm was determined via time-dependent density functional theory (TDDFT).

Calculations were carried out with TURBOMOLE[50] employing Becke's three parameter hybrid functional with Lee–Yang–Parr correlation (B3LYP) and polarized double zeta valence basis sets Def2SV(P).[51-53] These transitions involve the highest 8 occupied and the lowest 16 unoccupied orbitals. The latter are part of the π-system of the NHCs, the former mainly show contributions of the 3p orbitals of sulfur (55%), the 5s/4d orbitals of silver (29%) and the 6s/5d orbitals of the gold centers (13%); as determined from Mulliken population analysis.[54] The character of this transition is also evident from the difference density (Figure 2.5B) between the excited states and the ground state.[55] The lowest energy electronic state in **2.2a** may thus be formulated as metal-metal to ligand charge transfer (MMLCT; $AuAg_2 \rightarrow IPr$) with an intraligand (IL; $S \rightarrow IPr$) admixture. As more electron density is injected into the $\{M_4E_4\}$ core (via replacement of S with Se/Te or Ag with Au), a higher-lying HOMO should induce a bathochromic shift of the transition energy. The computational results (Figure 2.5A) support this view for replacement of Ag with Au but fail to differentiate the HOMO energy for homologous S and Se clusters. Emission energy differences from the triplet state are also a consequence of structural rearrangement, which may be more sensitive to the chalcogen atom and account for the differences in the emission energy.

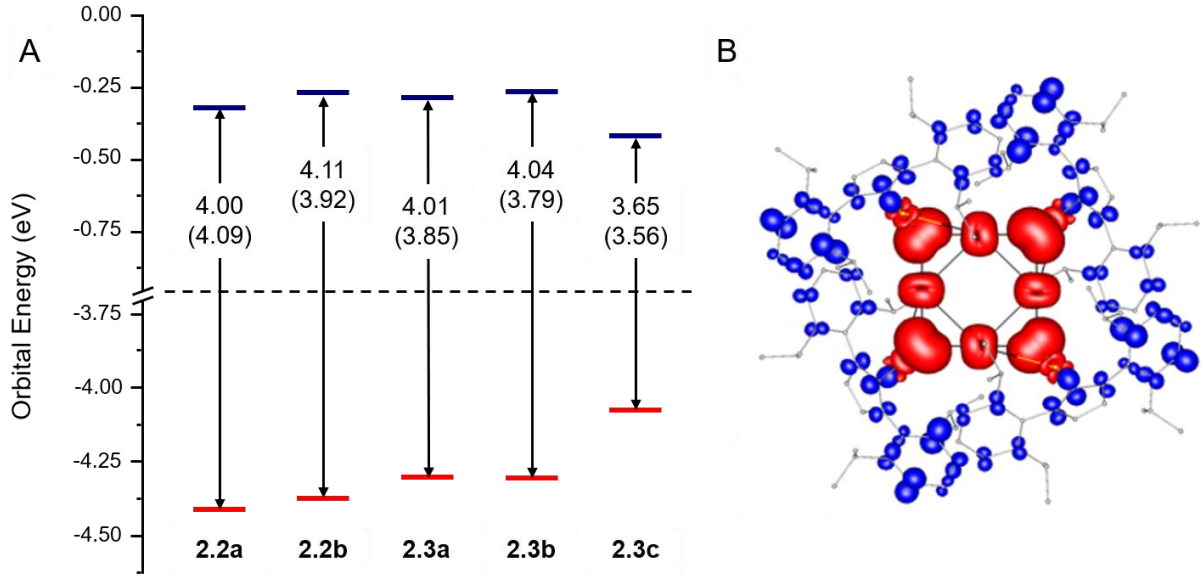

Figure 2.5 A) Orbital energy diagram for **2.2-3**. The HOMO and LUMO are plotted in red and blue, respectively. The calculated $\Delta E_{LUMO\text{-}HOMO}$ (eV) is compared to the experimental value in parentheses derived from the PLE spectra. B) Difference density plot for the first excited singlet state of **2.2a**. Regions of red indicate a surplus of electron density in the ground state and blue a surplus in the excited state. All calculations are at B3LYP/Def2SV(P).

2.3 Experimental Section

2.3.1 General Considerations

All syntheses described were conducted under an atmosphere of high-purity dry nitrogen using standard double-manifold Schlenk line techniques. Non-chlorinated solvents (tetrahydrofuran, pentane, hexanes, and toluene) were dried and collected using an MBraun MB-SP Series solvent purification system. Deuterated chloroform was purchased from Caledon, and dried over P_2O_5 by refluxing under N_2 prior to collecting by distillation and stored over 3Å molecular sieves. Diethyl ether was dried and distilled over sodium benzophenone ketyl radical and stored over 3Å molecular sieves. Anhydrous 2-methyltetrahydrofuran (2-MeTHF) was purchased from Sigma and degassed by three freeze-pump-thaw cycles prior to use in photophysical experiments. [(IPr)AuCl],[56] Li[ESiMe$_3$] (E = S, Se, Te),[57] [(Ph$_3$P)AuOAc],[58] [({2,4-^{t}Bu(C$_6$H$_3$)O}$_3$P)AuOAc],[58] and [(Ph$_3$P)AgOAc] [59] were prepared following literature procedures. Other chemicals were used as received from commercial sources (Alfa Aesar and Aldrich).

NMR spectra were recorded on Inova 400 and Inova 600 spectrometers. ^{1}H, ^{13}C{^{1}H} and ^{29}Si chemical shifts are referenced to external solvent peaks and quoted in ppm relative to SiMe$_4$. ^{77}Se and ^{125}Te chemical shifts are quoted relative to Me$_2$Se and Me$_2$Te, respectively. Heteronuclear Multiple Bond Correlation (HMBC) experiments were performed for ^{29}Si-^{1}H, ^{77}Se-^{1}H, and ^{125}Te-^{1}H to confirm signal assignments or to improve signal-to-noise through indirect detection of coupled protons. Elemental analysis was performed by Laboratoire d'analyse élémentaire at the Université de Montréal, Montreal, Canada. Samples were dried under dynamic vacuum (< 10 mTorr) for at least 12 hours prior to shipment. For sample **2.3c**, the presence of an amorphous black powder upon vacuum drying single crystals of the sample prevented the acquisition of satisfactory elemental analysis data.

Samples of **2.2a**,**b** and **2.3a**,**b** for solution-state electronic spectroscopy were prepared in a nitrogen filled glovebox by dissolving pure compound in 2-MeTHF which had been degassed by three freeze-pump-thaw cycles directly before transfer into the glovebox. The photoluminescence and photoluminescence excitation spectra at 77K were acquired on a PTI Quantamaster (PTI, London, Ontario) fluorimeter. At 298K, no emissions were observed from these samples. A quartz dewar was filled with liquid nitrogen and solutions were added dropwise into this holder, forming

randomly oriented beads of the frozen sample. A 250-400 cut-off filter was employed to remove unwanted stray exciting light that scatters from the frozen sample. The microsecond decay traces at 77 K were measured from decay traces using the PTI Xenoflash system with analysis using a sum of exponentials model. Photoluminescence measurements for **2.3a** and **2.3b** in the solid state using the same setup by immobilizing powdered samples on a sample holder (in air) which was then submerged into liquid nitrogen in the same quartz dewar. This holder was positioned at 45° relative to the source beam.

Photoluminescence measurements for solid samples of **2.2a**,**b** and **2.3c** were performed on a Horiba JobinYvon Fluorolog-3 spectrometer equipped with a Hamamatsu R5509 vis-NIR photomultiplier (~300 – 1400 nm) and an optical close-cycle cryostat (Leybold) for measurements at cryogenic temperatures down to ca. 15 K. Solid state spectra were measured in transmission for samples which were prepared as micron-sized crystalline powders dispersed in a mineral oil layer between two quartz plates. The emission spectra were corrected for the wavelength-dependent response of the spectrometer and detector (in relative photon flux units). Emission decay traces were recorded by connecting the photomultiplier to an oscilloscope (typically with a 500 or 50 Ohm load) and using a N_2-laser for pulsed excitation at 337 nm (~2 ns, ~5μJ per pulse).

2.3.2 Synthesis

Synthesis of [(IPr)AuSSiMe$_3$] (2.1a):

A Schlenk flask was charged with [(IPr)AuCl] (300 mg, 0.48 mmol) and a magnetic stir bar. The solid was dissolved in 15 mL THF and the resulting clear, colourless solution cooled to -30°C. A freshly prepared solution of Li[SSiMe$_3$] (0.48 mmol in 5 mL THF) was added to [(IPr)AuCl] at -30°C. The clear, colourless solution was warmed to room temperature and then stirred for an additional 2 hours. The solvent was removed *in vacuo*, leaving a white residue that was extracted in toluene. This was then doubly filtered through dry Celite® and the colourless filtrate concentrated. Layering with pentane and storing this solution at -25°C overnight resulting in the formation of colourless, rapidly desolvating crystals of [(IPr)AuSSiMe$_3$] which were dried under dynamic vacuum (78% yield); **m.p.** 185-186°C. **^{1}H NMR** ($CDCl_3$, 25°C, 599.301 MHz) δ7.48 (2H, t, $^3J_{H\text{-}H}$ = 7.9 Hz, CH_{Ar}), 7.29 (4H, d, $^3J_{H\text{-}H}$ = 7.9 Hz, CH_{Ar}), 7.14 (2H, s, CH_{imid}), 2.61 (4H, sept, $^3J_{H\text{-}H}$ = 7.0 Hz, C*H*$(CH_3)_2$), 1.37 (12H, d, $^3J_{H\text{-}H}$ = 7.0 Hz, CH(C*H*$_3)_2$), 1.22 (12H, d, $^3J_{H\text{-}}$

$_H$ = 7.0 Hz, CH(C*H*$_3$)$_2$), -0.11 (9H, s, Si(C*H*$_3$)$_3$). **^{13}C{^{1}H} NMR** (CDCl$_3$, 25°C, 150.78 MHz) δ187.1 (s, *C*-Au), 145.6 (s, C$_{Ar}$), 134.4 (s, C$_{Ar}$), 130.4 (s, C$_{Ar}$), 124.1 (s, C$_{Ar}$), 122.7 (s, C$_{imid}$), 28.8 (s, *C*H(CH$_3$)$_2$), 24.4 (s, CH(*C*H$_3$)$_2$), 24.1 (s, CH(*C*H$_3$)$_2$), 6.4 (SSi(*C*H$_3$)$_3$); **^{29}Si NMR** (CDCl$_3$, 25°C, 119.055 MHz) δ12 (s, S*Si*(CH$_3$)$_3$). **Anal. Calcd** for C$_{30}$H$_{45}$AuN$_2$SSi: C, 52.16; H, 6.57; N, 4.06; S, 4.64. Found C, 52.92; H, 6.82; N, 3.86; S, 4.80.

Synthesis of [(IPr)AuSeSiMe$_3$] (2.1b):

As described for **1a** with 0.5 mmol Li[SeSiMe$_3$] in 5 mL THF (67% yield); **m. p.** 184-187°C. **^{1}H NMR** (CDCl$_3$, 25°C, 599.301 MHz) δ7.48 (2H, t, $^3J_{H\text{-}H}$ = 7.6 Hz, CH$_{Ar}$), 7.29 (4H, d, $^3J_{H\text{-}H}$ = 7.6 Hz, CH$_{Ar}$), 7.14 (2H, s, CH$_{imid}$), 2.62 (4H, sept, $^3J_{H\text{-}H}$ = 6.8 Hz, C*H*(CH$_3$)$_2$), 1.38 (12H, d, $^3J_{H\text{-}H}$ = 6.8 Hz, CH(C*H*$_3$)$_2$), 1.22 (12H, d, $^3J_{H\text{-}H}$ = 6.8 Hz, CH(C*H*$_3$)$_2$), 0.01 (9H, s, Si(C*H*$_3$)$_3$). **^{13}C{^{1}H} NMR** (CDCl$_3$, 25°C, 150.78 MHz) δ188.9 (s, *C*-Au), 145.6 (s, C$_{Ar}$), 134.4 (s, C$_{Ar}$), 130.4 (s, C$_{Ar}$), 124.1 (s, C$_{Ar}$), 122.6 (s, C$_{imid}$), 28.8 (s, *C*H(CH$_3$)$_2$), 24.5 (s, CH(*C*H$_3$)$_2$), 24.1 (s, CH(*C*H$_3$)$_2$), 7.0 (SeSi(*C*H$_3$)$_3$); **^{29}Si NMR** (CDCl$_3$, 25°C, 119.055 MHz) δ8 (s, Se*Si*(CH$_3$)$_3$); **^{77}Se NMR** (CDCl$_3$, 25°C, 114.38 MHz) δ32 (s, *Se*Si(CH$_3$)$_3$, $^1J_{Se\text{-}Si}$ not resolved). **Anal. Calcd** for C$_{30}$H$_{45}$AuN$_2$SeSi: C, 48.84; H, 6.15; N, 3.80. Found C, 48.28; H 6.14; N 3.47.

Synthesis of [(IPr)AuTeSiMe$_3$] (2.1c):

A flame-dried Schlenk flask was charged with [(IPr)AuCl] (300 mg, 0.48 mmol) and a magnetic stir bar. The solid was dissolved in 15 mL THF and the resulting clear, colourless solution cooled to -78°C. A freshly prepared solution of Li[TeSiMe$_3$] (0.48 mmol in 5 mL THF) was added to [(IPr)AuCl] at -78°C. The clear, orange solution was warmed to room temperature and then stirred for an additional 1 hour. The solvent was removed *in vacuo*, leaving an orange/white residue that was extracted in toluene. This was then doubly filtered through dry Celite® and the light yellow filtrate concentrated. Layering with pentane and storing this solution at -25°C overnight resulting in the formation of colourless, rapidly desolvating crystals of [(IPr)AuTeSiMe$_3$] which were dried under dynamic vacuum to give a light brown solid (55% yield); **m.p.** 177-182°C (dec). **^{1}H NMR** (CDCl$_3$, 25°C, 599.301 MHz) δ7.48 (2H, t, $^3J_{H\text{-}H}$ = 7.6 Hz, CH$_{Ar}$), 7.28 (4H, d, $^3J_{H\text{-}H}$ = 7.6 Hz, CH$_{Ar}$), 7.14 (2H, s, CH$_{imid}$), 2.63 (4H, sept, $^3J_{H\text{-}H}$ = 7.1 Hz, C*H*(CH$_3$)$_2$), 1.38 (12H, d, $^3J_{H\text{-}H}$ = 7.1 Hz, CH(C*H*$_3$)$_2$), 1.22 (12H, d, $^3J_{H\text{-}H}$ = 7.1 Hz, CH(C*H*$_3$)$_2$), 0.18 (9H, s, Si(C*H*$_3$)$_3$). **^{13}C{^{1}H} NMR** (CDCl$_3$, 25°C, 150.78 MHz) δ194.0 (s, *C*-Au), 145.6 (s, C$_{Ar}$), 134.3 (s, C$_{Ar}$), 130.4 (C$_{Ar}$), 124.1 (s, C$_{Ar}$), 122.5 (s, C$_{imid}$), 28.8 (s, *C*H(CH$_3$)$_3$), 24.5 (s, CH(*C*H$_3$)$_3$), 24.1 (s, CH(*C*H$_3$)$_3$), 8.2

(TeSi(CH_3)$_3$); **^{29}Si NMR** ($CDCl_3$, 25°C, 119.055 MHz) δ-12 (s, Te*Si*(CH_3)$_3$, $^1J_{Te\text{-}Si}$ not resolved); **^{125}Te NMR** ($CDCl_3$, 25°C, 189.32 MHz) δ -1071 (s, *Te*Si(CH_3)$_3$), -1071(d, $^1J_{Te\text{-}Si}$ = 296 Hz, *Te*^{29}Si(CH_3)$_3$). **Anal. Calcd** for $C_{30}H_{45}AuN_2SiTe$: C, 45.82; H, 5.77; N, 3.56. Found C, 46.06; H 5.91; N 3.45.

Synthesis of [$Au_4Ag_4S_4$(IPr)$_4$] (2.2a)

[(IPr)AuSSiMe_3] (100 mg, 0.145 mmol) and [(Ph_3P)AgOAc] (62 mg, 0.145 mmol) were transferred into separate Schlenk flasks under nitrogen and each was dissolved in 5 mL anhydrous THF. The solutions were cooled to -78°C. [(IPr)AuSSiMe_3] was added to [(Ph_3P)AgOAc] and the solution slowly warmed to -25°C, resulting in a golden-brown colour. This was stored at -25°C overnight then stirred at room temperature for five hours at which point the reaction mixture was layered with 30 mL pentane. Storing the solution for 3 days resulted in the formation of colourless crystals of [$Au_4Ag_4S_4$(IPr)$_4$] and some brown material at the bottom of the flask. This dark material was dissolved in THF and removed selectively. The remaining crystals were washed with pentane and vacuum dried, affording [$Au_4Ag_4S_4$(IPr)$_4$] as an analytically pure white solid (49% yield); **m. p.** 242-246°C (dec) **^{1}H NMR** ($CDCl_3$, 25°C, 599.301 MHz) δ7.44 (2H, t, $^3J_{H\text{-}H}$ = 7.2 Hz, CH_{Ar}), 7.26 (4H, d, $^3J_{H\text{-}H}$ = 7.2 Hz, CH_{Ar}), 7.03 (2H, s, CH_{imid}), 2.55 (4H, sept, $^3J_{H\text{-}H}$ = 6.6 Hz, C*H*(CH_3)$_2$), 1.34 (12H, d, $^3J_{H\text{-}H}$ = 6.6 Hz, CH(C*H*$_3$)$_2$), 1.15 (12H, d, $^3J_{H\text{-}H}$ = 6.6 Hz, CH(C*H*$_3$)$_2$). **^{13}C{^{1}H} NMR** ($CDCl_3$, 25°C, 150.78 MHz) δ189.7 (s, *C*-Au), 145.3 (s, C_{Ar}), 134.6 (s, C_{Ar}), 130.4 (s, C_{Ar}), 124.5 (s, C_{Ar}), 121.8 (s, C_{imid}), 28.8 (s, *C*H(CH_3)$_2$), 25.4 (s, CH(*C*H$_3$)$_2$), 24.2 (s, CH(*C*H$_3$)$_2$). **Anal. Calcd** for $C_{108}H_{144}Ag_4Au_4N_8S_4$: C, 44.70; H, 5.00; N, 3.86; S, 4.42. Found C, 44.48; H, 4.91; N, 3.68; S, 4.14.

Synthesis of [$Au_4Ag_4Se_4$(IPr)$_4$] (2.2b)

As described for **2.2a** with 100 mg (0.136 mmol) **1a** and 58 mg (0.136 mmol) [Ph_3PAgOAc] in 5 mL THF (36% yield); **^{1}H NMR** ($CDCl_3$, 25°C, 599.301 MHz) δ7.44 (2H, t, $^3J_{H\text{-}H}$ = 7.8 Hz, CH_{Ar}), 7.26 (4H, d, $^3J_{H\text{-}H}$ = 7.8 Hz, CH_{Ar}), 7.02 (2H, s, CH_{imid}), 2.55 (4H, sept, $^3J_{H\text{-}H}$ = 6.8 Hz, C*H*(CH_3)$_2$), 1.35 (12H, d, $^3J_{H\text{-}H}$ = 6.8 Hz, CH(C*H*$_3$)$_2$), 1.15 (12H, d, $^3J_{H\text{-}H}$ = 6.8 Hz, CH(C*H*$_3$)$_2$). **^{13}C{^{1}H} NMR** (CDCl, 25°C, 150.78 MHz) δ192.5 (s, *C*-Au), 145.2 (s, C_{Ar}), 134.5 (s, C_{Ar}), 130.4 (s, C_{Ar}), 124.4 (s, C_{Ar}), 121.8 (s, C_{imid}), 28.8 (s, *C*H(CH_3)$_2$), 25.5 (s, CH(*C*H$_3$)$_2$), 24.1 (s, CH(*C*H$_3$)$_2$). **^{77}Se NMR** ($CDCl_3$, 0°C, 114.38 MHz) δ-655 (t, $^1J_{Se\text{-}Ag}$ = 17 Hz, *Se*Ag_2Au;

resolution between ^{107}Ag and ^{109}Ag not obtained). **Anal. Calcd** for $C_{108}H_{144}Ag_4Au_4N_8Se_4$: C, 41.99; H, 4.70; N, 3.63. Found C, 42.38; H, 4.73; N, 3.56.

Synthesis of [$Au_8S_4(IPr)_4$] (2.3a)

[(IPr)AuSSiMe$_3$] (55 mg, 0.0796 mmol) and [({2,4-^{t}Bu(C_6H_3)O}$_3$P)AuOAc] (72 mg, 0.0796 mmol) were dissolved separately in 4 mL THF each and cooled to -78°C. The solutions were combined and stirred while slowly warming to -25°C. The mixture was stored overnight at this temperature then stirred an additional hour at room temperature. The solvent was removed in vacuo and the residual oily solid was dissolved in 4 mL Et_2O. Colourless prismatic crystals suitable for X-ray diffraction were grown by layering with 30 mL hexanes and leaving the solution at -25°C for three days. The resulting crystals were washed with 3:1 diethyl ether/hexanes and obtained as a white powder (48% yield); **^{1}H NMR** ($CDCl_3$, 25°C, 599.301 MHz) δ7.42 (2H, t, $^3J_{H-H}$ = 7.8 Hz, CH_{Ar}), 7.23 (4H, d, $^3J_{H-H}$ = 7.8 Hz, CH_{Ar}), 7.04 (2H, s, CH_{imid}), 2.60 (4H, sept, $^3J_{H-H}$ = 6.9 Hz, C*H*(CH_3)$_2$), 1.35 (12H, d, $^3J_{H-H}$ = 6.9 Hz, CH(C*H*$_3$)$_2$), 1.15 (12H, d, $^3J_{H-H}$ = 6.9 Hz, CH(C*H*$_3$)$_2$). **^{13}C{^{1}H} NMR** (CDCl3, 25°C, 150.78 MHz) δ186.2 (s, *C*-Au), 145.4 (s, C_{Ar}), 134.6 (s, C_{Ar}), 130.3 (s, C_{Ar}), 124.2 (s, C_{Ar}), 121.9 (s, C_{imid}), 28.8 (s, *C*H(CH_3)$_2$), 25.0 (s, CH(*C*H$_3$)$_2$), 24.2 (s, CH(*C*H$_3$)$_2$). **Anal. Calcd** for $C_{108}H_{144}Ag_4Au_4N_8S_4$: C, 39.81; H, 4.45; N, 3.44; S, 3.94 Found C, 39.35; H, 4.59; N, 3.20; S, 4.40.

Synthesis of [$Au_8Se_4(IPr)_4$] (2.3b)

As described for **2.3a** with 0.108 mmol [(IPr)AuSeSiMe$_3$] (39% yield); **^{1}H NMR** ($CDCl_3$, 25°C, 599.301 MHz) δ7.43 (2H, t, $^3J_{H-H}$ = 7.8 Hz, CH_{Ar}), 7.22 (4H, d, $^3J_{H-H}$ = 7.8 Hz, CH_{Ar}), 7.03 (2H, s, CH_{imid}), 2.59 (4H, sept, $^3J_{H-H}$ = 6.7 Hz, C*H*(CH_3)$_2$), 1.34 (12H, d, $^3J_{H-H}$ = 6.7 Hz, CH(C*H*$_3$)$_2$), 1.15 (12H, d, $^3J_{H-H}$ = 6.7 Hz, CH(C*H*$_3$)$_2$). **^{13}C{^{1}H} NMR** (CDCl3, 25°C, 150.78 MHz) δ188.4 (s, *C*-Au), 145.4 (s, C_{Ar}), 134.6 (s, C_{Ar}), 130.2 (s, C_{Ar}), 124.2 (s, C_{Ar}), 121.8 (s, C_{imid}), 28.8 (s, *C*H(CH_3)$_2$), 25.1 (s, CH(*C*H$_3$)$_2$), 24.2 (s, CH(*C*H$_3$)$_2$). **^{77}Se NMR** ($CDCl_3$, 0°C, 114.38 MHz) δ-517 (s, *Se*Au_3) **Anal. Calcd** for $C_{108}H_{144}Ag_4Au_4N_8Se_4$: C, 37.64; H, 4.21; N, 3.25 Found C, 38.33; H, 4.11; N, 3.25.

Synthesis of [$Au_8Te_4(IPr)_4$] (2.3c)

[(IPr)AuTeSiMe_3] (55 mg, 0.0698 mmol) and [(Ph_3P)AuOAc] (36 mg, 0.0698 mmol) were dissolved separately in 3 mL cold (-78°C) THF each and stirred to aid dissolution. The two compounds were mixed and stirred for a few minutes at -78°C to afford a red solution. The mixture was then layered with 30 mL hexanes and stored on dry ice for four days after which time, the Schlenk tube was transferred to -25°C. After another four days, colourless crystals formed above a red film. The crystals were removed and recrystallized from THF/pentane at room temperature to afford the title complex as colourless crystals which discolour to brown over time (28% yield); **^{1}H NMR** ($CDCl_3$, 0°C, 599.301 MHz) δ7.43 (2H, t, $^3J_{H\text{-}H}$ = 7.8 Hz, CH_{Ar}), 7.23 (4H, d, $^3J_{H\text{-}H}$ = 7.8 Hz, CH_{Ar}), 7.02 (2H, s, CH_{imid}), 2.60 (4H, sept, $^3J_{H\text{-}H}$ = 6.7 Hz, C*H*(CH_3)$_2$), 1.34 (12H, d, $^3J_{H\text{-}H}$ = 6.7 Hz, CH(C*H*$_3$)$_2$), 1.15 (12H, d, $^3J_{H\text{-}H}$ = 6.7 Hz, CH(C*H*$_3$)$_2$). **^{125}Te NMR** ($CDCl_3$, 0°C, 189.32 MHz) δ -1050 (s, *Te*Au_3).

2.3.3 X-Ray Crystallography Details

X-ray measurements were made on a Bruker Kappa Axis Apex2 diffractometer equipped with graphite monochromated Mo Kα (λ=0.71073 Å) radiation at a temperature of 110 K. The samples were mounted on a Mitegen polyimide micromount with a small amount of Paratone N oil. The structure was solved by using direct methodologies using the SHELXT program.[60] All non-hydrogen atoms were obtained from the initial solution and hydrogen atoms were introduced at idealized positions and were allowed to ride on the parent atom. The structural model was fit to the data using full matrix least-squares based on *F*. The calculated structure factors included corrections for anomalous dispersion from the usual tabulation. The structures were refined using the SHELXL-2014 program from the SHELXTL suite of crystallographic software. For compounds **2.2b** and **2.3b** a twin law was derived using COSET software.[61]

CCDC 1526645-1526646 for **2.2a** and **2.2b**, respectively, and CCDC 1559057-1559059 for **2.3a-c**, respectively, contain the supplementary crystallographic data for this paper. These data are provided free of charge by The Cambridge Crystallographic Data Center via www.ccdc.cam.ac.uk/data_request/cif.

2.4 Conclusions and Outlook

In summary, NHC ligands provide remarkable stability to [LAuESiMe$_3$] reagents, while retaining their high cluster-forming reactivity; readily yielding highly crystalline, solution processable, and functional gold(I) chalcogenide clusters. NHCs are found to be valuable for stabilizing a particular cluster framework, allowing the photophysical properties to be fine-tuned by the choice of metal ions and chalcogen centres. Furthermore, the nature of the emission is found to be influenced by the electron accepting ability of the NHC ligands, allowing even greater tunability of the optical properties through ancillary ligand modifications. Bidentate ligands are of special interest as they may lead to clusters of higher nuclearity through their bridging modes and help to increase quantum yield through greater structural rigidity.

We are also interested in exploring the reduction chemistry of the metal chalcogenide clusters reported in this chapter. It is well-known that reduction of gold(I)-thiolate precursors [Au(SR)]$_n$ gives thiolate-capped gold nanoclusters. In 2007, the first structural characterization of such species was provided for Au$_{102}$(*p*-MBA)$_{44}$ (*p*-MBA = *p*-mercaptobenzoic acid) .[62] Since then the field of atomically precise reduced gold nanostructures has gained widespread interest.[63] In 2017, Schnepf showed that gold nanoclusters with a Au(0) core stabilized by a gold(I)-sulfide and gold(I)-phosphine shell could be prepared by reduction of the precursor [(Ph$_3$P)AuSC(SiMe$_3$)$_3$].[64,65] Considering the clusters reported here as metal "aurachalcogenolate" precursors [M{EAu(IPr)}]$_4$, it is reasonable to suppose that their reduction could lead to similar clusters; potentially bimetallic group 11 nanoclusters with an M(0) core stabilized by a gold(I)-chalcogenide and gold(I)-NHC shell. This work would parallel that of Crudden *et al.* in introducing NHC ligands to gold(I) nanoparticle systems.[37]

2.5 References

[1] R. F. Ziolo, S. Lipton, Z. Dori. *J. Chem. Soc. D* **1970**, 1124
[2] V. W.-W. Yam, V. K.-M. Au, S. Y.-L. Leung. *Chem. Rev.* **2015**, *115*, 7589.
[3] V. W.-W. Yam, K. M.-C. Wong. *Chem. Commun.* **2011**, *47*, 11579.
[4] *Modern Supramolecular Gold Chemistry: Gold-Metal Interactions and Applications*; Laguna, A., Ed.; Wiley: Weinheim, Germany, 2008.
[5] H. Schmidbaur, A. Schier. *Chem. Soc. Rev.* **2008**, *37*, 1931.
[6] P. Pyykkö. *Angew. Chem. Int. Ed.* **2004**, *43*, 4412.
[7] C. King, J.-C. Wang, Md. N. I. Khan, J. P. Fackler, Jr. *Inorg. Chem.* **1989**, *28*, 2145.
[8] H. Schmidbaur, A. Schier, *Chem. Soc. Rev.* **2012**, *41*, 370.
[9] M. C. Gimeno, A. Laguna. *Chem. Soc. Rev.* **2008**, *37*, 1952.
[10] W. W. Xu, X. C. Zeng, Y. Gao. *Nanoscale* **2017**, *9*, 8990.
[11] J. R. Shakirova, E. V. Grachova, V. V. Sizov, G. L. Starova, I. O. Koshevoy, A. S. Melnikov, M. C. Gimeno, A. Laguna, S. P. Tunik. *Dalton Trans.* **2017**, *46*, 2516.
[12] L.-Y. Yao, V. W.-W. Yam. *J. Am. Chem. Soc.* **2015**, *137*, 3506.
[13] W. Yu, L. Guggolz, O. Fuhr, D. Fenske, S. Dehnen. *Dalton Trans.* **2015**, *44*, 9363.
[14] L.-Y. Yao, F. K.-W. Hau, V. W.-W. Yam. *J. Am. Chem. Soc.* **2014**, *136*, 10801.
[15] E. C.-C. Cheng, W.-Y. Lo, T. K.-M. Lee, N. Zhu, V. W.-W. Yam. *Inorg. Chem*. **2014**, *53*, 3854.
[16] L.-Q. Mo, J.-H. Jia, L.-j. Sun, Q.-M. Wang. *Chem. Commun.* **2012**, *48*, 8691.
[17] T. K.-M. Lee, N. Zhu, V. W.-W. Yam. *J. Am. Chem. Soc.* **2010**, *132*, 17646.
[18] Q.-M. Wang, Y.-A. Lee, O. Crespo, J. Deaton, C. Tang, H. J. Gysling, M. C. Gimeno, C. Larraz, M. D. Villacampa, A. Laguna, R. Eisenberg. *J. Am. Chem. Soc.* **2004**, *126*, 9488.
[19] J. Olkowska- Oetzel, P. Sevillano, A. Eichhöfer, D. Fenske. *Eur. J. Inorg. Chem.* **2004**, 1100.
[20] V. W.-W. Yam, E. C.-C. Cheng, N. Zhu. *Angew. Chem. Int. Ed.* **2001**, *40*, 1763.
[21] V. W.-W. Yam, E. C.-C. Cheng, Z.-Y. Zhou, *Angew. Chem. Int. Ed.* **2000**, *39*, 1683.
[22] S. Canales, O. Crespo, M. C. Gimeno, P. G. Jones, A. Laguna, F. Mendizabal. *Organometallics* **2000**, *19*, 4985.
[23] D. Fenske, T. Langetepe, M. M. Kappes, O. Hampe, P. Weis. *Angew. Chem. Int. Ed.* **2000**, *39*, 1857.
[24] K. Angermaier, H. Schmidbaur. *Z. Naturforsch., B: J. Chem. Sci.* **1996**, *51*, 879.
[25] F. Canales, M. C. Gimeno, A. Laguna, M. D. Villacampa. *Inorg. Chim. Acta* **1996**, *244*, 95.
[26] E. M. Gussenhoven, J. C. Fettinger, D. M. Pham, M. M. Malwitz, A. L. Balch. *J. Am. Chem. Soc.* **2005**, *127*, 10838.
[27] J. Vicente, M.-T. Chicote, P. Gonzàlez-Herrero, C. Grünwald. *Organometallics* **1997**, *16*, 3381.
[28] F. Canales, M. C. Gimeno, A. Laguna, P. G. Jones. *J. Am. Chem. Soc.* **1996**, *118*, 4839.
[29] *N-Heterocyclic Carbenes: From Laboratory Curiosities to Efficient Synthetic Tools*; Díez-González, S., Ed.; Royal Society of Chemistry: Cambridge, U.K., 2011.
[30] N. Marion, S. P. Nolan. *Chem. Soc. Rev.* **2008**, *37*, 1776.
[31] C.-H. Wang, W.-C. Shih, H. C. Chang, Y.-Y. Kuo, W.-C. Hung, T.-G. Ong, W.-S. Li. *J. Med. Chem.* **2011**, *54*, 5245.
[32] K. M. Hindi, M. J. Panzner, C. A. Tessier, C. L. Cannon, W. J. Youngs. *Chem. Rev.* **2009**, *109*, 3859.

[33] N. Sinha, T. T. Y. Tan, E. Peris, F. E. Hahn. *Angew. Chem. Int. Ed.* **2017**, *56*, 7393.
[34] J. Ruiz, L. García, D. Sol, M. Vivanco. *Angew. Chem. Int. Ed.* **2016**, *55*, 8386.
[35] C. M. Crudden, J. H. Horton, I. I. Ebralidze, O. V. Zenkina, A. B. McLean, B. Drevniok, Z. She, H.-B. Kraatz, N. J. Mosey, T. Seki, E. C. Keske, J. D. Leake, A. Rousina-Webb, G. Wu. *Nat. Chem.* **2014**, *6*, 409.
[36] X. Ling, S. Roland, M.-P. Pileni. *Chem. Mater.* **2015**, *27*, 414.
[37] K. Salorinne, R. W. Y. Man, C.-H. Li, M. Taki, M. Nambo, C. M. Crudden. *Angew. Chem., Int. Ed.* **2017**, *56*, 6198.
[38] C. E. Strasser, V. J. Catalano. *J. Am. Chem. Soc.* **2010**, *132*, 10009.
[39] R. Visbal, M. C. Gimeno. *Chem. Soc. Rev.* **2014**, *43*, 3551.
[40] A. A. Penney, V. V. Sizov, E. V. Grachova, D. V. Krupenya, V. V. Gurzhiy, G. L. Starova, S. P. Tunik. *Inorg. Chem.* **2016**, *55*, 4720.
[41] B. Choi, D. W. Paley, T. Siegrist, M. L. Steigerwald, X. Roy. *Inorg. Chem.* **2015**, *54*, 8348.
[42] M. Azizpoor Fard, F. Weigend, J. F. Corrigan. *Chem. Commun.* **2015**, *51*, 8361.
[43] M. Azizpoor Fard, T. I. Levchenko, C. Cadogan, W. J. Humenny, J. F. Corrigan. *Chem. - Eur. J.* **2016**, *22*, 4543.
[44] J. Zhai, A. S. Filatov, G. L. Hillhouse, M. D. Hopkins. *Chem. Sci.* **2016**, *7*, 589.
[45] D. T. T. Tran, J. F. Corrigan. *Organometallics* **2000**, *19*, 5202.
[46] J. E. Drake, B. M. Glanvincevski, R. Humphries, A. Majid. *Can. J. Chem.* **1979**, *57*, 3253.
[47] P. J. Bonasia, D. E. Gindelberger, J. Arnold. *Inorg. Chem.* **1993**, *32*, 5126.
[48] H. Lange, U. Herzog. *J. Organomet. Chem.* **2002**, *660*, 36.
[49] O. Bumbu, C. Ceamanos, O. Crespo, M. C. Gimeno, A. Laguna, C. Silvestru, M. D. Villacampa. *Inorg. Chem.* **2007**, *46*, 11457.
[50] F. Furche, R. Ahlrichs, C. Hättig, W. Klopper, M. Sierka, F. Weigend. *Wiley Interdiscip. Rev.: Comput. Mol. Sci.* **2014**, *4*, 91.
[51] A. D. Becke. *J. Chem. Phys.* **1993**, *98*, 5648.
[52] C. Lee, W. Yang, R. G. Parr. *Phys. Rev. B: Condens. Matter Mater. Phys*. **1988**, *37*, 785.
[53] F. Weigend, R. Ahlrichs. *Phys. Chem. Chem. Phys.* **2005**, *7*, 3297.
[54] Mulliken, R. S. J. Chem. Phys. 1955, 23, 1833.
[55] M. Kühn, F. Weigend. *J. Chem. Phys.* **2014**, *141*, 224302.
[56] A. Collado, A. Gómez-Suárez, A. R. Martin, A. M. Z. Slawin, S. P. Nolan, *Chem. Commun.* **2013**, *49*, 5541-5543.
[57] D. Taher, A. I. Wallbank, E. A. Turner, H. L. Cuthbert, J. F. Corrigan, *Eur. J. Inorg. Chem.* **2006**, 4616-4620.
[58] D. I. Nichols, A. S. Charleston, *J. Chem. Soc. A* **1969**, 2581-2583.
[59] J. McNulty, K. Keskar, *Eur. J. Org. Chem.* **2012**, 5462-5470.
[60] Sheldrick, G. M.; SHELXTL PC Version 6.1 An Integrated System for Solving, Refining, and Displaying Crystal Structures from Diffraction Data, Bruker Analytical X-ray Systems, **2000**.
[61] P. D. Boyle, *J. Appl. Cryst.*, **2014**, *47*, 467-470.
[62] P. D. Jadzinsky, G. Calero, C. J. Ackerson, D. A. Bushnell and R. D. Kornberg, *Science*, **2007**, *318*, 430.
[63] R. Jin, C. Zeng, M. Zhou, Y. Chen. *Chem. Rev.* **2016**, *116*, 10346.
[64] S. Kenzler, C. Schrenk, A. Schnepf. *Angew. Chem. Int. Ed.* **2017**, *56*, 393.
[65] S. Kenzler, C. Schrenk, A. R. Frojd, H. Häkkinen, A. Z. Clayborne, A. Schnepf. *Chem. Commun.* **2018**, *54*, 248.

Chapter 3

3 Plug and Play: Tunable Metal/Chalcogen Composition in Copper(I)-Chalcogenide Self-Assemblies Enabled by Cyclic (Alkyl)(amino)carbenes

3.1 Introduction

Copper(I) chalcogenide complexes are of substantial research interest because of their dramatic structural variability and important roles as N_2O reductase model compounds,[1,2] semiconducting nanomaterials,[3] and precursors to ternary semiconductors.[4] With the emergence of Cu(I) complexes as inexpensive alternatives to phosphors based on the platinum group metals,[5] Cu(I) chalcogenides have also generated interest as phosphorescent materials. Eichhöfer, and co-workers have quantified luminescence efficiencies in a series of red-emitting '$Cu_{12}E_6$' (E = S, Se) clusters with quantum yields up to 0.67 in the solid state.[6,7] Mixed coinage-metal-chalcogenide clusters have tunable emissions over the visible range of the spectrum, for example in the series [(μ_3-E){Au(P-N)}$_3$M] (E = O, S, Se; P-N = pyridylphosphine; M = Cu, Ag; λ_{em} 520 – 725 nm).[8]

Motivated by the favourable properties of Cu(I) carbene complexes (e.g. stability, solubility, tunability, ease of synthesis, and intense luminescence),[9-14] an interest has developed in Cu(I) chalcogenide clusters with carbene ancillary ligands.[15-18] To date, imidazolylidene-based carbenes have been used as ligands in these assemblies, and one luminescent compound has been reported.[18] Cyclic (alkyl)(amino)carbenes (CAACs) have comparatively superior σ-donating and π-accepting abilities,[19] and Cu(I)-CAAC complexes are intensely researched due to their rich photophysical properties.[20-24] Cu(I) chalcogenide clusters with CAAC ancillary ligands are therefore attractive synthetic targets for new types of structural chemistry and potential photophysical properties. Herein, CAACs are found to be uniquely capable of stabilizing self-assembled homo- and heterometallic clusters with a tunable coinage metal-chalcogenide core and fixed CAAC-Cu(I) surface, with photophysical properties that vary as a function of metal/chalcogen composition.

In this section, a series of homo- and heterometallic copper(I) chalcogenide clusters with the CAAC 2-(2,6-diisopropylphenyl)-3,3-dimethyl-2-azaspiro[4.5]dec-1-ylidene (**CAAC^{Cy}**) is described.[25] From [(CAAC^{Cy})CuOAc] (**3.1**), copper(I) trimethylsilyl-thiolate and -selenolates [(CAAC^{Cy})CuESiMe$_3$] (E = S **3.2a**; Se **3.2b**) are synthesized in good yields. These react with phosphine- or phosphite-solubilized group 11 metal acetate complexes to yield octanuclear clusters [Cu$_4$M$_4$(μ_3-E)$_4$(CAAC^{Cy})$_4$] (M = Cu, **3.3**; Ag, **3.4**; Au, **3.5**). Attempts to produce analogous IPr-stabilized clusters from [(IPr)CuESiMe$_3$] (IPr = 1,3-bis(2,6-diisopropylphenyl)imidazole-2-ylidene)[17] were unsuccessful, giving instead thermally unstable mixtures of products. The enhanced donor properties of CAACs are clearly crucial in stabilizing the Cu(I) chalcogenide cluster framework. For all compounds, long lived (τ > 30 μs) phosphorescence was observed. The emission colour of the clusters varies from green (538 nm) to orange (618 nm), depending on the identity of both the heterometal (M) and the chalcogen.

3.2 Results and Discussion

CAAC^{Cy} was generated by treating CAAC^{Cy}·HBF$_4$ with 1.25 equivalents of K[N(SiMe$_3$)$_2$] in toluene. Adding this to a suspension of CuOAc in toluene yielded the mononuclear carbene adduct [(CAAC^{Cy})CuOAc] (**3.1**) in 30% yield after 8 hours (Scheme 3.1). Prolonged reaction times resulted in decomposition via disproportionation of the Cu(I) complex, as also reported for related compounds.[20] Reactions of equimolar amounts of **3.1** and E(SiMe$_3$)$_2$ in THF at -30°C, followed by extraction of the product into hydrocarbons, filtration, and removal of the solvent yield analytically pure [(CAAC^{Cy})CuESiMe$_3$] (E = S, **3.2a**; E = Se, **3.2b**) as thermally-stable off-white solids in 41 and 59% yield, respectively (Scheme 3.1). Based on the similarity in steric bulk between IPr (%V$_{bur}$ = 47.6)[26] and CAAC^{Cy} (44.8%),[27] we propose mononuclear linear complexes like [(IPr)CuESiMe$_3$].[17]

The NMR spectra of **3.1** and **3.2** are consistent with the proposed linear structures (Figure 3.1). In all cases, a singlet set of signals for CAAC^{Cy} is present, accompanied by a broad singlet (1.87 ppm) for the acetate group of **3.1** and high field singlets at 0.11 and 0.23 ppm, respectively for the trimethylsilyl protons of **3.2a** and **3.2b**, respectively. In the aromatic region, a triplet (7.37 – 7.38 ppm) and doublet (7.23 – 7.24 ppm) are assigned to the *para*- and *meta*- protons of 2,6-diisopropylphenyl. At lower fields, the septet (2.82 – 2.83 ppm) and two doublets (1.34 – 1.29

ppm) are present for the isopropyl moieties. A singlet at 2.06 ppm in all three complexes integrating to two protons is assigned to the methylene protons in the pyrrolidylidene backbone. Another singlet at 1.33 – 1.34 ppm corresponds to the two chemically equivalent methyl groups on the pyrrolidylidene backbone. The remaining signals, integrating to ten protons, are for the cyclohexyl moiety.

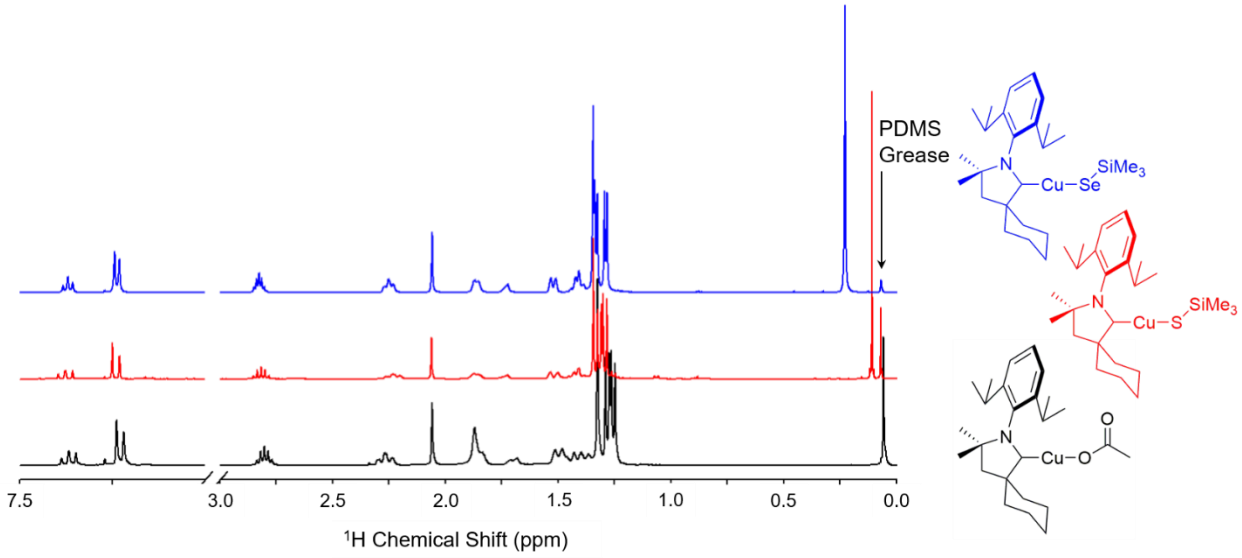

Figure 3.1 ^{1}H NMR spectra for **3.1-2** in $CDCl_3$ at 298K.

In metal trimethylsilylchalcogenolate compounds, the reactive E-Si bond can be cleaved with metal halide or carboxylate (M-X) compounds to yield homo- or heterometallic chalcogen cluster compounds, driven by the formation of X-$SiMe_3$. It was recently communicated that phosphine- or phosphite-supported coinage metal acetate compounds can react analogously, while limiting uncontrolled condensation side-reactions.[28] Reactions of equimolar amounts of **3.2a** and **3.2b** with [(Ph_3P)MOAc] (M = Cu, Ag) yield octanuclear clusters [$Cu_8(\mu_3\text{-E})_4(CAAC^{Cy})_4$] (E = S, **3.3a**; Se, **3.3b**) and [$Cu_4Ag_4(\mu_3\text{-E})_4(CAAC^{Cy})_4$] (E = S, **3.4a**; Se **3.4b**) in yields of 40 – 59%. Reaction with [{$(ArO)_3P$}AuOAc] (Ar = 2,4-*t*Bu(C_6H_3O)) gives different results for E = S and Se. For **3.2b**, only $AcOSiMe_3$ elimination occurs, yielding [$Cu_4Au_4(\mu_3\text{-Se})_4(CAAC^{Cy})_4$] (**3.5b**) selectively in 66% yield (Scheme 3.1). For **3.2a**, $AcOSiMe_3$ elimination occurs alongside carbene transfer from Cu to Au, as also observed between [($CAAC^{Cy}$)CuCl] and [(Me_2S)AuCl].[29] Energy Dispersive X-Ray Spectroscopy on single crystals of **3.5a** indicate the expected 1:1:1 ratio of Cu,

Au, and S in the product, however no satisfactory structural model for the eight metal positions could be obtained from single-crystal X-ray diffraction (SCXRD) analysis. The different reaction products might be attributed to the more reactive nature of **3.2b** relative to **3.2a**, resulting in greater kinetic control at low reaction temperatures.

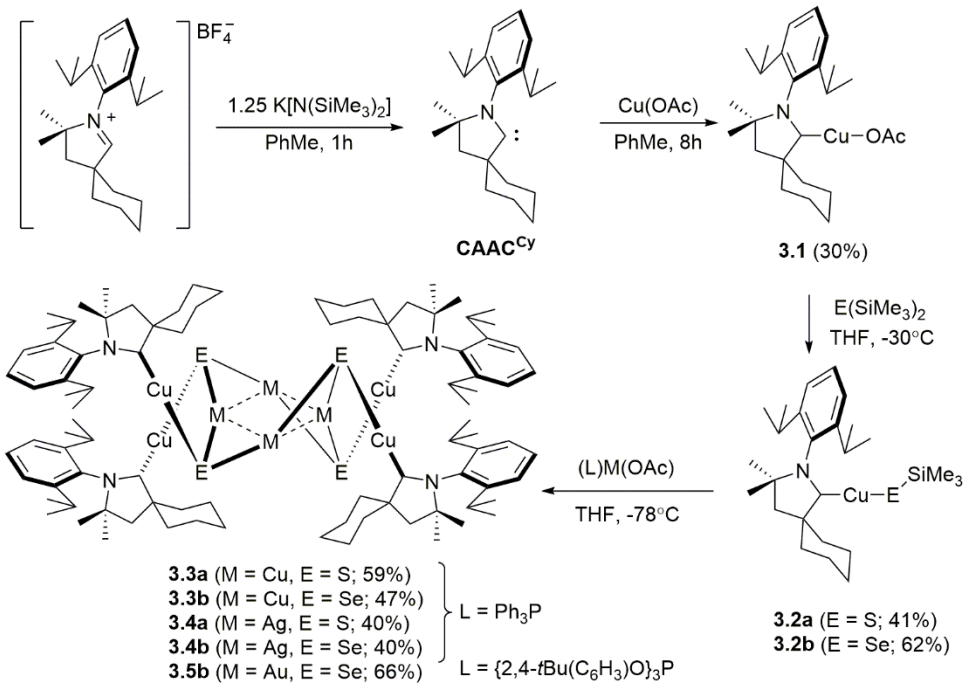

Scheme 3.1 Synthesis of **CAAC^{Cy}** and **3.1–5**. Dashed lines are drawn between the four central centers to indicate metallophilic interactions. Interactions between Au and M are omitted for clarity.

SCXRD analysis of **3.3**–**5** indicates that the clusters are isostructural and isomorphous, crystallizing in the monoclinic space group C2/*c* (Figure 3.2). The inorganic core consists of four 'CuM$_2$E' tetrahedra linked through the M atoms into a cyclic tetramer. The capping μ_3-E^{2-} ligands are pyramidally coordinated and adjacent units are *trans*-disposed to prevent steric clash of outer Cu(CAAC^{Cy}) moieties. CAAC^{Cy} is oriented with the smaller cyclohexyl groups toward the interior of the cluster. Short, non-bonding M-M′ contacts below the sum of the corresponding van der Waals radii are observed, indicating attractive metallophilic interactions are probably present and important in cluster formation and stability. Selected bond lengths and angles are presented in Table 3.1.

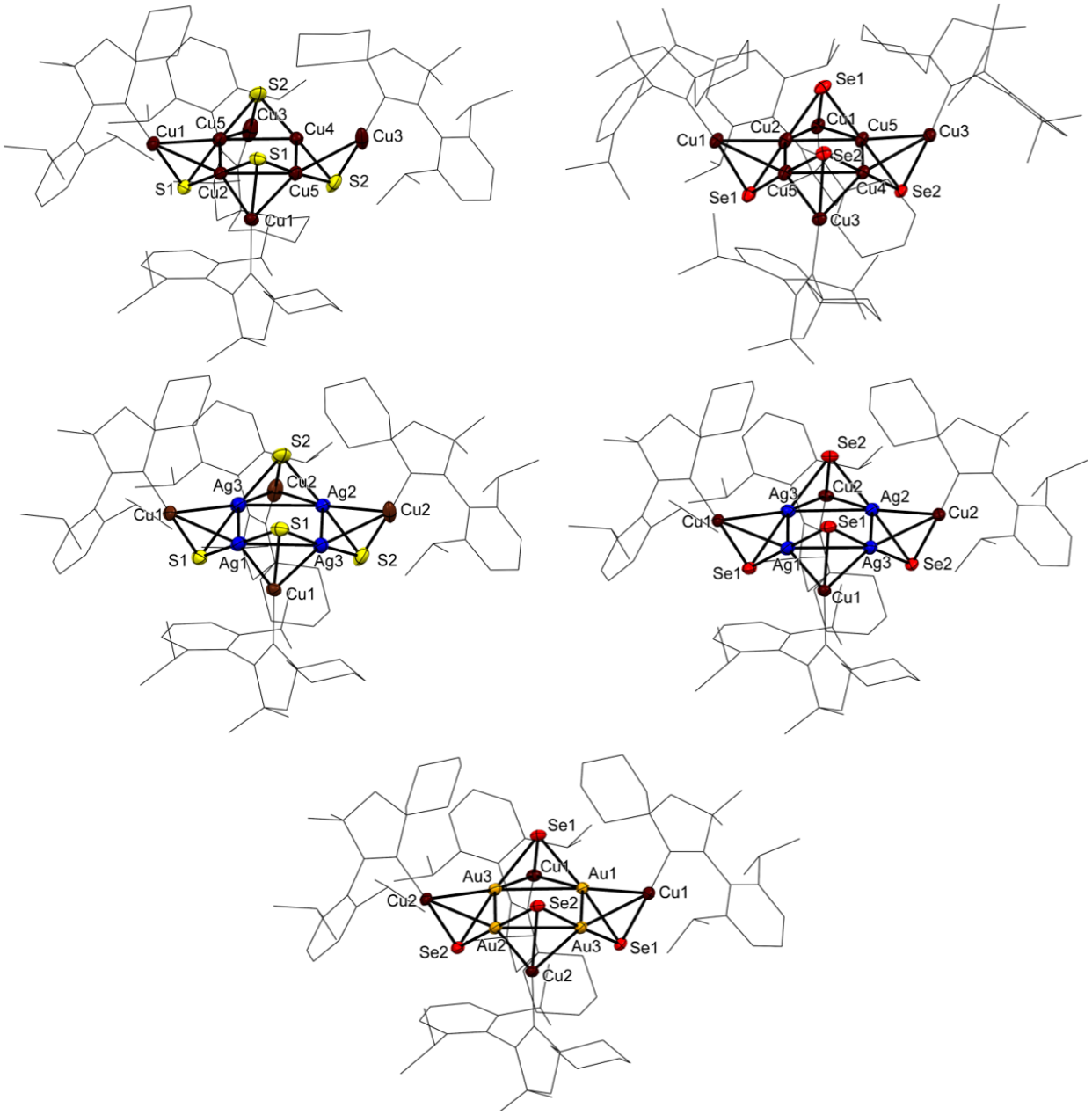

Figure 3.2 Molecular structures of **3.3**–**5** in the crystal. The core metal and chalcogen atoms are represented by thermal ellipsoids plotted at the 50% probability level. CAAC ligands are represented as wireframe drawings. Bonds are drawn between two metal atoms when their separation is less than the sum of their van der Waals radii, but should not be interpreted as covalent interactions. All hydrogen atoms and one co-crystallizing THF molecules have been omitted for clarity. The molecules crystallized about the intersection of a 2-fold axis through M1-M2/Cu2-Cu4 and a c-glide containing M3/Cu5. Colour scheme: S, yellow; Se, red; Cu, brown; Au, orange; Ag, blue.

Table 3.1 Selected bonds lengths (Å) and angles (°) for **3.3-5**. See Figure 3.2 for the atomic numbering scheme.

	3.3a **M = Cu**[a] **E = S**	**3.3b** **M = Cu**[a] **E = Se**	**3.4a** **M = Ag** **E = S**	**3.4b** **M = Ag** **E = Se**	**3.5b** **M = Au** **E = Se**
C-Cu	1.881(4)3	1.881(6)	1.879(4)	1.881(5)	1.886(6)
Cu-E	2.1321(11)[b] – 2.1596(10)	2.2509(10)[b] – 2.2532(10)	2.1166(19) – 2.1250(14)	2.2420(8) – 2.2438(7)	2.2641(9) – 2.2654(9)
M-E	2.1779(11) – 2.1806(13)	2.2812(6) – 2.3072(10)	2.3422(14) – 2.3876(15)	2.4603(5) – 2.5012(6)	2.4372(6) – 2.4636(6)
Cu-M	2.6599(5) – 2.9134(6)	2.6597(8) – 2.8469(10)	2.7589(6) – 2.9470(7)	2.7846(6) – 2.9080(6)	2.7422(7) – 2.9450(7)
M-M	2.6297(7) – 2.6916(7)	2.6199(11) – 2.6675(11)	2.8711(5) – 2.9499(5)	2.8162(7) – 2.9604(7)	2.9413(3) – 3.0245(3)
C-Cu-E	174.70(13)	173.49(19)	174.90(15)	174.20(15)	176.2(2)
Cu-E-M	76.21(4) – 85.41(5)	71.66(3) – 77.54(3)	75.81(5) – 81.92(5)	72.00(2) – 77.24(2)	70.82(3) – 77.06(3)
M-E-M	74.22(4) – 76.60(4)	69.66(3) – 71.09(3)	74.68(4) – 77.16(4)	71.06(2) – 73.010(19)	73.504(19) – 76.214(18)
E-M-E	175.88(5) – 178.85(7)	177.26(4) – 178.48(6)	175.29(5) – 177.43(7)	176.62(3) – 176.96(4)	172.58(3) – 174.73(3)
M-M-M	88.26(3) – 90.91(3)	88.35(4) – 90.63(3)	87.36(2) – 91.122(16)	87.21(2) – 91.597(16)	87.639(12) – 90.795(13)

[a] M = Cu2, Cu4, Cu5
[b] Cu = Cu1, Cu3

NMR data for **3.3**, **3.4**, and **3.5b** are consistent with the clusters remaining intact in solution, only showing one set of resonances for $CAAC^{Cy}$ in the ^{1}H and $^{13}C\{^{1}H\}$ NMR and one signal in the $^{77}Se\{^{1}H\}$ NMR spectrum for **3.3b** (-447 ppm), **3.4b** (-618 ppm), and **3.5b** (-449 ppm). In contrast to the previously reported cluster $[Au_4Ag_4Se_4(IPr)_4]$, where the $^{77}Se\{^{1}H\}$ NMR spectrum shows a triplet due to *J*-coupling between $^{107/109}Ag$ and ^{77}Se, the spectrum of **3.4b** contains a broad singlet (FWHM ≈ 25 Hz). This is likely a consequence of coupling to adjacent quadrupolar nuclei ^{63}Cu and ^{65}Cu, both with I = 3/2 and natural abundance 69.15% and 30.85%, respectively.

UV-Visible absorption and 77K photoluminescence excitation/emission (PLE/PL) spectra were recorded for **3.1**–**5** and free carbene $\mathbf{CAAC^{Cy}}$ in 2-methyltetrahydrofuran (2-MeTHF; Figure 3.3 and Table 3.2). No emission was observed at 298K in either 2-MeTHF or toluene under N_2. $\mathbf{CAAC^{Cy}}$ has a high energy absorption at 248 nm assigned to an IL $\pi \rightarrow \pi^*$ transition. A lower intensity shoulder at 330 nm (ε = 270 M^{-1} cm^{-1}) is assigned to the forbidden $n \rightarrow \pi^*$ state (Figure 3.3a). $\mathbf{CAAC^{Cy}}$ is blue emissive (λ_{em} = 488 nm) at 77K with a sub-μs decay time (Figure 3.3b).

The PLE spectrum is maximized at 343 nm, indicating that the n → π* state is involved in photoluminescence. Mononuclear complexes **3.1**–**2** have two distinct bands in their absorption spectra (Figure 3.3a). The higher energy bands (280 – 293 nm) are bathochromically shifted relative to the free carbene and are assigned to ^{1}MLCT (Cu $d_{\pi}\rightarrow\pi^*$) absorptions, similar to what is observed in [CuX(CAAC^{Me})] (X = Cl, Br, I).[22] The low energy bands (332 – 355 nm) are assigned to ^{1}XLCT (AcO^{-}/Me_3SiE^{-} → CAAC^{Cy}) in correspondence with the linear halides. The 77K PLE spectra also show two peaks which are red-shifted ca. 10 – 20 nm compared to the absorption bands at 298K (Figure 3.3b). The complexes are phosphorescent in the green-yellow region (**3.1**, 532 nm; **3.2a**, 552 nm; **3.2b**, 567 nm) with emission maxima that vary with the non-bonding pair energy of the anionic ligand, indicating that emission occurs from the ^{3}XLCT state.

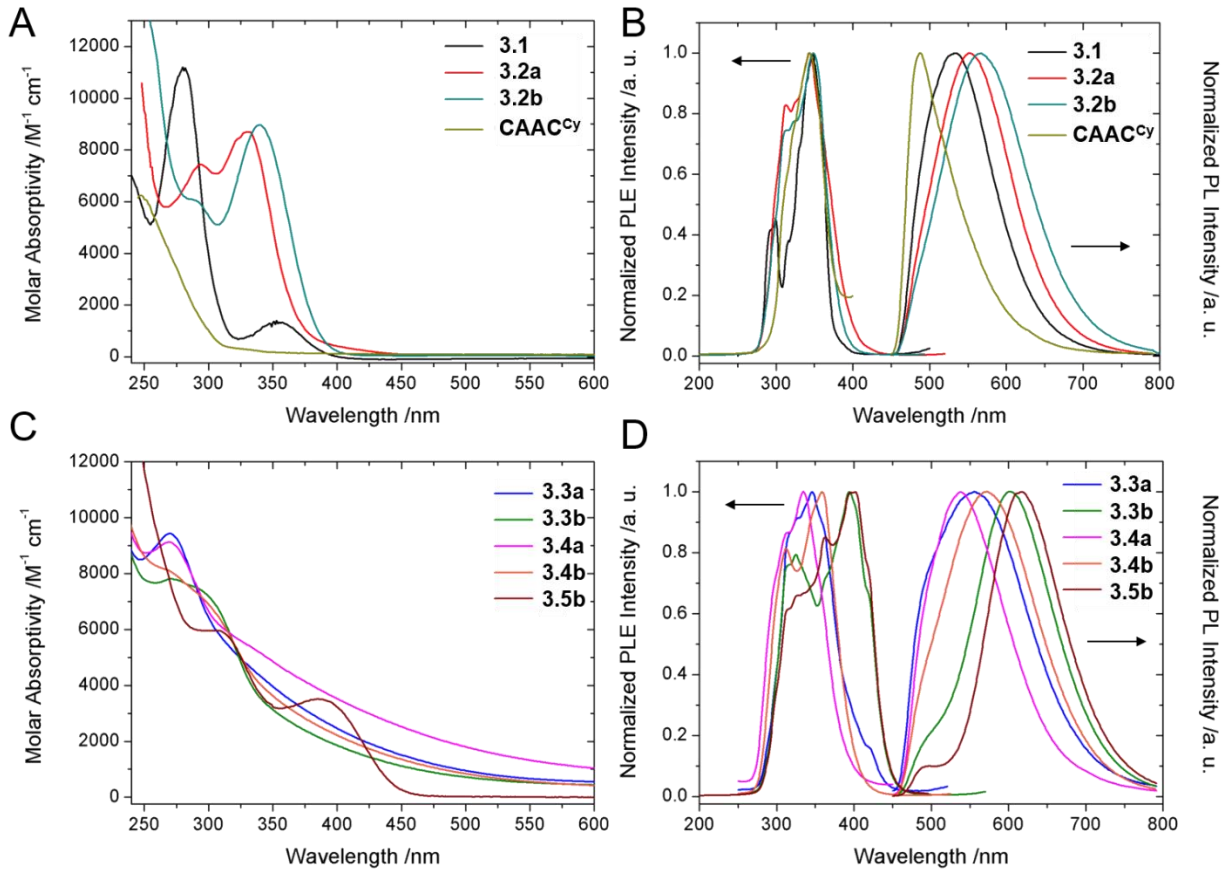

Figure 3.3 Absorption spectra of **A**) mononuclear complexes **3.1-2** and **CAAC^{Cy}** and **C**) cluster compounds **3.3-5** in 2-MeTHF at 298K. Photoluminescence excitation (PLE) and emission (PL) spectra of **B**) mononuclear complexes **3.1-2** and **CAAC^{Cy}** and **D**) cluster compounds **3.3-5** in glassy 2-MeTHF at 77K.

In contrast to the mononuclear complexes, the absorption spectra of **3.3** and **3.4** are dominated by broad, featureless tails over most of the visible region (Figure 3.3c) which are ascribed to electronic transitions between the '$Cu_4M_4E_4$' core and surface ligands (cluster-to-ligand charge transfer; ^{1}CLCT). Additional high energy bands around 270 nm are ascribed to a surface state of ^{1}MLCT (Cu → CAAC^{Cy}) character. For **3.5b**, both absorptions are distinct maxima at 308 and 390 nm. **3.3**–**5** mainly emit in the green to orange regions of the spectrum (538 – 612 nm) with an additional, excitation wavelength-independent, low-intensity band at 490 nm which likely arises from surface ^{3}IL states of **CAAC^{Cy}** (Figure 3.3d). Structured PLE bands between 312 – 405 nm indicate that the major emission originates from ^{3}CLCT. As with the mononuclear complexes, the selenide ligand shifts the emission to lower energies compared to sulfide ($\Delta E_{em} \approx$ 0.15 eV) due to the higher-lying lone pair orbitals. For a fixed chalcogenide, the emission energy varies over a range of ca. 0.10 – 0.15 eV according to M = Ag > Cu > Au. This is consistent with the observed trend in M→SR ^{1}MLCT energies for Ag (5.37 eV), Cu (4.90 eV), and Au (4.82 eV).[30]

Table 3.2 Spectroscopic data for **3.1-5** and **CAAC^{Cy}** in frozen (77K) 2-MeTHF.

	λ_{abs} [nm] (ε [$\times 10^3$ M^{-1} cm^{-1}])	λ_{ex} [nm]	λ_{em} [nm]	$\tilde{\nu}_{ST}$ [$\times 10^3$ cm^{-1}]	τ [μs]
CAAC^{Cy}	248 (6.2)	343	488	8.66	-
	330 sh (0.27)				
3.1	280 (11.2)	299			
	355 (1.3)	348	532	9.94	47.6
3.2a	293 (7.4)	313			
	332 (6.3)	343	552	11.0	56.6
3.2b	290 (6.0)	314			
	340 (4.1)	348	567	11.1	30.8
3.3a	270 (9.4)	346	556	10.9	34.9
3.3b	271 (7.8)	324	489 sh		
		394	602	8.77	41.3
3.4a	269 (9.1)	335	538	11.3	35.9
3.4b	268 (8.1)	312			
		359	572	10.4	35.7
3.5b	308 (5.9)		489 sh		49.9 (88%)
	390 (3.4)	405	618	8.51	211.4 (12%)

Quantum chemical calculations suggest that ground state effects contribute to this ordering, as the cluster-based S_0 is significantly stabilized for **3.4** compared to **3.3** and **3.5** (ΔE_{HOMO} > 0.15

eV; Figure 3.4). Structural reorganization of the cluster core and intramolecular M-M′ contacts upon intersystem-crossing will also have a marked effect on emission energy. In S_0, M-M′ interactions are principally antibonding/non-bonding in nature. A contraction of the M-M′ distances would be expected as the metal-based σ* orbitals are depopulated in the ^{3}CLCT state, as has been shown in a related system.[31] The energy of T_1 will then depend on the stabilizing metallophilic interactions present – which are highly sensitive to the nature of the heterometal.

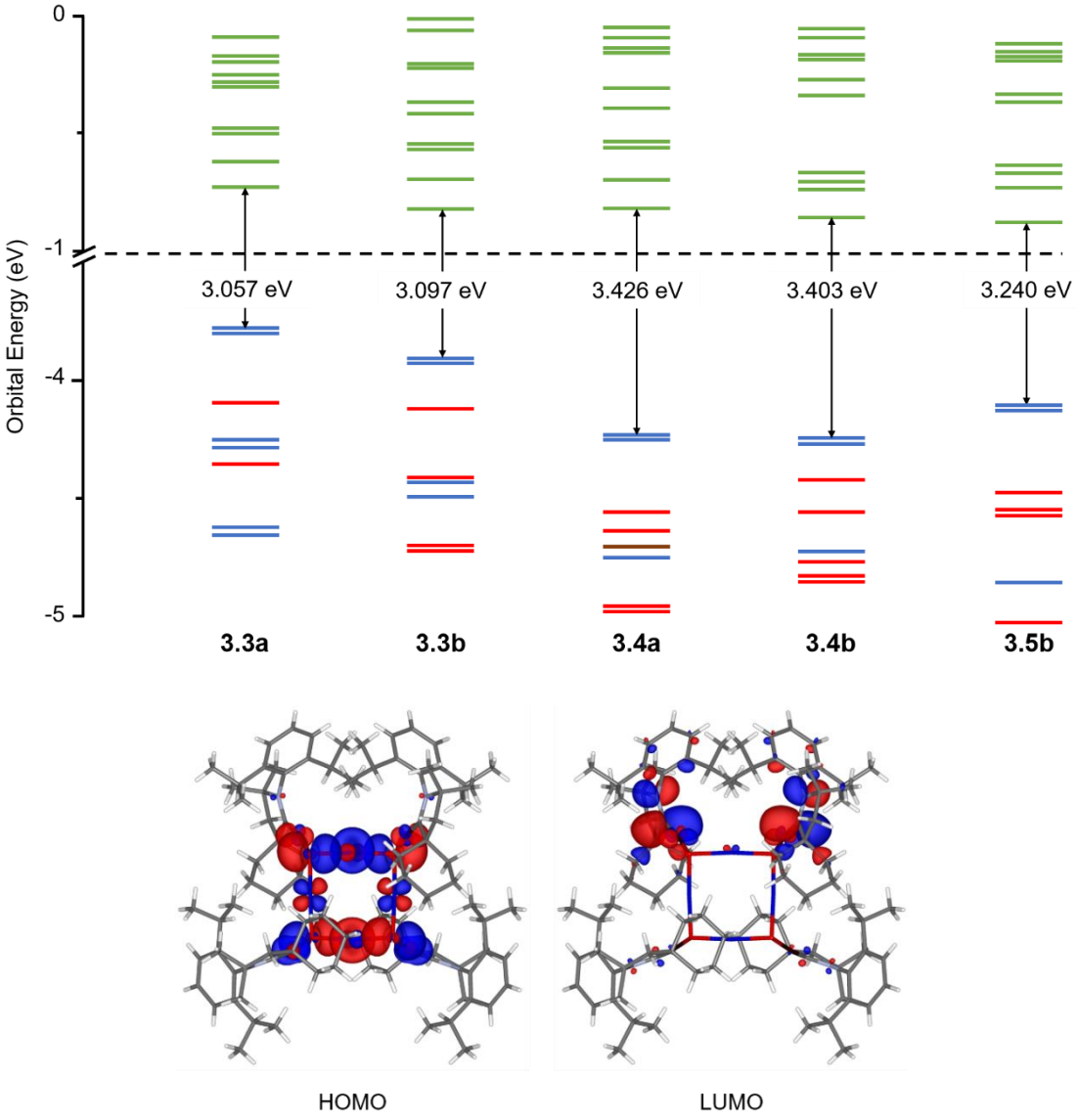

Figure 3.4 Orbital energy diagram for the singlet states of **3.3-5**. Orbitals are coloured according to their major contributors as determined from Mulliken population analysis: brown = Cu, blue = M, red = E, green = CAAC^{Cy}. Orbital energies were calculated at B3LYP/Def-2SV(P) for the molecular geometry obtained from SCXRD. Below, the HOMO and LUMO for **3.3a** are plotted.

3.3 Experimental Section

3.3.1 General Considerations

All syntheses described were conducted under an atmosphere of high-purity dry nitrogen using standard double-manifold Schlenk line techniques. Non-chlorinated solvents (tetrahydrofuran, pentane, hexanes, and toluene) were dried and collected using an MBraun MB-SP Series solvent purification system and stored over 3Å molecular sieves. Deuterated chloroform was purchased from Caledon and dried over P_2O_5 by refluxing under N_2 prior to collecting by distillation and stored over 3Å molecular sieves. Diethyl ether was dried and distilled over sodium benzophenone ketyl radical and stored over 3Å molecular sieves. Anhydrous 2-Methyl tetrahydrofuran (2-Me-THF) was purchased from Sigma, degassed by three freeze-pump-thaw cycles and transfer into an inert atmosphere glovebox prior to use in photophysical experiments. Celite® was dried under dynamic vacuum at 220°C for 24 hours and stored under vacuum in a sealed flask. $CAAC^{Cy}\cdot HCl$,[25] Cu(OAc),[32] $E(SiMe_3)_2$,[33] [({2,4-^{t}Bu(C_6H_3)O}$_3$P)AuOAc],[34] and [(Ph_3P)AgOAc][35] were prepared following literature procedures. Other chemicals were used as received from commercial sources (Alfa Aesar and Aldrich).

NMR spectra were recorded on Inova 400 and Inova 600 spectrometers. ^{1}H, ^{13}C{^{1}H} and ^{29}Si chemical shifts are referenced to $SiMe_4$. ^{77}Se chemical shifts are relative to Me_2Se. Heteronuclear Multiple Bond Correlation (HMBC) experiments were performed for ^{29}Si-^{1}H, ^{77}Se-^{1}H to confirm signal assignments or to improve signal-to-noise through indirect detection of coupled protons. Elemental analysis was performed by Laboratoire d'analyse élémentaire at the Université de Montréal, Montreal, Canada. Samples were dried under dynamic vacuum (< 10 mTorr) for at least 12 hours prior to shipment.

Samples of **3.1**–**5** for solution-state electronic spectroscopy were prepared in a nitrogen filled glovebox by dissolving pure compound in 2-MeTHF which had been degassed by three freeze-pump-thaw cycles directly before transfer into the glovebox. UV-Vis spectra were recorded in a quartz cuvette with a Teflon cap on a Cary 100 Bio instrument. The photoluminescence and photoluminescence excitation spectra at 77K were acquired on a PTI Quantamaster (PTI, London, Ontario) fluorimeter. A quartz dewar was filled with liquid nitrogen and solutions were added dropwise into this holder, forming randomly oriented beads of the frozen sample. A 250-400 cut-off filter was employed to remove unwanted stray exciting light that scatters from the frozen

sample. The microsecond decay traces at 77 K were measured from decay traces using the PTI Xenoflash system with analysis using a sum of exponentials model.

Quantum chemical calculations were performed in Gaussian 09 Revision B.01[36] on the crystallographically determined structures of **3.3**–**5** at the level B3LYP/Def2SVP.[37-40] Mulliken population analysis[41] of the frontier orbitals was performed in Chemissian Version 4.53. Molecular orbital isosurfaces were plotted from Gaussian .cub files in Visualization for Electronic Structure Analysis, version 4.4.0.[42]

3.3.2 Synthesis

Synthesis of [(CAAC^{Cy})CuOAc] (3.1):

In a modification of a literature procedure, free CAAC^{Cy} was produced by mixing CAAC^{Cy}·HBF_4 (1g, 2.418 mmol) and KHMDS (603 mg, 3.023 mmol) in 25 mL toluene, stirring for one hour then removing the solvent and extracting the product into 40 mL pentane. The extract was filtered through Celite®, the solvent of the filtrate removed, and the resulting yellow oil dispersed in 25 mL toluene. CuOAc (296 mg, 2.418 mmol) was suspended in 25 mL toluene and the two solutions were combined. The resulting mixture was stirred overnight at ambient temperature to yield a grey suspension. This was filtered through Celite® to yield clear, light yellow solution. The volume of the filtrate was reduced and a 5x excess of hydrocarbons was added. Full precipitation of the product was obtained by cooling to -25°C for 3 hours. The mother liquor was removed by pipette and the remaining white solid was washed with hydrocarbons and dried under dynamic vacuum. **Yield** 321 mg (30%). **^{1}H NMR** ($CDCl_3$, 25°C, 400.08 MHz) δ 7.37 (t, 1H, 7.8 Hz, C_pH), 7.23 (d, 2H, 7.8 Hz, C_mH), 2.80 (sept, 2H, 6.9 Hz, C$\underline{H}(CH_3)_2$), 2.32 – 2.21 (m, 2H, $C_{Cy}H_2$), 2.06 (s, 2H, CH_2), 1.87 (s, 3H, OC(O)CH_3), 1.93 – 1.65 (m, 3H, $C_{Cy}H_2$), 1.55 – 1.33 (m, 5H, $C_{Cy}H_2$), 1.33 (s, 6H, CH_3), 1.28 (d, 6H, 6.8 Hz, CH(C$\underline{H}_3)_2$), 1.26 (d, 6H, 6.8 Hz, CH(C$\underline{H}_3)_2$). **^{13}C{^{1}H} NMR** ($CDCl_3$, 25°C, 100.62 MHz) δ 249.5 ($C_{carbenic}$), 178.4 (O*C*(O)CH_3), 144.9 ($C_{o,ar}$), 134.5 ($C_{i,ar}$), 129.5 ($C_{p,ar}$), 124.6 ($C_{m,ar}$), 80.3 (C^{IV}), 59.6 (C^{IV}), 45.8 (CH_2), 35.8 (CH_2), 29.6 (*C*H($CH_3)_2$), 29.0 (CH_3), 27.0 (CH(*C*$H_3)_2$), 25.1 ($C_{Cy}H_2$), 23.2 (OC(O)*C*H_3), 22.3 ($C_{Cy}H_2$), 21.9 (CH(*C*$H_3)_2$).

Synthesis of [(CAAC^{Cy})CuSSiMe$_3$] (3.2a):

[(CAAC^{Cy})CuOAc] (220 mg, 0.491 mmol) was dissolved in 5 mL THF and cooled to -30°C. 0.1 mL (0.491 mmol) S(SiMe$_3$)$_2$ was added neat and the solution was warmed to 0°C over one hour. The solution was stirred for 2 hours at room temperature then the solvent was removed under vacuum. The product was taken up into 2x 60 mL heptane and filtered through Celite® on a frit. The volume of the filtrate was reduced by ~1/4 and then stored at -25°C to induce precipitation of the product over one night. The title compound was collected as colourless needles by removal of the mother liquor, which was recrystallized to give a second crop of crystals. **Yield** 99 mg (41%). **M.p.** 168 – 171°C. **^{1}H NMR** ($CDCl_3$, 25°C, 400.08 MHz) δ 7.38 (t, 1H, 7.7 Hz, C$_p$H), 7.24 (d, 2H, 7.7 Hz, C$_m$H), 2.82 (sept, 2H, 6.8 Hz, C$\underline{H}$(CH$_3$)$_2$), 2.28 – 2.18 (m, 2H, C$_{Cy}$H$_2$), 2.06 (s, 2H, CH$_2$), 1.91 – 1.71 (m, 3H, C$_{Cy}$H$_2$), 1.56 – 1.37 (m, 5H, C$_{Cy}$H$_2$), 1.34 (s, 6H, CH$_3$), 1.32 (d, 6H, 6.8 Hz, CH(C$\underline{H}_3$)$_2$), 1.29 (d, 6H, 6.8 Hz, CH(C$\underline{H}_3$)$_2$), 0.11 (Si(CH$_3$)$_3$). **^{13}C{^{1}H} NMR** ($CDCl_3$, 25°C, 100.62 MHz) δ 249.1 (C$_{carbenic}$), 145.0 (C$_{o,ar}$), 134.4 (C$_{i,ar}$), 129.6 (C$_{p,ar}$), 124.7 (C$_{m,ar}$), 80.3 (C^{IV}), 59.6 (C^{IV}), 46.0 (CH$_2$), 36.1 (CH$_2$), 29.6 (*C*H(CH$_3$)$_2$), 29.1 (CH$_3$), 27.5 (CH(*C*H$_3$)$_2$), 25.3 (C$_{Cy}$H$_2$), 22.5 (C$_{Cy}$H$_2$), 22.0 (CH(*C*H$_3$)$_2$), 7.0 (Si(CH$_3$)$_3$). **^{29}Si NMR** ($CDCl_3$, 25°C, 119.055 MHz) δ 10 (^{29}Si-^{1}H HMBC). **Anal. Calc'd** $C_{26}H_{44}CuNSSi$: C 63.17, H 8.97, N 2.83, S 6.49; Found C 62.84, H 8.91, N 2.84, S 6.30.

Synthesis of [(CAAC)CuSeSiMe$_3$] (3.2b):

As for **3.2a** with 108 mg (0.24 mmol) **3.1** and 0.06 mL (0.24 mmol) Se(SiMe$_3$)$_2$. **Yield** 80 mg (62%). **M.p.** 169 – 173°C. **^{1}H NMR** ($CDCl_3$, 25°C, 599.23 MHz) δ 7.37 (t, 1H, 7.8 Hz, C$_p$H), 7.24 (d, 2H, 7.8 Hz, C$_m$H), 2.83 (sept, 2H, 6.9 Hz, C*H*(CH$_3$)$_2$), 2.29 – 2.21 (m, 2H, C$_{Cy}$H$_2$), 2.06 (s, 2H, CH$_2$), 1.90 – 1.70 (m, 3H, C$_{Cy}$H$_2$), 1.55 – 1.37 (m, 5H, C$_{Cy}$H$_2$), 1.34 (s, 6H, CH$_3$), 1.34 (d, 6H, 6.8 Hz, CH(C$\underline{H}_3$)$_2$), 1.29 (d, 6H, 6.8 Hz, CH(C$\underline{H}_3$)$_2$), 0.23 (Si(CH$_3$)$_3$). **^{13}C{^{1}H} NMR** ($CDCl_3$, 25°C, 150.70 MHz) δ 249.2 (C$_{carbenic}$), 145.0 (C$_{o,ar}$), 134.4 (C$_{i,ar}$), 129.5 (C$_{p,ar}$), 124.6 (C$_{m,ar}$), 80.1 (C^{IV}), 59.6 (C^{IV}), 46.0 (CH$_2$), 36.0 (CH$_2$), 29.6 (*C*H(CH$_3$)$_2$), 29.1 (CH$_3$), 27.6 (CH(*C*H$_3$)$_2$), 25.2 (C$_{Cy}$H$_2$), 22.5 (C$_{Cy}$H$_2$), 22.0 (CH(*C*H$_3$)$_2$), 7.5 (Si(CH$_3$)$_3$). **^{29}Si NMR** ($CDCl_3$, 25°C, 119.055 MHz) δ 6 (^{29}Si-^{1}H HMBC). **^{77}Se NMR** ($CDCl_3$, 25°C, 114.22 MHz) δ -468.0 (s), -468.0 (d, $^1J_{Se\text{-}29Si}$ = 122.4 Hz). **Anal. Calc'd** $C_{26}H_{44}CuNSeSi$: C 57.70, H 8.19, N 2.59; Found C 57.75, H 8.18, N 2.70.

Synthesis of [$Cu_8S_4(CAAC^{Cy})_4$] (3.3a)

[(Ph_3P)CuOAc] was prepared by adding 24 mg (0.091 mmol) Ph_3P in 2 mL THF to 11 mg CuOAc (0.091 mmol) and stirring until the solution is clear and yellow in colour. 45 mg (0.091 mmol) **3.2a** was dissolved in 2 mL THF and cooled to -78°C. Dropwise addition of [(Ph_3P)CuOAc] to a cold solution of **3.2a** produces a clear orange solution. This was warmed to -25°C, layered with 20 mL heptane and stored at -25°C for two days. The product precipitates as yellow crystals which are washed with 2x 10 mL Et_2O and dried under dynamic vacuum. **Yield** 26 mg (59%). **^{1}H NMR** ($CDCl_3$, 25°C, 599.23 MHz) δ 7.29 (t, 1H, 7.8 Hz, C_pH), 7.17 (d, 2H, 7.8 Hz, C_mH), 3.00 – 2.90 (m, 2H, $C_{Cy}H_2$), 2.82 (sept, 2H, 6.8 Hz, $CH(CH_3)_2$), 1.95 (s, 2H, CH_2), 1.91 – 1.74 (m, 3H, $C_{Cy}H_2$), 1.48 – 1.14 (m, 5H, $C_{Cy}H_2$), 1.33 (d, 6H, 6.8 Hz, $CH(CH_3)_2$), 1.25 (s, 6H, CH_3), 1.22 (d, 6H, 6.8 Hz, $CH(CH_3)_2$). **^{13}C{^{1}H} NMR** ($CDCl_3$, 25°C, 150.70 MHz) δ 251.5 ($C_{carbenic}$), 145.6 ($C_{o,ar}$), 134.9 ($C_{i,ar}$), 128.6 ($C_{p,ar}$), 124.2 ($C_{m,ar}$), 79.1 (C^{IV}), 60.5 (C^{IV}), 46.1 (CH_2), 36.2 (CH_2), 29.6 ($CH(CH_3)_2$), 29.0 (CH_3), 28.3 ($CH(CH_3)_2$), 25.0 ($C_{Cy}H_2$), 22.5 ($C_{Cy}H_2$), 22.3 ($CH(CH_3)_2$). **Anal. Calc'd** $C_{92}H_{140}Cu_8N_4S_4$: C 57.00, H 7.28, N 2.89, S 6.61; Found C 56.06, H 6.67, N 2.85, S 6.25.

Synthesis of [$Cu_8Se_4(CAAC^{Cy})_4$] (3.3b)

As for **3.3a** with 65 mg (0.12 mmol) **3.2b**, 15 mg (0.12 mmol) Ph_3P, and 32 mg (0.12 mmol) CuOAc, **Yield** 30 mg (47%). **^{1}H NMR** ($CDCl_3$, 25°C, 599.23 MHz) δ 7.31 (t, 1H, 7.7 Hz, C_pH), 7.17 (d, 2H, 7.7 Hz, C_mH), 3.03 – 2.91 (m, 2H, $C_{Cy}H_2$), 2.83 (sept, 2H, 6.6 Hz, $CH(CH_3)_2$), 1.95 (s, 2H, CH_2), 2.02 – 1.71 (m, 3H, $C_{Cy}H_2$), 1.56 – 1.11 (m, 5H, $C_{Cy}H_2$), 1.33 (d, 6H, 6.6 Hz, $CH(CH_3)_2$), 1.25 (s, 6H, CH_3), 1.22 (d, 6H, 6.6 Hz, $CH(CH_3)_2$). **^{13}C{^{1}H} NMR** ($CDCl_3$, 25°C, 150.70 MHz) δ 251.6 ($C_{carbenic}$), 145.6 ($C_{o,ar}$), 134.8 ($C_{i,ar}$), 128.7 ($C_{p,ar}$), 124.2 ($C_{m,ar}$), 79.0 (C^{IV}), 60.5 (C^{IV}), 46.1 (CH_2), 36.0 (CH_2), 29.6 ($CH(CH_3)_2$), 28.9 (CH_3), 28.4 ($CH(CH_3)_2$), 24.9 ($C_{Cy}H_2$), 22.6 ($C_{Cy}H_2$), 22.2 ($CH(CH_3)_2$). **^{77}Se NMR** ($CDCl_3$, 25°C, 114.22 MHz) δ -447.2 (s). **Anal. Calc'd** $C_{92}H_{140}Cu_8N_4Se_4$: C 51.97, H 6.64, N 2.63; Found C 52.64, H 5.74, N 2.59.

Synthesis of [$Cu_4Ag_4S_4(CAAC^{Cy})_4$] (3.4a)

As for **3.3a** with 48 mg (0.097 mmol) **3.2a** and 42 mg (0.097 mmol) [(Ph_3P)AgOAc]. **Yield** 21 mg (40%). **^{1}H NMR** ($CDCl_3$, 25°C, 599.23 MHz) δ 7.31 (t, 1H, 7.9 Hz, C_pH), 7.18 (d, 2H, 7.9 Hz, C_mH), 2.95 – 2.76 (m, 2H, $C_{Cy}H_2$), 2.81 (sept, 2H, 6.6 Hz, $CH(CH_3)_2$), 1.95 (s, 2H, CH_2), 1.91 – 1.76 (m, 3H, $C_{Cy}H_2$), 1.52 – 1.17 (m, 5H, $C_{Cy}H_2$), 1.37 (d, 6H, 6.6 Hz, $CH(CH_3)_2$), 1.25 (s, 6H, CH_3), 1.23 (d, 6H, 6.6 Hz, $CH(CH_3)_2$). **^{13}C{^{1}H} NMR** ($CDCl_3$, 25°C, 150.70 MHz) δ 250.5

($C_{carbenic}$), 145.5 ($C_{o,ar}$), 134.8 ($C_{i,ar}$), 128.9 ($C_{p,ar}$), 124.3 ($C_{m,ar}$), 79.2 (C^{IV}), 60.4 (C^{IV}), 46.0 (CH_2), 36.6 (CH_2), 29.6 ($CH(CH_3)_2$), 29.0 (CH_3), 28.5 ($CH(CH_3)_2$), 25.1 ($C_{Cy}H_2$), 22.5 ($C_{Cy}H_2$), 22.2 ($CH(CH_3)_2$). **Anal. Calc'd** $C_{92}H_{140}Cu_4Ag_4N_4S_4$: C 52.22, H 6.67, N 2.65, S 6.06; Found C 51.97, H 6.64, N 2.63, S 6.07.

Synthesis of [$Cu_4Ag_4Se_4(CAAC^{Cy})_4$] (3.4b)

As for **3.3a** with 80 mg (0.148 mmol) **3.2b** and 63 mg (0.148 mmol) [(Ph_3P)AgOAc]. **Yield** 34 mg (40%). **^{1}H NMR** ($CDCl_3$, 25°C, 599.23 MHz) δ 7.32 (t, 1H, 7.9 Hz, C_pH), 7.19 (d, 2H, 7.9 Hz, C_mH), 2.93 – 2.76 (m, 2H, $C_{Cy}H_2$), 2.82 (sept, 2H, 6.6 Hz, $CH(CH_3)_2$), 1.95 (s, 2H, CH_2), 2.03 – 1.75 (m, 3H, $C_{Cy}H_2$), 1.55 – 1.06 (m, 5H, $C_{Cy}H_2$), 1.38 (d, 6H, 6.6 Hz, $CH(CH_3)_2$), 1.25 (s, 6H, CH_3), 1.23 (d, 6H, 6.6 Hz, $CH(CH_3)_2$). **^{13}C{^{1}H} NMR** ($CDCl_3$, 25°C, 150.70 MHz) δ 250.8 ($C_{carbenic}$), 145.5 ($C_{o,ar}$), 134.7 ($C_{i,ar}$), 128.9 ($C_{p,ar}$), 124.3 ($C_{m,ar}$), 79.2 (C^{IV}), 60.5 (C^{IV}), 46.1 (CH_2), 36.3 (CH_2), 29.6 ($CH(CH_3)_2$), 28.9 (CH_3), 28.5 ($CH(CH_3)_2$), 25.0 ($C_{Cy}H_2$), 22.6 ($C_{Cy}H_2$), 22.1 ($CH(CH_3)_2$). **^{77}Se NMR** ($CDCl_3$, 25°C, 114.22 MHz) δ -617.8 (s). **Anal. Calc'd** $C_{92}H_{140}Cu_4Ag_4N_4Se_4$: C 47.97, H 6.13, N 2.43; Found C 48.83, H 6.51, N 2.34.

Synthesis of [$Cu_4Au_4Se_4(CAAC^{Cy})_4$] (3.5b)

As for **3.3a** with 68 mg (0.126 mmol) **3.2b** and 113 mg (0.126 mmol) [{(2,4-*t*Bu(C_6H_3)O)$_3$P}AuOAc]. **Yield** 55 mg (66%). **^{1}H NMR** ($CDCl_3$, 25°C, 599.23 MHz) δ 7.32 (t, 1H, 7.7 Hz, C_pH), 7.18 (d, 2H, 7.7 Hz, C_mH), 3.14 – 3.03 (m, 2H, $C_{Cy}H_2$), 2.83 (sept, 2H, 6.6 Hz, $CH(CH_3)_2$), 1.96 (s, 2H, CH_2), 1.94 – 1.73 (m, 3H, $C_{Cy}H_2$), 1.50 – 1.11 (m, 5H, $C_{Cy}H_2$), 1.36 (d, 6H, 6.7 Hz, $CH(CH_3)_2$), 1.25 (s, 6H, CH_3), 1.23 (d, 6H, 6.7 Hz, $CH(CH_3)_2$). **^{13}C{^{1}H} NMR** ($CDCl_3$, 25°C, 150.70 MHz) δ 249.9 ($C_{carbenic}$), 145.7 ($C_{o,ar}$), 134.8 ($C_{i,ar}$), 128.7 ($C_{p,ar}$), 124.2 ($C_{m,ar}$), 79.0 (C^{IV}), 60.8 (C^{IV}), 46.0 (CH_2), 35.8 (CH_2), 29.6 ($CH(CH_3)_2$), 29.0 (CH_3), 28.5 ($CH(CH_3)_2$), 24.8 ($C_{Cy}H_2$), 22.6 ($C_{Cy}H_2$), 22.2 ($CH(CH_3)_2$). **^{77}Se NMR** ($CDCl_3$, 25°C, 114.22 MHz) δ -448.8 (s). **Anal. Calc'd** $C_{92}H_{140}Cu_4Au_4N_4Se_4$: C 41.54, H 5.31, N 2.11; Found C 41.52, H 5.42, N 2.19.

3.3.3 X-Ray Crystallography Details

X-ray measurements were made on a Bruker Kappa Axis Apex2 diffractometer equipped with graphite monochromated Mo $K\alpha_1$ (λ=0.71073 Å) radiation at a temperature of 110 K. The samples were mounted on a Mitegen polyimide micromount with a small amount of Paratone N

oil. The collection strategy was a number of ω and φ scans with data collected up to >50° (2θ). The frame integration was performed using SAINT.[43] The resulting raw data was scaled and absorption corrected using a multi-scan averaging of symmetry equivalent data using SADABS.[44] The structure was solved by using a dual space methodology using the SHELXT program.[45] All non-hydrogen atoms were obtained from the initial solution. The hydrogen atoms were introduced at idealized positions and were allowed to ride on the parent atom. The structural model was fit to the data using full matrix least-squares based on F^2. The calculated structure factors included corrections for anomalous dispersion from the usual tabulation.

The structures were refined using the SHELXLE program from the SHELXTL suite of crystallographic software.[46] Unless otherwise stated, all non-hydrogen atoms were refined anisotropically. For **3.3**–**5**, positional disorder in the pyrrolidylidene backbone and cyclohexyl moiety of the ligands were jointly treated with a split occupancy model. Two orientations of C4 (above and below the C_3N plane) were detected by analysis of the residual electron density. This was coupled with two distinct chair conformations of cyclohexane and, for **3.3b**, **3.4b**, and **3.5b**, one methyl group on C3. All disordered atoms were refined isotropically and occupancy ratios for the two conformations were 60:40 (**3.3a**), 65:35 (**3.4a**), 65:35 (**3.4b**), and 70:30 (**3.5b**). Two disordered solvent molecules were modelled in **3.3a**,**b**, and **3.4a** by split occupancy models, using the SADI command to constrain the C-C and C-O bond lengths. In **3.4b** and **3.5b**, only one THF molecule was directly modelled. Residual electron density suggests the presence of a second THF molecule in both cases, but no satisfactory structure model could be obtained.

CCDC 1845227-1845231 for **3.3a** – **3.5b**, respectively, contain the supplementary crystallographic data for this paper. These data can be obtained free of charge from The Cambridge Crystallographic Data Center via www.ccdc.cam.ac.uk/data_request/cif.

3.4 Conclusions and Outlook

In conclusion, the enhanced donor properties of CAACs compared to imidazolylidene-based NHCs are crucial in the preparation of a series of luminescent polynuclear Cu(I) chalcogenide complexes. Modulation of the complex nuclearity, bridging ligands, and metal composition – made possible by the metal-stabilizing properties of CAACs – were found to be effective in tuning the light absorption and emission characteristics in these assemblies. We are currently investigating methods to improve the quantum yield in these and related systems through control of the cluster geometry.

The copper(I) silylchalcogenolate precursors presented in this chapter are the most versatile variants of the cuprachalcogenolate, "Cu-E$^-$", moiety prepared to date in our lab. It therefore would be interesting to test the analogy between these fragments with organic chalcogenolates further. The clusters presented may be analogised to copper(I) chalcogenolate oligomers $[Cu(ER)]_n$ like those seen in Section 1.1.1 with R = $(CAAC^{Cy})Cu$, and n = 4. Massive Cu(I) chalcogen clusters are obtained from the reaction of Cu(I) precursors with a source of RE^- and E^{2-} (Section 1.1.3). Therefore, the combination of RE^- = $(CAAC^{Cy})CuESiMe_3$, E^{2-} = $E(SiMe_3)_2$, and CuOAc could give rise to larger copper(I) chalcogenide clusters with NHC ancillary ligands. Alternatively, treating the clusters $[Cu\{E(Cu\text{-}CAAC^{Cy})\}]_4$ directly with $E(SiMe_3)_2$ could cause aggregation to larger assemblies in an analogous manner to clusters like $[Cu_{136}S_{56}(SCH_2C_4H_3O)_{24}(dpppt)_{10}]$ (Section 1.1.3).[47]

3.5 References

[1] S. R. Pauleta, S. Dell'Acqua, I. Moura. *Coord. Chem. Rev.* **2013**, *257*, 332.
[2] B. J. Johnson, W. E. Antholine, S. V. Lindeman, M. J. Graham, N. P. Mankad. *J. Am. Chem. Soc.* **2016**, *138*, 13107.
[3] O. Fuhr, S. Dehnen, D. Fenske. *Chem. Soc. Rev.* **2013**, *42*, 1871.
[4] O. Kluge, R. Biedermann, J. Holldorf, H. Krautscheid. *Chem. – Eur. J.* **2014**, *20*, 1318.
[5] V. W.-W. Yam, V. K.-M. Au, S. Y. L. Leung. *Chem. Rev.* **2015**, *115*, 7589.
[6] X.-X. Yang, I. Issac, S. Lebedkin, M. Kühn, F. Weigend, D. Fenske, O. Fuhr, A. Eichhöfer. *Chem. Commun.* 2014, *50*, 11043.
[7] A. Eichhöfer, G. Buth, S. Lebedkin, M. Kühn, F. Weigend. *Inorg. Chem.* **2015**, *54*, 9413.
[8] O. Crespo, M. C. Gimeno, A. Laguna, C. Larraz, M. D. Villacampa. *Chem. – Eur. J.* **2007**, *13*, 235-46.
[9] R. Visbal, M. C. Gimeno. *Chem. Soc. Rev.* **2014**, *43*, 3551.
[10] B. Hupp, C. Schiller, C. Lenczyk, M. Stanoppi, K. Edkins, A. Lorbach, A. Steffen. *Inorg. Chem.* **2017**, *56*, 8896.
[11] J. Nitsch, F. Lacemon, A. Lorbach, A. Eichhorn, F. Cisnetti, A. Steffen. *Chem. Commun.* **2016**, *52*, 2932.
[12] V. A. Krylova, P. I. Djurovich, B. L. Conley, R. Haiges, M. T. Whited, T. J. Williams, M. E. Thompson. *Chem. Commun.* **2014**, *50*, 7176.
[13] M. J. Leitl, V. A. Krylova, P. I. Djurovich, M. E. Thompson, H. Yersin. *J. Am. Chem. Soc.* **2014**, *136*, 16032.
[14] V. A. Krylova, P. I. Djurovich, M. T. Whited, M. E. Thompson. *Chem. Commun.* **2010**, *46*, 6696.
[15] J. Zhai, M. D. Hopkins, G. L. Hillhouse. *Organometallics* **2015**, *34*, 4637.
[16] J. Zhai, A. S. Filatov, G. L. Hillhouse, M. D. Hopkins. *Chem. Sci.* **2016**, *7*, 589.
[17] M. Azizpoor Fard, F. Weigend, J. F. Corrigan. *Chem. Commun.* **2015**, *51*, 8361.
[18] M. Azizpoor Fard, T. I. Levchenko, C. Cadogan, W. J. Humenny, J. F. Corrigan. *Chem. – Eur. J.* **2016**, *22*, 4543.
[19] M. Melaimi, R. Jazzar, M. Soleilhavoup, G. Bertrand. *Angew. Chem. Int. Ed.* **2017**, *56*, 10046.
[20] R. Hamze, R. Jazzar, M. Soleilhavoup, P. I. Djurovich, G. Bertrand, M. E. Thompson. *Chem. Commun.* **2017**, *53*, 9008.
[21] A. S. Romanov, C. R. Becker, C. E. James, D. Di, D. Credgington, M. Linnolahti, M. Bochmann. *Chem. – Eur. J.* **2017**, *23*, 4625.
[22] M. Gernert, U. Müller, M. Haehnel, J. Pflaum, A. Steffen. *Chem. – Eur. J.* **2017**, *23*, 2206.
[23] A. S. Romanov, D. Di, L. Yang, J. Fernandez-Cestau, C. R. Becker, C. E. James, B. Zhu, M. Linnolahti, D. Credgington, M. Bochmann. *Chem. Commun.* **2016**, *52*, 6379.
[24] D. Di, A. S. Romanov, L. Yang, J. M. Richter, J. P. H. Rivett, S. Jones, T. H. Thomas, M. A. Jalebi, R. H. Friend, M. Linnolahti, M. Bochmann, D. Credgington. *Science*, **2017**, *356*, 159.
[25] R. Jazzar, R. D. Dewhurst, J.-B. Bourg, B. Donnadieu, Y. Canac, G. Bertrand. *Angew. Chem. Int. Ed.* **2007**, *46*, 2899.
[26] H. Clavier, S. P. Nolan. *Chem. Commun.* **2010**, *46*, 841.
[27] Y. D. Bidal, M. Lesieur, M. Melaimi, F. Nahra, D. B. Cordes, K. S. Athukorala Arachchige, A. M. Z. Slawin, G. Bertrand, C. S. J. Cazin. *Adv. Synth. Catal.* **2015**, *357*, 3155.

[28] A. M. Polgar, F. Weigend, A. Zhang, M. J. Stillman, J. F. Corrigan. *J. Am. Chem. Soc.* **2017**, *139*, 14045.
[29] Y. D. Bidal, O. Santoro, M. Melaimi, D. B. Cordes, A. M. Z. Slawin, G. Bertrand, C. S. J. Cazin. *Chem. – Eur. J.* **2016**, *22*, 9404.
[30] K. Fujisawa, S. Imai, Y. Moro-oka. *Chem. Lett.* **1998**, *27*, 167.
[31] A. M. Polgar, C. B. Khadka, M. Azizpoor Fard, B. Nikkel, T. O'Donnell, T. Neumann, K. Lahring, K. Thompson, C. Cadogan, F. Weigend, J. F. Corrigan. *Chem. – Eur. J.* **2016**, *22*, 18378.
[32] D. A. Edwards, R. Richards. *J. Chem. Soc., Dalton Trans*. **1973**, *0*, 2463.
[33] J.-H. So, P. Boudjouk. *Synthesis*, **1989**, *4*, 306.
[34] S. Hosseyni, C. A. Smith, X. Shi. *Org. Lett.* **2016**, *18*, 6336.
[35] J. McNulty, K. Keskar. *Eur. J. Org. Chem*. **2012**, 5462.
[36] Frisch, M. J.; Trucks, G. W.; Schlegel, H. B.; Scuseria, G. E.; Robb, M. A.; Cheeseman, J. R.; Scalmani, G.; Barone, V.; Petersson, G. A.; Nakatsuji, H.; Li, X.; Caricato, M.; Marenich, A.; Bloino, J.; Janesko, B. G.; Gomperts, R.; Mennucci, B.; Hratchian, H. P.; Ortiz, J. V.; Izmaylov, A. F.; Sonnenberg, J. L.; Williams-Young, D.; Ding, F.; Lipparini, F.; Egidi, F.; Goings, J.; Peng, B.; Petrone, A.; Henderson, T.; Ranasinghe, D.; Zakrzewski, V. G.; Gao, J.; Rega, N.; Zheng, G.; Liang, W.; Hada, M.; Ehara, M.; Toyota, K.; Fukuda, R.; Hasegawa, J.; Ishida, M.; Nakajima, T.; Honda, Y.; Kitao, O.; Nakai, H.; Vreven, T.; Throssell, K.; Montgomery, J. A., Jr.; Peralta, J. E.; Ogliaro, F.; Bearpark, M.; Heyd, J. J.; Brothers, E.; Kudin, K. N.; Staroverov, V. N.; Keith, T.; Kobayashi, R.; Normand, J.; Raghavachari, K.; Rendell, A.; Burant, J. C.; Iyengar, S. S.; Tomasi, J.; Cossi, M.; Millam, J. M.; Klene, M.; Adamo, C.; Cammi, R.; Ochterski, J. W.; Martin, R. L.; Morokuma, K.; Farkas, O.; Foresman, J. B.; Fox, D. J. Gaussian 09, Revision B.01, Gaussian, Inc., Wallingford CT, 2016.
[37] A. D. Becke. *Phys. Rev. A* **1988**, *38*, 3098.
[38] C. Lee, W. Yang, R. G. Parr. *Phys. Rev. B* **1988**, *37*, 785.
[39] F. Weigend, R. Ahlrichs. *Phys. Chem. Chem. Phys*. **2005**, *7*, 3297.
[40] F. Weigend. *Phys. Chem. Chem. Phys.* **2006**, *8*, 1057.
[41] R. S. Mulliken. *J. Chem. Phys.* **1955**, *23*, 1833.
[42] K. Momma, F. Izumi. *J. Appl. Cryst.* **2014**, *44*, 1272.
[43] Bruker-AXS, SAINT version 2013.8, 2013, Bruker-AXS, Madison, WI 53711, USA.
[44] Bruker-AXS, SADABS version 2012.1, 2012, Bruker-AXS, Madison, WI 53711, USA.
[45] G. M. Sheldrick. *Acta Cryst.* **2015**, *A71*, 3.
[46] G. M. Sheldrick. *Acta Cryst.* **2015**, *C71*, 3.
[47] M. L. Fu, I. Issac, D. Fenske, O. Fuhr, *Angew. Chem. Int. Ed.* **2010**, *49*, 6899.

Chapter 4

4 Gold(I)-Copper(I)-Sulfido Clusters: Structure-Dependent Luminescence and Thermally Activated Delayed Fluorescence

4.1 Introduction

Over the past several decades, interest in polynuclear d^{10} metal chalcogenide systems has grown immensely. Reports throughout the 1990's highlighted the great structural diversity in the chalcogenides of d^{10} group 11 metals. Fenske and co-workers have shown that the combination of Cu(I) or Ag(I) salts with silylated chalcogen sources and ancillary phosphine ligands can give rise to nanoscopic Cu(I) and Ag(I) chalcogen clusters, containing hundreds of metal atoms.[1-4] Several research groups have studied the electronic and optical properties of small-to-medium-sized chalcogenide clusters, including those of Au(I).[5-22] These systems show a rich diversity in their excited states and dynamics because of a lack of non-emissive d-d states, strong spin-orbit coupling, and the influence of non-covalent d^{10}-d^{10} interactions, including low-energy emission and supramolecular assembly.[23-27]

The reaction chemistry of group 11 trimethylsilylchalcogenolate compounds [$L_nMESiMe_3$] (L = phosphine, *N*-heterocyclic carbene; M = Cu, Ag, Au; E = S, Se, Te) with metal halide and acetate compounds has proven fruitful in the preparation of polynuclear 11-16 assemblies and their heterometallic derivatives.[28-36] Recently, this method was applied in the preparation of luminescent 11-11′-16 clusters stabilized by *N*-heterocyclic carbene (NHC) ancillary ligands. [28] Phosphorescence was observed at 77K in glass matrices, with energies that vary as a function of metal/chalcogen composition. Room temperature emission was not observed, suggesting that relaxation processes compete with phosphorescence and quench emission at ambient temperatures. Herein, two Au(I)-Cu(I)-S clusters of distinct nuclearity and geometry are prepared from an NHC-stabilized gold(I) trimethylsilylthiolate reagent [(IPr)AuSSiMe$_3$]. [$Au_6Cu_{10}(\mu_3\text{-}S)_6(\mu_4\text{-}S)_2(IPr)_6$] (**4.1**) is a Cu(I)-S core/Au(I)-IPr shell cluster which exhibits efficient yellow phosphorescence at 77K (λ_{em} = 595 nm, Φ_{PL} = 0.92) and remains emissive at 298K (Φ_{PL} = 0.05) by the thermally-

activated delayed fluorescence (TADF) mechanism. $[Au_4Cu_4(\mu_3\text{-}S)_4(IPr)_4]$ (**4.2**) is isostructural to the previously reported clusters $[Au_4Ag_4(\mu_3\text{-}S)_4(IPr)_4]$ and $[Au_8(\mu_3\text{-}S)_4(IPr)_4]$. Like these clusters, **4.2** shows solid state phosphorescence at 77K which is quenched at higher temperatures. The enhancement in luminescence in **4.1** versus **4.2** can be attributed to its rigid, high-connectivity core, small $\Delta E(S_1\text{-}T_1)$ and strong charge transfer character, favouring emission from thermally equilibrated S_1 and T_1 states.[37]

4.2 Results and Discussion

Stoichiometric reaction of equimolar amounts of $[(IPr)AuSSiMe_3]$ and $(Ph_3P)CuOAc$ in THF leads to the mixed-metal sulfido cluster $[Au_6Cu_{10}(\mu_3\text{-}S)_6(\mu_4\text{-}S)_2(IPr)_6]$ (**4.1**) in 32% yield based on Cu (Scheme 1A). Notably, the 1:1:1 Au:Cu:S reaction stoichiometry is not retained in the final product. Attempts to improve the yield of this reaction were undertaken by combining $[(IPr)AuSSiMe_3]$, $(Ph_3P)CuOAc$, and $S(SiMe_3)_2$ in the ratio found in cluster **4.1**, i.e. 6:10:2 (Scheme 1B). This synthetic strategy can be likened to the preparation of metal chalcogenolate-chalcogenide clusters with MX_n, $E(SiMe_3)_2$, and $RE(SiMe_3)_2$, where in this case R = (IPr)Au. The major products of this reaction were uncharacterized brown solids, but white crystals of $[Au_4Cu_4(\mu_3\text{-}S)_4(IPr)_4]$ (**4.2**) were obtained in low yield (5%). Replacing $S(SiMe_3)_2$ with $Se(SiMe_3)_2$ produces a mixed-chalcogenide cluster $[Au_4Cu_4(\mu_3\text{-}S)_x(\mu_3\text{-}Se)_{4-x}(IPr)_4]$ ($x \approx 2.37$ by Energy-Dispersive X-ray Spectroscopy). The E^{2-} source is therefore necessary to form the smaller assembly as it becomes incorporated into the structural framework.

The structures of **4.1** and **4.2** were determined by SCXRD analysis (Figure 4.1). **4.2** is isostructural and isomorphous to our previously reported clusters $[Au_4M_4(\mu_3\text{-}E)_4(IPr)_4]$ (M = Ag, Au; E = S, Se, Te), and completes the series of mixed-group 11 metal sulfido clusters.[28] Four $AuCu_2(\mu_3\text{-}S)$ tetrahedra are linked at the Cu vertices to form a cyclic tetramer. S-Au distances of 2.2896(11) Å and Cu-S distances of 2.1821(13) – 2.1954(13) Å are typical for binary Cu(I) and Au(I) sulfido clusters.[5-22] Cu-Cu contacts are 2.7755(7) Å and thus slightly below twice the van der Waals radius of copper. Au-Cu contacts are asymmetric with one long (3.295(8) Å) and one short (3.0903(8) Å) contact. All metal atoms exhibit linear coordination geometry with the largest deviations of 3.5° arising for C-Au-S. Cu-S-Cu angles of 78.70(4)° and Au-S-Cu angles between 84.74(4)° and 91.19(4)° fall within the normal ranges for μ_3-coordinated sulfido ligands.

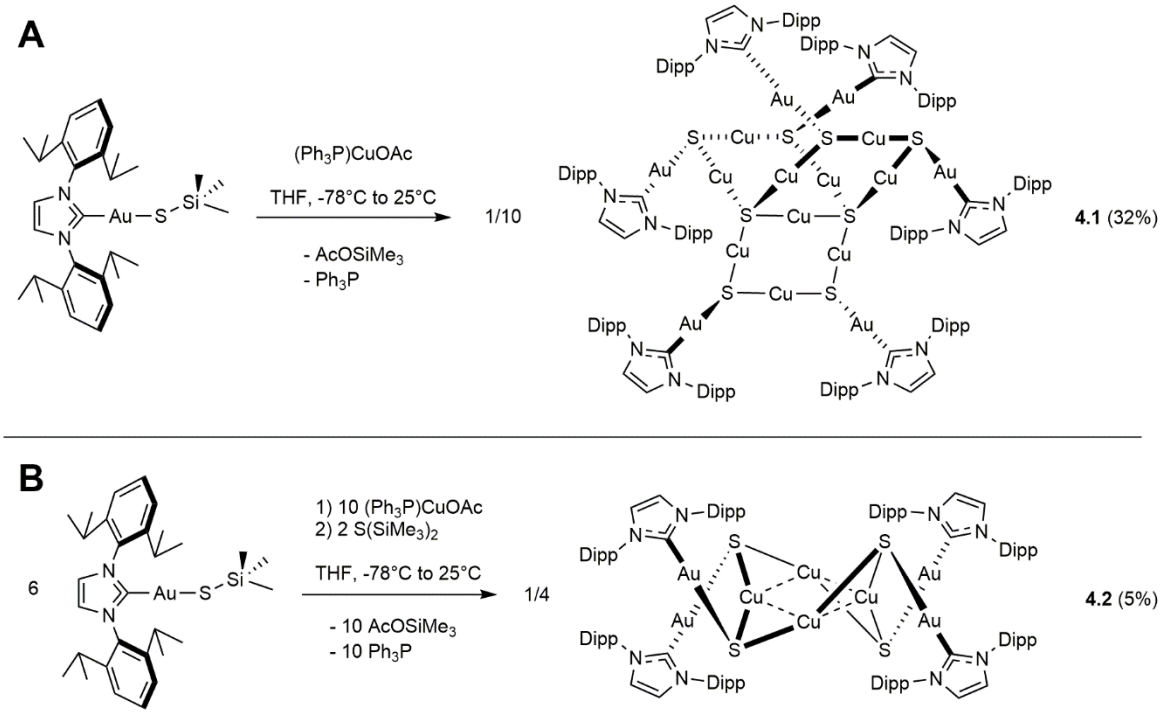

Scheme 4.1 Syntheses of A) **4.1** and B) **4.2**.

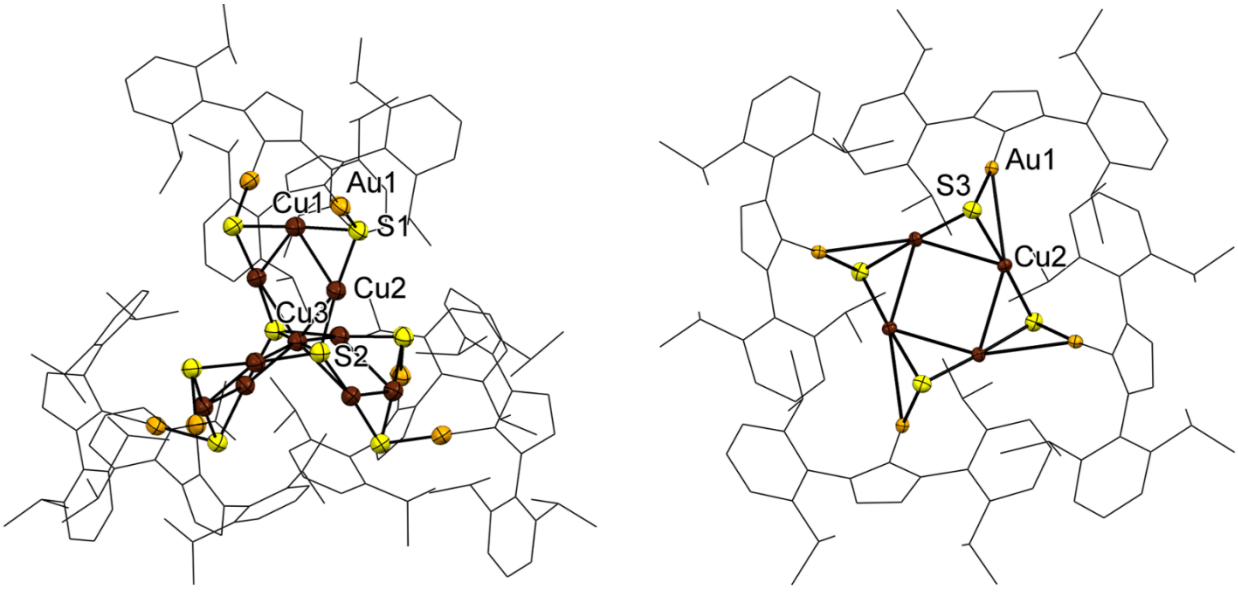

Figure 4.1 Molecular structures of Λ-**4.1** (left) and **4.2** (right) in the crystal. Thermal ellipsoids are plotted at the 50% probability level. All hydrogen atoms and solvent molecules are omitted, and the ligands are represented as wireframe drawings for clarity. **4.1** crystallizes about the intersection of a 3-fold axis passing through S2-Cu3-S2′ and a 2-fold axis passing through Cu1-Cu3. **4.2** crystallizes about a $\bar{4}$ center.

4.1 crystallizes in the trigonal space group $R\bar{3}c$ centered about the intersection of a 3-fold axis and three 2-fold axes (Figure 4.1). The cluster adopts a pinwheel-type structure which may be thought of as the combination of three Cu_4S_4 cycles found in **4.2**, fused along a single CuS_2 edge. The (IPr)Au groups are pendent on the outer edges and *trans* disposed relative to the M_4 plane. The cluster exhibits helical chirality, with both Δ and Λ enantiomers present in the crystal lattice. All metal atoms are linearly coordinated, with the largest deviations of 5° for S1-Cu2-S2. Sulfur atoms exist in two distinct coordination environments. The six outer sulfur (S1) bound to two Cu and one Au are trigonal pyramidal (Cu1-S1-Au1 87.87(8) – 95.57(10)°; Cu2-S1-Cu1 76.68(9)°), whereas the two inner sulfur atoms (S2) bound to four Cu are trigonal bipyramidal with a lone pair of electrons occupying the apical position.[19] S2 exhibits acute Cu3-S2-Cu2 (75.46(11)) and Cu2-S2-Cu2 which deviate less than 7° from 120°. Shorter Cu-Cu contacts (2.6814(12) – 2.6870(19) Å) are observed in **4.1** compared to **4.2**.

The ^{1}H and $^{13}C\{^{1}H\}$ NMR spectra of **4.2** are nearly identical to the related clusters $[Au_4M_4(\mu_3\text{-}E)_4(IPr)_4]$ (Section 2.2) and remain unchanged after several days at room temperature, indicating that conversion from **4.2** to **4.1** does not occur spontaneously in solution. The ^{1}H NMR spectrum of **4.1** differs significantly from that of **4.2**. In the aromatic region, three sets of signals are present: a multiplet from 7.37 – 7.41 ppm integrating to four protons, an apparent doublet of doublets from 7.28 – 7.30 ppm integrating to two protons and a singlet at 7.04 ppm integrating to two protons. In the aliphatic region, two overlapping septets at 2.61 and 2.58 ppm are present, integrating to four protons, alongside four partially overlapping doublets integrating to twenty-four protons in total (Figure 4.2). The observed signals indicate that the typical aromatic AB_2 spin system for 2,6-diisopropylphenyl is reduced to an ABC system. The simulated spin system produces good agreement with experiment to support this assignment (Figure 4.2). The ABC system is also verified by $^{13}C\{^{1}H\}$ NMR. In **4.2**, four signals appear in the aromatic region, as typical for a 2,6-disubstituted phenyl with identical 2- and 6-substituents. In **4.1**, six aromatic signals are observed, indicating all carbon atoms in the aromatic ring are inequivalent. This represents a rare example of an asymmetric cluster core imposing lower symmetry on its surroundings.[38]

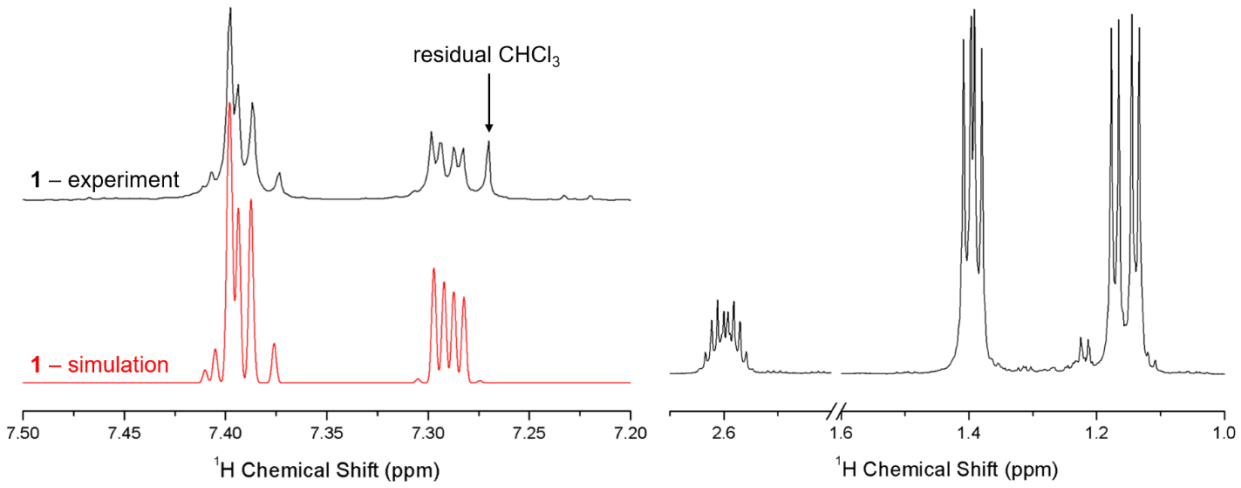

Figure 4.2 A) Simulated (lower, red) and experimental (upper, black) ^{1}H NMR spectra for the aromatic region of **4.1**. The spectrum was simulated as an ABC spin system with δ_A = 7.290 ppm, δ_B = 7.389 ppm, δ_C = 7.399 ppm, J_{AB} = 6.57 Hz, J_{AC} = 2.33 Hz, and J_{BC} = 6.87 Hz. B) Experimental ^{1}H NMR spectrum for the aliphatic region of **4.1**. Experimental spectra were obtained in $CDCl_3$ at 298K.

Single crystals of **4.1** are bright yellow luminescent in the solid state under UV (365 nm) excitation, whereas crystals of **4.2** are not visibly emissive unless cooled to 77K, at which temperature blue-green emission is observed. The bright solid-state emission of **4.1** prompted investigation of its photophysical properties as a function of temperature (Figure 4.3). In addition to measurements of steady state PL and PLE spectra from 15K to 298K, excited state lifetimes were obtained from mono-exponential fits to the time-resolved photoluminescence decay trace, and quantum yields were obtained using an integrating sphere by the method outlined in Section 4.3.1. The radiative rate constant was obtained from the ratio of Φ_{PL} and τ (see Section 1.2.1).

At 298K, **4.1** has a photoluminescence quantum yield of 0.05 in the solid state and excited state lifetime of 42 μs. Decreasing the temperature results in an increase in quantum yield and lifetime until 77K, at which point both plateau at 0.92 and ca. 470 μs, respectively. From 298K to 77K, the wavelength of maximum emission shifts from 578 nm to 595 nm. In addition to the tenfold decrease in excited state lifetime and blue-shifted emission upon raising the temperature, a twofold increase in the radiative rate constant (k_r) from 225K (789 s^{-1}) to 250K (1708 s^{-1}) suggests thermal population of an excited state with more allowed radiative relaxation to S_0. Such features are suggestive of a thermally-activated delayed fluorescence (TADF) mechanism.

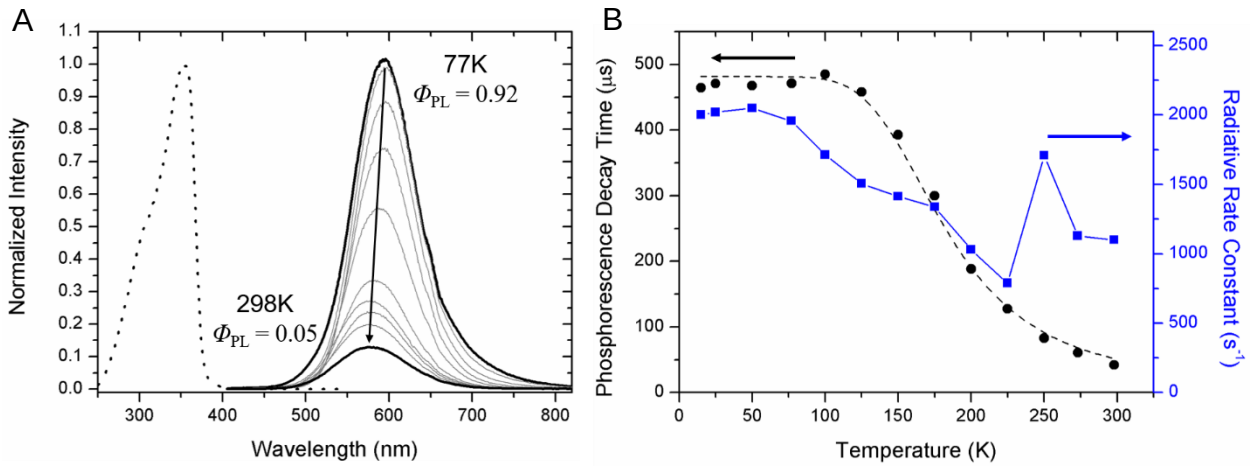

Figure 4.3 A) Temperature-dependent emission spectra of **4.1** in the solid state from 77K to 298K (solid lines). The dotted line is the excitation spectrum at 77K. B) Temperature-dependence of the phosphorescence lifetime (black circles) and radiative rate constant $k_r = \Phi_{PL}/\tau$ (blue squares) of **4.1**. The dashed black line is the least squares fit of the lifetime data to equation 4.1.

Least-squares fitting to the thermally-equilibrated two-state model of TADF (Equation 4.1) gives good agreement with the observed temperature dependence of τ (Figure 4.3). [39]

$$\tau(T) = \frac{3 + \exp\left(-\frac{\Delta E(S_1 - T_1)}{k_B T}\right)}{\frac{3}{\tau(T_1)} + \frac{1}{\tau(S_1)}\exp\left(-\frac{\Delta E(S_1 - T_1)}{k_B T}\right)} \qquad \textbf{(4.1)}$$

From the fitting procedure, a singlet-triplet gap $\Delta E(S_1\text{-}T_1)$ = 720 cm^{-1} is obtained, comparable to the experimental blueshift of 500 cm^{-1} from 77K to 298K. This procedure gives pure radiative lifetimes $\tau(T_1)$ = 482 μs and $\tau(S_1)$ = 600 ns, which, combined with low radiative lifetimes, indicate low oscillator strength for the $S_1 \rightarrow S_0$ and $T_1 \rightarrow S_0$ transitions compared to other TADF materials based on group 11 complexes.[39-43]

Density-functional modelling of the frontier orbitals of **4.1** suggests that the emissive state involves a charge transfer from the $Cu_{10}S_8$ cluster core to the NHC ancillary ligands (Figure 4.4). From Mulliken population analysis, the HOMO contains contributions from Cu (59%), S (27%), and Au (11%) and the LUMO is based mainly on the π system of the ligands (98%). Because there is minimal overlap in the orbitals involved in the S_0 and S_1 states, it is to be expected that the $S_1 \rightarrow S_0$ transition dipole moment will be small, and so delayed fluorescence will be inefficient, as

reflected in the long $S_1 \rightarrow S_0$ radiative decay time. On the other hand, minimal overlap between the HOMO and LUMO and the strong MLCT (Cu d$\rightarrow\pi^*$) character is connected to a small exchange integral and therefore contributes to the low singlet-triplet splitting $\Delta E(S_1\text{-}T_1)$ observed in **4.1**.

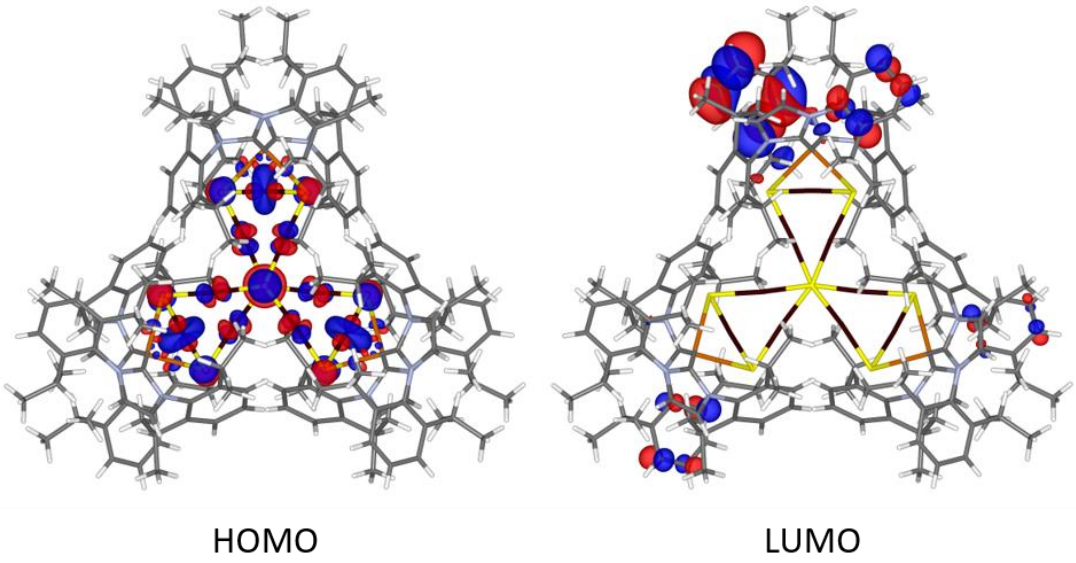

Figure 4.4 Highest occupied molecular orbital (HOMO) and lowest unoccupied molecular orbital (LUMO) isosurfaces (isoval = 0.03) for **4.1**.

4.3 Experimental Section

4.3.1 General Considerations

All syntheses described were conducted under an atmosphere of high-purity dry nitrogen using standard double-manifold Schlenk line techniques. Non-chlorinated solvents (tetrahydrofuran, pentane, hexanes, and toluene) were dried and collected using an MBraun MB-SP Series solvent purification system and stored over 3Å molecular sieves. Deuterated chloroform was purchased from Caledon and dried over P_2O_5 by refluxing under N_2 prior to collecting by distillation and stored over 3Å molecular sieves. Diethyl ether was dried and distilled over sodium benzophenone ketyl radical and stored over 3Å molecular sieves. Cu(OAc),[44] and $E(SiMe_3)_2$[45] were prepared following literature procedures. [(IPr)AuSSiMe$_3$] was prepared as outlined in Section 2.3.2. Other chemicals were used as received from commercial sources (Alfa Aesar and Aldrich).

NMR spectra were recorded on Inova 400 and Inova 600 spectrometers. ^{1}H and $^{13}C\{^{1}H\}$ chemical shifts are referenced to $SiMe_4$. Elemental analysis was performed by Laboratoire d'analyse élémentaire at the Université de Montréal, Montreal, Canada. Samples were dried under dynamic vacuum (< 10 mTorr) for at least 12 hours prior to shipment.

Photoluminescence measurements for solid samples of **4.1** and **4.2** were performed on a Horiba JobinYvon Fluorolog-3 spectrometer equipped with a Hamamatsu R5509 vis-NIR photomultiplier (~300 – 1400 nm) and an optical close-cycle cryostat (Leybold) for measurements at cryogenic temperatures down to ca. 15 K. Solid state spectra were measured in transmission for samples which were prepared as micron-sized crystalline powders dispersed in a mineral oil layer between two quartz plates. The emission spectra were corrected for the wavelength-dependent response of the spectrometer and detector (in relative photon flux units). Emission decay traces were recorded by connecting the photomultiplier to an oscilloscope (typically with a 500 or 50 Ohm load) and using a N_2-laser for pulsed excitation at 337 nm (~2 ns, ~5μJ per pulse).

Quantum yield for **4.1** was determined using a Teflon-lined integrating sphere by the method of Friend *et al.* [46] Briefly, six measurements were made: The area under the emission × wavelength profile is obtained (a) in absence of the sample, (b) with the sample directly illuminated by the source beam, and (c) with the sample diffusely illuminated by the source beam. The area under the excitation profile is also determined under the same experimental conditions. The quantum yield is determined by Equation 4.2.

$$\Phi_{PL} = \frac{P_c - (1 - A)P_b}{L_a A} \qquad \textbf{(4.2)}$$

Here, P_c = area under the emission profile in (c), $A = 1 - L_c/L_b$ is the absorption coefficient, where L_c and L_b are the area under the excitation profile in (c) and (b), P_b = area under the emission profile in (b) and L_a = area under the excitation profile in (a). For a complete experimental description, see reference 46.

Quantum chemical calculations were performed in Gaussian 09 Revision B.01[47] on the crystallographically determined structure of **4.1** at the level B3LYP/Def2SVP.[48-51] Mulliken population analysis[52] of the frontier orbitals was performed in Chemissian Version 4.53. Molecular

orbital isosurfaces were plotted from Gaussian .cub files in Visualization for Electronic Structure Analysis, version 4.4.0.[53]

4.3.2 Synthesis

Synthesis of $[Au_6Cu_{10}S_8(IPr)_6]$ (4.1)

$(Ph_3P)CuOAc$ was generated by the addition of PPh_3 (15 mg, 0.0579 mmol in 3 mL THF) to solid CuOAc followed by stirring until the solution is golden coloured. $[(IPr)AuSSiMe_3]$ (40 mg, 0.0579 mmol) was dissolved in 2 mL THF and both solutions were cooled to -78°C. The solutions were combined and the resulting clear yellow mixture was allowed to warm to -25°C with stirring and then held at this temperature overnight. The solution was then layered with 30 mL hexanes and stored at room temperature for two days, at which point colourless block crystals and yellow oil formed in solution. The crystals were removed and washed with Et_2O to afford the title complex as a pure white solid. Yield was increased by recrystallizing the mother liquor from THF/hexanes (9 mg, 32%). **^{1}H NMR** ($CDCl_3$, 25°C, 599.301 MHz) δ7.37-7.41 (4H, m, CH_{Ar}), 7.28-7.30 (2H, dd, CH_{Ar}), 7.04 (2H, s, CH_{imid}), 2.61 (sept, $J_{H\text{-}H}$ = 7.0 Hz, $CH(CH_3)_2$), 2.58 (sept, $J_{H\text{-}H}$ = 7.0 Hz, $CH(CH_3)_2$); overlapping signals at 2.61 and 2.58 integrate to 4H in total; 1.40 (d, $J_{H\text{-}H}$ = 7.0 Hz, $CH(CH_3)_2$), 1.38 (d, $J_{H\text{-}H}$ = 7.0 Hz, $CH(CH_3)_2$); overlapping signals at 1.40 and 1.38 integrate to 12H in total; 1.17 (d, $J_{H\text{-}H}$ = 7.0 Hz, $CH(CH_3)_2$); 1.13 (d, $J_{H\text{-}H}$ = 7.0 Hz, $CH(CH_3)_2$); overlapping signals at 1.17 and 1.13 integrate to 12H in total. **^{13}C{^{1}H} NMR** ($CDCl_3$, 25°C, 150.78 MHz) δ190.2 (s, C-Au), 145.3 (s, C_{Ar}), 145.0 (s, C_{Ar}), 134.4 (s, C_{Ar}), 130.8 (s, C_{Ar}), 125.0 (s, C_{Ar}), 124.2 (s, C_{Ar}), 121.9 (s, C_{imid}), 28.9 (s, $CH(CH_3)_2$), 28.9 (s, $CH(CH_3)_2$), 25.6 (s, $CH(CH_3)_2$), 25.5 (s, $CH(CH_3)_2$), 24.3 (s, $CH(CH_3)_2$), 24.1 (s, $CH(CH_3)_2$). **Anal. Calcd** for $C_{162}H_{216}Au_6Cu_{10}N_{12}S_8 \bullet C_4H_8O$: C, 44.53; H, 5.04; N, 3.75; S, 5.73. Found C, 44.89; H, 5.15; N, 3.58; S, 5.47. The presence of 1 molecule of THF per molecule of the title cluster is confirmed by both single-crystal X-ray diffraction and the integration of the THF signals in the ^{1}H NMR spectrum after vacuum drying

Synthesis of $[Au_4Cu_4S_4(IPr)_4]$ (4.2)

$(Ph_3P)CuOAc$ was generated by the addition of PPh_3 (32 mg, 0.1206 mmol in 2 mL THF) to solid CuOAc (15 mg, 0.1206 mmol) followed by stirring until the solution is golden coloured. $[(IPr)AuSSiMe_3]$ (50 mg, 0.0724 mmol) was dissolved in 2 mL THF and both solutions were cooled to -78°C. The solutions were combined, and the resulting clear yellow mixture was allowed

to warm to -25°C with stirring and stirred at this temperature for 20 minutes. The mixture was cooled to -78°C and 5 μL (0.0241 mmol) $S(SiMe_3)_2$ was added with a micropipette. The solution was allowed to warm to -25°C with stirring and then stored at this temperature overnight. The solution was brought to room temperature and layered with hexanes (40 mL). After 1 day, white crystals and brown solids form. The brown solids were removed with a pipette and the crystals were recrystallized from THF/hexanes to afford 4 mg of the title complex (5%). **^{1}H NMR** ($CDCl_3$, 25°C, 599.301 MHz) δ7.41 (2H, t, $J_{H\text{-}H}$ = 7.8 Hz, CH_{Ar}), 7.22 (4H, d, $J_{H\text{-}H}$ = 7.8 Hz, CH_{Ar}), 6.99 (2H, s, CH_{imid}), 2.58 (4H, sept, $J_{H\text{-}H}$ = 6.7 Hz, C*H*$(CH_3)_2$), 1.30 (12H, d, $J_{H\text{-}H}$ = 6.7 Hz, CH(C*H*$_3)_2$), 1.15 (12H, d, $J_{H\text{-}H}$ = 6.7 Hz, CH(C*H*$_3)_2$). **^{13}C{^{1}H} NMR** ($CDCl_3$, 25°C, 150.78 MHz) δ190.9 (s, C-Au), 145.4 (s, C_{Ar}), 134.7 (s, C_{Ar}), 130.1 (s, C_{Ar}), 124.1 (s, C_{Ar}), 121.8 (s, C_{imid}), 28.7 (s, *C*H$(CH_3)_2$), 25.2 (s, CH(*C*H$_3)_2$), 24.1 (s, CH(*C*H$_3)_2$).

4.3.3 X-Ray Crystallography Details

X-ray measurements were made on a Bruker Kappa Axis Apex2 diffractometer equipped with graphite monochromated Mo $K\alpha_1$ (λ=0.71073 Å, **4.2**) radiation or a Nonius KappaCCD Apex2 with Cu $K\alpha_1$ (λ=1.5418 Å, **4.1**) radiation at a temperature of 110 K. The samples were mounted on a Mitegen polyimide micromount with a small amount of Paratone N oil. The collection strategy was a number of ω and φ scans with data collected up to >50° (2θ). The frame integration was performed using SAINT.[54] The resulting raw data was scaled and absorption corrected using a multi-scan averaging of symmetry equivalent data using SADABS.[55] The structure was solved by using a dual space methodology using the SHELXT program.[56] All non-hydrogen atoms were obtained from the initial solution. The hydrogen atoms were introduced at idealized positions and were allowed to ride on the parent atom. The structural model was fit to the data using full matrix least-squares based on F^2. The calculated structure factors included corrections for anomalous dispersion from the usual tabulation.

The structures were refined using the SHELXLE program from the SHELXTL suite of crystallographic software.[57] Unless otherwise stated, all non-hydrogen atoms were refined anisotropically. In **4.1**, a disordered THF molecule was refined with a split occupancy model over two positions and all atoms were refined isotropically using the SADI command to constrain the C-C and C-O bond lengths.

4.4 Conclusions and Outlook

In conclusion, two new Au(I)-Cu(I)-S clusters, $[Au_6Cu_{10}S_8(IPr)_6]$ and $[Au_4Cu_4S_4(IPr)_4]$, have been prepared from reactions of the NHC-stabilized gold(I) trimethylsilylchalcogenolate reagent $[(IPr)AuSSiMe_3]$. The larger of the two clusters exhibits efficient phosphorescence at low temperatures and long-lived thermally activated delayed fluorescence at room temperature. At low temperatures, the smaller of the two clusters was phosphorescent but became completely non-emissive upon warming. Thus, the combination of the increased structural rigidity in **1** compared to **2**, and its capacity for emission from thermally equilibrated S_1 and T_1 states is responsible for the overall enhancements observed in solid state luminescence efficiency. These principles can help in the design new emissive materials based on polynuclear clusters of d^{10} centers.

In general, it is difficult to control the nuclearity and geometry of metal chalcogenide clusters. The choice of ancillary ligand often produces large variations in the size of cluster obtained from reaction mixtures of metal acetates, $E(SiMe_3)_2$, and/or $RESiMe_3$. For Au(I), high nuclearity (ca. 10 – 30 Au atoms) clusters generally involve bidentate phosphines. Therefore, it would be of interest to attempt the types of reactions described herein in the presence of bidentate NHC ligands. Dinuclear complexes of the form $[(L\hat{}L)Au_2(ESiMe_3)_2]$ (L^L = bidentate ligand) prepared in the Corrigan lab are known to be unstable towards formation of $[(L\hat{}L)Au_2(\mu\text{-}E)]$ and $E(SiMe_3)_2$. Cluster formation must therefore bypass formation of the trimethylsilylchalcogenolate compound. This might be achieved by the combination of $[(L\hat{}L)Au_2X_2]$ (L^L = bidentate carbene, X = halide, acetate) with substoichiometric amounts of $E(SiMe_3)_2$. Alternatively, ligand-exchange reactions (which are commonly exploited in nanocluster chemistry)[58-60] between bidentate NHCs and monodentate-NHC-stabilized clusters such as $[Au_4M_4(\mu_3\text{-}E)_4(IPr)_4]$ could produce a rearrangement of the cluster core to one of higher nuclearity, facilitated by bridging interactions in the ligand sphere. Rigid bidentate ligands should additionally help to improve quantum yield by limiting molecular distortion in the excited state.

4.5 References

[1] O. Fuhr, S. Dehnen, D. Fenske. *Chem. Soc. Rev.* **2013**, *42*, 1871.
[2] S. Bestgen, O. Fuhr, B. Breitung, V. S. K. Chakravadhanula, G. Guthausen, F. Hennrich, W. Yu, M. M. Kappes, P. W. Roesky, D. Fenske. *Chem. Sci.* **2017**, *42*, 1871.
[3] S. Bestgen, X. Yang, I. Issac, O. Fuhr, P. W. Roesky, D. Fesnke. *Chem. Eur. J.* **2016**, *22*, 9933.
[4] S. Bestgen, O. Fuhr, P. W. Roesky, D. Fenske. *Dalton Trans.* **2016**, *45*, 14907.
[5] L.-Y. Yao, T. K.-M. Lee, V. W.-W. Yam. *J. Am. Chem. Soc.* **2016**, *138*, 7260.
[6] L.-Y. Yao, V. W.-W. Yam. *J. Am. Chem. Soc.* **2015**, *137*, 3506.
[7] L.-Y. Yao, F. K.-W. Hau, V. W.-W. Yam. *J. Am. Chem. Soc.* **2014**, *136*, 10801.
[8] T. K.-M. Lee, N. Zhu, V. W.-W. Yam. *J. Am. Chem. Soc.* **2010**, *132*, 17646.
[9] V. W.-W. Yam, E. C.-C. Cheng, N Zhou. *Angew. Chem. Int. Ed.* **2001**, *40*, 1763.
[10] V. W.-W. Yam, E. C.-C. Cheng, Z.-Y. Zhou. *Angew. Chem. Int. Ed.* **2000**, *39*, 1683.
[11] V. W.-W. Yam, E. C.-C. Cheng. *Angew. Chem. Int. Ed.* **2000**, *39*, 4240.
[12] V. W.-W. Yam, E. C-C. Cheng, K.-K. Cheung. *Angew. Chem. Int. Ed.* **1999**, *38*, 197.
[13] V. W.-W. Yam, K. K.-W. Lo, C.-R. Wong, K.-K. Cheung. *Inorg. Chem.* **1996**, *35*, 5116.
[14] V. W.-W. Yam, W.-K. Lee, T.-F. Lai. *J. Chem. Soc. Chem. Commun.* **1993**, *4*, 1571.
[15] J. R. Shakirova, E. V. Grachova, V. V. Sizov, G. L. Starova, I. O. Koshevoy, A. S. Melnikov, M. C. Gimeno, A. Laguna, S. P. Tunik. *Dalton Trans.* **2017**, *46*, 2516.
[16] O. Crespo, M. C. Gimeno, A. Laguna, C. Larraz, M. D. Villacampa, *Chem. Eur. J.* **2007**, *13*, 235.
[17] Q.-M. Wang, Y.-A. Lee, O. Crespo, J. Deaton, C. Tang, H. J. Gysling, M. C. Gimeno, C. Larraz, M. D. Villacampa, A. Laguna, R. Eisenberg. *J. Am. Chem. Soc.* **2004**, *126*, 9488.
[18] S. Canales, O. Crespo, M. C. Gimeno, P. G. Jones, A. Laguna, F. Mendizabal. *Organometallics* **2000**, *19*, 4985.
[19] F. Canales, M. C. Gimeno, A. Laguna, P. G. Jones. *J. Am. Chem. Soc.* **1996**, *118*, 4839.
[20] A. Eichhöfer, M. Kühn, S. Lebedkin, M. Kehry, M. M. Kappes, F. Weigend. *Inorg. Chem.* **2017**, *56*, 9330.
[21] A. Eichhöfer, G. Buth, S. Lebedkin, M. Kühn, F. Weigend. *Inorg. Chem.* **2015**, *54*, 9413.
[22] X.-X. Yang, I. Issac, S. Lebedkin, M. Kühn, F. Weigend, D. Fenske, O. Fuhr, A. Eichhöfer. *Chem. Commun.* **2014**, *50*, 11043.
[23] V. W.-W. Yam, V. K.-M. Au, S. Y.-L. Leung. *Chem. Rev.* **2015**, *115*, 7589.
[24] C.-W. Hsu, C.-C. Lin, M. W. Chung, Y. Chi, G.-H. Lee, P.-T. Chou, C.-H. Chang, P.-Y. Chen. *J. Am. Chem. Soc.* **2011**, *133*, 12085.
[25] V. W.-W. Yam, K. M.-C. Wong. *Chem. Commun.* **2011**, *47*, 11579.
[26] A. Barbieri, G. Accorsi, N. Armaroli. *Chem. Commun.* **2008**, 2185.
[27] V. W.-W. Yam, K. K.-W. Lo. *Chem. Soc. Rev.* **1999**, *28*, 323.
[28] A. M. Polgar, F. Weigend, A. Zhang, M. J. Stillman, J. F. Corrigan. *J. Am. Chem. Soc.* **2017**, *139*, 14045.
[29] A. M. Polgar, C. B. Khadka, M. Azizpoor Fard, B. Nikkel, T. O'Donnell, T. Neumann, K. Lahring, K. Thompson, C. Cadogan, F. Weigend, J. F. Corrigan. *Chem. Eur. J.* **2016**. *22*, 18378.
[30] M. Azizpoor Fard, T. I. Levchenko, C. Cadogan, W. J. Humenny, J. F. Corrigan. *Chem. – Eur. J.* **2016**, *22*, 4543.
[31] J. Zhai, A. S. Filatov, G. L. Hillhouse, M. D. Hopkins. *Chem. Sci.* **2016**, *7*, 589.

[32] J. Zhai, M. D. Hopkins, G. L. Hillhouse, *Organometallics*, **2015**, *34*, 4637.
[33] M. Azizpoor Fard, F. Weigend, J. F. Corrigan. *Chem. Commun.* **2015**, *51*, 8361.
[34] R. Biedermann, O. Kluge, D. Fuhrmann, H. Krautscheid. *Eur. J. Inorg. Chem.* **2013**, *27*, 4727.
[35] A. Borecki, J. F. Corrigan. *Inorg. Chem.* **2007**, *46*, 2478.
[36] M. W. DeGroot, J. F. Corrigan. *Z. Anorg. Allg. Chem.* **2006**, *632*, 19.
[37] H. Yersin, R. Czerwieniec, M. Z. Shafikov, A. F. Suleymanova. *ChemPhysChem* **2017**, *18*, 3508.
[38] G. Deng, S. Malola, J. Yan, Y. Han, P. Yuan, C. Zhao, X. Yuan, S. Lin, Z. Tang, B. K. Teo, H. Häkkinen, N. Zheng. *Angew. Chem. Int. Ed.* **2018**, *57*, 3421.
[39] R. Czerwieniec, M. J. Leitl, H. H. H. Homeier, H. Yersin. *Coord. Chem. Rev.* **2016**, *325*, 2.
[40] K. Shimada, A. Kobayashi, Y. Ono, H. Ohara, T. Hasegawa, T. Taketsugu, E. Sakuda, S. Akagi, N. Kitamura, M. Kato. *J. Phys. Chem. B* **2016**, *120*, 16002.
[41] X.-L. Chen, R. Yu, X.-Y. Wu, D. Liang, J.-H. Jia, C.-Z. Lu. *Chem. Commun.* **2016**, *52*, 6288.
[42] J. Nitsch, F. Lacemon, A. Lorbach, A. Eichhorn, F. Cisnetti, A. Steffen. *Chem. Commun.* **2016**, *52*, 2932.
[43] M. Osawa, M.-a. Aino, T. Nagakura, M. Hoshino, Y. Tanaka, M. Akita. *Dalton Trans.* **2018**, DOI: 10.1039/C8DT01097H
[44] D. A. Edwards, R. Richards. *J. Chem. Soc., Dalton Trans*. **1973**, *0*, 2463.
[45] J.-H. So, P. Boudjouk. *Synthesis*, **1989**, *4*, 306.
[46] J. C. de Mello, H. F. Wittmann, R. H. Friend. *Adv. Mater.* **1997**, *9*, 230.
[47] Frisch, M. J.; Trucks, G. W.; Schlegel, H. B.; Scuseria, G. E.; Robb, M. A.; Cheeseman, J. R.; Scalmani, G.; Barone, V.; Petersson, G. A.; Nakatsuji, H.; Li, X.; Caricato, M.; Marenich, A.; Bloino, J.; Janesko, B. G.; Gomperts, R.; Mennucci, B.; Hratchian, H. P.; Ortiz, J. V.; Izmaylov, A. F.; Sonnenberg, J. L.; Williams-Young, D.; Ding, F.; Lipparini, F.; Egidi, F.; Goings, J.; Peng, B.; Petrone, A.; Henderson, T.; Ranasinghe, D.; Zakrzewski, V. G.; Gao, J.; Rega, N.; Zheng, G.; Liang, W.; Hada, M.; Ehara, M.; Toyota, K.; Fukuda, R.; Hasegawa, J.; Ishida, M.; Nakajima, T.; Honda, Y.; Kitao, O.; Nakai, H.; Vreven, T.; Throssell, K.; Montgomery, J. A., Jr.; Peralta, J. E.; Ogliaro, F.; Bearpark, M.; Heyd, J. J.; Brothers, E.; Kudin, K. N.; Staroverov, V. N.; Keith, T.; Kobayashi, R.; Normand, J.; Raghavachari, K.; Rendell, A.; Burant, J. C.; Iyengar, S. S.; Tomasi, J.; Cossi, M.; Millam, J. M.; Klene, M.; Adamo, C.; Cammi, R.; Ochterski, J. W.; Martin, R. L.; Morokuma, K.; Farkas, O.; Foresman, J. B.; Fox, D. J. Gaussian 09, Revision B.01, Gaussian, Inc., Wallingford CT, 2016.
[48] A. D. Becke. *Phys. Rev. A* **1988**, *38*, 3098.
[49] C. Lee, W. Yang, R. G. Parr. *Phys. Rev. B* **1988**, *37*, 785.
[50] F. Weigend, R. Ahlrichs. *Phys. Chem. Chem. Phys*. **2005**, *7*, 3297.
[51] F. Weigend. *Phys. Chem. Chem. Phys.* **2006**, *8*, 1057.
[52] R. S. Mulliken. *J. Chem. Phys.* **1955**, *23*, 1833.
[53] K. Momma, F. Izumi. *J. Appl. Cryst.* **2014**, *44*, 1272.
[54] Bruker-AXS, SAINT version 2013.8, 2013, Bruker-AXS, Madison, WI 53711, USA.
[55] Bruker-AXS, SADABS version 2012.1, 2012, Bruker-AXS, Madison, WI 53711, USA.
[56] G. M. Sheldrick. *Acta Cryst.* **2015**, *A71*, 3.
[57] G. M. Sheldrick. *Acta Cryst.* **2015**, *C71*, 3.
[58] C. Zeng, Y. Chen, A. Das, R. Jin. *J. Phys. Chem. Lett.* **2015**, *6*, 2976.
[59] T.-A. D. Nguyen, Z. R. Jones, D. F. Leto, G. Wu, S. L. Scott, T. W. Hayton. *Chem. Mater.* **2016**, *28*, 8385.
[60] Y. Kamei, Y. Shichibu, K. Konishi. *Angew. Chem. Int. Ed.* **2011**, *50*, 7442.

Chapter 5

5 Conclusions and Outlook

5.1 Summary and Conclusions

The work in this thesis describes the reaction chemistry of group 11 silylchalcogenolate reagents stabilized by *N*-heterocyclic carbene ligands for the preparation of luminescent coinage metal chalcogenide clusters. Reagents of the form [(NHC)MESiMe$_3$] are prepared in a single step from readily accessible precursors. One further step converts these into polynuclear homo- and heterometallic chalcogenide assemblies with tunable metal/chalcogen compositions. The photophysical properties of the clusters vary depending on their composition, with independent contributions from the metal atoms and chalcogenide ligands. Variation in the ancillary NHC ligand allows for stabilization of a wider range of structural frameworks and new photophysical properties are observed as a result. Control over cluster geometry and nuclearity are the most difficult to obtain but may have the most significant effects on the excited state dynamics in group 11 chalcogenide clusters.

Building on previous work in the Corrigan lab regarding NHC-stabilized copper(I) and silver(I) trimethylsilylchalcogenolate compounds [(IPr)CuESiMe$_3$] and [(IPr)AgESiMe$_3$],[1,2] the gold(I) analogues [(IPr)AuESiMe$_3$] (**2.1a-c**, E = S, Se, Te) were first synthesized. These exhibited exceptional thermal stability in solution and the solid state, compared to the Cu(I) and Ag(I) derivatives and [(Ph$_3$P)AuESiMe$_3$].[3] Reactions of **2.1a-c** with [(Ph$_3$P)AgOAc], [(Ph$_3$P)AuOAc] or [({2,4-^{t}Bu(C$_6$H$_3$)O}$_3$P)AuOAc] yielded a series of isostructural octanuclear clusters [Au$_4$M$_4$(μ_3-E)$_4$(IPr)$_4$] (**2.2a,b**, M = Ag, E = S, Se; **2.3a-c**, M = Au, E = S, Se, Te). These were emissive in 2-methyltetrahydrofuran (2-MeTHF) and the solid state at 77K, with emission energies varying from green (562 nm) to the near-infrared (745 nm) as a function of M, E, and the medium in which emission occurs. In general, Au(I)-E clusters emitted at lower energies than Au(I)-Ag(I)-E for fixed E, and Au(I)-M(I)-Se clusters emitted at lower energies than Au(I)-M(I)-S for fixed M. Quantum chemical calculations suggest that emission arises from a charge transfer between the cluster-based HOMO and ligand-based LUMO. Higher-lying lone-pair orbitals on Se compared to S contribute to lower energy photoluminescence. Similarly, destabilization of the core-based

HOMO for M = Au compared to M = Ag is calculated to produce low energy emission. Chart 5.1 summarizes the compounds prepared and their photophysical properties.

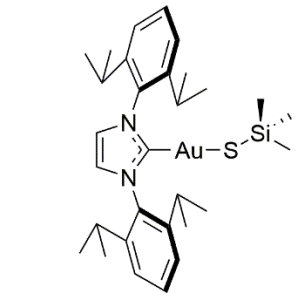

2.1a

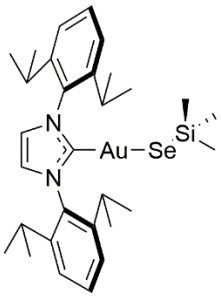

2.1b

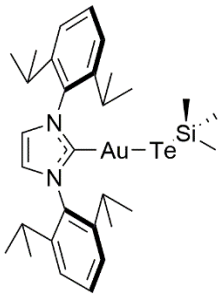

2.1c

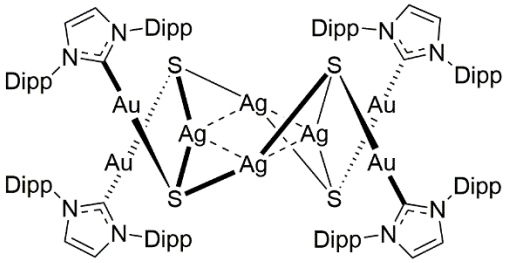

2.2a

λ_{em} = 562 nm; τ = 17.7 μs (2-MeTHF)
λ_{em} = 669 nm; τ = 19.2 μs (Solid)

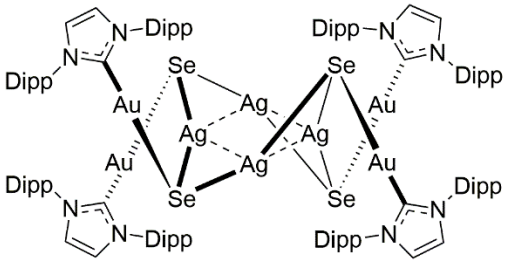

2.2b

λ_{em} = 592 nm; τ = 20.5 μs (2-MeTHF)
λ_{em} = 682 nm; τ = 20.4 μs (Solid)

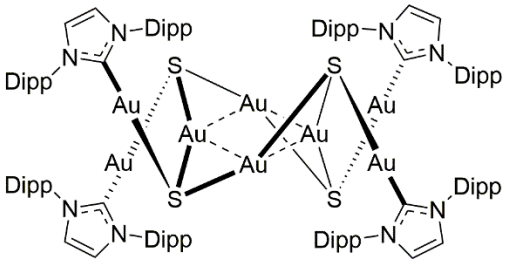

2.3a

λ_{em} = 596 nm; τ = 42.4 μs (2-MeTHF)
λ_{em} = 670 nm; τ = 31.0 μs (Solid)

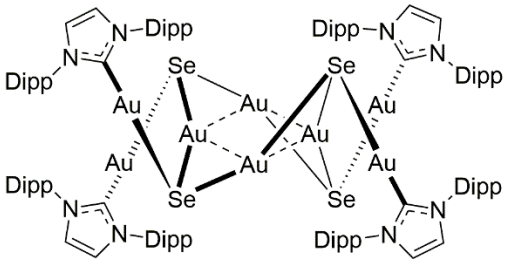

2.3b

λ_{em} = 657 nm; τ = 37.8 μs (2-MeTHF)
λ_{em} = 745 nm; τ = 30.3 μs (Solid)

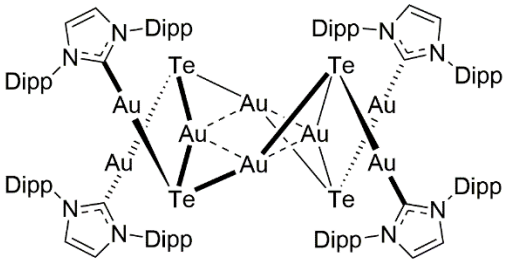

2.3c

λ_{em} = 694 nm
τ = 9.78 μs (Solid)

Chart 5.1 New compounds reported in Section 2 and their associated spectroscopic parameters at 77K. Dipp = 2,6-diisopropylphenyl.

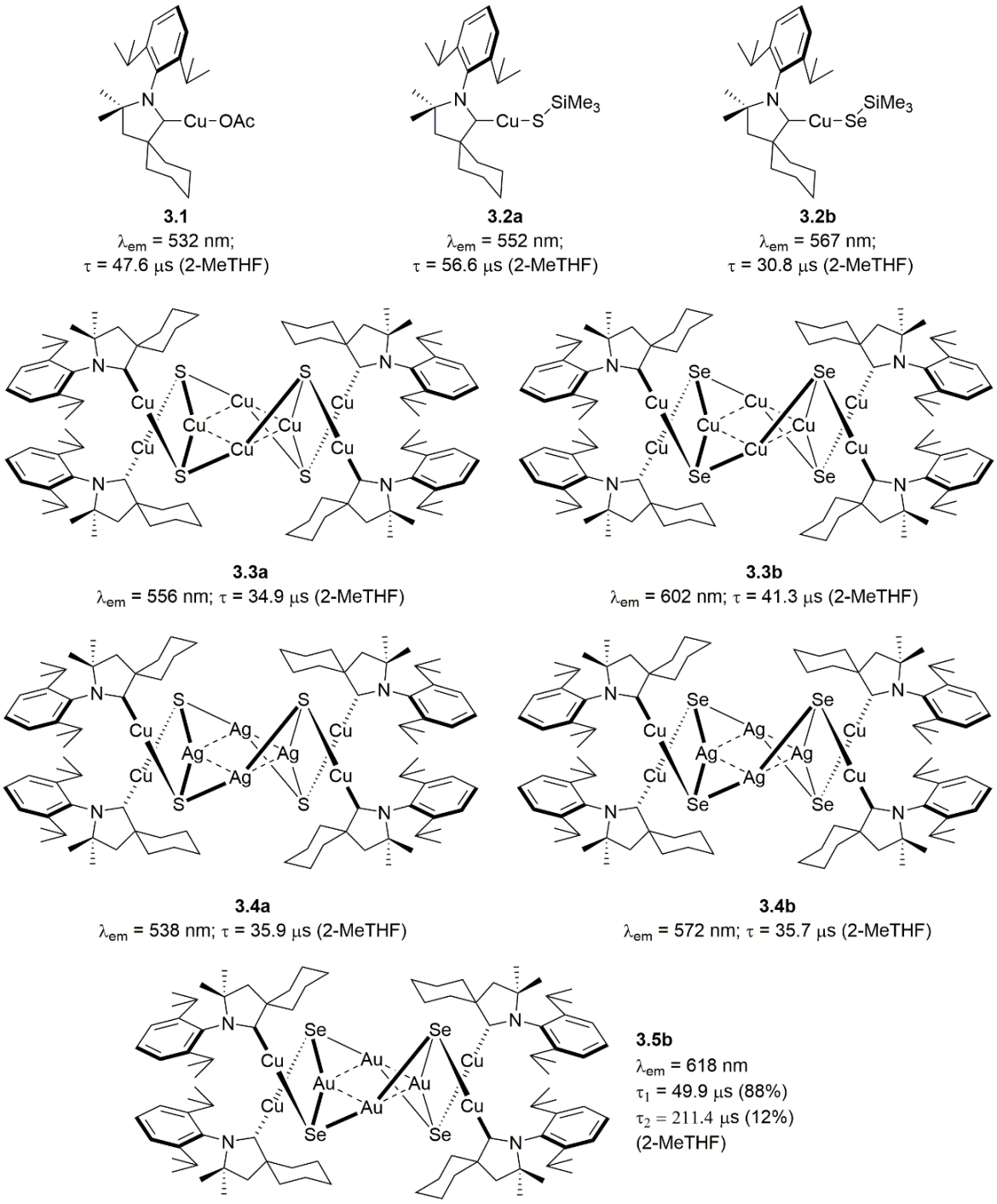

Chart 5.2 New compounds reported in Section 3 and their associated spectroscopic parameters at 77K.

Attempts to produce analogous 11-11′-16 clusters using [(IPr)CuESiMe$_3$] were unsuccessful, with only thermally unstable mixtures produced by reaction with [(L)M(OAc)]. A

stronger σ-donor ancillary ligand based on a cyclic (alkyl)(amino)carbene ($CAAC^{Cy}$) was instead employed, [4] and found to give stable complexes. From [($CAAC^{Cy}$)CuOAc] (**3.1**), the trimethylsilylchalcogenolates [($CAAC^{Cy}$)$CuESiMe_3$] (**3.2a,b**, E = S, Se) were prepared. The mononuclear complexes were luminescent in 2-MeTHF at 77K, with emission maxima red-shifted with higher-lying non-bonding pairs on the chalcogen-containing ligand (O < S < Se). Reactions with [(Ph_3P)CuOAc], [(Ph_3P)AgOAc] or [({2,4-^{t}Bu(C_6H_3)O}$_3$P)AuOAc] yielded a second series of isostructural octanuclear clusters [$Cu_4M_4(\mu_3\text{-}E)_4(CAAC^{Cy})_4$] (**3.3a,b**, M = Cu, E = S, Se; **3.4a,b**, M = Ag, E = S, Se; **3.5b**, M = Au, E = Se). These were emissive at 77K in glassy 2-MeTHF, with emission energies that vary as a function of the chalcogen lone-pair energy and the ability of the metal atom to stabilize the cluster-based HOMO (Ag > Cu > Au). This sequencing of the group 11 metals is also observed for the ^{1}MLCT (M→SR) energy, [5] indicating the strong MLCT contribution to the emissive states. Chart 5.2 summarizes the compounds prepared and their photophysical properties.

Reaction of **2.1a** with [(Ph_3P)CuOAc] produced an unexpected cluster [$Au_6Cu_{10}(\mu_3\text{-}S)_6(\mu_4\text{-}S)_2(IPr)_6$] (**4.1**) when reacted in equimolar amounts, and another cluster [$Au_4Cu_4(\mu_3\text{-}S)_4(IPr)_4$] (**4.2**), isostructural to **2.2-3**, when carried out with $S(SiMe_3)_2$ and substoichiometric Au relative Cu. **4.1** was emissive in the solid state at room temperature and the efficiency of the emission maximized (Φ_{PL} = 0.92) at 77K. **4.2**, although similar in composition, was emissive at 77K but became non-emissive upon warming the solid. The different spectroscopic behaviour for the two related clusters was related to the enhanced size and structural rigidity of **4.1** relative to **4.1** and the observation of thermally activated delayed fluorescence in **4.1** at room temperature.[6] A small singlet-triplet gap $\Delta E(S_1\text{-}T_1)$ allows **4.1** to thermally populate the S_1 state by reverse intersystem crossing from the excited triplet state. Fully allowed $S_1 \rightarrow S_0$ emission is observed in an increase in the radiative rate constant at higher temperature and blue-shifted emission energy at 298K compared to 77K. Quantum chemical calculations show that emission in **4.1** originates from a charge transfer between the $Cu_{10}S_8$ core and NHC ancillary ligands. The minimal overlap in HOMO and LUMO is thought to be responsible for both the small $\Delta E(S_1\text{-}T_1)$, which allows for TADF, and the relatively low radiative $S_1 \rightarrow S_0$ rates, which limits the efficiency of emission. Chart 5.3 summarizes the compounds prepared and their photophysical properties.

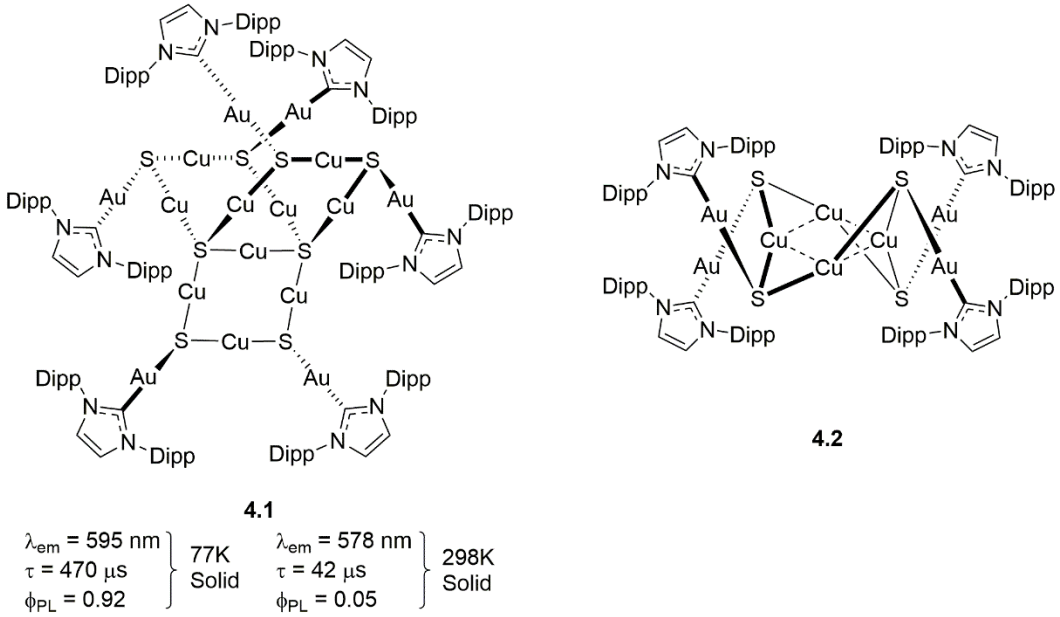

Chart 5.3 New compounds reported in Section 4 and their associated spectroscopic parameters.

5.2 Outlook – NHCs in Nanocluster Chemistry

The complexes and clusters reported in this thesis are promising precursors to nanoclusters of the group 11 metals passivated with metal-chalcogenide surfaces and NHC ancillary ligands. The reaction of the clusters $[Au_4M_4E_4(IPr)_4]$ with reducing agents could result in the formation of an M(0) nanocluster core and a stabilizing Au_2E shell, with NHCs occupying the coordination sphere of surface metal atoms. Recently, Schnepf has provided a proof of this concept in the preparation of nanoclusters with a gold(0) core and a gold(I)-sulfide shell through the reduction of a gold(I) thiolate precursor.[7,8] These types of clusters would represent a fundamentally new type of nanoscopic assembly, which could be a source of versatile functional materials. The functional properties of homometallic nanoclusters are already broadly exploited in chemistry.[9] Bimetallic nanoclusters have also emerged, in which synergistic effects between the two metals produce enhancements in physical properties like catalytic activity, photoluminescence, and redox activity.[10] The favourable ligation properties of NHCs could be advantageous in such systems by increasing stability and solubility, and by limiting surface isomerization.

5.3 Outlook – Metal Chalcogenide-Metallachalcogenolate clusters

Metal chalcogenide-chalcogenolate clusters are some of the largest discrete molecules to have been characterized by crystallographic methods.[11] Based on the analogy between the reaction chemistry organic chalcogenolates, RE^-, and metallachalcogenolates, such as $(CAAC^{Cy})CuE^-$, it may be possible to prepare similar large structures in which the stabilizing shell is composed of metallic, rather than organic fragments. Reactions of $(CAAC^{Cy})CuESiMe_3$ with M(OAc) (M = Cu, Ag) and $E(SiMe_3)_2$, or reactions of $[Cu_4M_4E_4(CAAC^{Cy})]_4$ with $E(SiMe_3)_2$ directly parallel the chemistry of metal chalcogenide-chalcogenolate nanoclusters and deserve exploration. In principle this would allow the preparation of an M_2E core stabilized by a $(CAAC^{Cy})CuE^-$ shell. The ability to tune this system by different choices of M and E could produce libraries of nanosized-clusters with different metal/chalcogen composition, as shown in this thesis for smaller $\{(NHC)MM'E\}_n$ oligomers. The production of organic soluble metal-chalcogenide nanoclusters is a relatively recent advancement,[12] which could be expanded upon using NHC ancillary ligands.

5.4 Outlook – Modulation of the Ancillary NHC Ligands

The understanding in this thesis of how different cluster geometries drive different photophysical behaviours should encourage the exploration of how to control cluster geometry and nuclearity. One previously established principle involves the use of smaller NHC ligands to facilitate cluster growth, at the cost of lower overall stability.[2] This thesis explored only carbenes of similar size, so variation in ligand steric environment should be investigated more fully. The use of polydentate NHCs is also promising for new structural types. Furthermore, higher denticity should promote greater molecular rigidity and therefore positively impact the excited state properties of metal chalcogenide cluster. For example, NHCs with pyridyl groups as the *N*-substituents should change the way clusters aggregate (particularly those of Cu(I), which interacts well with N-donor ligands),[13] while not interfering with the formation of the silylchalcogenolate precursor. Ligand exchange reactions with preformed clusters and bidentate NHCs also have potential in this regard and would mirror the well-developed chemistry of phosphine- and thiolate-exchange reactions.[14-16]

5.5 References

[1] M. Azizpoor Fard, F. Weigend, J. F. Corrigan. *Chem. Commun.* **2015**, *51*, 8361.
[2] M. Azizpoor Fard, T. I. Levchenko, C. Cadogan, W. J. Humenny, J. F. Corrigan. *Chem. – Eur. J.* **2016**, *22*, 4543.
[3] A. M. Polgar, F. Weigend, A. Zhang, M. J. Stillman, J. F. Corrigan. *J. Am. Chem. Soc.* **2017**, *139*, 14045.
[4] R. Jazzar, R. D. Dewhurst, J.-B. Bourg, B. Donnadieu, Y. Canac, G. Bertrand. *Angew. Chem. Int. Ed.* **2007**, *46*, 2899.
[5] K. Fujisawa, S. Imai, Y. Moro-oka. *Chem. Lett.* **1998**, *27*, 167.
[6] H. Yersin, R. Czerwieniec, M. Z. Shafikov, A. F. Suleymanova. *ChemPhysChem* **2017**, *18*, 3508.
[7] S. Kenzler, C. Schrenk, A. Schnepf. *Angew. Chem. Int. Ed.* **2017**, *56*, 393.
[8] S. Kenzler, C. Schrenk, A. R. Frojd, H. Häkkinen, A. Z. Clayborne, A. Schnepf. *Chem. Commun.* **2018**, *54*, 248.
[9] I. Chakraborty, T. Pradeep. *Chem. Rev.* **2017**, *117*, 8208.
[10] N. Yan, L. Liao, J. Yuan, Y.-j. Lin, L.-h. Weng, J. Yang, Z. Wu. *Chem. Mater.* **2016**, *28*, 8240.
[11] O. Fuhr, S. Dehnen, D. Fenske. *Chem. Soc. Rev.* **2013**, *42*, 1871.
[12] S. Bestgen, O. Fuhr, B. Breitung, V. S. K. Chakravadhanula, G. Guthausen, F. Hennrich, W. Yu, M. M. Kappes, P. W. Roesky, D. Fenske. *Chem. Sci.* **2017**, *42*, 1871.
[13] C. E. Strasser, V. J. Catalano. *J. Am. Chem. Soc.* **2010**, *132*, 10009.
[14] C. Zeng, Y. Chen, A. Das, R. Jin. *J. Phys. Chem. Lett.* **2015**, *6*, 2976.
[15] T.-A. D. Nguyen, Z. R. Jones, D. F. Leto, G. Wu, S. L. Scott, T. W. Hayton. *Chem. Mater.* **2016**, *28*, 8385.
[16] Y. Kamei, Y. Shichibu, K. Konishi. *Angew. Chem. Int. Ed.* **2011**, *50*, 7442.

Appendices

Appendix 1. Permission to Reuse Copyright Material

Chapter 1 – De Gruyter Reproduction Permission

Dear Alex,

thank you for your e-mail. I am pleased to inform you that we grant you, as one of the authors, the permission to reuse the requested article free of charge in the introduction of your graduate thesis, provided that full credit is given to the original publication and publisher.

Please note that our consent is given to the mentioned reuse only and this permission is non-exclusive and non-transferable. We kindly ask you to ensure, that any electronic content is password-protected, we cannot grant open access.

The permission is subject to full acknowledgement of the source material used and provides that full credit is given to the original publication and the publisher at appropriate place and according to the following credit line:

author(s)/editor(s) (ed.), title. subtitle, place: publisher, year, pp. xx – xx, fig./ill. xx – xx. or

author(s), "title of article"; in: author(s)/editors(s) (ed.) of book/journal, title of book/journal, vol./issue number (if journal), place: publisher, year, pp. xx – xx, fig./ill. xx – xx.

Please do not hesitate to contact us in case you have any questions.

Best regards,

i.A. Lars Goldbach

Associate Rights & Licenses

DE GRUYTER

Genthiner Straße 13

10785 Berlin, Germany

T +49 (0)30.260 05-337

F +49 (0)30.260 05-264

rights@degruyter.com

www.degruyter.com

Walter de Gruyter GmbH. Genthiner Str. 13. 10785 Berlin.

Domicile Berlin. Amtsgericht Charlottenburg HRB 143490 B. Rechtsform: GmbH.

Executive Board: Dr. Anke Beck, Carsten Buhr

Chairman of the Advisory Board: Rüdiger Gebauer

Chapter 2 – American Chemical Society Reproduction Permission

Copyright Clearance Center RightsLink®

Home | Create Account | Help

ACS Publications
Most Trusted. Most Cited. Most Read.

Title: A N-Heterocyclic Carbene-Stabilized Coinage Metal-Chalcogenide Framework with Tunable Optical Properties

Author: Alexander M. Polgar, Florian Weigend, Angel Zhang, et al

Publication: Journal of the American Chemical Society

Publisher: American Chemical Society

Date: Oct 1, 2017

Copyright © 2017, American Chemical Society

LOGIN

If you're a copyright.com user, you can login to RightsLink using your copyright.com credentials.

Already **a RightsLink user** or want to learn more?

PERMISSION/LICENSE IS GRANTED FOR YOUR ORDER AT NO CHARGE

This type of permission/license, instead of the standard Terms & Conditions, is sent to you because no fee is being charged for your order. Please note the following:

- Permission is granted for your request in both print and electronic formats, and translations.
- If figures and/or tables were requested, they may be adapted or used in part.
- Please print this page for your records and send a copy of it to your publisher/graduate school.
- Appropriate credit for the requested material should be given as follows: "Reprinted (adapted) with permission from (COMPLETE REFERENCE CITATION). Copyright (YEAR) American Chemical Society." Insert appropriate information in place of the capitalized words.
- One-time permission is granted only for the use specified in your request. No additional uses are granted (such as derivative works or other editions). For any other uses, please submit a new request.

Appendix 2. Supporting Information for Chapter 2

2.1a – ^{1}H NMR $CDCl_3$ - 298K

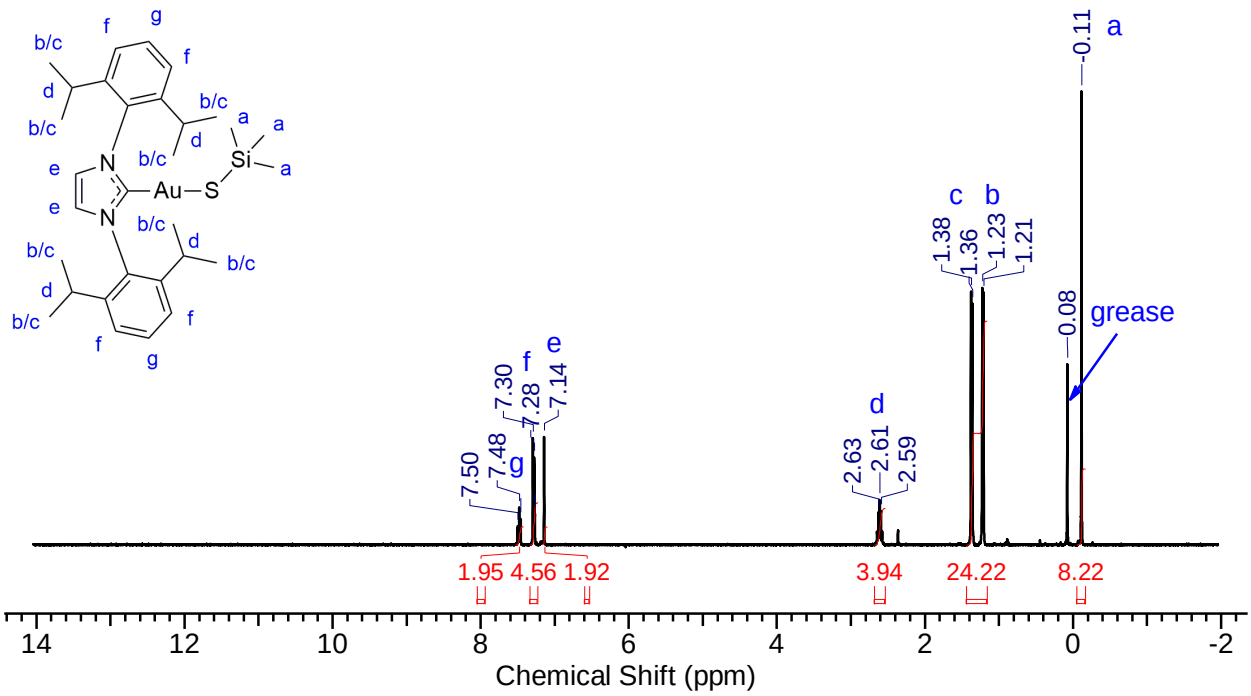

2.1a – ^{13}C{^{1}H} NMR $CDCl_3$ - 298K

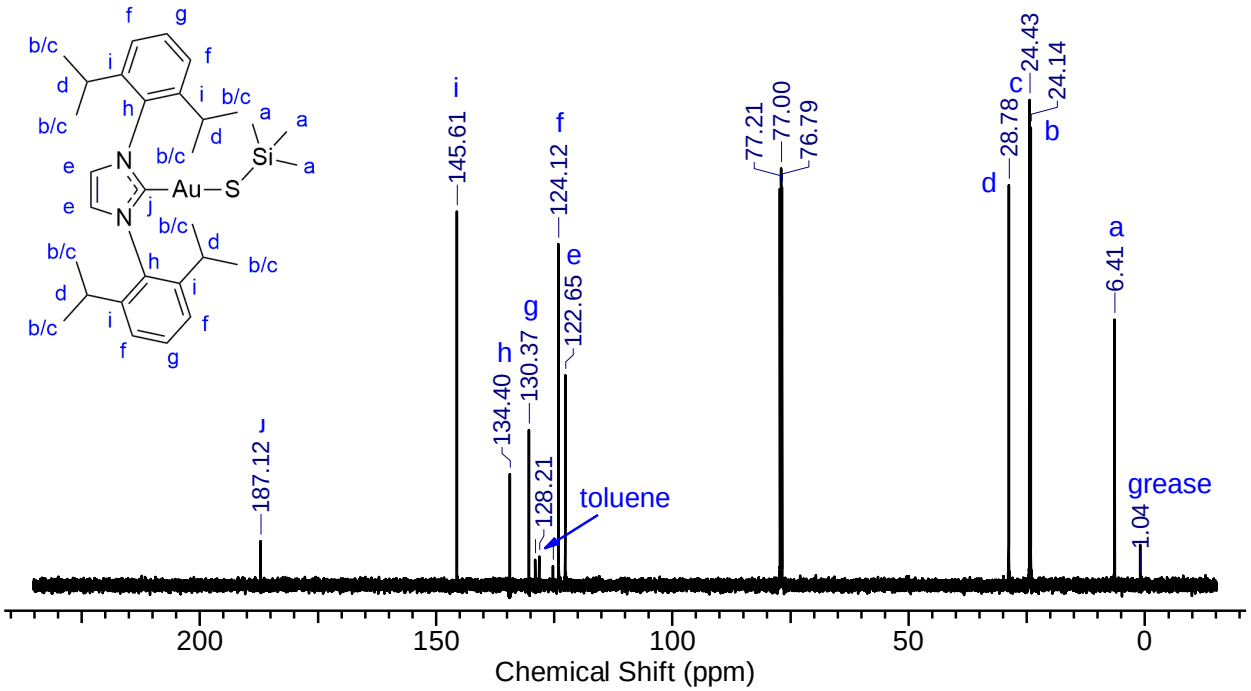

2.1a – ^{29}Si-^{1}H HMBC $CDCl_3$ - 298K

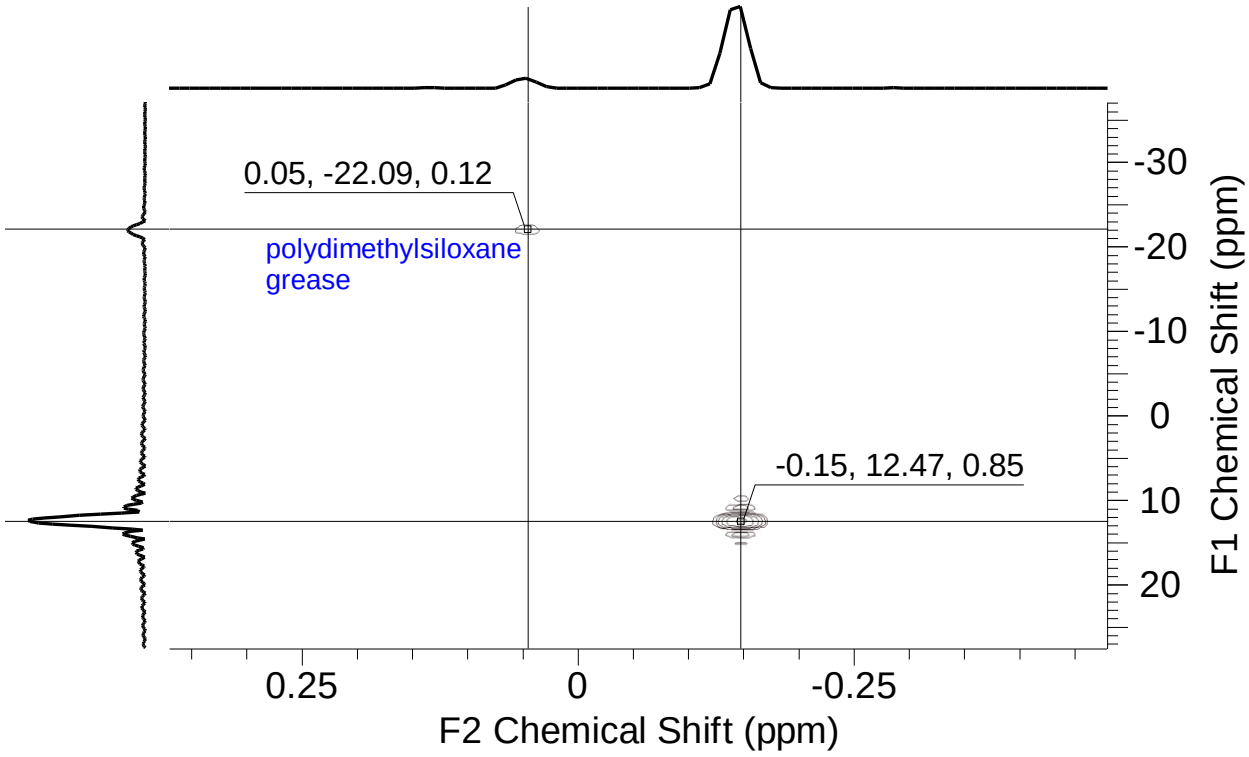

2.1b – ^{1}H NMR $CDCl_3$ - 298K

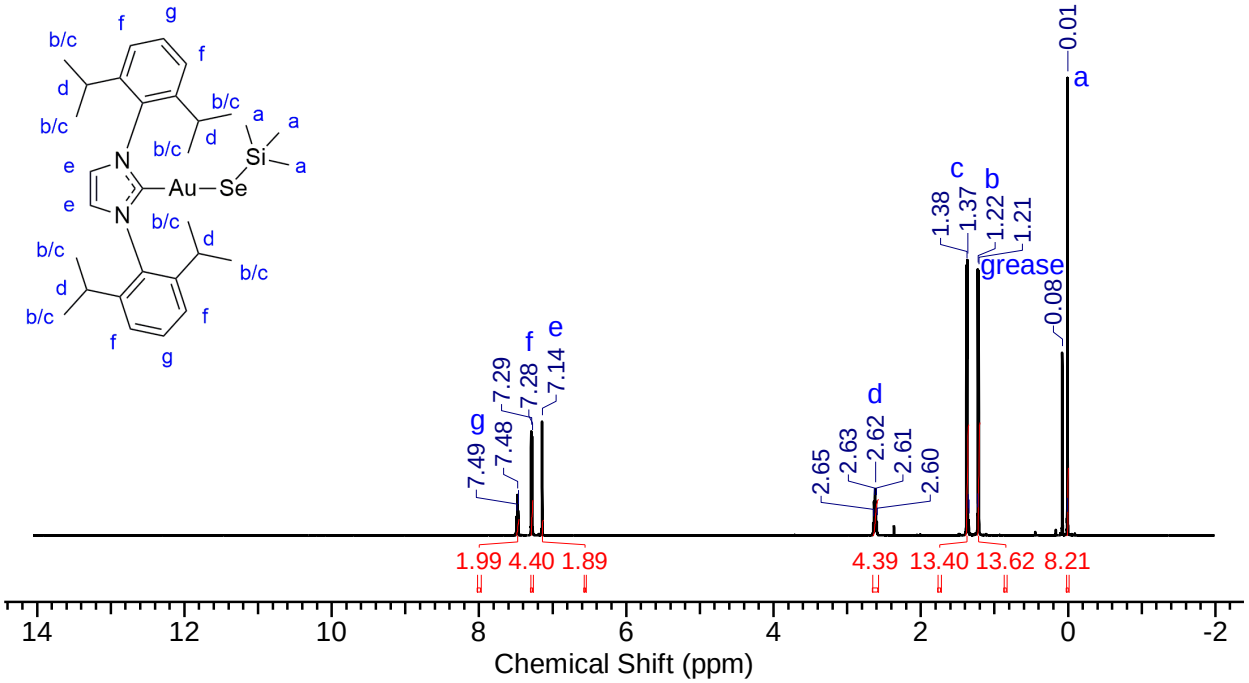

2.1b – $^{13}C\{^{1}H\}$ NMR $CDCl_3$ - 298K

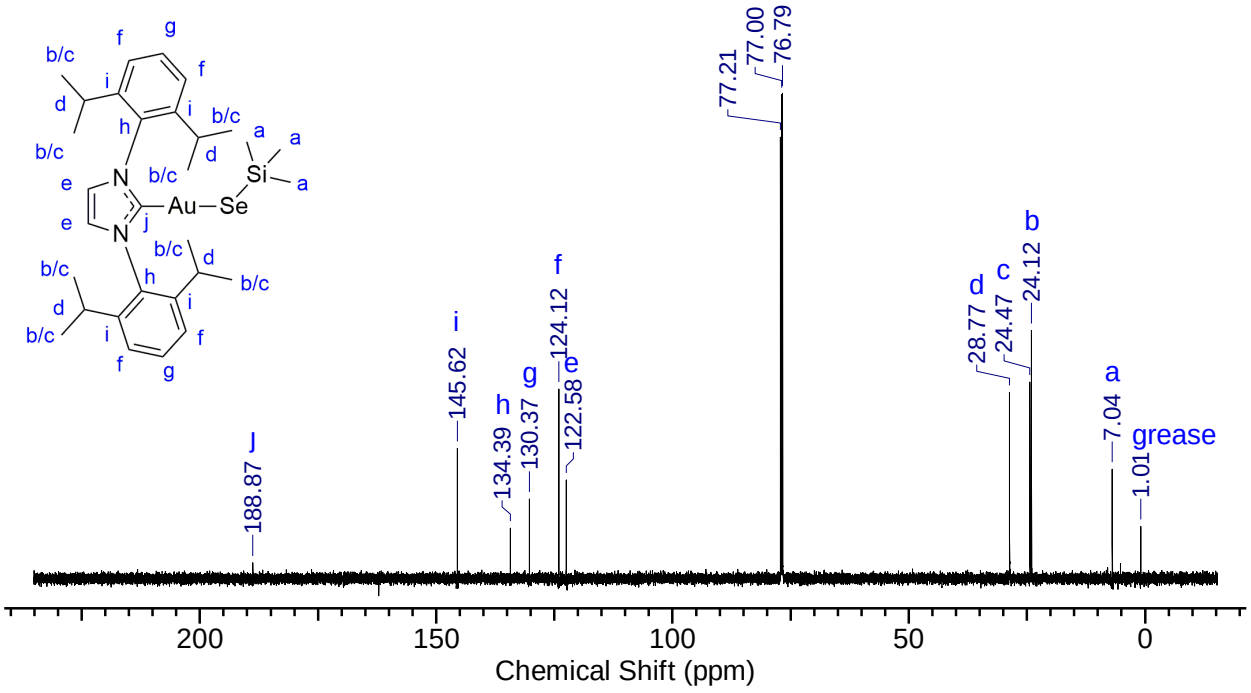

2.1b – ^{29}Si – ^{1}H HMBC $CDCl_3$ - 298K

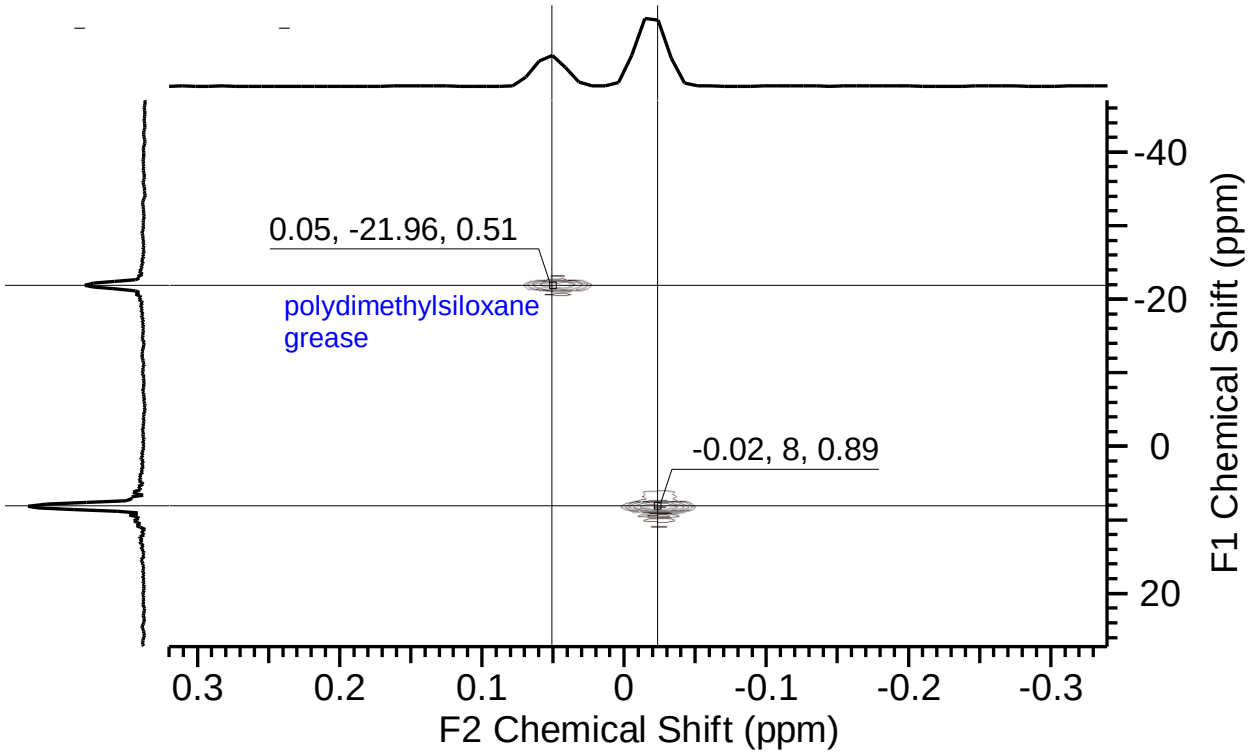

2.1b – ^{77}Se – ^{1}H HMBC $CDCl_3$ - 298K

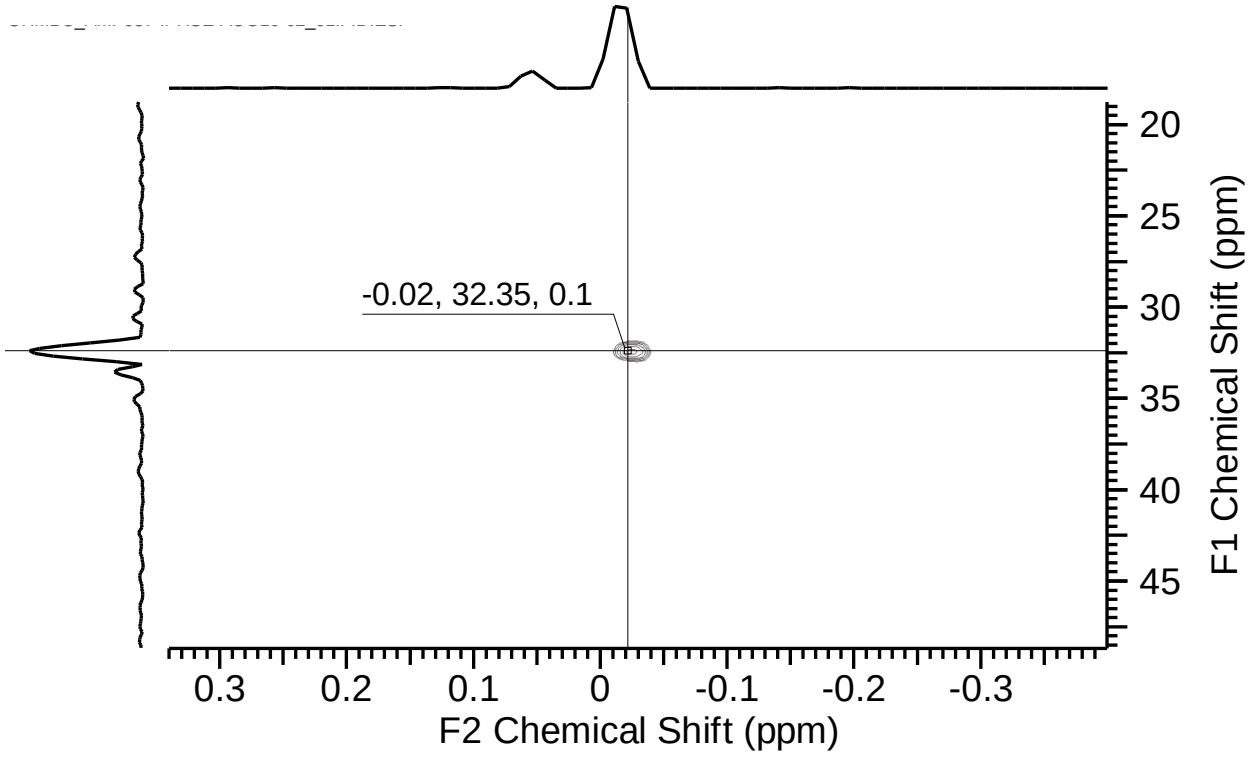

2.1c – ^{1}H NMR $CDCl_3$ - 298K

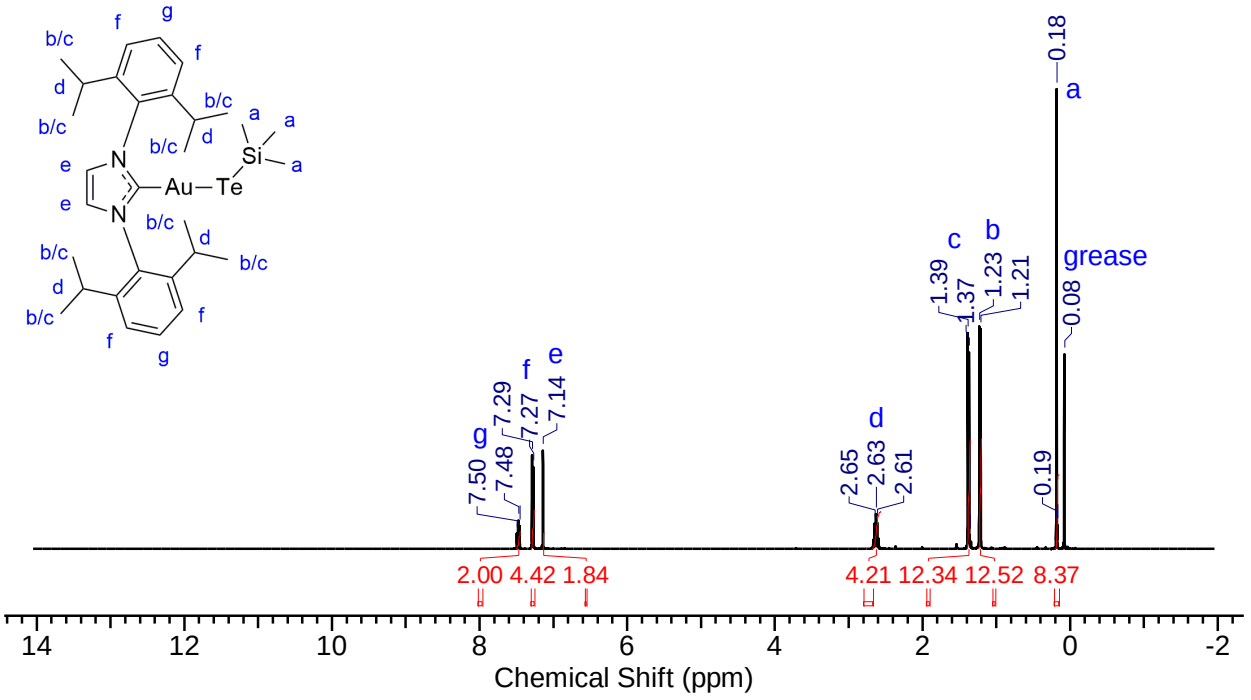

2.1c – $^{13}C\{^{1}H\}$ NMR $CDCl_3$ - 298K

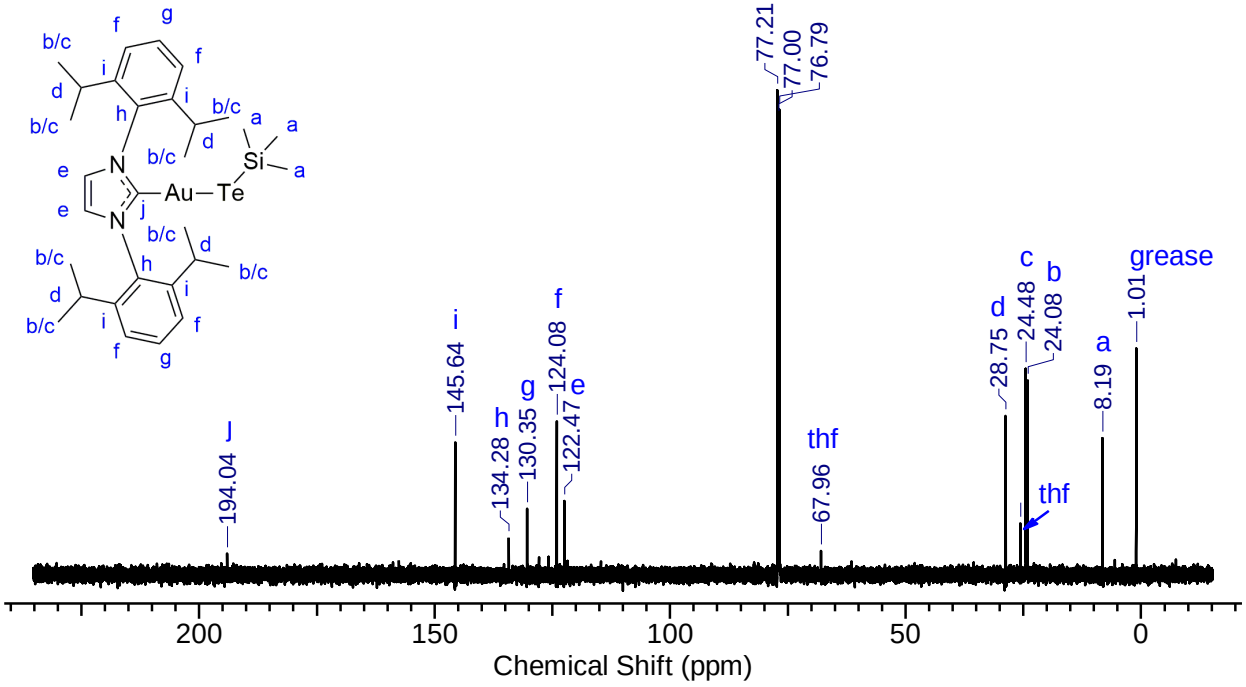

2.1c – ^{29}Si – ^{1}H HMBC $CDCl_3$ - 298K

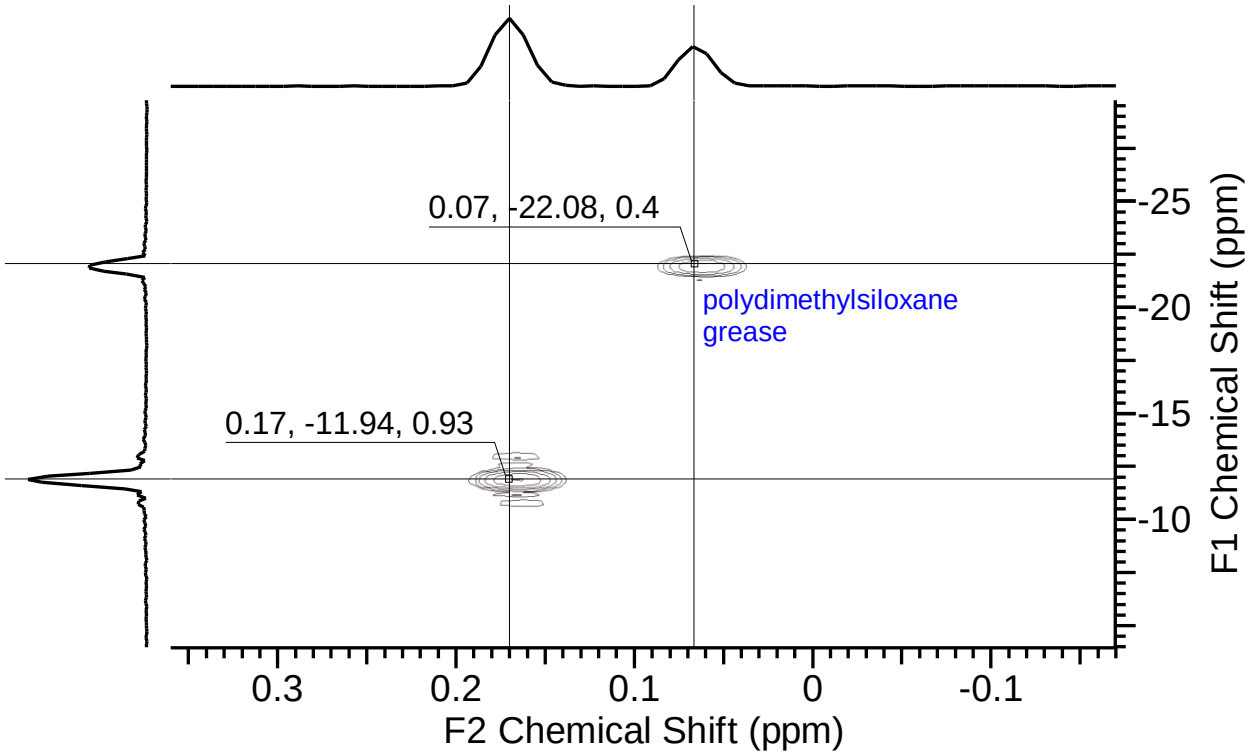

2.1c – ^{125}Te – ^{1}H HMBC $CDCl_3$ - 298K

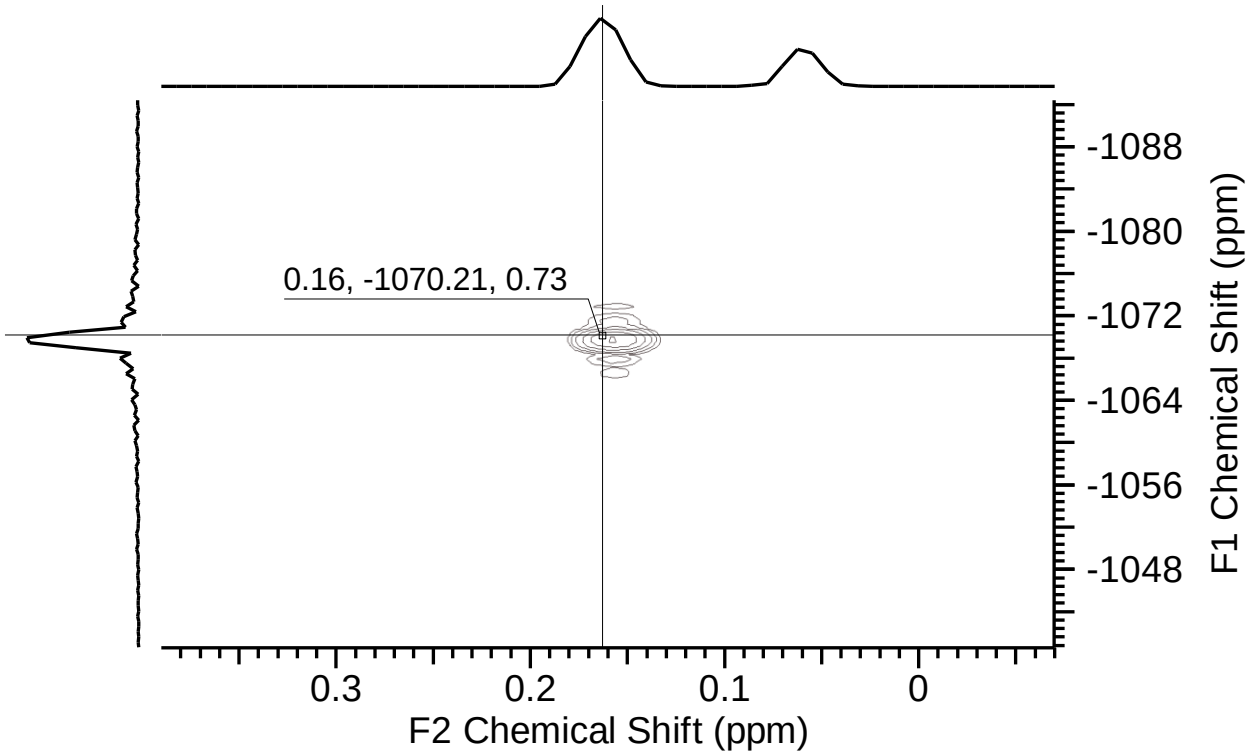

2.1c – $^{125}Te\{^{1}H\}$ NMR $CDCl_3$ - 298K

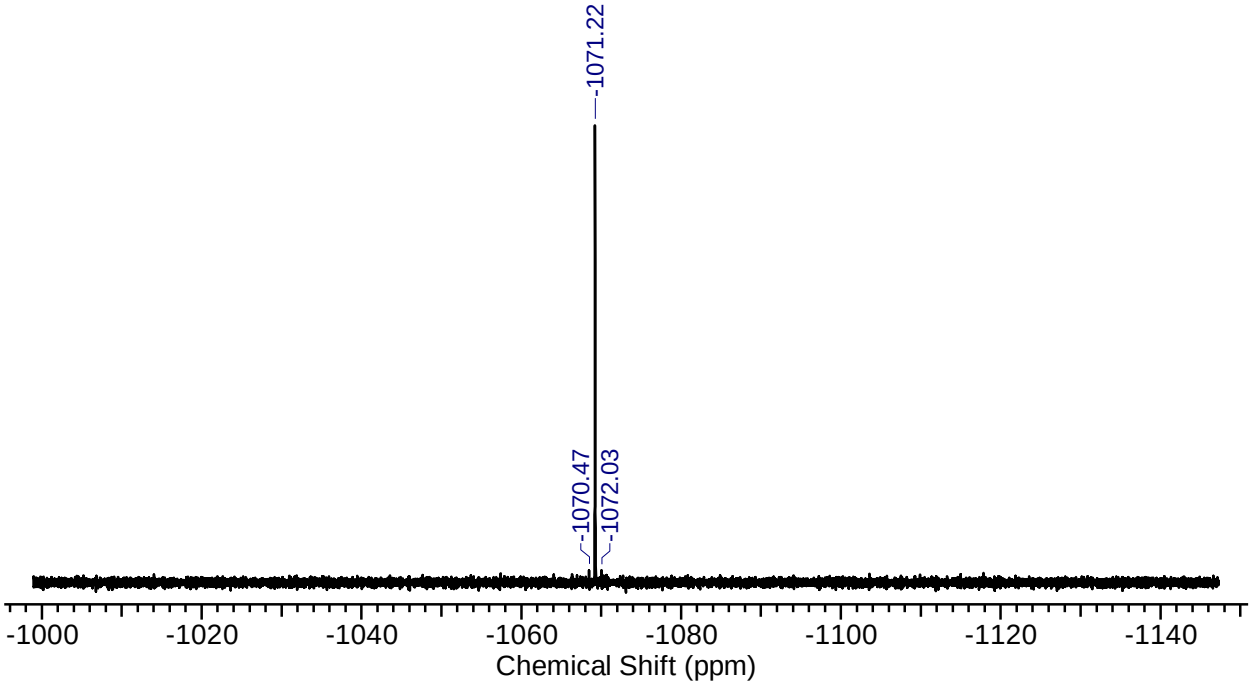

2.1c – $^{125}Te\{^{1}H\}$ NMR expanded view

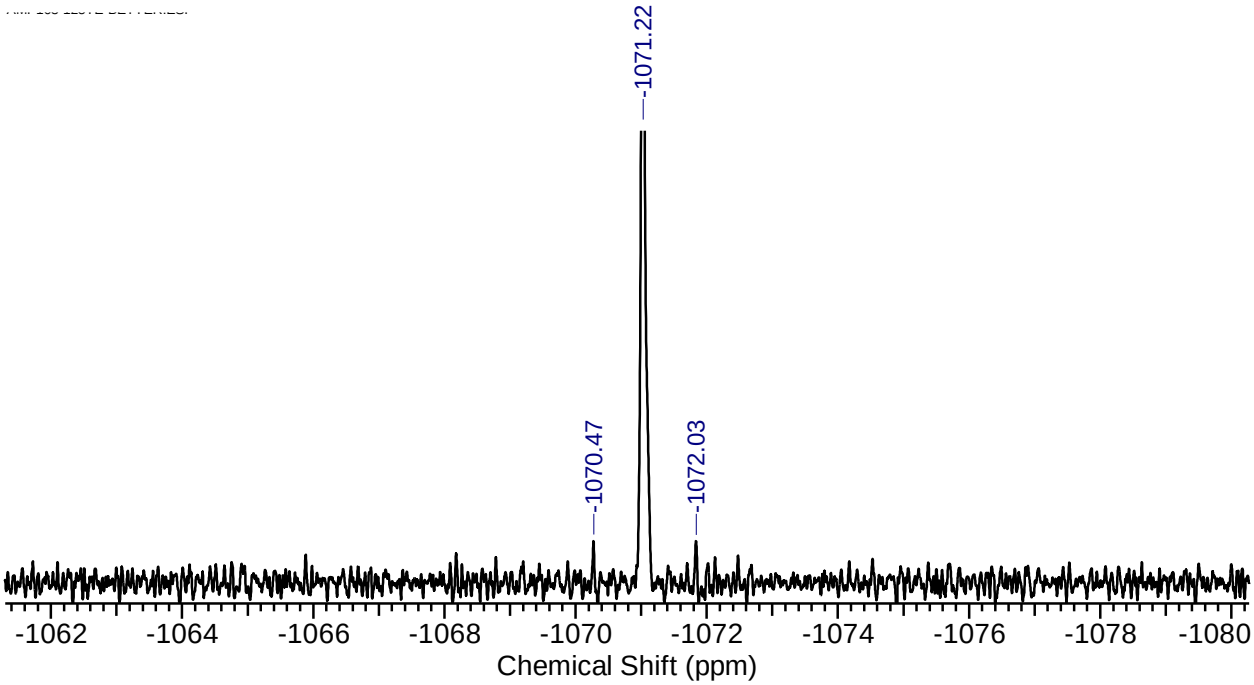

2.2a – ^{1}H NMR $CDCl_3$ - 298K

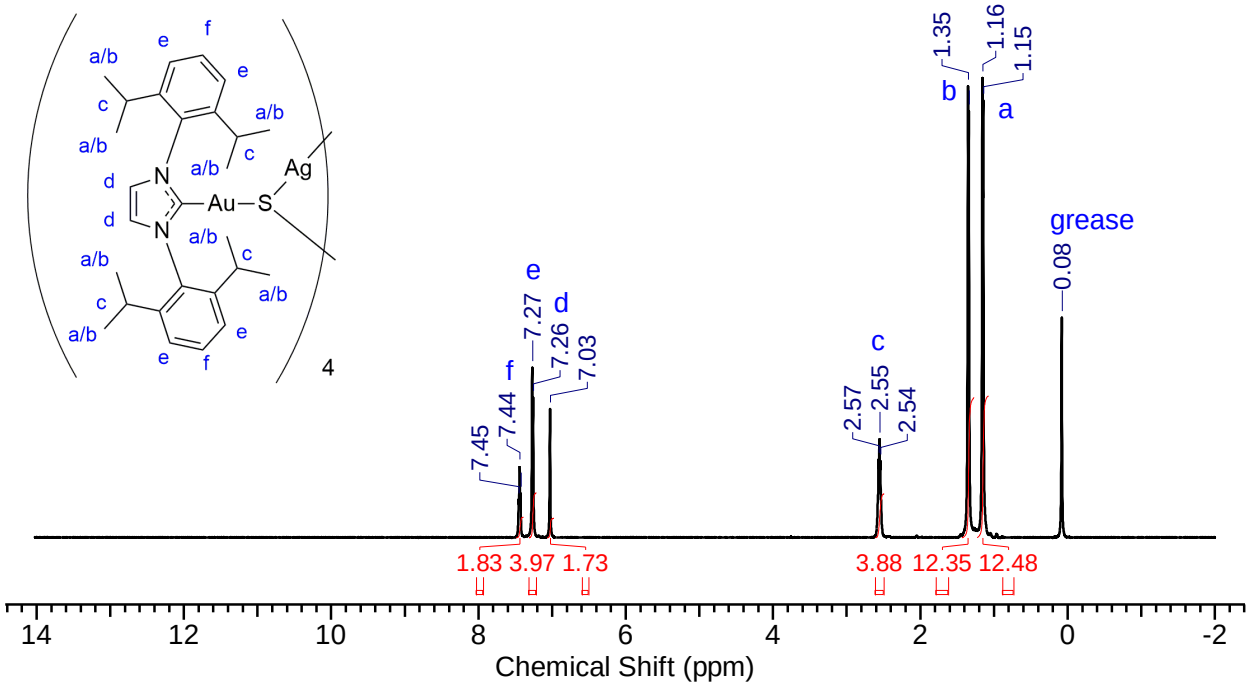

2.2a – $^{13}C\{^{1}H\}$ NMR $CDCl_3$ - 298K

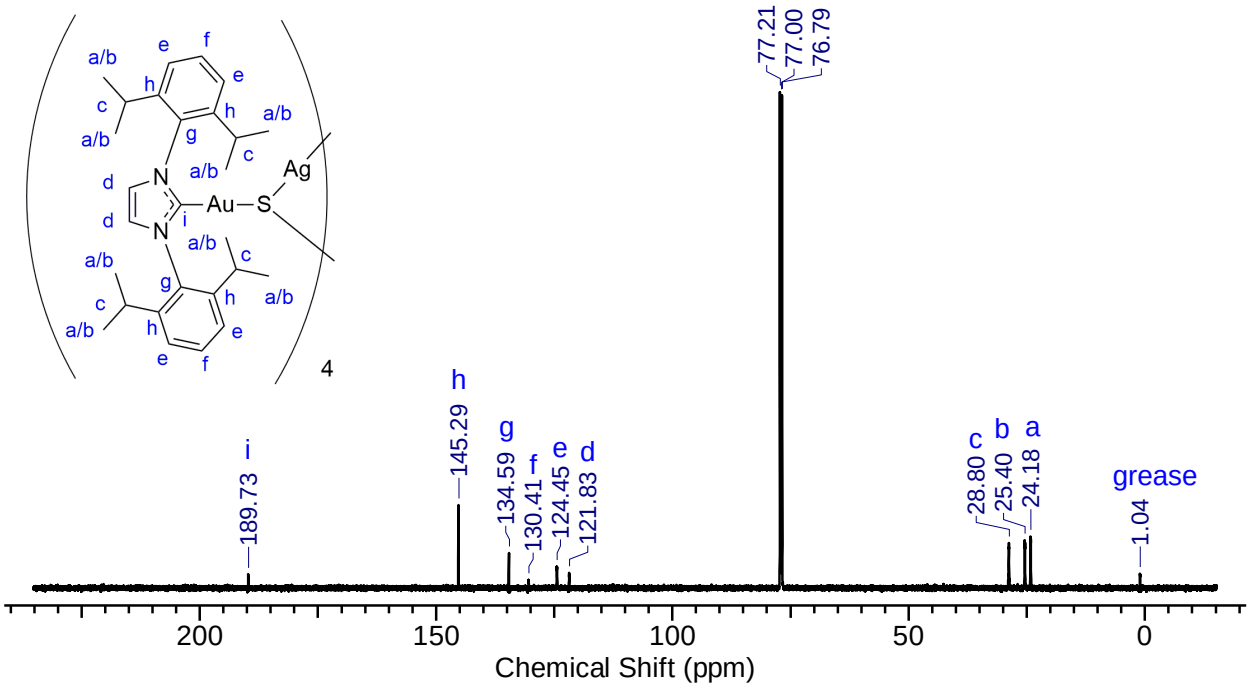

2.2b – ^{1}H NMR $CDCl_3$ - 298K

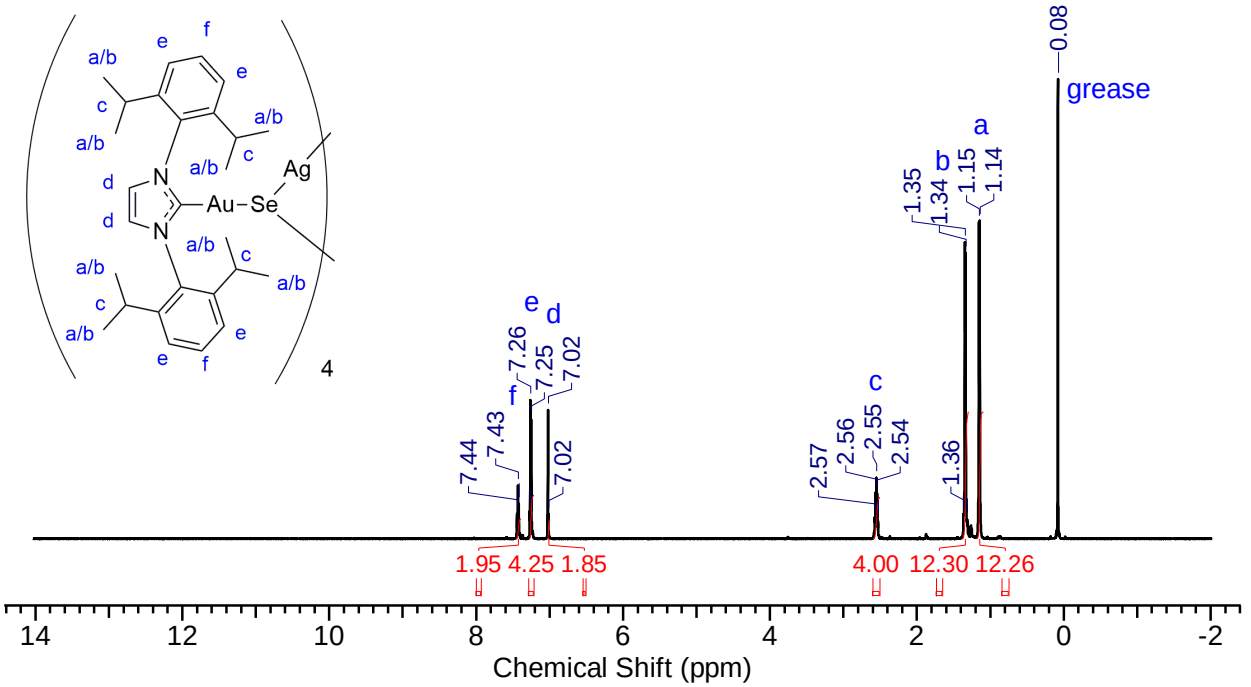

2.2b – $^{13}C\{^{1}H\}$ NMR $CDCl_3$ - 298K

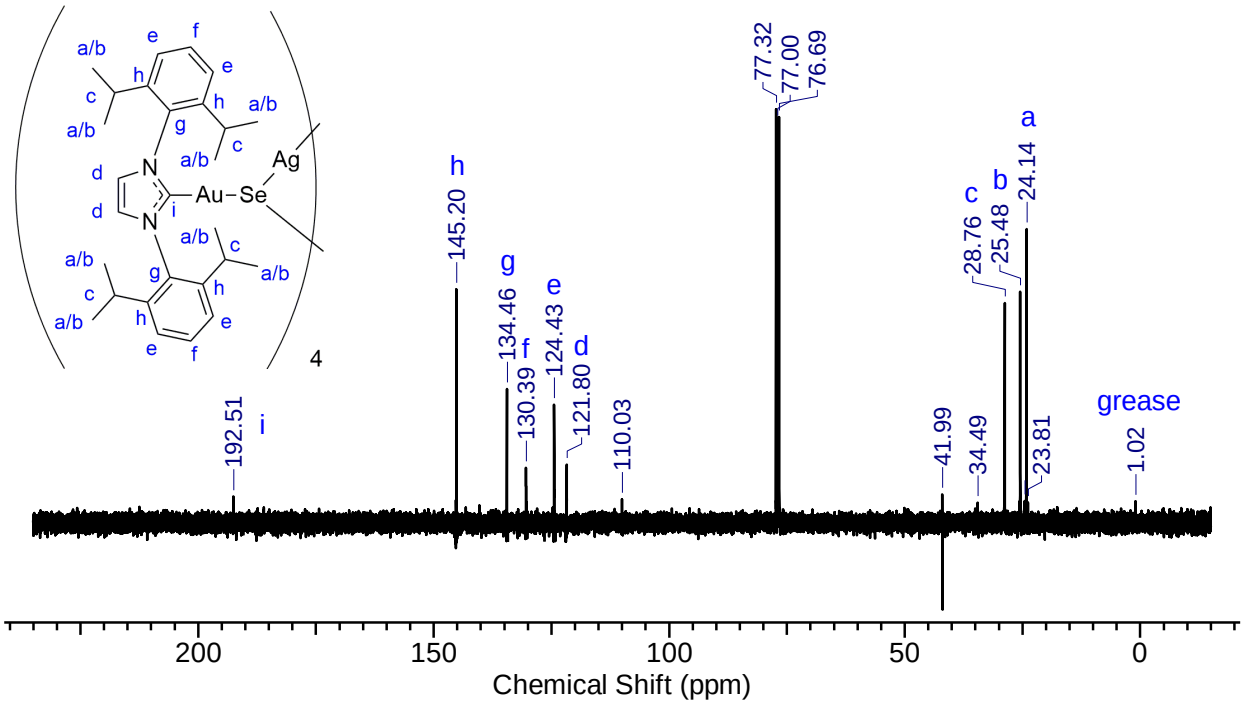

2.2b – $^{77}Se\{^{1}H\}$ NMR $CDCl_3$ - 273K

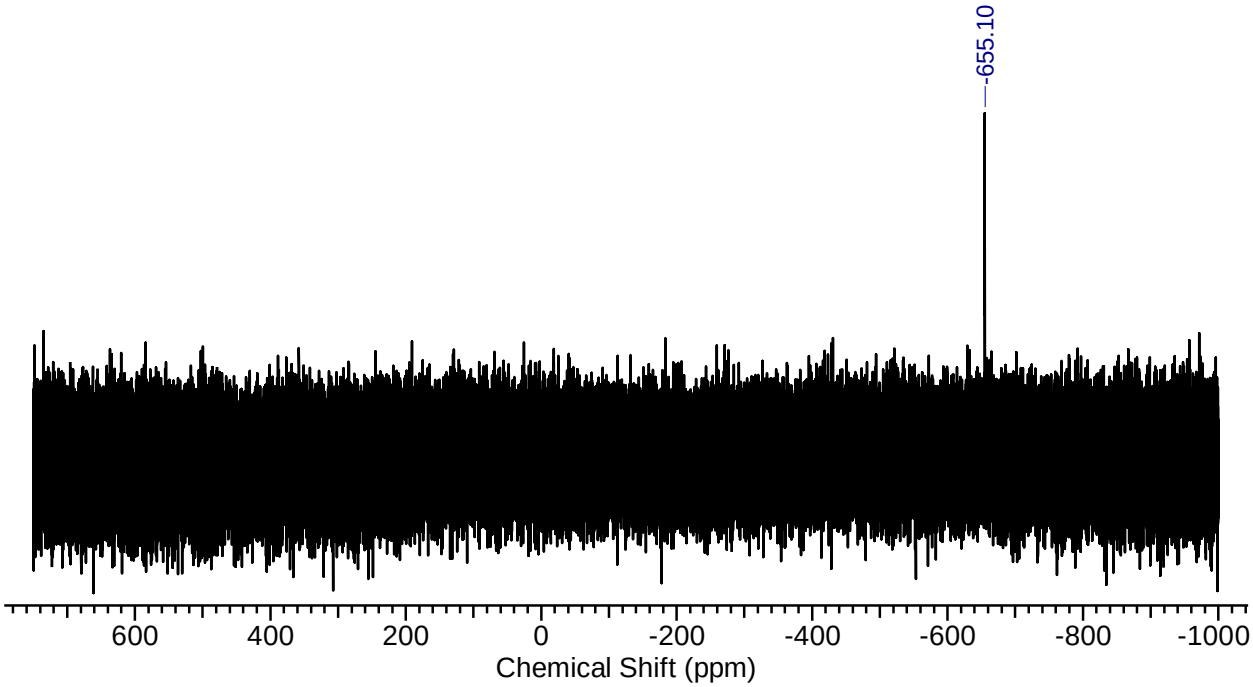

2.2b – $^{77}Se\{^{1}H\}$ NMR expanded view

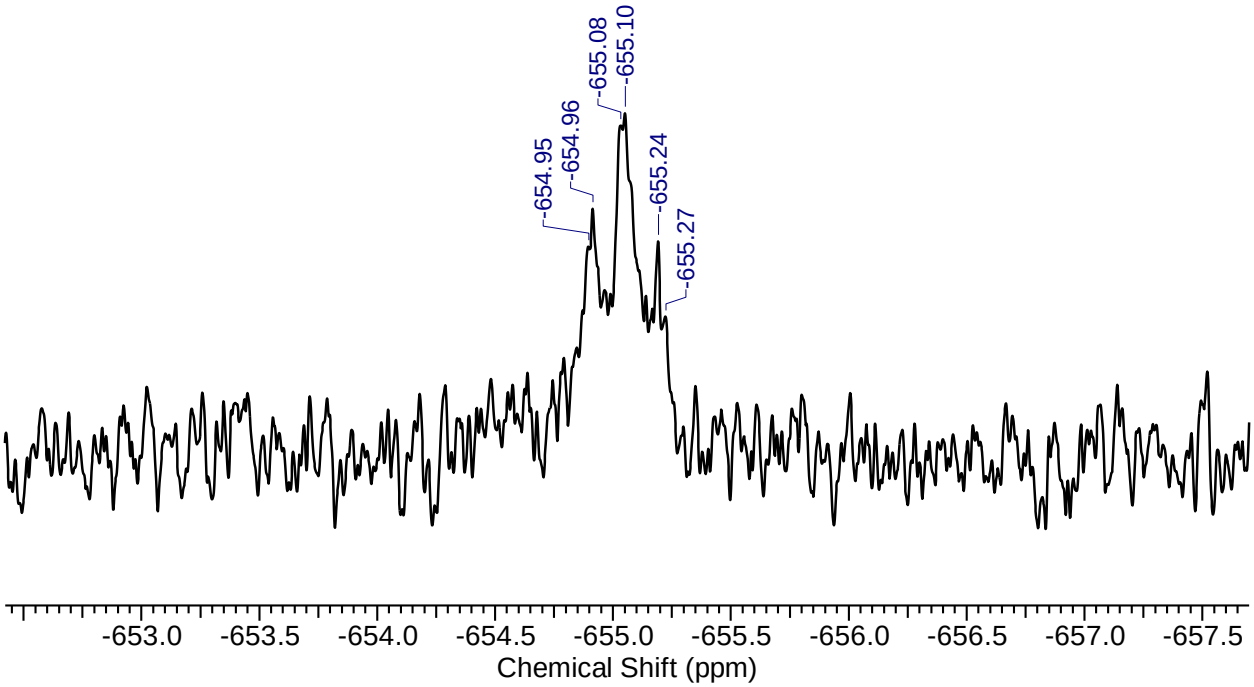

2.3a – ^{1}H NMR $CDCl_3$ - 298K

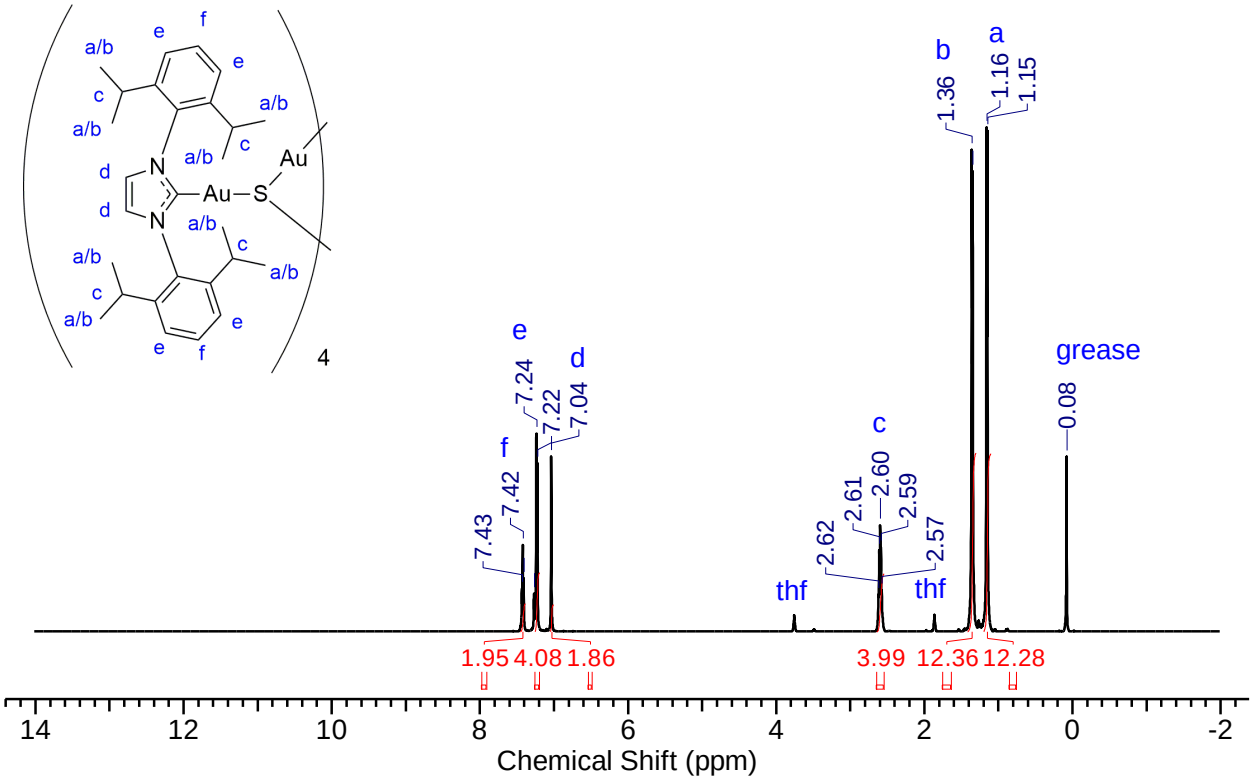

2.3a – $^{13}C\{^{1}H\}$ NMR $CDCl_3$ - 298K

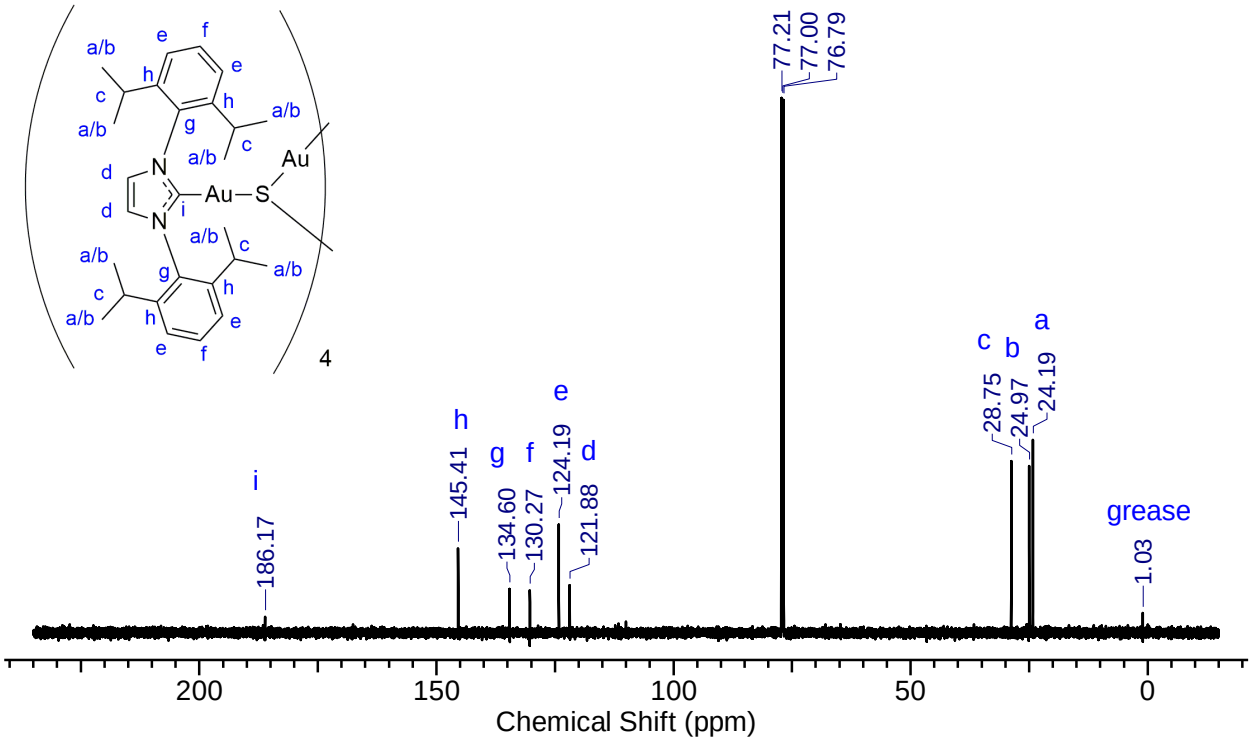

2.3b – ^{1}H NMR $CDCl_3$ - 273K

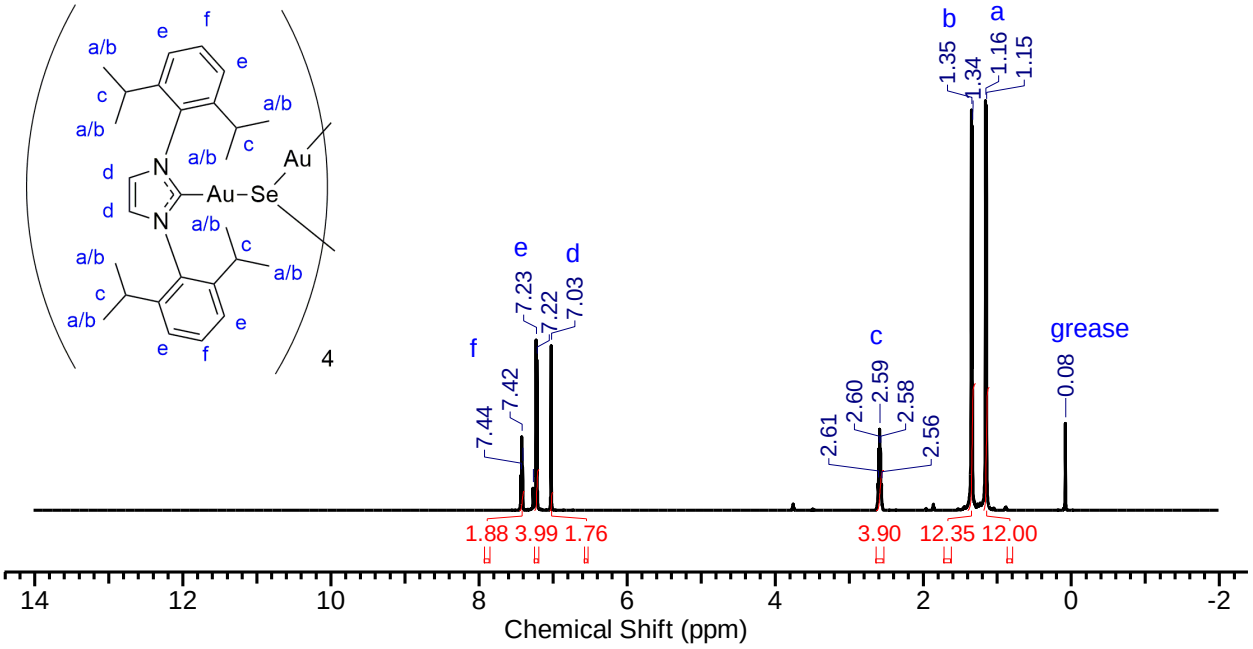

2.3b – ^{13}C NMR $CDCl_3$ - 273K

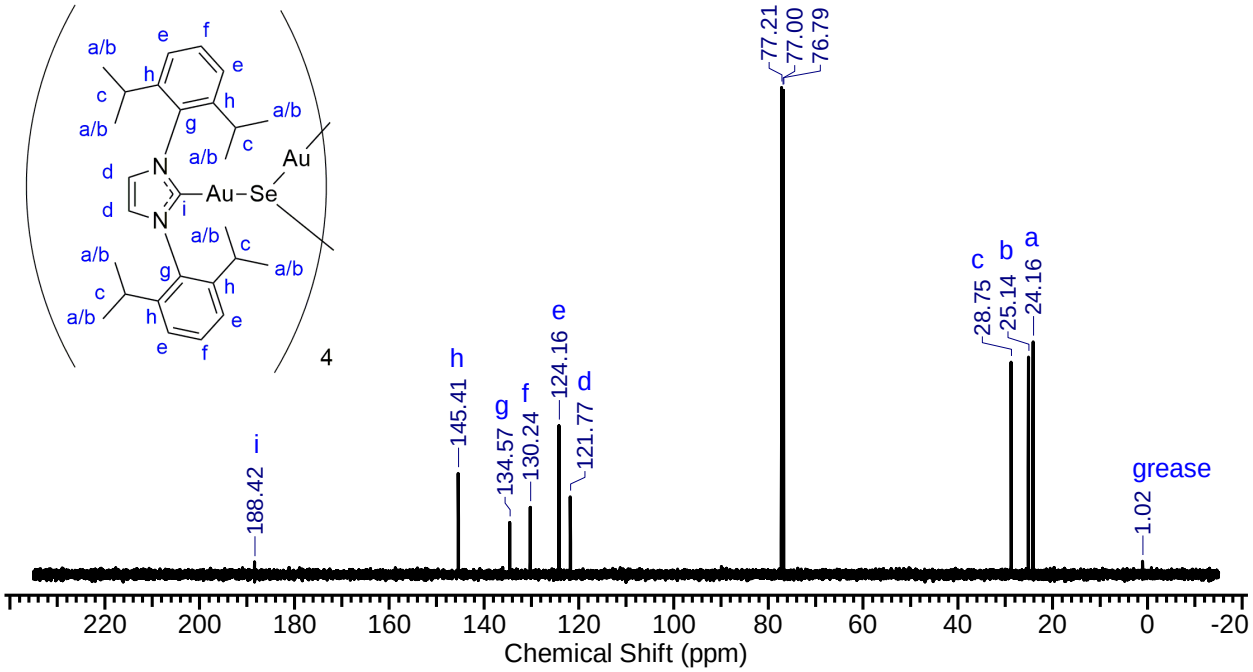

2.3b – ^{77}Se{^{1}H} NMR $CDCl_3$ - 273K

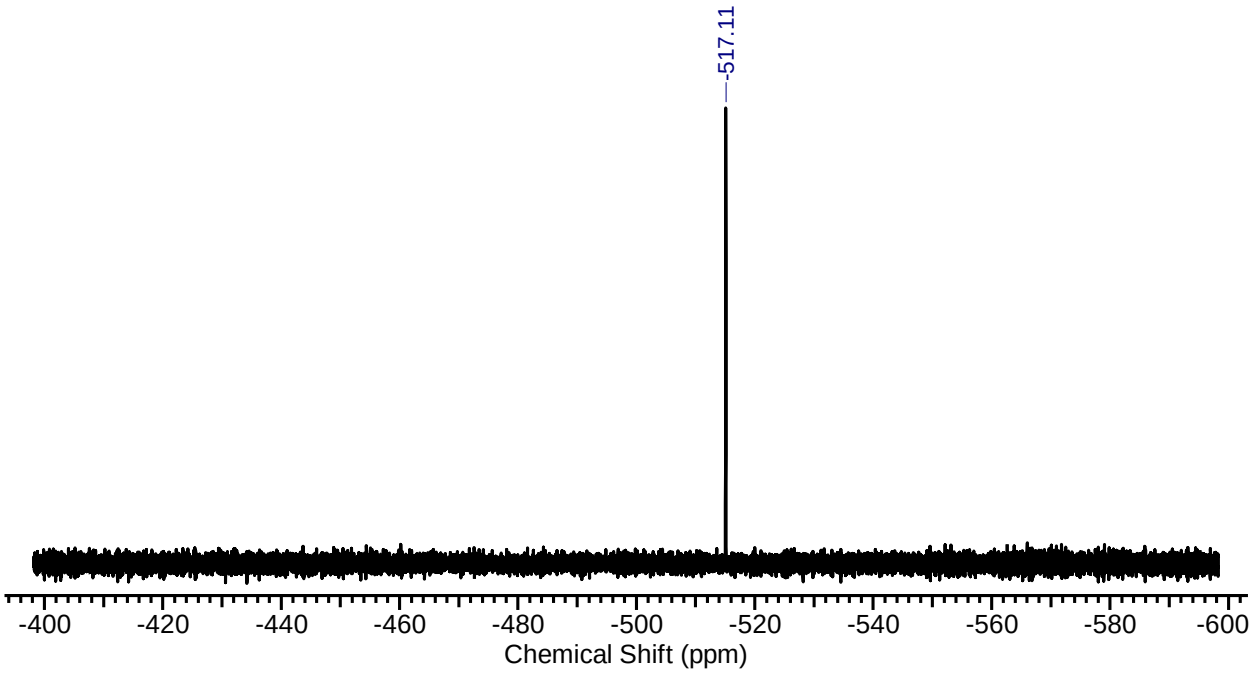

2.3c – ^{1}H NMR $CDCl_3$ - 298K

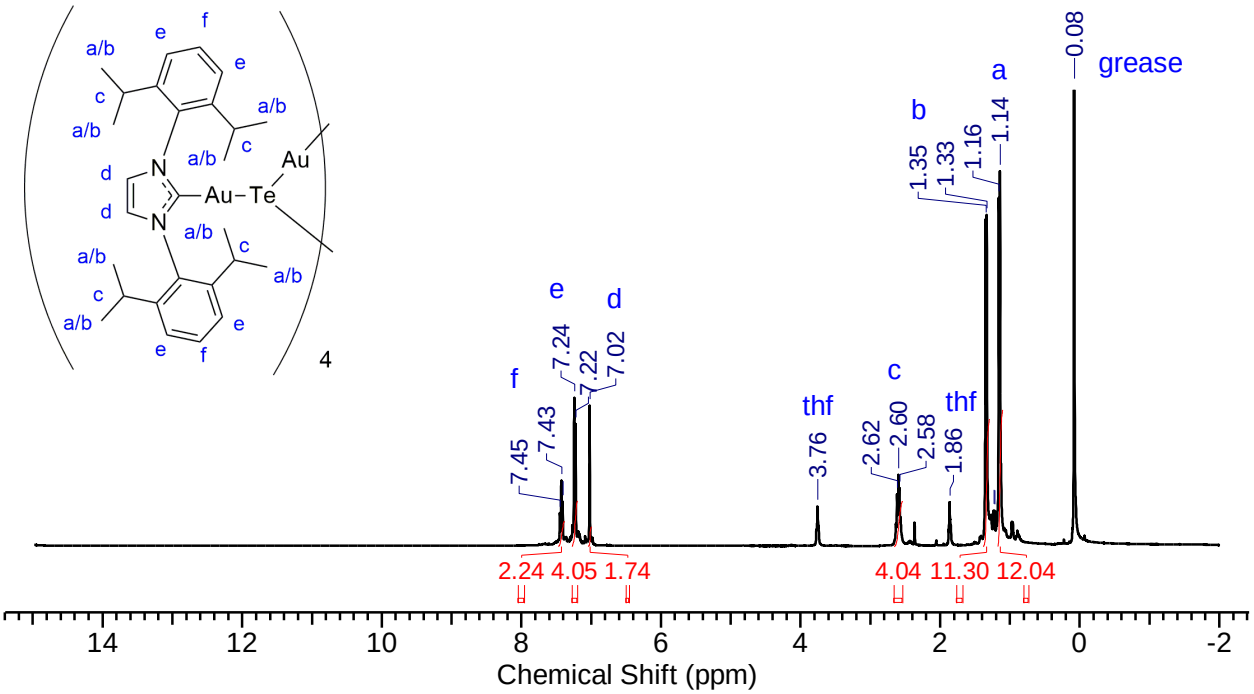

2.3c – ^{125}Te{^{1}H} NMR $CDCl_3$ - 298K

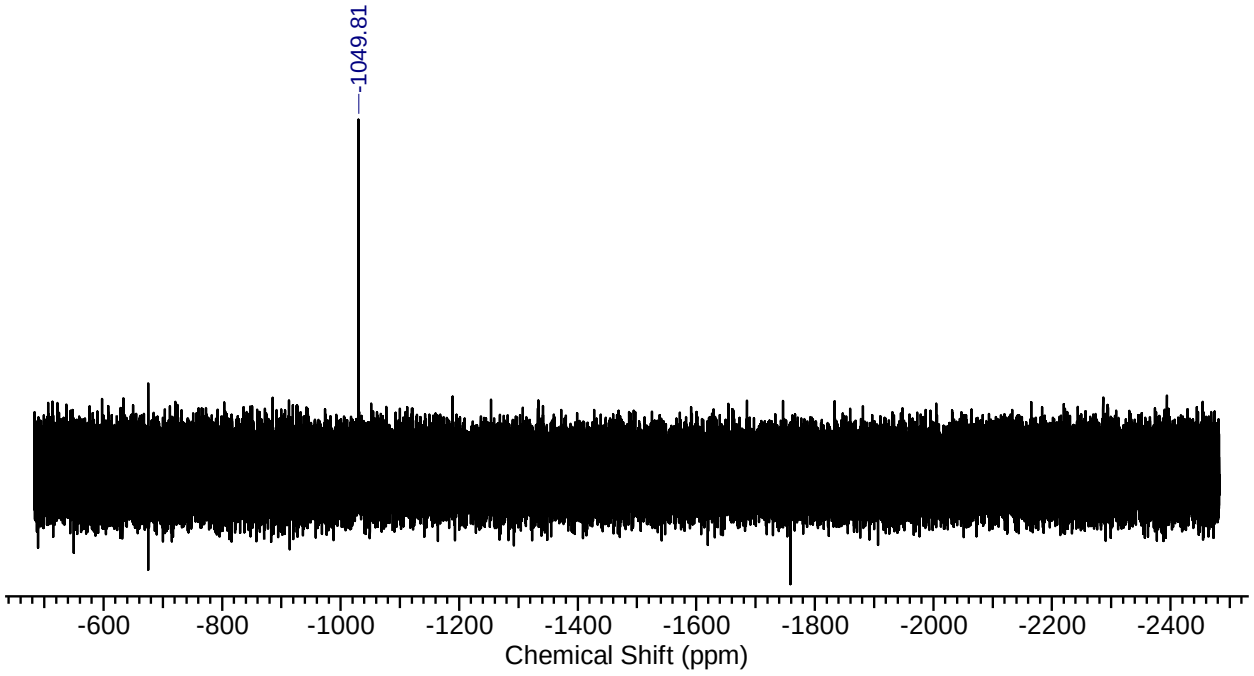

Reaction of 2.1a with $Ph_3PAuOAc$: ^1H NMR $CDCl_3$ - 298K

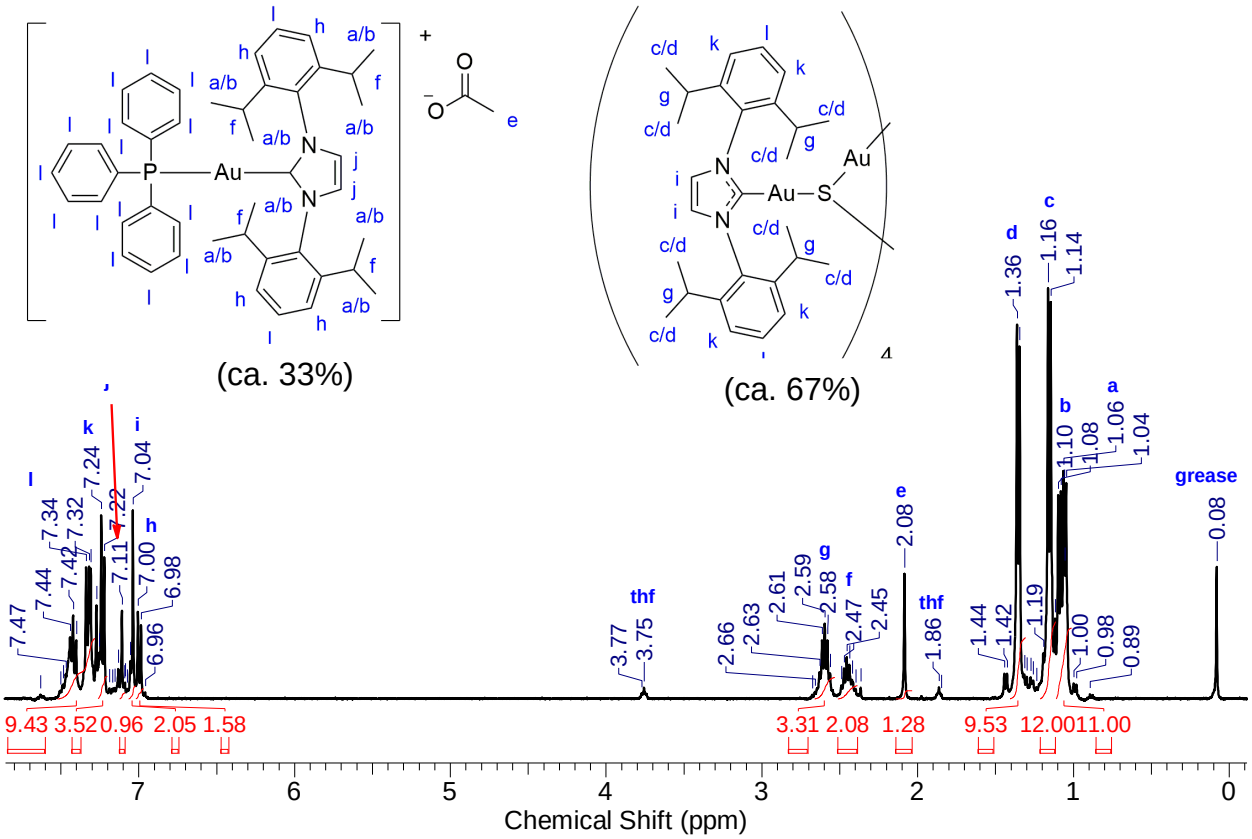

Reaction of 2.1a with $Ph_3PAuOAc$: $^{31}P\{^1H\}$ NMR $CDCl_3$ - 298K

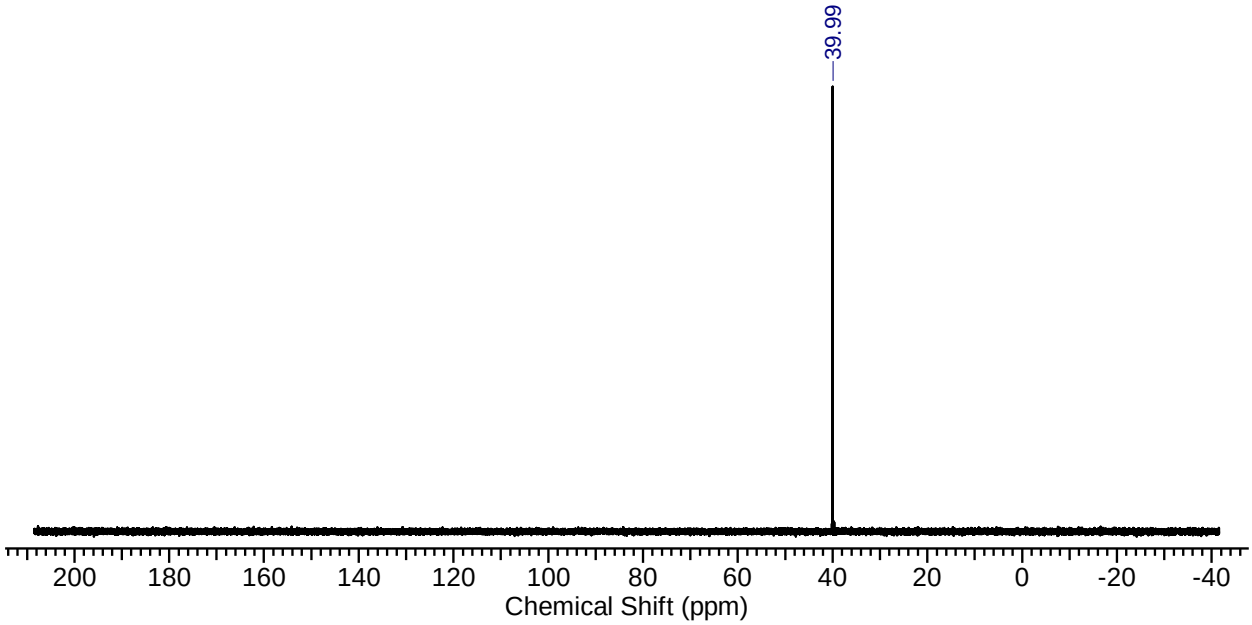

	2.2a	**2.2b**	**2.3a**	**2.3b**	**2.3c • THF**
Molecular Formula	$C_{108}H_{144}Ag_4Au_4N_8S_4$	$C_{108}H_{144}Ag_4Au_4N_8Se_4$	$C_{108}H_{144}Au_8N_8S_4$	$C_{108}H_{144}Au_8N_8Se_4$	$C_{108}H_{144}Au_8N_8Te_4 \bullet C_4H_8O$
Formula Weight	2901.91	3089.49	3258.28	3445.88	3712.54
Crystal Habit	Colourless Prism	Colourless Prism	Colourless Block	Colourless Prism	Yellow Plate
Crystal System	Tetragonal	Tetragonal	Tetragonal	Tetragonal	Orthorhombic
Space Group	$I\bar{4}$	$I\bar{4}$	$I\bar{4}$	$I\bar{4}$	$P2_12_12_1$
Temperature (K)	110	110	110	110	110
λ (Å)	0.71073	0.71073	0.71073	0.71073	0.71073
a (Å)	18.4029(19)	18.437(4)	18.389(5)	18.451(5)	14.9225(11)
b (Å)	18.4029(19)	18.437(4)	18.389(5)	18.451(5)	22.1262(18)
c (Å)	16.434(3)	16.477(6)	16.455(4)	16.458(6)	34.994(3)
α (deg)	90	90	90	90	90
β (deg)	90	90	90	90	90
γ (deg)	90	90	90	90	90
V (Å^3)	5565.5(15)	5601(3)	5565(3)	5603(3)	11554.3(16)
Z	2	2	2	2	4
μ (MoKα_1, mm^{-1})	6.061	7.247	10.625	11.777	11.155
$\rho_{calc.}$ (g cm^{-3})	1.732	1.832	1.945	2.043	2.134
$2\theta_{max}$	65.056	77.192	75.644	68.764	60.080
Reflections collected	48116	201468	134993	235900	254269
Ind. Reflections	10076	15805	14921	11789	33754
R_{merge}	0.0336	0.0485	0.0509	0.0744	0.0639
R_1, wR_2 [$I > 2\sigma(I)$]	0.0194, 0.0486	0.0261, 0.0394	0.0330, 0.0686	0.0238, 0.0437	0.0379, 0.0693
R_1, wR_2 (all data)	0.0218, 0.0497	0.0372, 0.0412	0.0560, 0.0755	0.0301, 0.0455	0.0635, 0.0784
GOF	0.740	0.974	0.987	1.006	1.049
Max, min residual electron density (e^-/Å^3)	1.245, -0.511	1.186, -1.208	4.977, -1.119	0.902, -0.672	5.799, -3.867

$R_1 = \Sigma(|F_o| - |F_c|) / \Sigma F_o$

$wR_2 = [\Sigma(w(F_o^2 - F_c^2)^2) / \Sigma(w F_o^4)]^{½}$

$GOF = [\Sigma(w(F_o^2 - F_c^2)^2) / (\text{No. of reflns.} - \text{No. of params.})]^{½}$

Table A2.1 Crystallographic data for **2.2-3**

Appendix 3. Supporting Information for Chapter 3

3.1 – ^{1}H NMR $CDCl_3$ - 298K

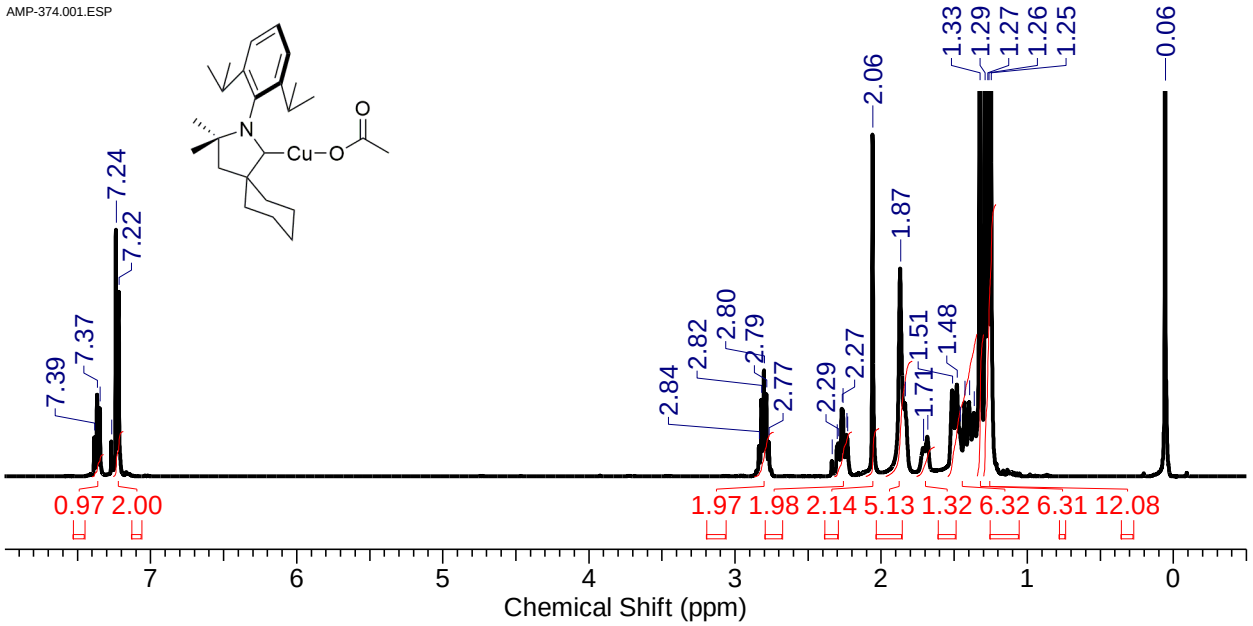

3.1 – ^{13}C{^{1}H} NMR $CDCl_3$ - 298K

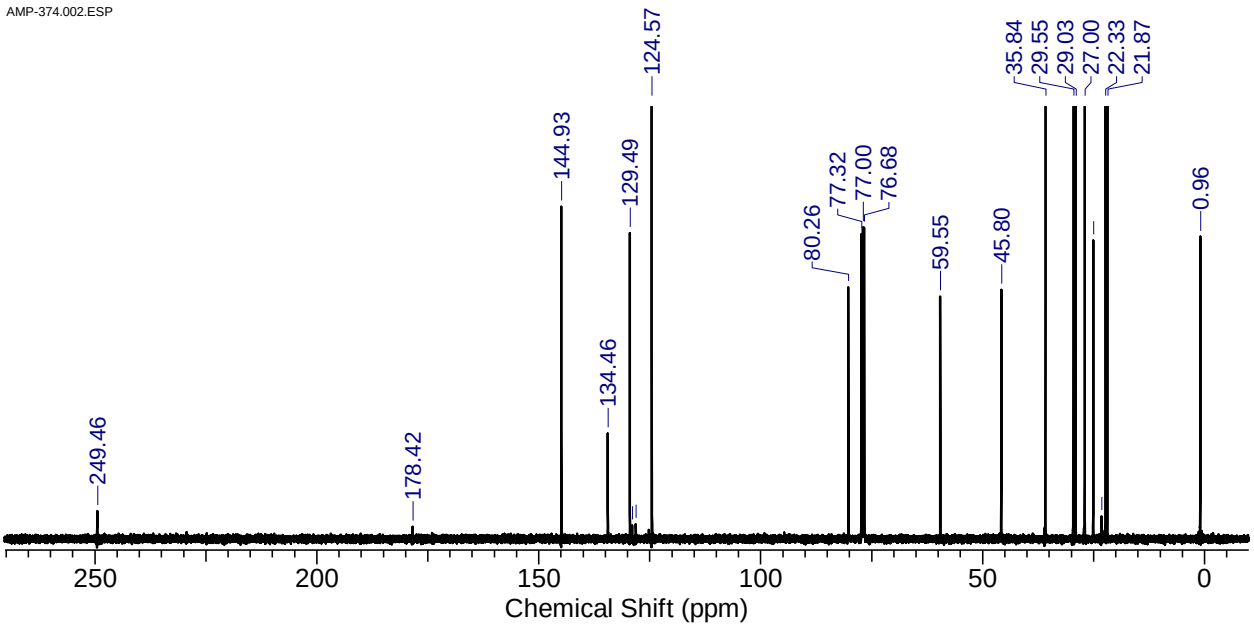

3.2a – ^{1}H NMR $CDCl_3$ - 298K

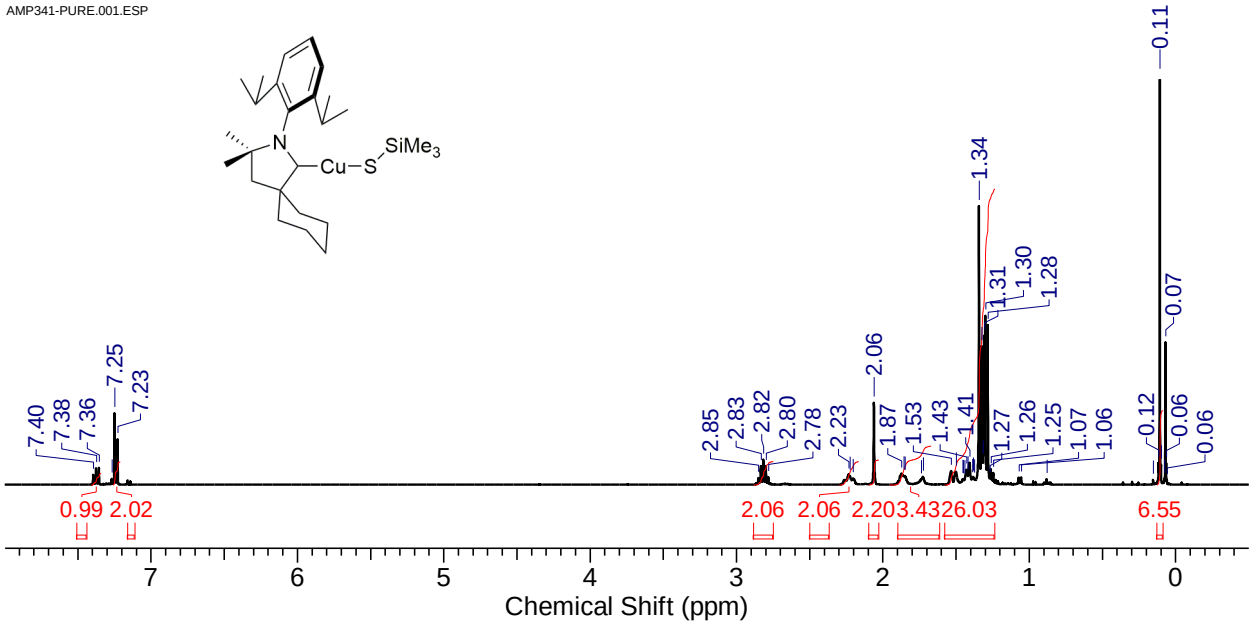

3.2a – ^{13}C{^{1}H} NMR $CDCl_3$ - 298K

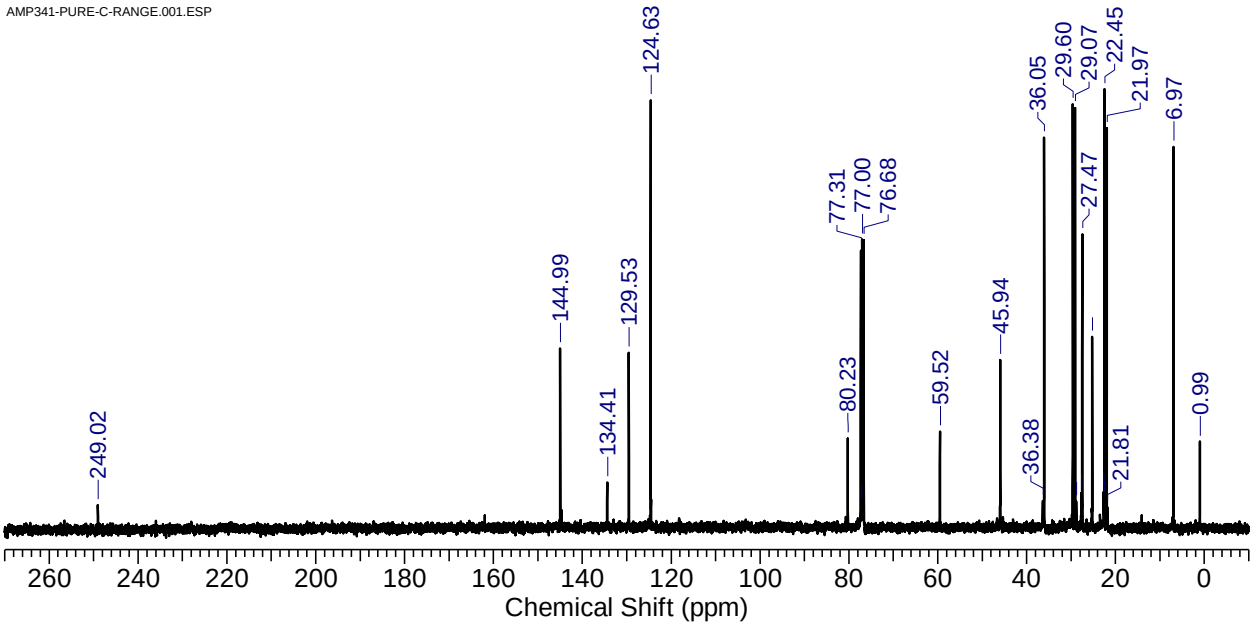

3.2a – ^{29}Si-^{1}H HMBC $CDCl_3$ - 298K

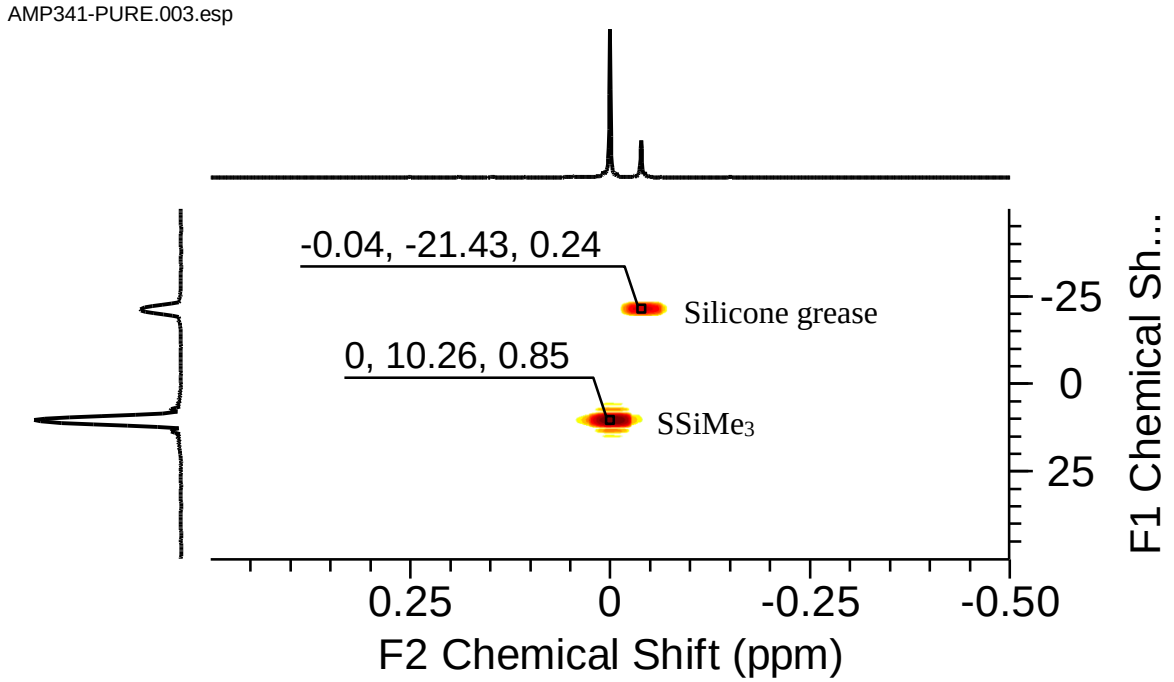

3.2b – ^{1}H NMR $CDCl_3$ - 298K

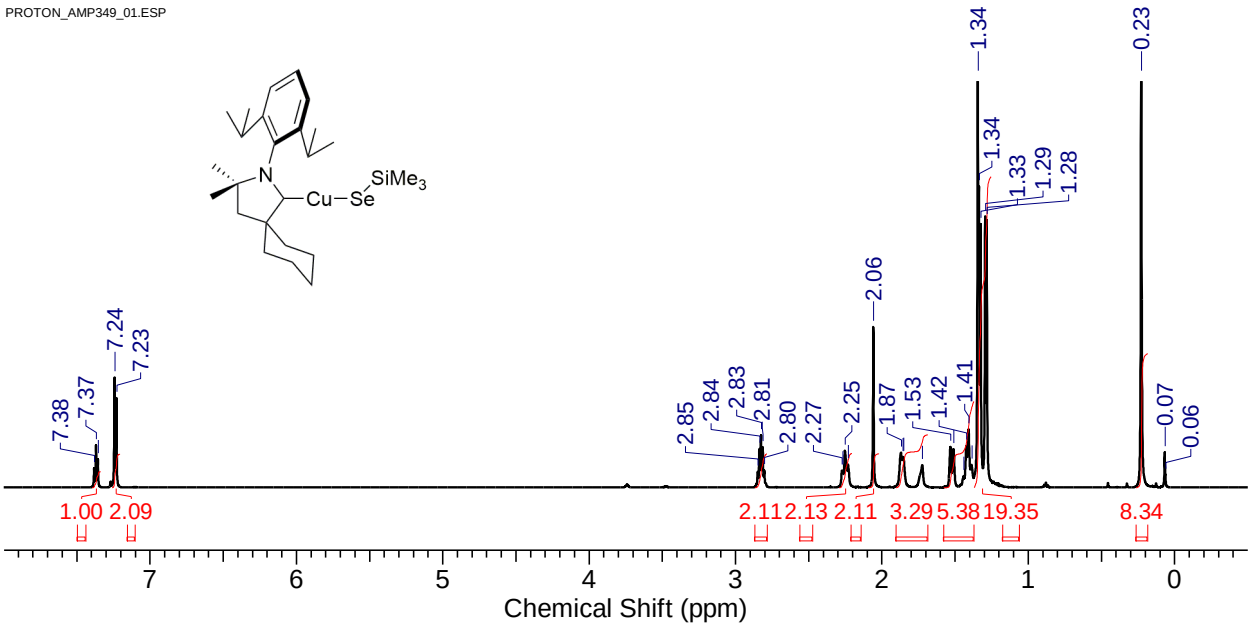

3.2b – $^{13}C\{^{1}H\}$ NMR $CDCl_3$ - 298K

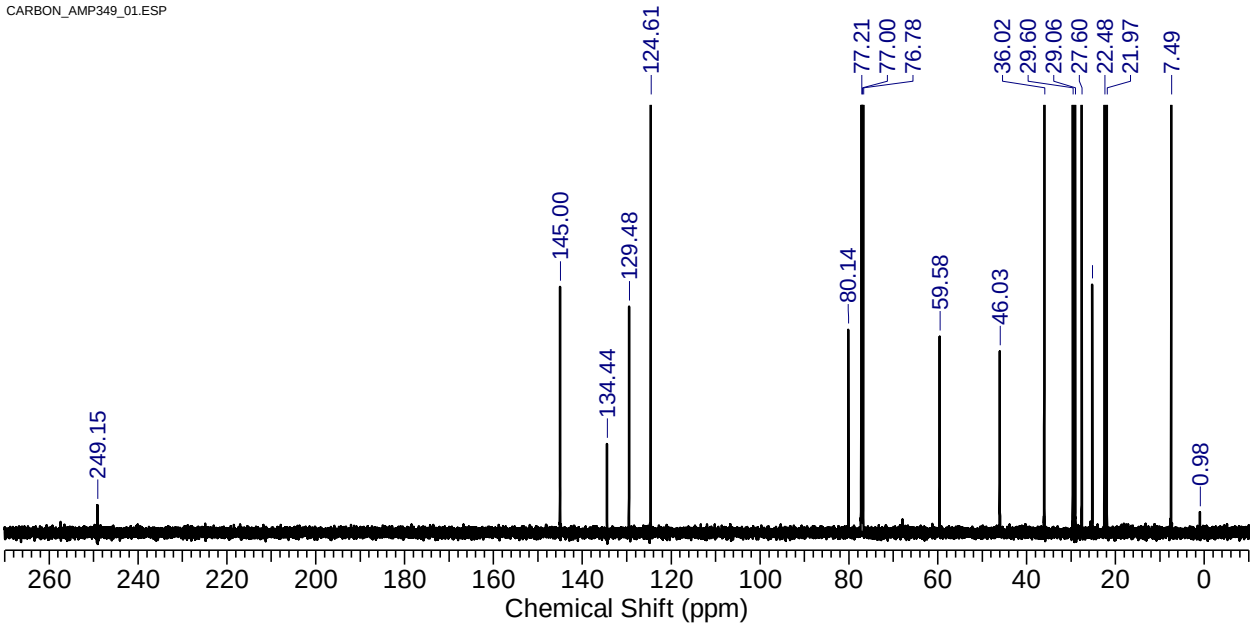

3.2b – ^{29}Si-^{1}H HMBC $CDCl_3$ - 298K

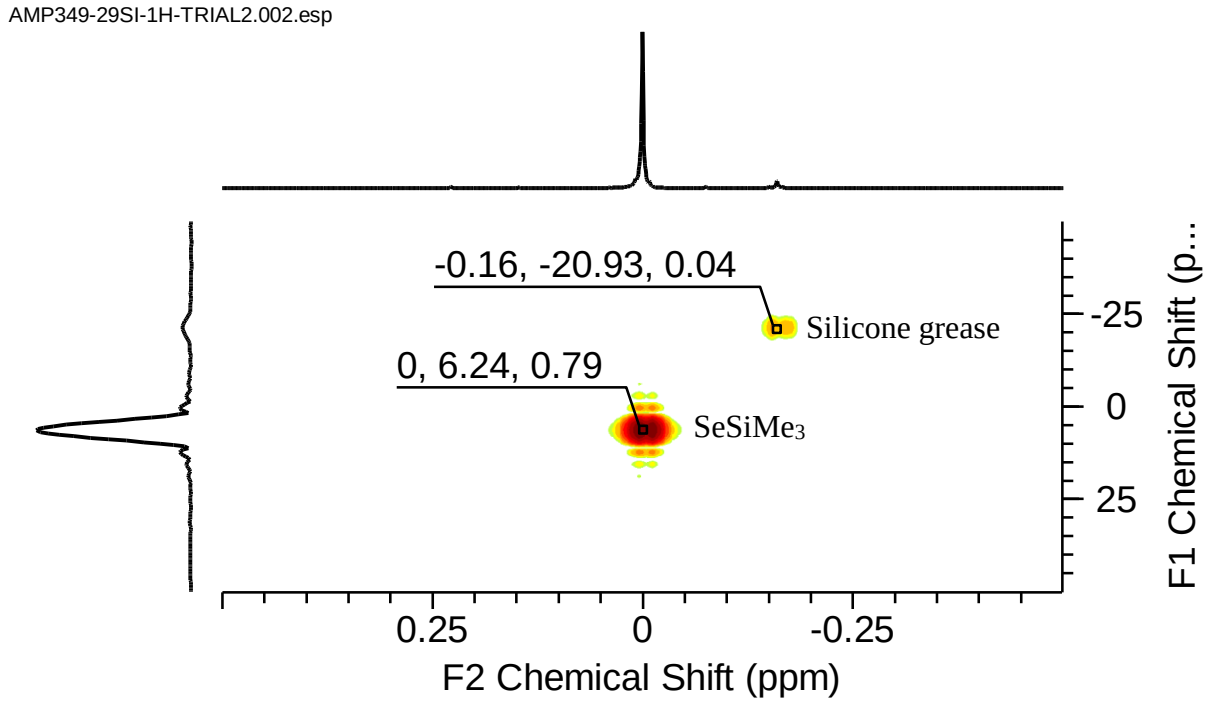

3.2b – $^{77}Se\{^{1}H\}$ NMR $CDCl_3$ - 298K

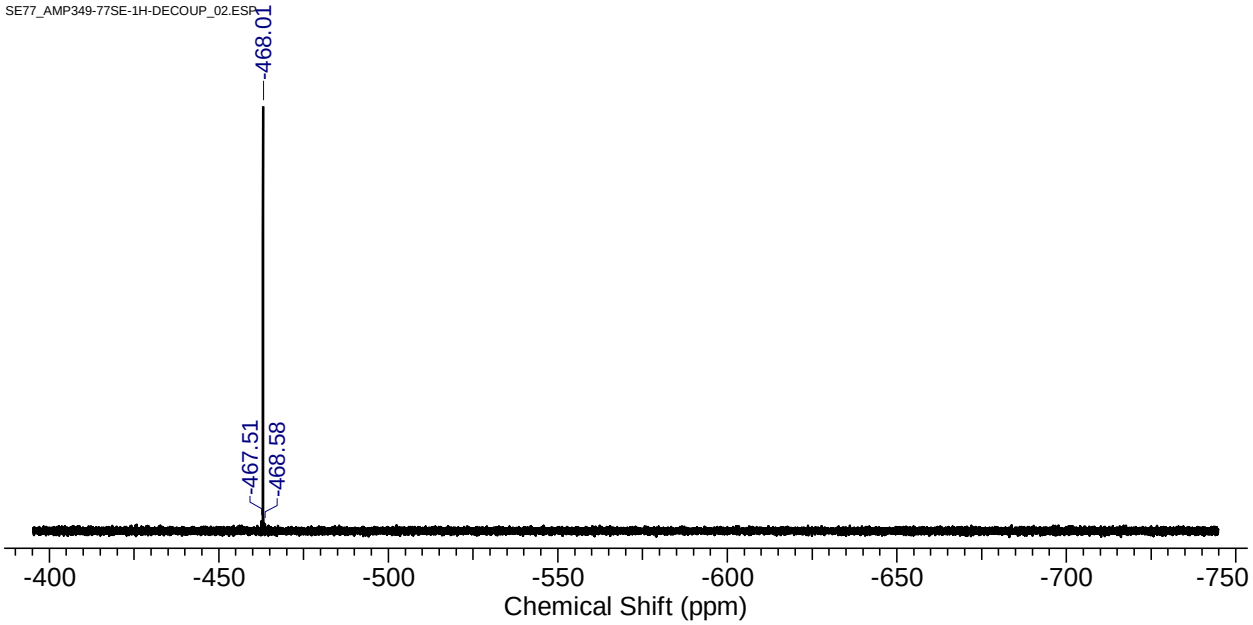

3.2b – ^{77}Se-^{1}H HMBC $CDCl_3$ - 298K

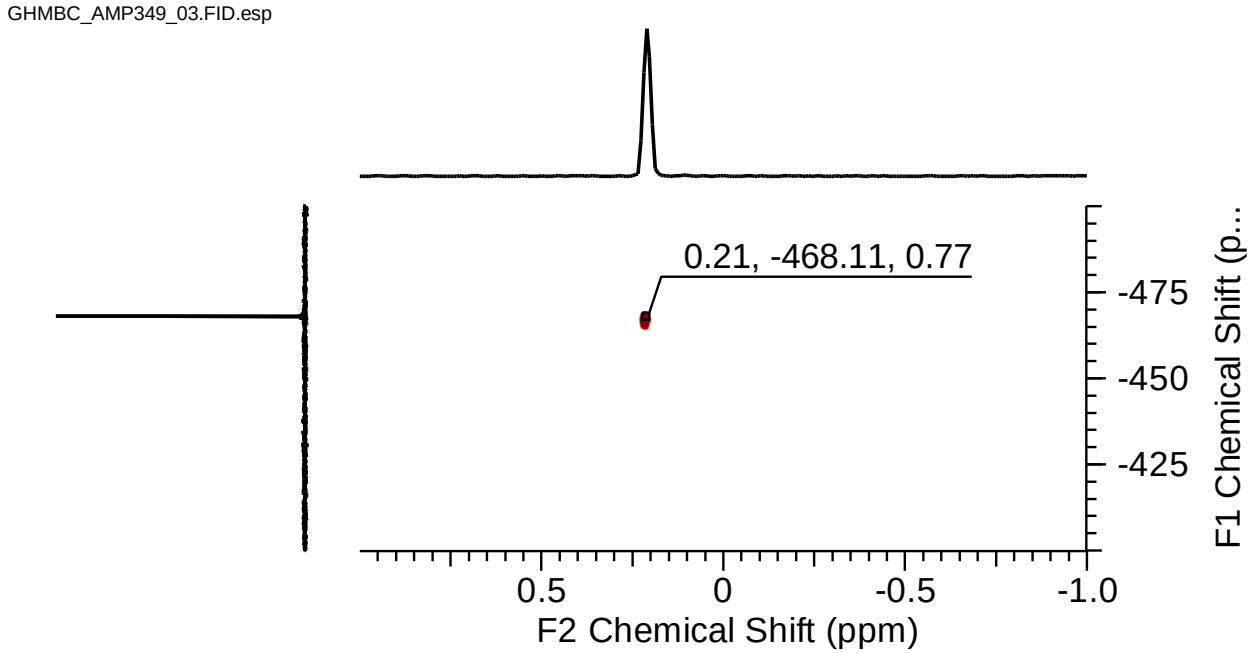

3.3a – ^{1}H NMR $CDCl_3$ - 298K

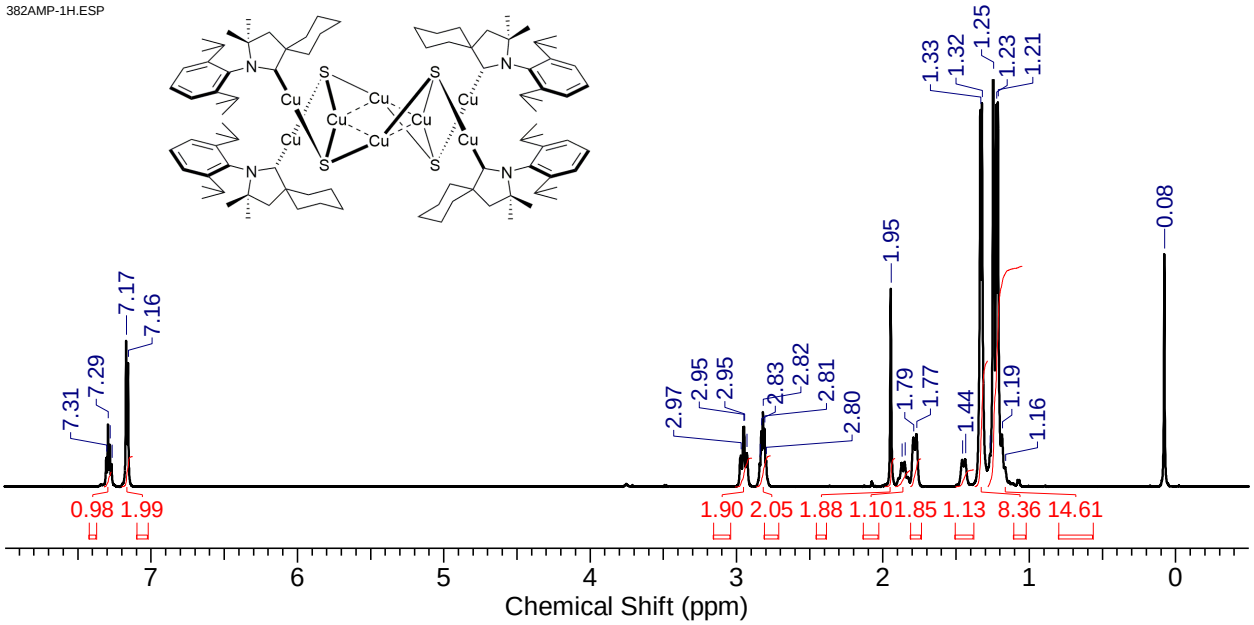

3.3a – ^{13}C{^{1}H} NMR $CDCl_3$ - 298K

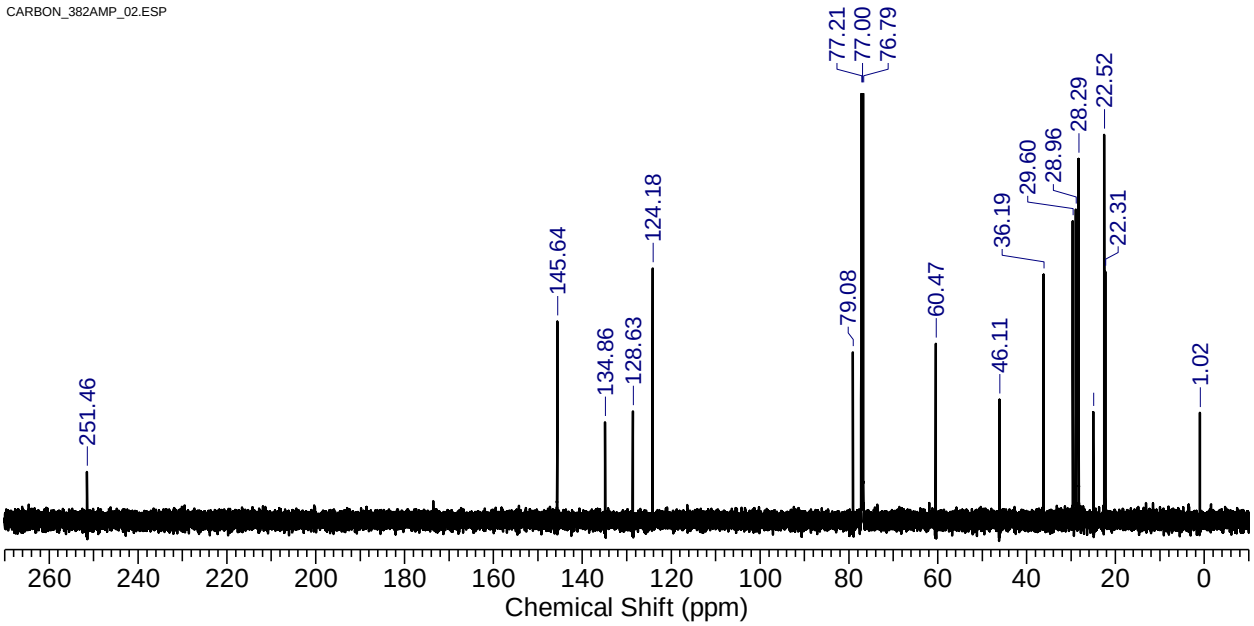

3.3b – ^{1}H NMR $CDCl_3$ - 298K

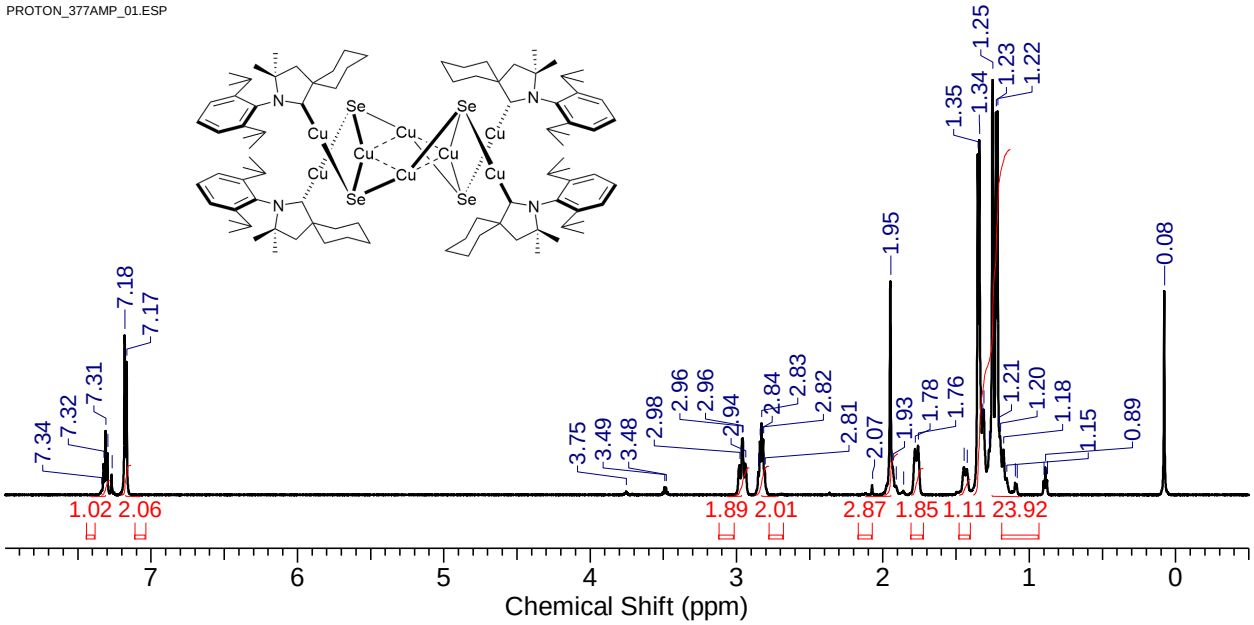

3.3b – ^{13}C{^{1}H} NMR $CDCl_3$ - 298K

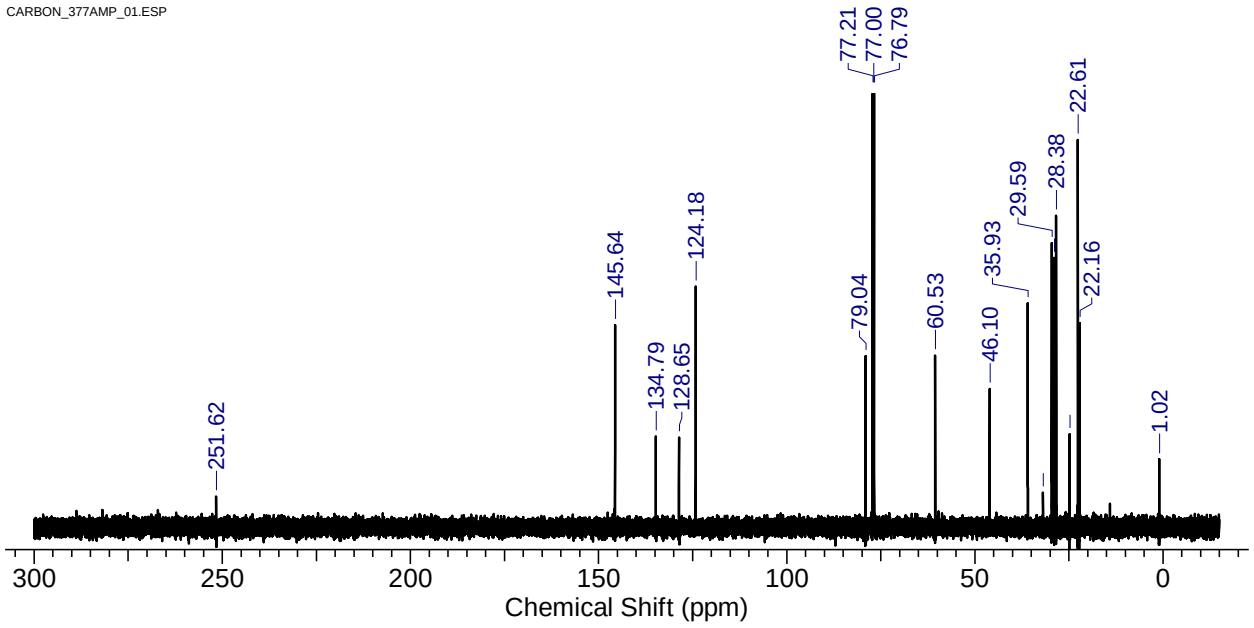

3.3b – $^{77}Se\{^{1}H\}$ NMR $CDCl_3$ - 298K

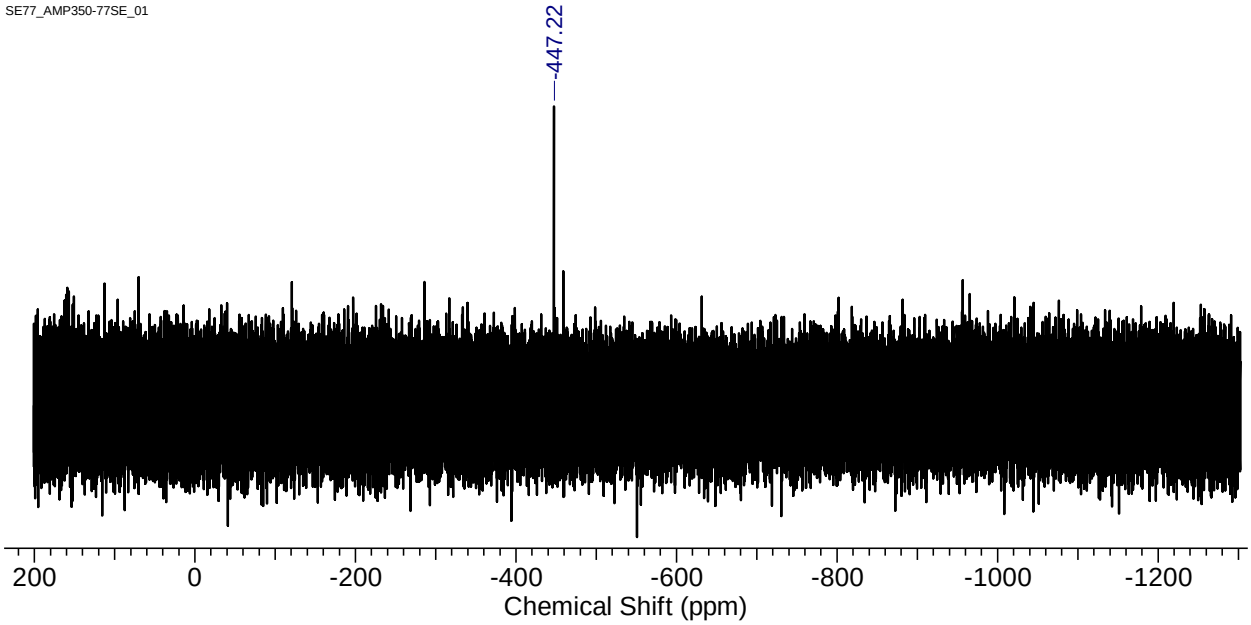

3.4a – ^{1}H NMR $CDCl_3$ - 298K

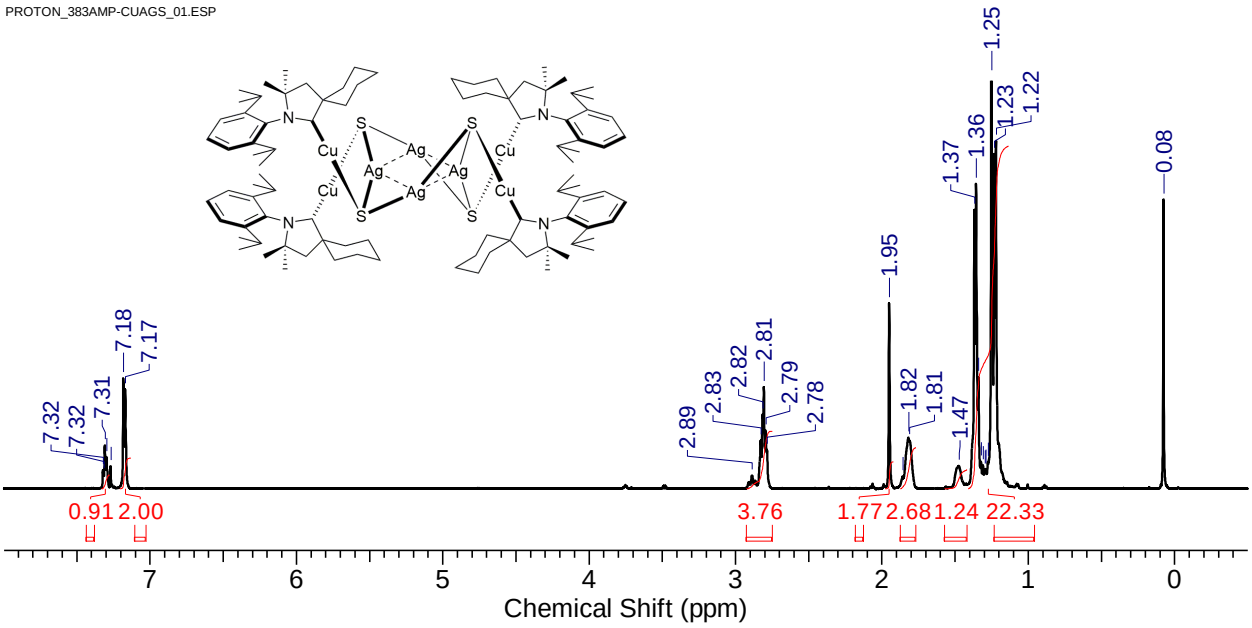

3.4a – $^{13}C\{^{1}H\}$ $CDCl_3$ - 298K

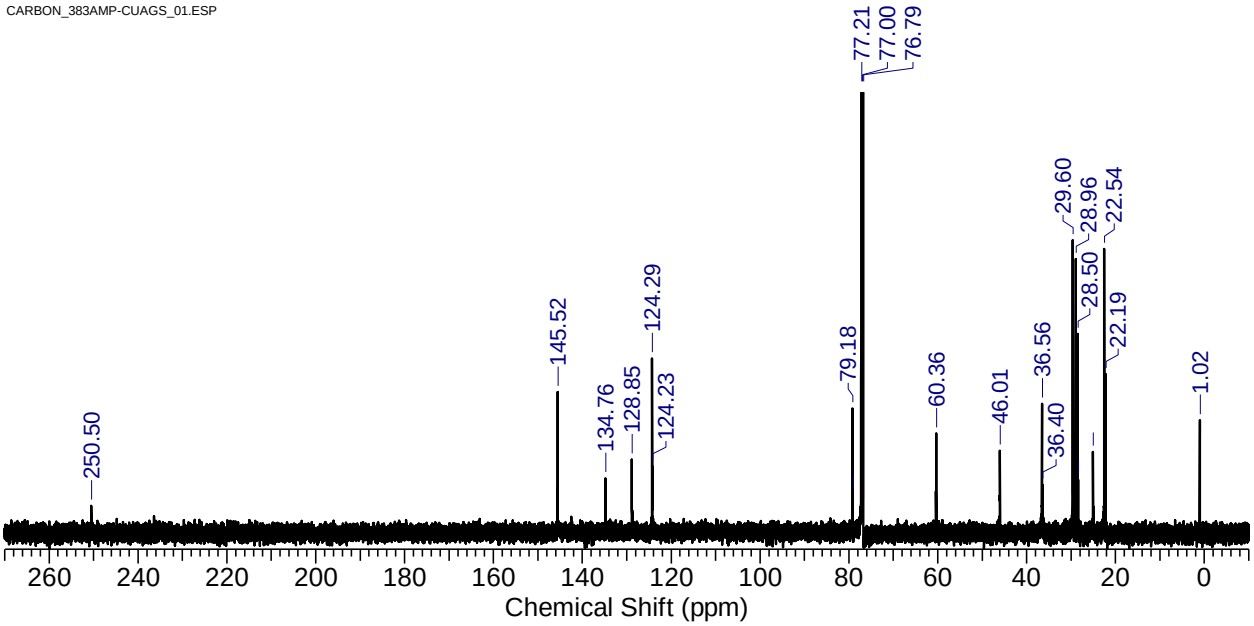

3.4b – ^{1}H NMR $CDCl_3$ - 298K

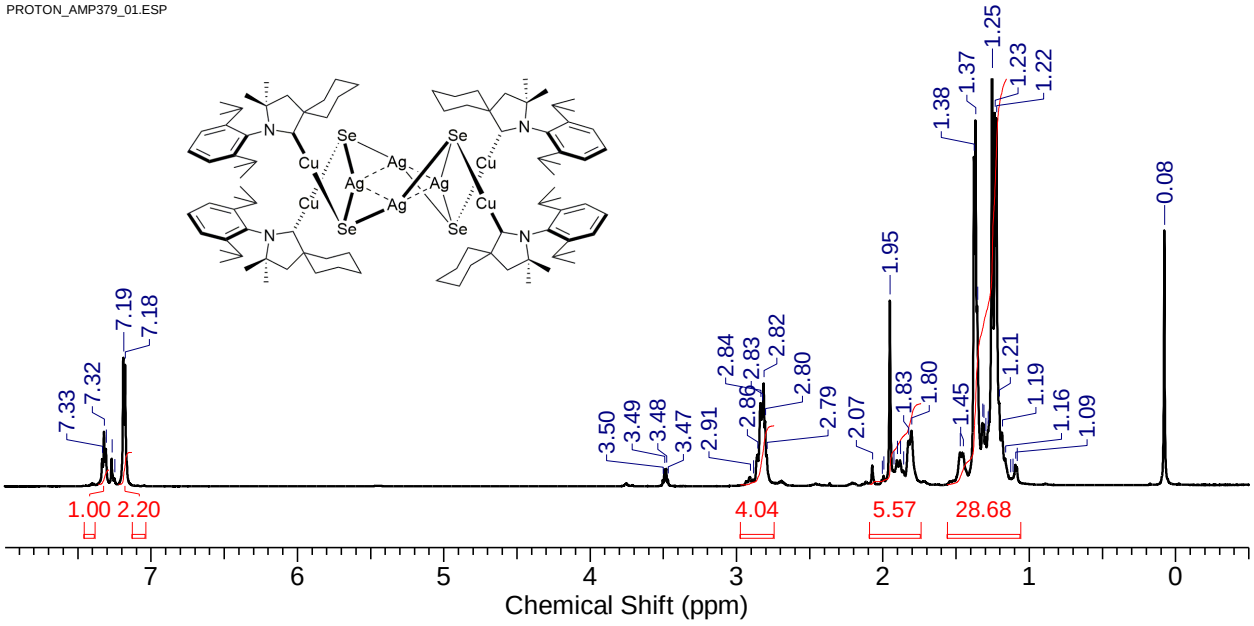

3.4b – $^{13}C\{^{1}H\}$ NMR $CDCl_3$ - 298K

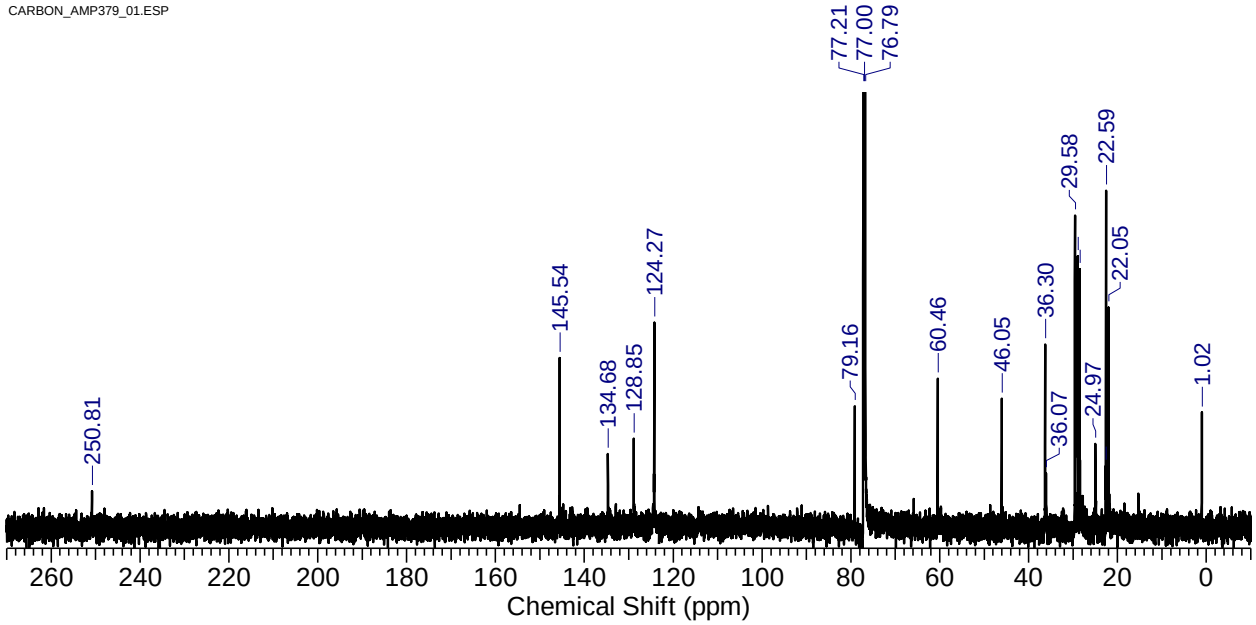

3.4b – $^{77}Se\{^{1}H\}$ NMR $CDCl_3$ - 298K

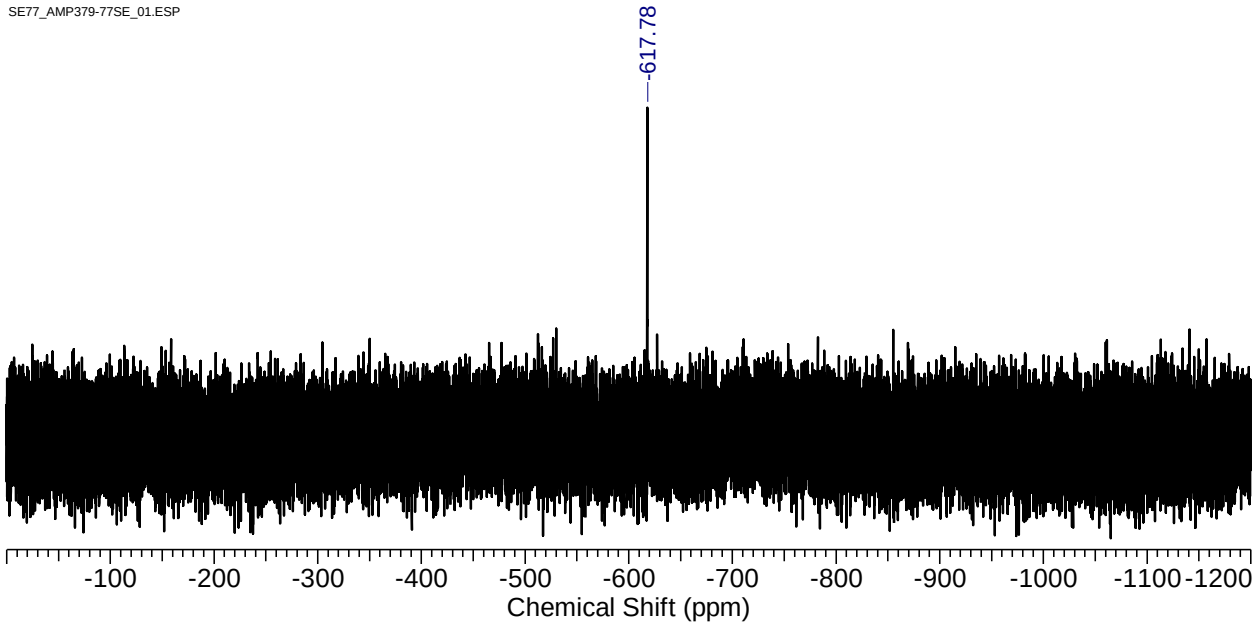

3.5b – ^{1}H NMR $CDCl_3$ - 298K

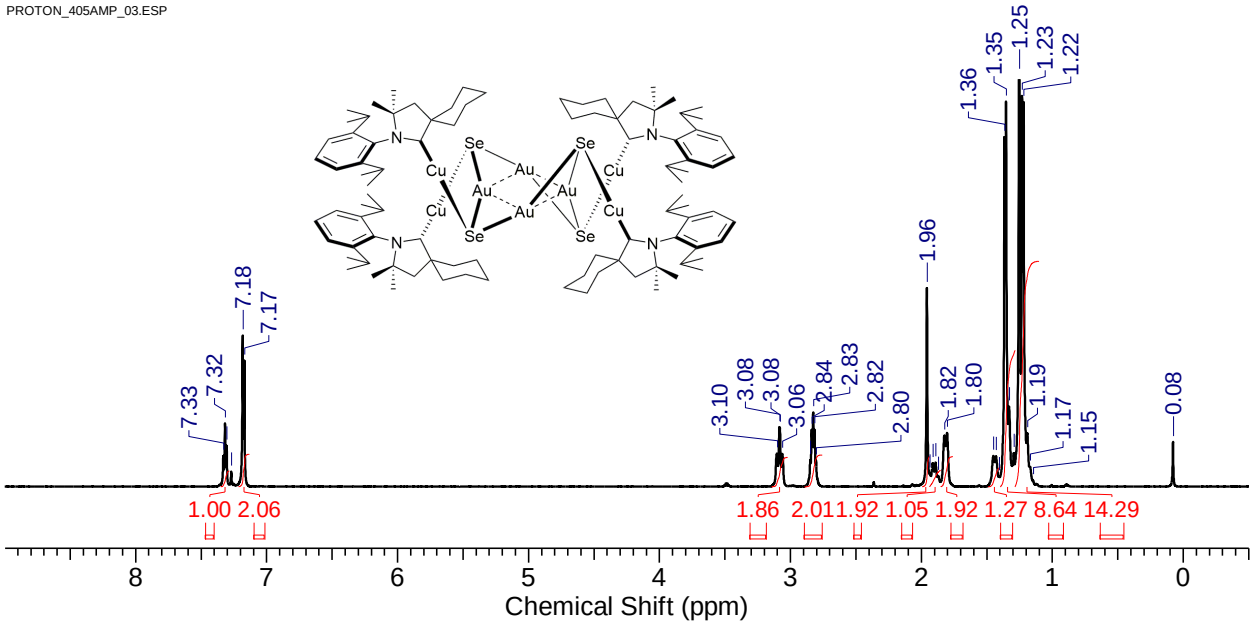

3.5b – ^{13}C{^{1}H} NMR $CDCl_3$ - 298K

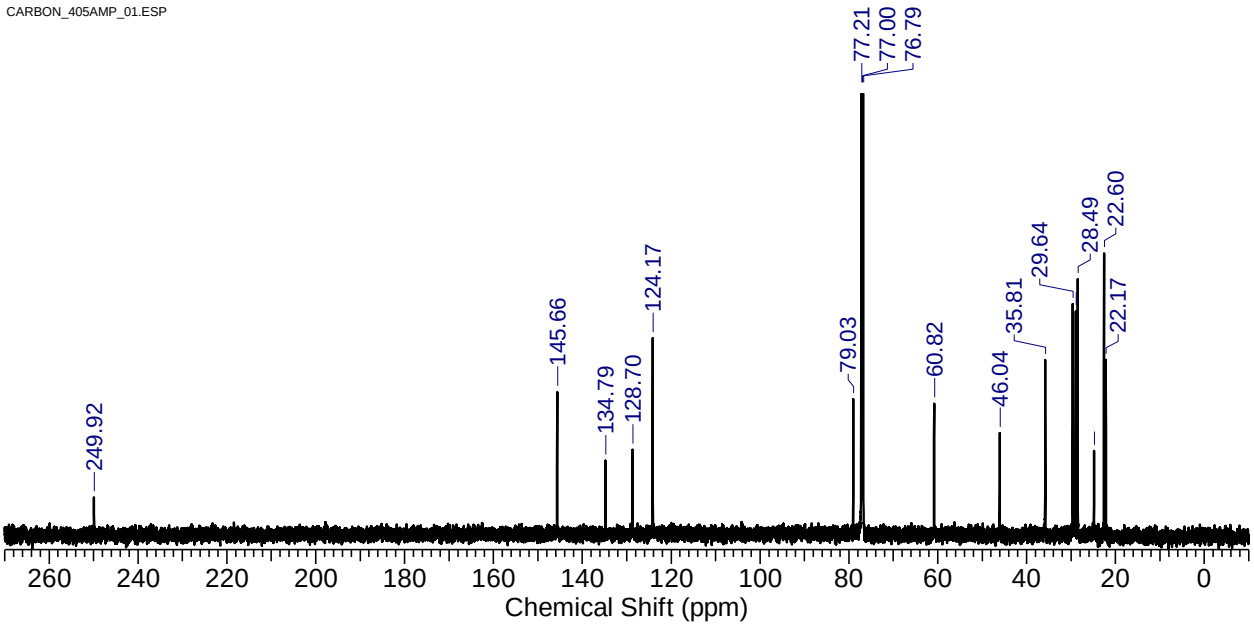

3.5b – $^{77}Se\{^{1}H\}$ NMR $CDCl_3$ - 298K

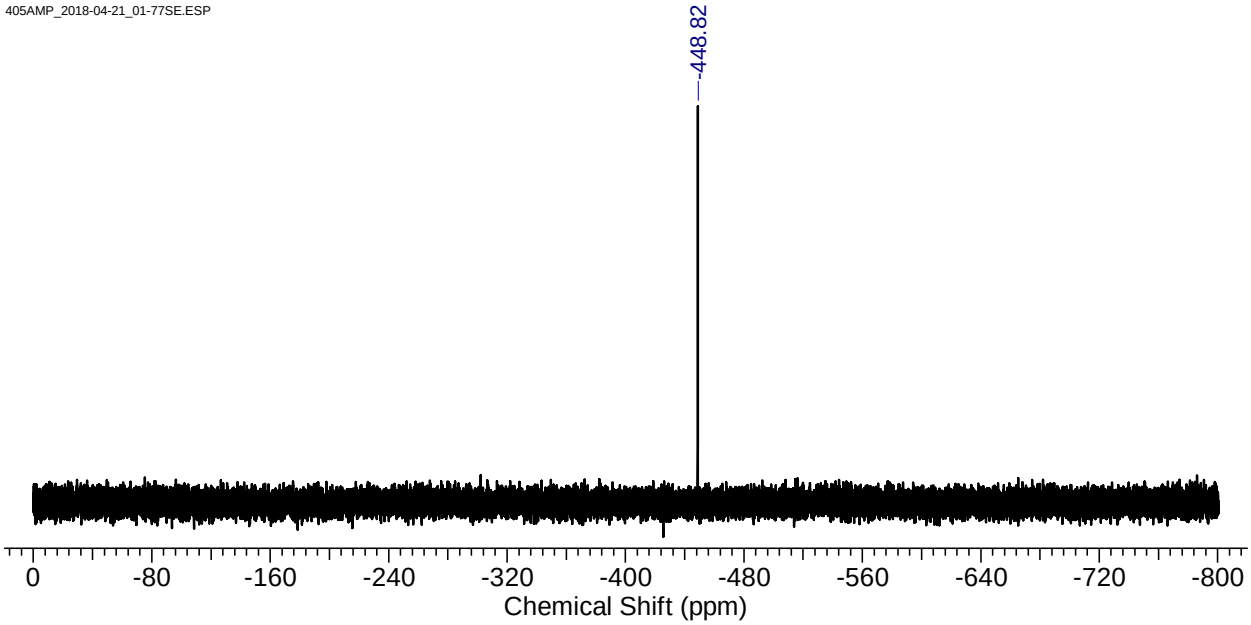

	3.3a	**3.3b**	**3.4a**	**3.4b**	**3.5b**
Molecular Formula	$C_{92}H_{140}Cu_8N_4S_4 \cdot 2\ C_4H_8O$	$C_{92}H_{140}Cu_8N_4Se_4 \cdot 2\ C_4H_8O$	$C_{92}H_{140}Ag_4Cu_4N_4S_4 \cdot 2\ C_4H_8O$	$C_{92}H_{140}Ag_4Cu_4N_4Se_4 \cdot C_4H_8O$	$C_{92}H_{140}Au_4Cu_4N_4Se_4 \cdot C_4H_8O$
Formula Weight	2082.84	2270.44	2260.16	2374.95	2723.37
Crystal Habit	Yellow Prism	Yellow Needle	Colourless Block	Yellow Prism	Yellow Polyhedron
Crystal System	Monoclinic	Monoclinic	Monoclinic	Monoclinic	Monoclinic
Space Group	*C2/c*	*C2/c*	*C2/c*	*C2/c*	*C2/c*
Temperature (K)	110	110	110	110	110
λ (Å)	0.71073	0.71073	0.71073	0.71073	0.71073
a (Å)	22.7609(8)	23.1908(6)	23.2250(15)	23.8586(6)	23.7945(5)
b (Å)	18.3905(6)	18.4282(4)	18.5523(13)	18.5564(6)	18.5897(5)
c (Å)	24.9373(8)	24.8244(6)	24.7158(16)	24.5983(6)	24.6375(6)
α (deg)	90	90	90	90	90
β (deg)	90.382(2)	91.5623(14)	90.414(3)	91.7430(10)	91.6880(10)
γ (deg)	90	90	90	90	90
V (Å^3)	10438.1(6)	10605.1(4)	10649.2(12)	10885.4(5)	10893.2(5)
Z	4	4	4	4	4
μ (MoKα_1, mm^{-1})	1.723	2.990	1.626	2.848	7.508
$\rho_{calc.}$ (g cm^{-3})	1.325	1.422	1.410	1.449	1.661
$2\theta_{max}$	55.498	50.000	55.176	57.446	50.484
Reflections collected	48525	72458	109959	36298	80084
Ind. Reflections	12217	9329	12240	13554	19757
R_{merge}	0.0532	0.0690	0.0496	0.0296	0.0331
R_1, wR_2 [$I > 2\sigma(I)$]	0.0572, 0.1473	0.0542, 0.1420	0.0533, 0.1415	0.0487, 0.1509	0.0520, 0.1317
R_1, wR_2 (all data)	0.1087, 0.1704	0.0811, 0.1520	0.0804, 0.1602	0.0700, 0.1614	0.0828, 0.1437
GOF	1.067	1.022	1.025	1.078	1.116
Max, min residual electron density (e^-/Å^3)	1.042, -1.449	1.578, -0.895	2.305, -2.807	1.742, -0.986	3.158, -1.269

$R_1 = \Sigma(|F_o| - |F_c|) / \Sigma F_o$

$wR_2 = [\Sigma(w(F_o^2 - F_c^2)^2) / \Sigma(w F_o^4)]^{½}$

$GOF = [\Sigma(w(F_o^2 - F_c^2)^2) / (\text{No. of reflns.} - \text{No. of params.})]^{½}$

Table A3.1 Crystallographic data for **3.3-5**.

Appendix 4. Supporting Information for Chapter 4

4.1 – ^{1}H NMR $CDCl_3$ - 298K

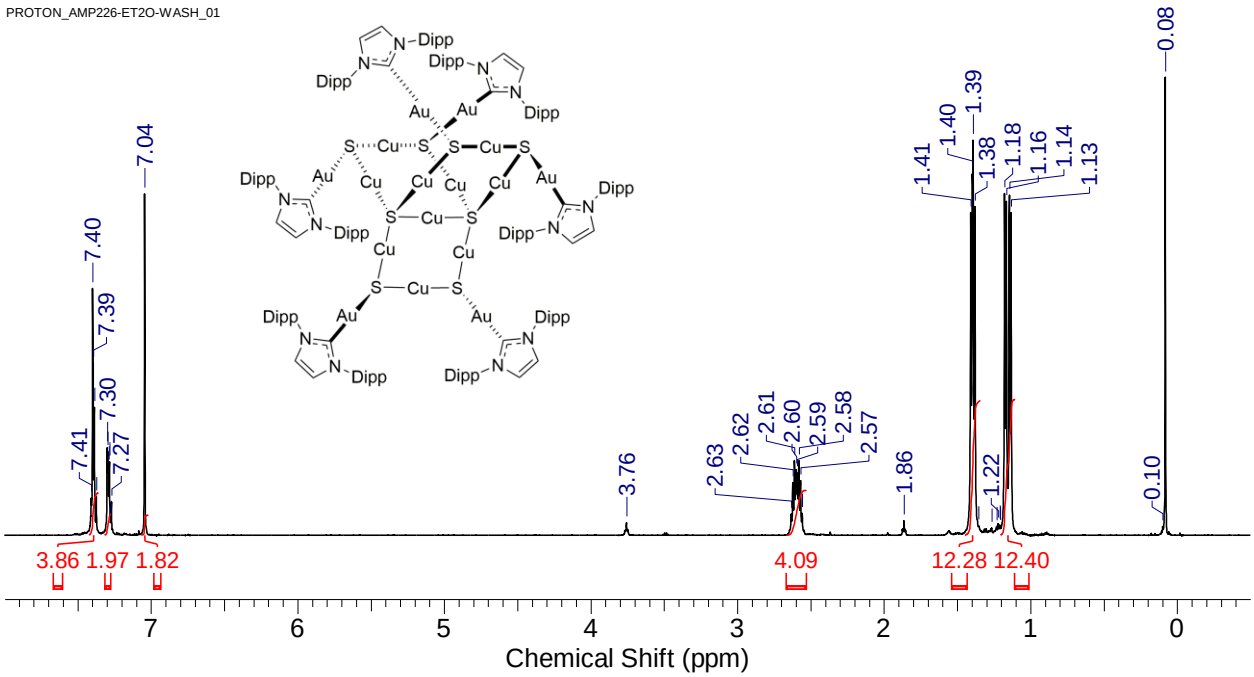

4.1 – ^{13}C{^{1}H} NMR $CDCl_3$ - 298K

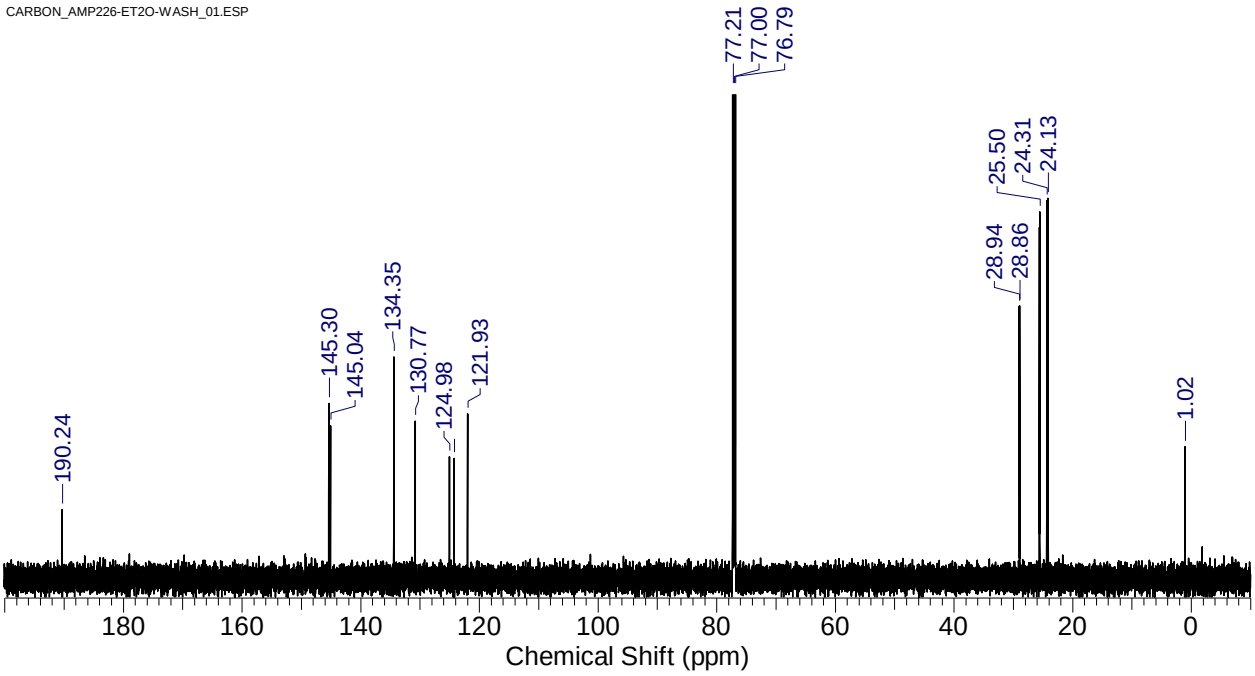

4.2 – ^{1}H NMR $CDCl_3$ - 298K

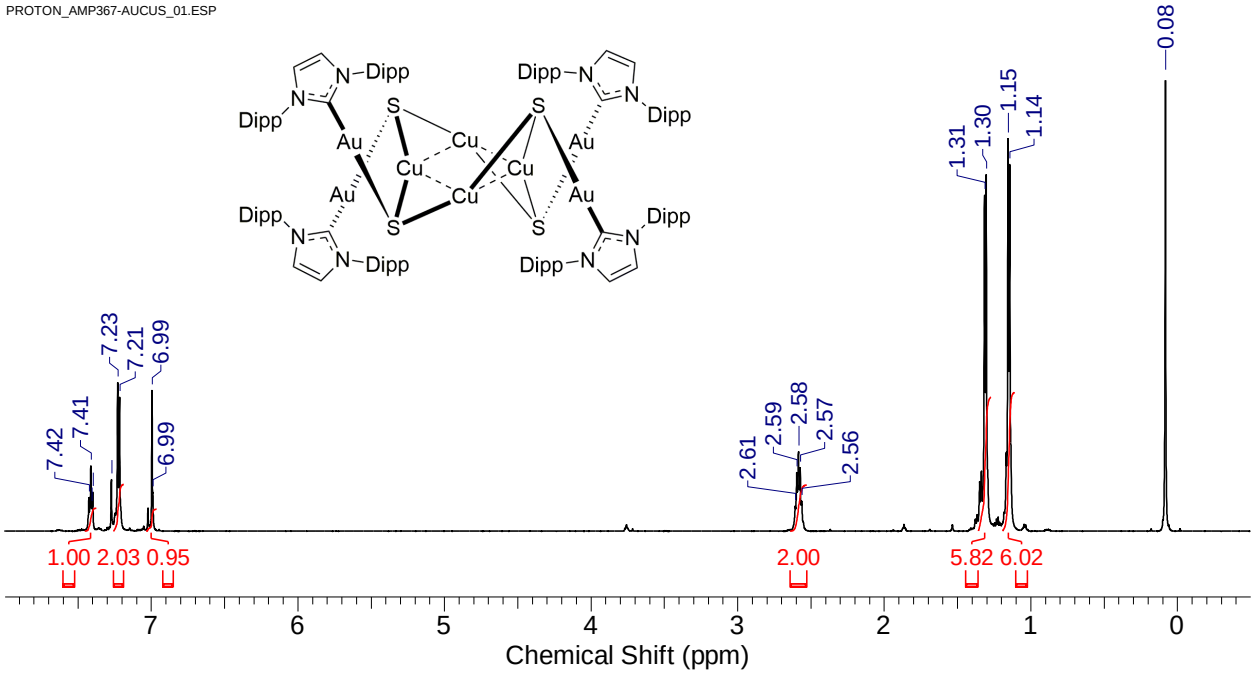

4.1 – ^{13}C{^{1}H} NMR $CDCl_3$ - 298K

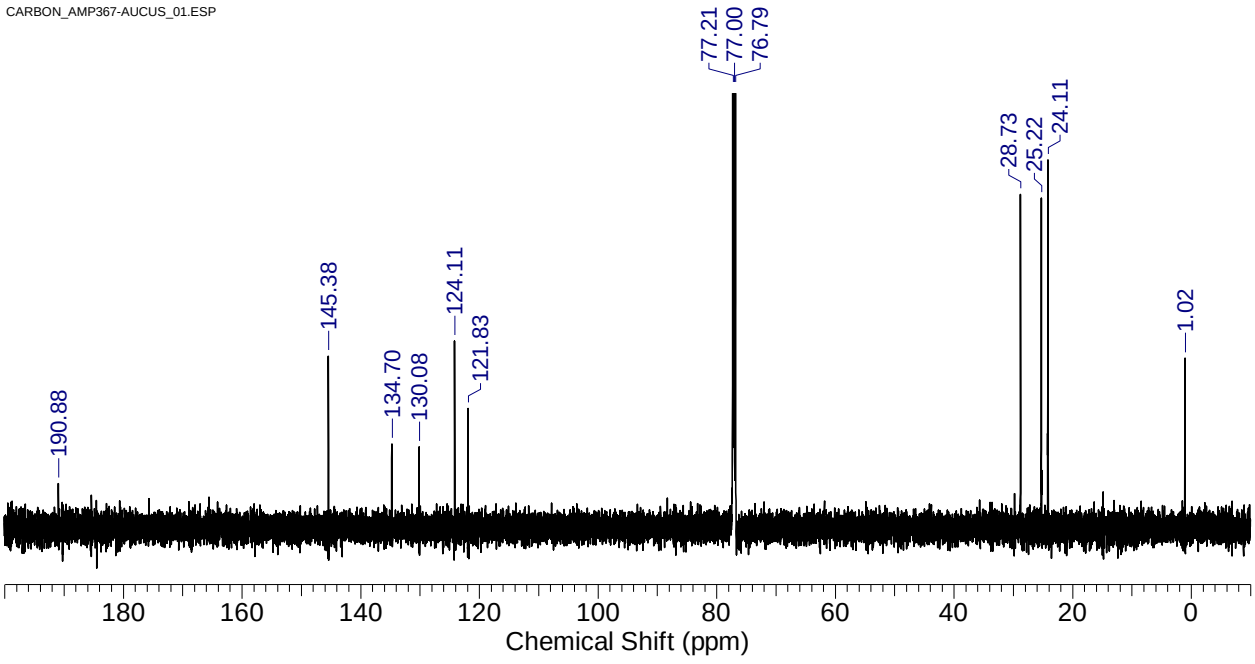

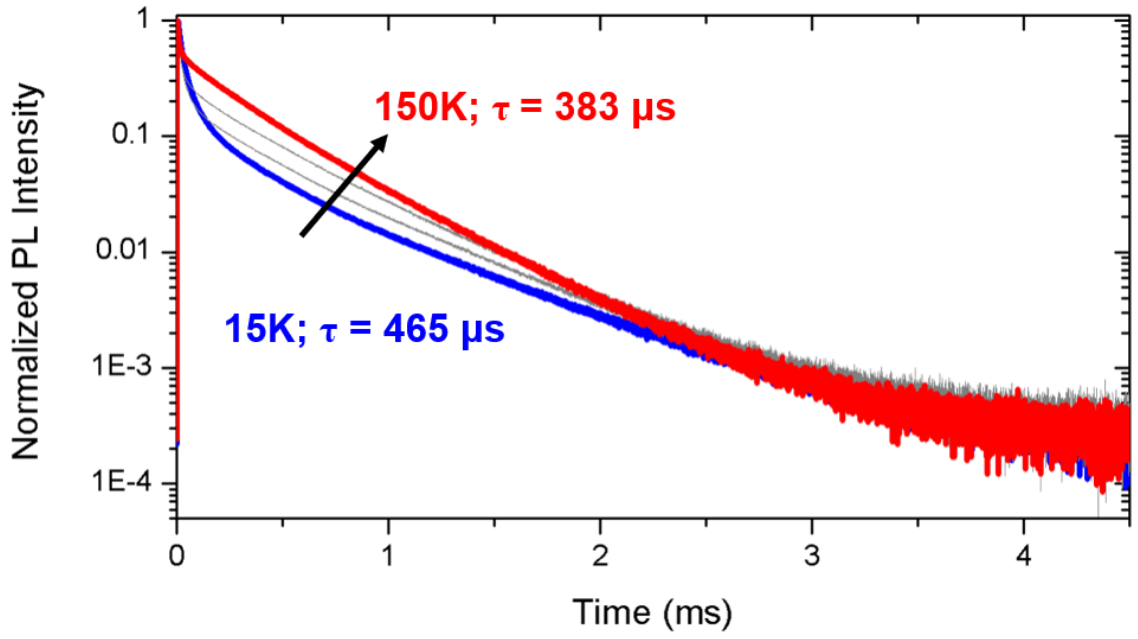

Figure A4.1 Photoluminescence decay traces for **4.1** (λ_{ex} = 337 nm, λ_{em} = 580 nm) at temperatures from 15K (blue) up to 150K (red). The values of τ are given for monoexponential fits to the data.

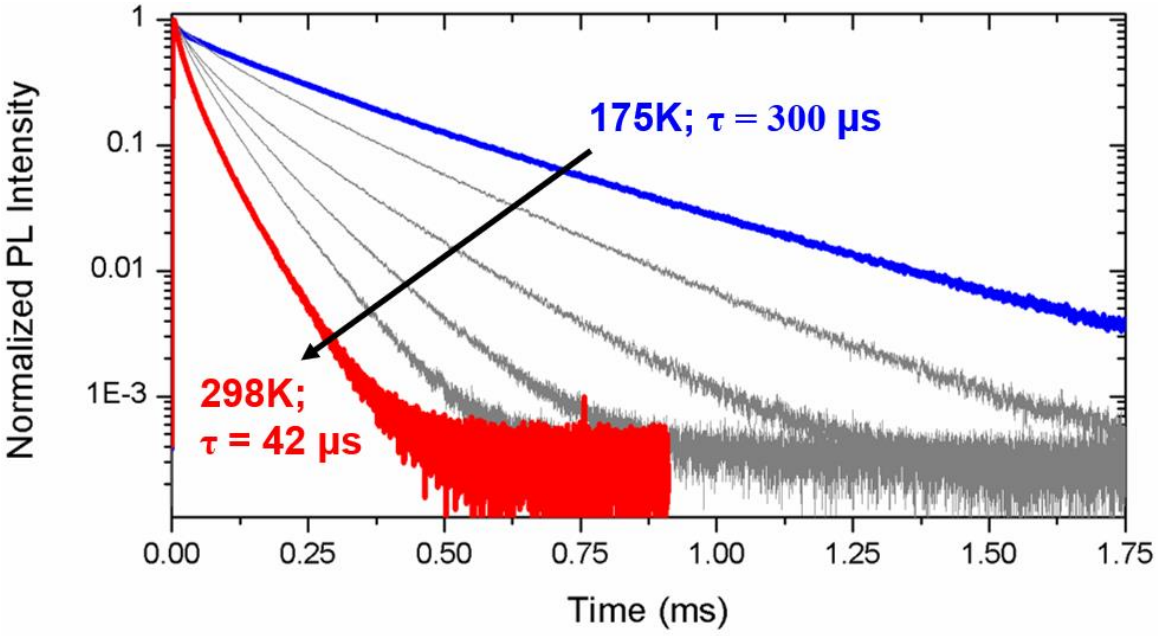

Figure A4.2 Photoluminescence decay traces for **4.1** (λ_{ex} = 337 nm, λ_{em} = 580 nm) at temperatures from 175K (blue) up to 298K (red). The values of τ are given for monoexponential fits to the data.

	4.1	**4.2**
Molecular Formula	$C_{162}H_{216}Au_6Cu_{10}N_{12}S_8 \cdot 3C_4H_8O$	$C_{108}H_{144}Au_4Cu_4N_8S_4$
Formula Weight	4621.44	2724.57
Crystal Habit	Colourless Prism	Colourless Block
Crystal System	Trigonal	Tetragonal
Space Group	$R\bar{3}c$	$I\bar{4}$
Temperature (K)	110	110
λ (Å)	1.54178	0.71073
a (Å)	28.6657(8)	18.3060(4)
b (Å)	28.6657(8)	18.3060(4)
c (Å)	52.375(2)	16.5326(6)
α (deg)	90	90
β (deg)	90	90
γ (deg)	120	90
V (Å^3)	37271(3)	5540.2(3)
Z	6	2
μ (mm^{-1})	8.285	6.149
$\rho_{calc.}$ (g cm^{-3})	1.235	1.633
$2\theta_{max}$	131.232	66.334
Reflections collected	118487	69757
Ind. Reflections	7124	10543
R_{merge}	0.1361	0.0284
R_1, wR_2 [$I > 2\sigma(I)$]	0.0537, 0.1743	0.0230, 0.0594
R_1, wR_2 (all data)	0.0831, 0.1974	0.0258, 0.0606
GOF	1.117	1.026
Max, min residual electron density (e^-/Å^3)	1.067, -1.545	2.342, -0.584

$R_1 = \Sigma(|F_o| - |F_c|) / \Sigma F_o$

$wR_2 = [\Sigma(w(F_o^2 - F_c^2)^2) / \Sigma(w F_o^4)]^{½}$

GOF = [$\Sigma(w(F_o^2 - F_c^2)^2) / ($No. of reflns. - No. of params.$)]^{½}$

Table A4.1 Crystallographic data for **4.1** and **4.2**

Curriculum Vitae

Alexander Mathias Polgar

Education

***The* University *of* Western Ontario** London, ON
M Sc candidate, Department of Chemistry, Sep. 2016 - present
Thesis: Coinage Metal Chalcogenide Clusters with *N*-Heterocyclic Carbene Ancillary Ligands

***The* University *of* Western Ontario** London, ON
B Sc Honours Chemistry, Sep. 2012 – May 2016
Thesis: Gold(I) Trimethylsilylchalcogenolate Reagents as Precursors to Luminescent Heterometallic Chalcogenide Clusters

Book Chapters

1. **A. M. Polgar**, J. F. Corrigan*, Recent Advances in the Self-Assembly of Polynuclear Metal-Selenium and -Tellurium Compounds from 14 – 16 Reagents *in* Selenium and Tellurium Reagents - In Chemistry and Materials Science. Edited by Risto Laitinen. De Gruyter, **2018**. (in press)

Journal Articles

7. **A. M. Polgar**, A. Zhang, M. J. Stillman, J. F. Corrigan*, Plug and Play: Tunable Metal/Chalcogen Composition in Copper(I)-Chalcogenide Self-Assemblies Enabled by Cyclic (Alkyl)(amino)carbenes, (submitted).

6. V. Somasundaram, **A. M. Polgar**, P. N. Gunawardene, M. S. Workentin, J. F. Corrigan*, NHC Ligated Group 11 Metal-Arylthiolates Containing an Azide Functionality Amenable to "Click" Reaction Chemistry, (submitted).

5. **A. M. Polgar**, F. Weigend, A. Zhang, M. J. Stillman, J. F. Corrigan*, Synthesis and Characterization of a Highly Tunable Octanuclear Coinage Metal Chalcogenide Framework with *N*-Heterocyclic Carbene Ancillary Ligands, *J. Am. Chem. Soc.* **2017**, *139*, 14045 – 14048.

4. **A. M. Polgar**, C. B. Khadka, M. Azizpoor Fard, B. Nikkel, T. O'Donnell, T. Neumann, K. Lahring, K. Thompson, C. Cadogan, F. Weigend, J. F. Corrigan*, A Controlled Route to a Luminescent $3d^{10}$-$5d^{10}$ Sulfido Cluster Containing Unique $AuCu_2(\mu_3\text{-}S)$ Motifs, *Chem. Eur. J.* **2016**, *22*, 18378 – 18382.

3. A. I. Wallbank, T. P. Lebold, A. Borecki, **A. M. Polgar**, B. M. Waters, M. S. Workentin, J. F. Corrigan*, Zn(II) and Cd(II) Ferrocenylchalcogenolate Complexes, *Eur. J. Inorg. Chem.* **2016**, 372 – 377.

2. N. K. Joshi, **A. M. Polgar**, R. P. Steer*, M. F. Paige*, White Light Generation using Förster Resonance Energy Transfer between 3-hyroxyisoquinoline and Nile Red, *Photochem. Photobiol. Sci.* **2016**, *15*, 609 – 617.

1. S. V. Kohut, **A. M. Polgar**, V. N. Staroverov*, Origin of the Step Structure of Molecular Exchange-Correlation Potentials, *Phys. Chem. Chem. Phys.* **2016**, *18*, 20938 – 20944.

Conference Presentations

4. Oral Presentation (National) **A. M. Polgar**, C. B. Khadka, M. Azizpoor Fard, C. Cadogan, A. Q. W. Zhang, M. J. Stillman, J. F. Corrigan*, Gold(I) Trimethylsilylchalcogenolate Precursors to Luminescent Mixed Coinage Metal-Chalcogenide Clusters, 100th Canadian Chemistry Conference and Exhibition, Toronto, ON. 28 May – 1 June 2017.

3. Poster Presentation (Institutional) **A. M. Polgar**, C. B. Khadka, C. Cadogan, F. Weigend, J. F. Corrigan*, Mixed Coinage Metal-Chalcogenide Clusters: Synthesis, Optoelectronics and Ligand Effects, Fallona Family Interdisciplinary Science Showcase, London, ON. 16 January 2017.

2. Oral Presentation (Regional): **A. M. Polgar**, C. B. Khadka, M. Azizpoor Fard, C. Cadogan, F. Weigend, J. F. Corrigan*, Preparation of Mixed Coinage Metal-Chalcogenide Clusters from Simple Precursors. 49th Inorganic Discussion Weekend, Hamilton, ON. 11-13 November 2016.

1. Oral Presentation (National): **A. M. Polgar**, M. F. Paige*, Single-Molecule Fluorescence Microscopy of a Nanocatalytic Chemical Reaction. Reactive Intermediates Student Exchange 2015 Conference, Calgary, AB. 21 August 2015.

Teaching Assistantships

***The* University *of* Western Ontario** London, ON

Chem 1302	Discovering Chemical Energetics	Winter 2017
Chem 2271	Structure and Bonding in Inorganic Chemistry	Fall 2017
Chem 2384	Microscopic Phenomena	Winter 2016
Chem 2271	Structure and Bonding in Inorganic Chemistry	Fall 2016

Scholarships and Awards (2016 and 2017)

6. Queen Elizabeth II Ontario Graduate Scholarship

5. Natural Sciences and Engineering Research Council - Canada Graduate Scholarship

4. UWO Department of Chemistry - ASPIRE Travel Grant

3. Canadian Society for Chemistry - Award for Undergraduate Research in Inorganic Chemistry

2. Society of Chemical Industry Canada - Merit Certificate

1. Andrew E. Scott Medal and Prize; N. B. Patel Award

Graduate Courses Completed and Grade Received

Chem 9503	Advanced NMR Spectroscopy I	97
Chem 9541	Crystallography I	99
Chem 9651	Organometallic Chemistry for Bond Activation	94